



NON-NEWTONIAN OPEN CHANNEL FLOW: THE EFFECT OF SHAPE

by

Johannes Hendrik Burger

Thesis submitted in fulfilment of the requirements for the degree

Doctor of Technology: Mechanical Engineering

in the

Faculty of Engineering

at the

Cape Peninsula University of Technology

Supervisor: Prof Rainer Haldenwang

Co-supervisor: Dr Neil J Alderman

Cape Town

February 2014

Declaration

I, Johannes Hendrik Burger, hereby declare that the contents of this thesis represent my own unaided work and that the thesis has not previously been submitted for academic examination towards any qualification. Furthermore, it represents my own opinions and not necessarily that of the Cape Peninsula University of Technology or the National Research Foundation of South Africa.

All intellectual concepts, theories, methodologies, mathematical derivations and model developments used in this thesis and published in various scientific journals (except those that were used for review articles) were derived solely by the candidate and first author of the published manuscripts. Where appropriate, the intellectual property of others were acknowledged by using appropriate references. The contribution of co-authors, for conference and published manuscripts, was in a supervisory capacity (Prof Rainer Haldenwang and Dr Neil J Alderman) to meet the requirements for the doctoral degree award.

(Signature)

Signed in Cape Town this _____ day of _____ 2014

Abstract

Open channels, flumes or launders are used in the mining industry to transport slurries during processing and to disposal sites. Water plays a major part in the makeup of these slurries, its usage and availability is critical in countries where there are strict water usage management programs. The optimisation of flume design involves the maximisation of solids transport efficiency whilst, at the same time reduces water usage. The design of open channels is complex as it is dependent on both the slurry rheology and the channel shape. Very little has been reported in the literature for predicting non-Newtonian laminar flow in open channels of arbitrary cross-section. The only method available was that proposed by Kozicki and Tiu (1967, 1986). The shape factors they used were those evaluated from analytical solutions for flow of Newtonian fluids in open channels of the same cross-section. However, they carried out no experimental work to validate their model. Few experimental studies have been made on the effect of shape on non-Newtonian flow in open channels. Naik (1983) tested kaolin in water suspensions in a rectangular channel. Coussot (1994) provided some data for the flow of a Herschel-Bulkley fluid in rectangular and trapezoidal channels. Fitton (2007; 2008) obtained data for flow of three different non-Newtonian fluids (carboxymethylcellulose, carbopol and thickened tailings) in a semi-circular channel. A large experimental database for non-Newtonian flow in rectangular open channels was published by Haldenwang (2003) at the Flow Process Research Centre, Cape Peninsula University of Technology. Guang et al. (2011) performed Direct Numerical Simulations of turbulent flow of a yield- pseudoplastic fluid in a semi-circular channel. They compared their simulations with actual field measurements and found them to over-predict the flow velocity by approximately 40%. The source for this discrepancy was difficult to ascertain.

A comprehensive database was compiled during this research of the flow of three non-Newtonian fluids in rectangular, trapezoidal, semi-circular and triangular channels. The flow of carboxymethylcellulose solutions and aqueous kaolin and bentonite suspensions was investigated in a 10 meter long flume at angles ranging from 1° to 5° from the horizontal plane. The effect of channel shape on the friction factor-Reynolds number relationship for laminar and turbulent open channel flow of these three fluids was investigated. New models for the prediction of laminar and turbulent flow of non-Newtonian fluids in open channels of different cross-sectional shapes are proposed. The new laminar and turbulent velocity models are compared with three previously-published velocity models for laminar flow and five previously-published velocity models for turbulent flow using average velocity as comparison criteria.

For each channel shape, the laminar flow data can be described by a general relationship, $f = K/Re$ where f is the Fanning friction factor and Re is the appropriate Haldenwang et al. (2002) Reynolds number. The K values were found to be 14.6 for triangular channels with a vertex angle of 90°, 16.2 for semi-circular channels, 16.4 for rectangular channels and 17.6 for trapezoidal channels with 60 degree sides. These K values were found to be in line with those reported by Straub et al. (1958) and Chow (1969) for open channel laminar flow of Newtonian fluids as opposed to the assumption made by Haldenwang et al. (2002; 2004) of using a constant value of 16 based on the pipe flow paradigm for all channel shapes.

This new laminar model gave a closer fit to the laminar flow data than those from the three previously-published models. However, the presence of the yield stress still presents a problem, which makes the flow prediction in laminar flow for such fluids not very accurate. The investigation on non-Newtonian turbulent flow of the three fluids in the four different shaped open channels revealed that the data was described by the modified Blasius equation $f = a Re^b$ where a and b are constant values determined for each channel shape and Re is the Haldenwang et al. (2002) Reynolds number. Values of a and b for a rectangular channel were found to be 0.12 and -0.330, for a semi-circular channel 0.048 and -0.205, for a trapezoidal channel with 60° sides, 0.085 and -0.266 and for a triangular channel with vertex angle of 90°, 0.042 and -0.202. New laminar and turbulent velocity models were derived from using the new laminar $f = K/Re$ and turbulent $f = a Re^b$, friction factor-Reynolds number relationship. The laminar velocity model did not always give the best result, but the majority of the time it did, compared to the three previously published models. The new turbulent velocity model yielded the best results when compared to the five previously published models using average velocity as comparison criteria. The composite power law modelling procedure of Garcia et al. (2003) used for pipe flow predictions was extended to the present work on non-Newtonian flow in open channels of various cross-sections. The results show that the modelling technique used by Garcia et al. (2003) for pipe flow can be used to adequately predict flow in an open channel of a given cross-sectional shape provided that an appropriate Reynolds number is used to take into account the non-Newtonian behaviour of the test fluid. It was found that the results using the Haldenwang et al. (2002) Reynolds number yielded better results than those based on the adapted Metzner-Reed Reynolds number.

The correlations and models developed and experimentally validated during this research can be used to further improve the design of rectangular, semi-circular, trapezoidal and triangular open channels to transport non-Newtonian fluids.

Dedication

To my children Johan, Dimitri and Zoe for the many, many family hours sacrificed.

Acknowledgements

I am very grateful to:

- My supervisors, Prof Rainer Haldenwang and Dr Neil J Alderman, for their guidance, motivation and patience.
- Dr Alta van der Merwe for her guidance on the complex issues of advanced mathematics encountered in verifying the models of Straub, et al. (1958) and Kozicki & Tiu (1967).
- The National Research Foundation and the Cape Peninsula University of Technology for funding the research.

Biographical Sketch

Johan obtained his H.N.D Mechanical engineering in 1984, his M.Dip. Mechanical Engineering in 1990 and his Government Certificate of Competency as a mechanical engineer in 1989.

Johan has been the external moderator for fluid-mechanics, turbo machines and hydraulic machines at final year degree level from 1993 to 2010. He has made meaningful contributions to the syllabus for hydraulic machines by being actively involved with lecturers in the School of Mechanical engineering (via the advisory committee between industry and this university) for many years. In addition, Johan was the deputy chairman of the advisory committee for a term. He was also involved with Dr Hannes Esterhuisen the person responsible for arguably formulating the best in-service training program in the country for engineering students. Further to the above university connections:

- Johan was a part of the team representing industry during the E.C.S.A inspection and certification for several years.
- He has been registered with E.C.S.A as a Pr. Tech Eng. since 1993.

On the industry side, Johan started his working career at the Caltex refinery as mechanical reliability engineer. In 1988, he joined Dresser Wayne as design and product development engineer. After success in the position, he was promoted to production manager in 1989 and then to operations manager the following year. During his years at Dresser Wayne, the turnover increased from R18.5 million to R65 million. Moreover, the company market share increased from 20% to 60%.

In 1994, he started his own manufacturing and engineering company. A few years later in 2003, he joined Colcab as production director where he put the necessary infrastructure in place to improve product quality and output, as well as to increase overall plant efficiency. Under his leadership the production output was increased by a four times magnitude and the turnover more than quadrupled.

In 2010, he was appointed managing director of Insulated Structures (a sister company to Colcab under the Universal Industries umbrella) to build an infrastructure, which included ensuring optimal product quality, increasing general productivity, optimising efficiency and increasing the business' overall profitability. When his tenure as managing director ended in 2013, the production output increased by 25% and the net profit on refrigerated cabinets manufactured increased by 290%. A major new corporate client was also acquired.

Johan is currently a consultant to the manufacturing and engineering industry.

Table of Contents

	Page
Declaration	i
Abstract	iii
Dedication	v
Acknowledgements.....	vii
Biographical Sketch	ix
Table of Contents.....	xi
List of Figures	xv
List of Tables	xix
List of Symbols	xxi
Terms, Concepts and Abbreviations	xxiii
Chapter 1 Introduction	1
1.1 Background and Motivation.....	1
1.2 Research Question	2
1.3 Aims, Objectives and Outcomes.....	2
1.4 Significance.....	3
1.5 Delineation	4
1.6 Methodology.....	4
1.7 Organisation of the Dissertation	5
Chapter 2 Literature and Theory	7
2.1 Newtonian Behaviour.....	7
2.2 Non-Newtonian Behaviour.....	8
2.2.1 Shear-thinning behaviour	9
2.2.2 Viscoplastic fluid behaviour.....	9
2.2.3 Flow curve model selection and parameter estimation.....	11
2.3 Open channel hydraulics	12
2.3.1 Determining the wall shear stress expression.....	13
2.3.2 Non-Newtonian sheet flow down an inclined plane	15
2.3.3 Flow of a power law fluid down an inclined plane	15
2.3.4 Laminar flow of a Herschel–Bulkley fluid down an inclined plane	16
2.3.5 Combined expression for the flow in non-circular cross sections of arbitrary shape	17
2.4 Effect of shape on Newtonian open channel flow	18
2.5 Effect of shape on non-Newtonian open channel flow.....	21
2.5.1 Laminar flow models	22
2.5.2 Turbulent flow models	28
2.6 Composite Power law friction factor vs. Reynolds number modelling	31
2.7 Summary	32

2.8	References.....	33
Chapter 3	Research method	37
3.1	Abstract	37
3.2	Introduction	37
3.3	Fundamentals.....	38
3.4	Research method	38
3.4.1	Data	39
3.5	Laminar flow.....	39
3.6	Laminar-turbulent transition.....	40
3.7	Turbulent flow.....	41
3.8	Conclusions	41
3.9	Notation	41
3.10	References.....	42
Chapter 4	Friction factor-Reynolds number relationship for laminar flow of non-Newtonian fluids in open channels of different cross-sectional shapes	51
4.1	Abstract	51
4.2	Introduction	51
4.3	Background	51
4.4	Materials and Methods	55
4.5	Results and Discussions.....	55
4.6	Conclusions	58
4.7	Acknowledgements.....	58
4.8	Notation	58
4.9	References.....	59
Chapter 5	Laminar and Turbulent Flow of non-Newtonian Fluids in Open Channels for Different Cross-sectional Shapes.....	73
5.1	Abstract	73
5.2	Introduction	73
5.3	Laminar flow.....	74
5.4	Turbulent flow.....	74
5.5	Literature and theory	75
5.5.1	Laminar flow models	75
5.5.2	Turbulent flow models	80
5.6	Experimental	83
5.6.1	Results and Discussion	84
5.7	Conclusions	86
5.8	Acknowledgements.....	86
5.9	Notation	86
5.10	References.....	88
Chapter 6	Laminar non-Newtonian open channel flow: Investigating velocity, wall shear stress and fluid	

depth	105
6.1 Introduction	105
6.2 Laminar non – Newtonian open channel flow	105
6.3 Experimental	108
6.4 Results	108
6.4.1 Comparison of actual and model velocities	109
6.4.2 Comparison of measured and model wall shear stresses	109
6.4.3 Flow depth sensitivity.....	110
6.5 Conclusions	110
6.6 References.....	111
Chapter 7 Power law and composite power law friction factor correlations for laminar and turbulent non-Newtonian open channel flow.....	121
7.1 Introduction	121
7.2 Dimensional Considerations.....	122
7.3 Experimental methods and materials	126
7.4 Results and Discussion	127
7.5 Conclusions	128
7.6 Acknowledgements.....	128
7.7 Notation	128
7.8 References.....	129
Chapter 8 Conclusions and recommendations	147
8.1 Conclusions	147
8.2 Recommendations	150
Appendices	151
Appendix A. Database for non-Newtonian flow in different channel shapes.....	151
Appendix B. Error propagation analysis.....	209
Appendix C. Fundamental derivations for non–Newtonian open channel flow.....	213
Appendix D. Experimental set-up.....	221

List of Figures

	Page
Figure 2.1	Schematic representation of one directional shearing flow..... 8
Figure 2.2	Newtonian and non-Newtonian behaviour 9
Figure 2.3.	Open channel flow 13
Figure 2.4	Equations for cross-sectional area and wetted perimeter for the four channel shapes used in this research. 15
Figure 2.5	Flow on an inclined plane. 15
Figure 2.6	Flow of a Herschel–Bulkley fluid on an inclined plane..... 16
Figure 2.7.	Slit flow. 17
Figure 2.8.	Friction factor vs. Reynolds number plots for smooth laminar flow in rectangular and triangular channels (Straub et al., 1958). The R used by Straub et al. (1958) is in fact Re. 19
Figure 2.9.	Friction factor vs. Reynolds number plots for smooth turbulent flow in rectangular and triangular channels Straub et al. (1958). The R used by Straub et al. (1958) is in fact Re. 20
Figure 3.1	Various flume shapes used in experiments for area and perimeter for channel shapes used in this research 44
Figure 3.2	Moody diagram with $f = 17.6/R_H$ for 7.1% kaolin suspension in 150 mm trapezoidal flume 45
Figure 3.3	Plots of (a) f versus R_H and (b) $f \times R_H$ versus R_H for laminar flow of three different non-Newtonian fluids in semi-circular flume at angles of 1° to 5° 46
Figure 3.4	Model comparison based on shear stress for laminar flow of 4.89% CMC solution in 300 mm triangular flume 46
Figure 3.5	Model comparison based on velocity for laminar flow of 4.89% CMC solution in 300 mm triangular flume 47
Figure 3.6	Model comparison based on shear stress for laminar flow of 5.4% kaolin suspension in 75 mm trapezoidal flume..... 47
Figure 3.7	Model comparison based on velocity for laminar flow of 5.4% kaolin suspension in 75 mm trapezoidal flume..... 48
Figure 3.8	Comparison of Herschel-Bulkley models for turbulent flow of 6% kaolin suspension ($\tau_y = 6.8 \text{ Pa}$, $K = 0.149 \text{ Pa s}^n$, $n = 0.52$) in 150 mm smooth rectangular flume 48
Figure 4.1	10 m flume rig..... 62
Figure 4.2	In-line pipe viscometer 62
Figure 4.3	Open channel shapes used in this study..... 63
Figure 4.4 A	f vs. Re_H plot for 4.6%, 6.2% bentonite, 3.1% CMC and 5.3%, 7.1% kaolin flowing in various cross sectional shape flumes at slope angles of 1 to 5 degrees. 64
Figure 4.5 A	f vs. Re_H plot for 10% kaolin in 150 mm rectangular flume with a best line fit of $f = 16.4/Re$ 64
Figure 4.6 A	f vs. Re_H plot for 6.2% bentonite in 150 mm semi-circular flume with a best line fit of $f = 16.2/Re$ 65
Figure 4.7 A	f vs. Re_H plot for 4.89% CMC in 300 mm triangular shape flume with a best line fit of

	$f = 14.6/Re$	65
Figure 4.8 A	f vs. Re_H plot for 7.1% kaolin in a 150 mm trapezoidal shape flume with a best line fit of $f = 17.6/Re$	66
Figure 4.9 A	f vs. Re_H plot for three different non-Newtonian fluids flowing in a rectangular flume at slope angles of 1 to 5 degrees.....	66
Figure 4.10	Measured $f \times Re_H$ versus Re_H corresponding to Figure 4.9.	67
Figure 4.11 A	f vs. Re_H plot for three different non-Newtonian fluids flowing in a semi-circular flume at slope angles of 1 to 5 degrees.	67
Figure 4.12	Measured $f \times Re_H$ versus Re_H plot corresponding to Figure 4.11.	68
Figure 4.13 A	f vs. Re_H plot for three different non-Newtonian fluids flowing in a triangular flume at slope angles of 1 to 5 degrees.....	68
Figure 4.14	Measured $f \times Re_H$ versus Re_H plot corresponding to Figure 4.13.	69
Figure 4.15	A f vs. Re_H plot for three different non-Newtonian fluids flowing in a trapezoidal flume at slope angles of 1 to 5 degrees	69
Figure 4.16	Measured $f \times Re_H$ versus Re_H plot corresponding to Figure 4.15.	70
Figure 4.17	A f vs. Re_H plot comparing the use of Re_H and Re^*P for 4% CMC in 150 mm semi-circular shaped flume at slope angles of 1 to 5 degrees	70
Figure 4.18	A f vs. Re_H plot comparing the use of Re_H and Re^*_B for 5.4% bentonite in 300 mm triangular shaped flume at slope angles of 1 to 5 degrees	71
Figure 5.1(a)	10 m rectangular tilting flume linked to (b) 3-tube in-line viscometers.....	90
Figure 5.2	Model comparison based on velocity of 3.1 and 4.9% CMC solution flowing in a 300 mm triangular shape channel.	91
Figure 5.3	Model comparison based on velocity of 3% and 4% CMC solution flowing in a 150 and 300 mm rectangular channel.....	91
Figure 5.4	Model comparison based on velocity of 3 and 4% CMC solution flowing in a 150 mm trapezoidal channel.	92
Figure 5.5	Model comparison based on velocity of 3 and 4% CMC solution flowing in a 150 mm and 300 mm semi-circular channel.....	92
Figure 5.6	Model comparison based on velocity of 4.86 and 5.38% bentonite suspension flowing in a 300 mm triangular shaped channel.....	93
Figure 5.7	Model comparison based on velocity of 4.6 and 6.2% bentonite suspension flowing in a 300 mm semi-circular channel.....	93
Figure 5.8	Model comparison based on velocity of 7.1 and 9% kaolin suspension flowing in a 150 and 300 mm rectangular channel.....	94
Figure 5.9	Model comparison based on velocity of 5.4 and 9% kaolin suspension flowing in a 75 and 150 mm trapezoidal channel.	94
Figure 5.10	Model velocity comparisons for turbulent flow of three different non-Newtonian fluids in a 150 mm trapezoidal open channel.	95
Figure 5.11	Model velocity comparisons for turbulent flow of three different non-Newtonian fluids in a 150 and 300 mm rectangular open channels.	95

Figure 5.12	Model velocity comparison for turbulent flow of three different non-Newtonian fluids in a 150 and 300 mm semi-circular open channels.	96
Figure 5.13	Model velocity comparison for turbulent flow of three different non-Newtonian fluids in a 300 mm triangular open channel.....	96
Figure 6.1	Various flume shapes used in this study.....	114
Figure 6.2 A	f vs. Re plot showing 647 data points for laminar flow of three different non-Newtonian fluids in a rectangular flume at slope angles of 1 to 5°	115
Figure 6.3 A	f vs. Re plot showing 485 data points for laminar flow of three different non-Newtonian fluids in a semi-circular flume at slope angles of 1 to 5°	115
Figure 6.4 A	f vs. Re plot showing 326 data points for laminar flow of three different non-Newtonian fluids flowing in a triangular flume at slope angles of 1 to 5°	116
Figure 6.5 A	f vs. Re plot showing 460 data points for laminar flow of three different non-Newtonian fluids flowing in a trapezoidal flume at slope angles of 1 to 5°	116
Figure 6.6	Velocity comparison for a typical power law fluid flowing in four different shaped channels.	117
Figure 6.7	Velocity comparison for a range of yield stress fluids flowing in four different shaped channels.	117
Figure 6.8	Wall shear stress comparison for a typical power law fluid flowing in four different shaped channels.	118
Figure 6.9	Wall shear stress comparison for a range of yield stress fluids flowing in four different shaped channels.	118
Figure 6.10	Initial flow depth versus volume concentration of three different non-Newtonian fluids flowing in four different shaped channels at slopes of 2° and 4°	119
Figure 6.11	Onset of transition flow depth versus volume concentration of three different non-Newtonian fluids flowing in four different shaped channels at slopes of 2° and 4°	119
Figure 6.12	Predicted versus measured flow depth at start and end of laminar flow for CMC solutions flowing in four different shaped channels.	120
Figure 6.13	Predicted versus measured flow depth at start and end of laminar flow for kaolin and bentonite suspensions flowing in four different shaped channels.	120
Figure 7.1	(a) 10 m rectangular tilting flume linked to (b) 3 in-line tube viscometers	132
Figure 7.2	f vs. Re relationship for rectangular flume using Re_H (all materials).....	133
Figure 7.3	f_{pred} vs. f_{exp} for rectangular flume using Re_H (all materials)	133
Figure 7.4	f vs. Re relationship for semi-circular flume using Re_H (all materials)	134
Figure 7.5	f_{pred} vs. f_{exp} for semi-circular flume using Re_H (all materials)	134
Figure 7.6	f vs. Re relationship for trapezoidal flume using Re_H (all materials)	135
Figure 7.7	f_{pred} vs. f_{exp} for trapezoidal flume using Re_H (all materials).....	135
Figure 7.8	f vs. Re relationship for triangular flume using Re_H (all materials).....	136
Figure 7.9	f_{pred} vs. f_{exp} for triangular flume using Re_H (all materials)	136
Figure 7.10	f vs. Re relationship for rectangular flume using Re_{MR} (all materials).....	137
Figure 7.11	f_{pred} vs. f_{exp} for rectangular flume using Re_{MR} (all materials)	137
Figure 7.12	f vs. Re relationship for semi-circular flume using Re_{MR} (all materials).....	138
Figure 7.13	f_{pred} vs. f_{exp} for semi-circular flume using Re_{MR} (all materials)	138

Figure 7.14	f vs. Re relationship for trapezoidal flume using Re_{MR} (all materials)	139
Figure 7.15	f_{pred} vs. f_{exp} for trapezoidal flume using Re_{MR} (all materials)	139
Figure 7.16	f vs. Re relationship for triangular flume using Re_{MR} (all materials)	140
Figure 7.17	f_{pred} vs. f_{exp} for triangular flume using Re_{MR} (all materials)	140
Figure 7.18	f vs. Re relationship for rectangular flume using Re_H (Coussot and Naik data)	141
Figure 7.19	f_{pred} vs. f_{exp} for rectangular flume using Re_H (Coussot and Naik data)	141

List of Tables

	Page
Table 2.1 Flow curve models.....	12
Table 2.2 Values of a and b for open semi-circular channels, numerically obtained by Sestak (1974).	26
Table 3.1 Materials tested	49
Table 3.2 Flume data for flow of 7.1% kaolin suspension in a 150 mm trapezoidal flume.....	50
Table 4.1 Summary of materials used	61
Table 5.1 Open channel shapes used in this study	97
Table 5.2 Summary of non-Newtonian, laminar flow models for open channels.....	98
Table 5.3 Turbulent Constants a and b used in the modified Blasius equation.....	99
Table 5.4 Summary of non-Newtonian, turbulent flow models for open channels	100
Table 5.5 Summary of test materials	101
Table 5.6 Log square error values for laminar model velocities compared with measured velocities for models tested.	102
Table 5.7 Turbulent velocity model comparison for the flow of bentonite, CMC and kaolin in channel shapes tested based on log squared error (LSE) and correlation coefficient (R^2).....	103
Table 7.1 Open channel shapes used in this study.	142
Table 7.2 Summary of materials used.....	143
Table 7.3 K-values of different shape channels (Burger et al., 2010)	143
Table 7.4 Modified Blasius c and d values for different shape channels (Burger et al., 2014)	144
Table 7.5 Parameters in composite power law correlation for each shape, (based on Re_H)	144
Table 7.6 Parameters in composite power law correlation for each shape, (based on Re_{MR})	144
Table 7.7 Statistical ranking of different friction factor vs. Re correlations.....	144
Table 7.8 Percentage of f_{pred} values differing by more than $\pm 30\%$ from f_{exp} values.....	145

List of Symbols

Symbol	Description	Units
A	cross-sectional area of flow	m^2
A_r	area ratio Eq. (2.63)	-
a	shape factor constant, Eq. (2.35)	-
a	shape factor constant, Eq. (5.6)	-
a	channel shape factor constant for laminar flow, Eq. (2.73)	-
B	channel width	m
b	shape factor constant, Eq. (2.35)	-
b	shape factor constant, Eq. (5.6)	-
b	power law exponent taken as -1, Eq. (2.73)	-
c	"Blasius" power law constant for turbulent flow, Eq. (2.74)	-
D	pipe diameter	m
d	"Blasius" power law exponent for turbulent flow, Eq. (2.74)	-
d_x	representative particle size of the solid particles	μm
e	composite power law friction factor exponent, Eq. (2.72)	-
F_1	laminar flow power law friction factor	-
F_2	turbulent flow power law friction factor	-
f	composite power law friction factor exponent, Eq. (2.72)	-
f	Fanning friction factor	-
f_{mB}	modified Blasius friction factor, Eq. (5.6)	-
f_{pred}	predicted Fanning friction factor based on Eq. (7.8)	-
f_{exp}	experimental Fanning friction factor, Eq. (7.8)	-
$f_{exp(ave)}$	averaged experimental Fanning friction factor, Eq. (7.8)	-
g	acceleration due to gravity	m/s^2
HB	Herschel-Bulkley number	-
h	flow depth	m
k	laminar flow constant in the f vs. Re relationship, Eq. (3.1)	-
K	consistency coefficient	$Pa \cdot s^n$
k^*	consistency coefficient as defined by Eq. (2.40)	$Pa \cdot s^n$
k'	apparent consistency coefficient, Eq. (7.4)	$Pa \cdot s$
N	number of points, Eq. (7.9)	-
n	flow behaviour index	-
n'	apparent Power law index, Eq. (7.3)	-
n^*	flow behaviour index as defined by Eq. (2.39)	-
$n_{Manning}$	Manning constant	$m^{1/3}/s$
P	wetted perimeter	m
R^2	correlation coefficient	-

Symbol	Description	Units
Re	Reynolds number	-
Re*	generalised Reynolds number, Eq. (2.38)	-
Re* _B	Kozicki and Tiu Bingham Reynolds number, Eq. (2.44)	-
Re* _P	Kozicki and Tiu power law Reynolds number, Eq. (2.41)	-
Re _H	Haldenwang et al Reynolds number, Eq. (2.59)	-
Re _{MR}	Metzner-Reed Reynolds number adapted for open channel flow, Eq.(7.2b)	-
Re _r	roughness Reynolds number, Eq. (2.71)	-
R _h	hydraulic radius	m
t	composite power law friction factor exponent, Eq. (2.72)	-
V	average velocity	m/s
V*	shear velocity, Eq. (2.65)	m/s
V _N	Newtonian mean velocity, Eq. (2.64)	m/s
W	channel width	m
α	Coussot shape factor, Eqs. (2.56) & (2.57)	-
γ̇	shear rate, Eq. (2.1)	s ⁻¹
λ	flow width to depth ratio, Eq. (2.52)	-
μ _{a(500)}	apparent viscosity at shear rate of 500 s ⁻¹	Pa.s
μ	dynamic viscosity, Eq.(2.1)	Pa.s
μ _B	Bingham plastic viscosity	Pa.s
μ _e	equivalent viscosity	Pa.s
μ _N	Newtonian viscosity	Pa.s
ξ	ratio of wall shear stress to Bingham yield stress Eq. (7.5)	
φ'	defined by Eq. (2.51)	-
ρ	density	kg/m ³
τ ₀ ^H	yield stress (notation used in appendix C)	Pa
τ _w	wall shear stress	Pa
τ _Y	yield stress	Pa
τ _{yB}	Bingham yield stress	Pa
τ _{yHB}	Herschel-Bulkley yield stress	Pa
θ	channel angle from the horizontal	degrees
X	ratio of Bingham yield stress to wall shear stress Eq.(2.44)	-
Ω	blunting effect of velocity profile, Eq. (2.66)	-

Terms, Concepts and Abbreviations

Bingham plastic behaviour:	This is observed when a non-zero shear stress is required to initiate significant flow and there is a linear relationship between the shear stress in excess of the yield stress, τ_y and the resulting shear rate.
CFD:	Computational fluid dynamics.
Flume:	Artificial open channel carrying fluids, slurries or tailings.
FPRC:	Flow Process and Rheology Centre (Cape Peninsula University of Technology)
Laminar flow:	Occurs when the viscous forces dominate over the inertial forces causing the particles to move in smooth paths or streamlines.
Launders:	In the mining industry, short flumes with steeper slopes are often called launders.
LSE:	Log square error.
Newtonian fluid:	Any incompressible fluid exhibiting behaviour where the shear stress is directly proportional to the shear rate.
Non-Newtonian fluid:	Any deviation from Newtonian behaviour is said to be non-Newtonian. This is when the flow curve (shear stress versus shear rate) becomes non-linear or does not pass through the origin.
Open channel:	Conduit for transporting liquids with a free surface open to atmosphere. A channel may be artificial or natural.
Reynolds number:	Defined as the ratio between viscous and inertial forces.
Rheology:	The science of flow behaviour.
Shear-thinning behaviour:	This is characterised by the viscosity decreasing non-linearly with increasing shear rate.
Transition region:	This is the region between the laminar and the turbulent regions.
Turbulent flow:	Occurs when the inertial forces dominate over the viscous forces causing the particles to move in irregular paths.
UVP:	Ultrasound velocity profiling.
Viscoplastic behaviour:	This is observed when a non-zero shear stress is required to initiate significant flow and the rate of increase in shear stress with shear rate in excess of the yield stress, τ_y decreases with increasing shear rate.

Chapter 1 Introduction

The flow of water in open channels has been well researched. The same cannot be said of the flow of homogeneous non-Newtonian slurries in open channels, and the fact that many of these open channels are designed without a properly researched and validated design makes this a research topic that requires urgent attention (Haldenwang, 2003). Datasets were published for non-Newtonian flow in rectangular open channels by Coussot (1994), Naik (1983), Haldenwang (2003), and Haldenwang & Slatter (2006) and Fitton (2007,2008) for non-Newtonian flow in semi-circular open channels. No data has been published for non-Newtonian flow in channels of other cross-sectional shapes.

1.1 Background and Motivation

The effect of channel shape on laminar flow of Newtonian and non-Newtonian fluids in open channels is of interest for a variety of industrial applications. Rectangular, semi-circular and trapezoidal cross-sectional channels are often encountered in the mining industry where tailings are transported from the mine to the disposal site (Haldenwang and Slatter, 2006). The flow of Non-Newtonian fluids in channels of different cross-sections also occurs in the wastewater and food processing industries (Fitton, 2008).

Flow of water in a variety of open channels has been investigated by several researchers (Straub et al. 1958 and Chow, 1959). Straub et al. (1958) presented a theory for laminar flow of Newtonian fluids in open channels of different cross-sectional shapes and they also supplied experimental data for the flow of water and kerosene.

They showed that the data in the laminar flow regime can be defined by a general relationship $f = K/Re$ where f is the Fanning friction factor and Re is the Newtonian Reynolds number and that K is “a purely numerical coefficient dependent on the channel shape” (Straub et al. 1958).

Analytical and numerical solutions for K were provided for rectangular, semi-circular, elliptical, 60° , 90° and 120° triangular and trapezoidal channels. Straub et al. (1958) found that the predicted f vs. Re line for smooth-walled, rectangular, triangular and semi-circular-shaped channels to be coincident with the experimental data when plotted as an f vs. Re plot. For rectangular channels where the water height to channel width (h/W) ratios ranged from 0.08 to 0.37, K was found to vary from 19.75 to 15.25. These values compared well with the corresponding analytical values of 21.5 to 16.25. For triangular channels where the vertex angle ranged from 30° to 150° , K was found to be 14.25 and independent of the vertex angle. This is in excellent agreement with the analytical value of 14.23 for the 90° triangular channel and the numerical value of 14.15 for the other triangular channels. For semi-circular channels, the f vs. Re plot showed the data to be “grouped” about the $f = K/Re$ line where K was found analytically to be 16.

In his authoritative book on open channel flow, Chow (1959) produced a friction factor vs. Reynolds number plot for flow of water in smooth-walled, rectangular and triangular channels based on the two datasets of Straub et al. (1958). Here, K was found to be approximately 24 for the rectangular channels and 14 for the triangular channels.

Very little has been reported in the literature for predicting non-Newtonian laminar flow in open channels of arbitrary cross-section. The only method available was that proposed by Kozicki and Tiu (1967; 1986). The shape factors used by Kozicki and Tiu (1967; 1986) were those evaluated from analytical solutions for flow of Newtonian fluids in the open channel of the same cross-section (Chhabra and Richardson, 2008). No experimental work was carried out by Kozicki and Tiu (1967; 1986) to validate their model.

Coussot (1994) provided some data for the flow of a Herschel-Bulkley fluid in rectangular and trapezoidal channels. Fitton (2007; 2008) obtained data for flow of three different non-Newtonian fluids (carboxymethyl cellulose, carbopol and thickened tailings) in semi-circular channels. Naik (1983) provided some data for turbulent flow of a Bingham fluid in a rectangular channel.

Haldenwang (2003) and Haldenwang & Slatter (2006) provided an extensive database for non-Newtonian flow in rectangular open channels. In this study, the database developed by Haldenwang (2003) for rectangular channels was extended to include non-Newtonian flow in semi-circular, trapezoidal and triangular channels. Using the Haldenwang et al. (2002) definition of Re , the effect of shape on the f vs. Re relationship for laminar, open channel flow of non-Newtonian fluids was investigated in some depth.

In this research a check was also made on the validity of the pipe flow paradigm of $f = 16/Re$ used by Haldenwang et al. (2002), Haldenwang (2003) and Haldenwang et al. (2004) for open rectangular channels to other shaped channels. During this research an investigation was also made on the effect of shape on the friction factor-Reynolds number relationship for turbulent non-Newtonian flow in rectangular, trapezoidal, semi-circular and triangular open channels. The application of the composite power law modelling procedure covering laminar, transitional and turbulent regimes for pipe flow used by Garcia et al. (2003) to open channel flow in various cross-sections was investigated.

1.2 Research Question

Does the channel cross-sectional shape have an effect on non-Newtonian flow in open channels?

1.3 Aims, Objectives and Outcomes

The aims of this research work were to:

- Determine the effect of channel shape on laminar and turbulent flow of non-Newtonian fluids in open channels of various cross sectional shapes.
- Provide a significant experimental database for the flow of three different homogeneous non-Newtonian fluids in four different shaped open channels. The test fluids to be used were various concentrations of carboxymethyl cellulose (CMC) solutions that exhibit shear-thinning behaviour, bentonite suspensions that show Bingham plastic behaviour and kaolin suspensions that are

characterised by yield-shear thinning behaviour. The channel shapes to be studied were rectangular, semi-circular, triangular and trapezoidal.

- Put forward new models for the prediction of laminar and turbulent non-Newtonian flow in open channels using average velocity as a criteria and comparing the new models with three previous published laminar models and five previously published turbulent models.
- Determine the composite power law friction factor correlations for laminar and turbulent non-Newtonian open channel flow.

The following outcomes are contributions by the candidate to scientific knowledge and future research during his doctoral candidacy:

Peer Reviewed Publications

- Burger, J.H., Haldenwang, R. and Alderman, N.J. 2010. Friction factor-Reynolds number relationship for laminar flow of non-Newtonian fluids in open channels of different cross-sectional shapes. *Chem. Eng. Sci.*, **65**: 3549-3556.
- Burger, J.H. Haldenwang, R. and Alderman, N.J. (2010), Experimental database for non-Newtonian flow in four channel shapes. *Journal of Hydraulic Research*, 48(3): 363–370.
- Burger, J.H., Haldenwang, R. and Alderman, N.J. (2010). Laminar non-Newtonian open channel flow: Investigating velocity, wall shear stress and fluid depth. *18th International Conference on Hydrotransport*, 22-24 September, Rio de Janeiro, Brazil, 193- 207.
- Burger, J.H., Haldenwang, R., Chhabra, R.P. and Alderman, N.J. (2014). Power law and composite power law friction factor correlations for laminar and turbulent non-Newtonian open channel flow. *J. Braz. Soc. Mech. Sci. Eng.* DOI 10.1007/S40430-014-0188-1

Manuscripts Submitted for Publication and still under review.

- Burger, J.H., Haldenwang, R. and Alderman, N.J. (2014). Laminar and turbulent flow of non-Newtonian fluids in open channels for different cross-sectional shapes. (*ASCE Journal of Hydraulic Engineering*).

Peer Reviewed conference presentation

- Laminar non-Newtonian open channel flow: Investigating velocity, wall shear stress and fluid depth. *18th International Conference on Hydrotransport*, 22-24 September 2010, Rio de Janeiro, Brazil.

1.4 Significance

The effect of channel cross-sectional shape on non-Newtonian open channel flow design has not yet been fully investigated. This research offers a significant database from which valuable observations were made which in turn resulted in finding appropriate friction factor–Reynolds number relationships for laminar and turbulent non-

Newtonian flow in open channels of different shapes. New laminar and turbulent velocity models as well as a double power-law model spanning both the laminar and turbulent flow regimes were derived to improve open channel flow design.

1.5 Delineation

This research was limited to determining the effect of shape on laminar and turbulent flow of carboxymethyl cellulose (CMC) solutions, bentonite and kaolin suspensions in rectangular, trapezoidal with 60° sides, triangular with a vertex angle of 90° and semi-circular open channels at inclination angles of 1 to 5 degrees. Since the tests were only conducted in smooth walled open channels, the issue of rough-walled channels was not addressed. The materials tested were treated as pseudo-homogeneous, non-Newtonian fluids showing no or very little time-dependant effects.

1.6 Methodology

Flume tests were carried out in a 10 m long, rectangular flume designed and built at the Flow Process Research Centre at the Cape Peninsula University of Technology, Cape Town, South Africa. This flume can be tilted up to 5° from the horizontal. By placing a partition insert, the flume width was changed from 300 mm to 150 mm. By inserting appropriate cross-sectional inserts, the rectangular flume can be changed into that of a triangular, semi-circular or trapezoidal cross-section. The flow, provided by a Power 100 mm progressive cavity, positive displacement pump and a Warman 4x3 centrifugal slurry pump, was controlled by variable speed drives and monitored by an electromagnetic flow meter. The maximum discharge capacity from the flume was 45 l/s. Flow depths were measured using digital depth gauges of $\pm 5\%$ accuracy fitted at the 5 m and 6 m positions from the flume entrance. These two positions were found to be optimum for depth measurement (Haldenwang, 2003). Since the difference in fluid height between these two positions was found to be minimal, the flow in the region can therefore be taken as steady.

A data logger was used to record the various outputs as a function of time. All data were then fed to a PC so that a Moody chart resulted as output. A Moody chart is a graphical representation of the friction factor-Reynolds number relationship where the friction factor values are recorded on the vertical axis and the Reynolds number values on the horizontal axis. For each of the cross sectional shapes, datasets were collected for each test material at various concentrations, slopes and flow rates. Flow curve measurements of the test material were also made in-situ using an inline tube viscometer fitted with three tubes of inner diameters 13, 28 and 80 mm. Each tube was fitted with a Krohne electromagnetic flow meter and two differential pressure transducers of high (0-30 kPa) and low measuring ranges (0-4 kPa) that were used to obtain the pressure drop across a fixed tube length. From these measurements, the wall shear stress τ_w and the nominal wall shear rate $8V/D$ were calculated. Error propagation analysis of measured variables and derived variables indicated errors of 0.5% and 0.6% in τ_w and $8V/D$, respectively. The τ_w vs. $8V/D$ dataset were then transformed by the Rabinowitsch-Mooney method to obtain the flow curve (Holland & Bragg, 1995). Since three different tube diameters over a fixed tube length were used, a check for the presence of wall slip was made. If all the flow curves obtained for the three tube diameters collapsed onto a single curve, this

indicated non-presence of wall slip. When the flow curves do not coincide, the slip velocity must be calculated for each tube and deducted from the measured mean velocity (Haldenwang, 2002).

Various model fits were then made to the flow curve data whilst ensuring the shear stress range used for the model fit was similar to that covered by the flume. It was found that the 1.5 to 5.3 % vol carboxymethyl cellulose solutions, 3.5 to 6.8 % vol. bentonite in water suspensions and 3.4 to 9.2% vol kaolin in water suspensions were best represented by the power law, Bingham plastic and Herschel-Bulkley models, respectively. The correlation coefficient was used as a criterion for determining the best model fit.

1.7 Organisation of the Dissertation

The overall aim of this work was to determine the effect of cross sectional shape of non-Newtonian flow in open channels. The thesis is written in article format. The Harvard style was used. The materials, methods and shapes for each part of the study are explained in the relevant chapters. The comprehensive database for the flow of non-Newtonian fluid in four different open channel shapes can be found in Appendix A, the error propagation analysis calculator used during this research in Appendix B, fundamental derivations on open channel flow in Appendix C and experimental setup in Appendix D.

The thesis is subdivided into the following chapters:

Chapter 1 serves as an overall introduction, providing the background and motivation for this study, the overall objectives and the delineation of the research that was done.

Chapter 2 contains the literature review on the effect of channel shape on the friction factor-Reynolds number relationship for laminar and turbulent, open channel flow of non-Newtonian fluids. Here, friction factor models were investigated as well as the various published laminar and turbulent velocity models.

Chapter 3 is the first of five results chapters. This chapter covers the research methodology, the materials used and the need that led to a comprehensive experimental database for non-Newtonian flow in four channel shapes to being compiled and published.

Chapter 4, the second results paper, presents the friction factor-Reynolds number relationship for laminar flow of non-Newtonian fluids in open channels of different cross-sectional shapes. Unique K shape factor constants in the $f = K/Re$ relationship for each different channel shape tested are developed.

Chapter 5, the third results paper, deals with the three previously published laminar and the five previously published turbulent flow velocity models which are compared to the new models. The successes of the new proposed models are discussed.

Chapter 6, the fourth results paper, discusses the average velocity, the wall shear stress and the fluid flow depth on non-Newtonian flow in open channels. This peer reviewed paper was presented at the *18th International Conference on Hydro transport*, 22-24 September 2010, Rio de Janeiro, Brazil.

Chapter 7, the fifth results paper, presents a new composite power law relationship spanning both laminar and turbulent flow in open channels by utilising data from the comprehensive database compiled during this research. This new composite power law relationship is independently verified by data published in laminar flow by Coussot (1994) and in turbulent flow by Naik (1983).

Chapter 8 presents the overall conclusions and recommendations.

Appendix A gives the comprehensive database of non-Newtonian flow in open channels of four different cross sectional shapes that was compiled during this research.

Appendix B describes the derivations behind the error propagation analysis calculator used for the second results paper.

Appendix C gives the fundamental derivations for non-Newtonian open channel flow.

Appendix D provides additional information to describe the experimental setup and procedures used, covering detail not published in the papers.

Chapter 2 Literature and Theory

Open channels, flumes or launders are used in the mining industry to transport non-Newtonian slurries during processing and to disposal sites. The usage of water for open channel flow has become critical in many countries due to its availability and the water management program used in that country. Open channels are also used in a variety of other industrial applications (Haldenwang, 2002). Two factors that are important in designing these flumes are the flow behaviour of materials transported and the design considerations of the flume. The material considerations deal with the development of non-Newtonian behaviour with increasing slurry concentration because of the need to reduce water consumption. The design considerations are concerned about the influence of the shape cross-section and the slope upon channel flow.

The effect of cross sectional shape on non-Newtonian open channel flow design has not been fully investigated and understood. Although datasets are available for non-Newtonian flow in rectangular open channels Coussot (1994), Haldenwang (2003) and Haldenwang & Slatter (2006) and in semi-circular open channels Fitton (2007; 2008), there were none available for non-Newtonian flow in other cross-sectional shaped channels. Guang et al. (2011) performed direct numerical simulations of turbulent flow of a yield shear-thinning fluid in a semi-circular channel. They compared their simulations with actual field measurements and found them to over predict the flow velocity by approximately 40%. They were unable to explain the source for this discrepancy.

In this review the following topics will be covered:

- Newtonian behaviour;
- Non-Newtonian behaviour;
- Rheological models;
- Open channel hydraulics;
- Effect of shape on Newtonian channel flow;
- Effect of shape on non-Newtonian open channel flow;
- Composite power law friction factor vs. Reynolds number modelling.

Before the literature on the effect of cross-sectional shape on non-Newtonian open channel flow, is reviewed, an understanding of the rheological behaviour of the test fluids to be used is required.

2.1 Newtonian Behaviour

Consider a thin layer of a fluid contained between two parallel planes of surface area A at a distance, dy apart as shown in Figure 2.1. Now, if under steady state conditions, the fluid is subjected to a shear by the application of a force, F in the direction of x as shown Figure 2.1. This will be balanced by an equal and opposite internal frictional force in the fluid. For an incompressible Newtonian fluid in laminar flow, the resulting shear stress is equal to the product of the shear rate and the viscosity of the fluid medium. The

shear rate may be expressed as the velocity gradient in the direction perpendicular to that of the shear force Chhabra and Richardson (2008), giving:

$$\frac{F}{A} = \tau_{yx} = \mu \left(\frac{dV_x}{dy} \right) = \mu \dot{\gamma}_{yx} \quad (2.1)$$

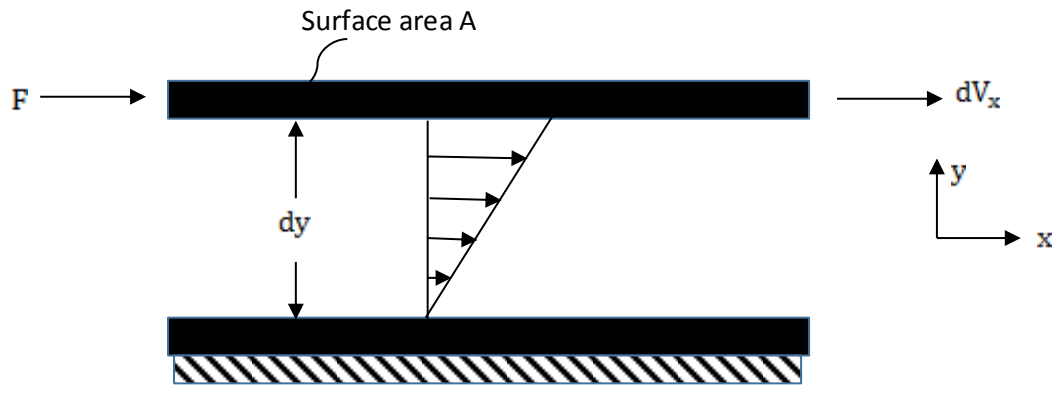


Figure 2.1 Schematic representation of one directional shearing flow

Note that the first subscript on both τ and $\dot{\gamma}$ indicates the direction normal to that of the shearing surface, whilst the second subscript refers to the direction of the force and the flow. The plot of shear stress against shear rate i.e. the flow curve, for a Newtonian fluid is therefore a straight line of slope, μ passing through the origin. The single constant, μ completely characterises the flow behaviour of a Newtonian fluid at a fixed temperature and pressure (Chhabra and Richardson, 2008).

2.2 Non-Newtonian Behaviour

Any deviation from Newtonian behaviour is said to be non-Newtonian. This is when the flow curve becomes non-linear or does not pass through the origin.

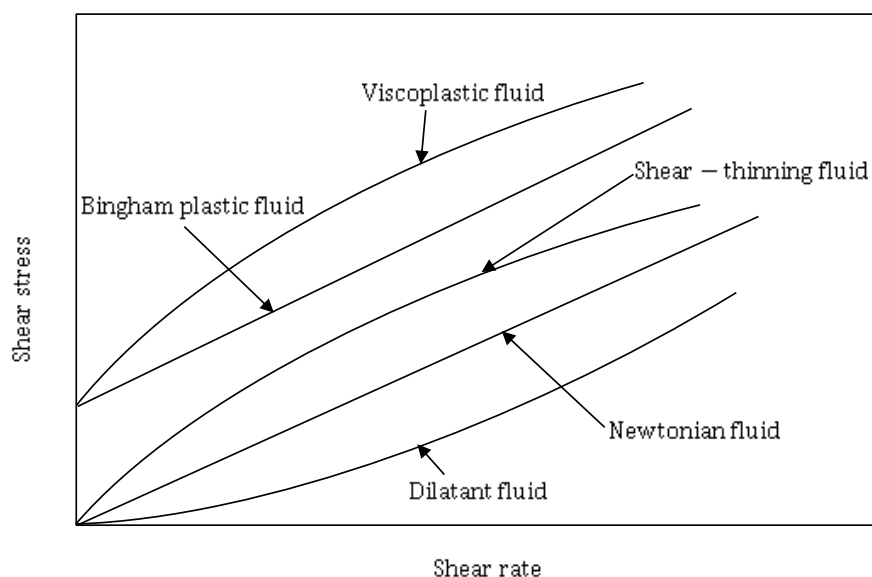


Figure 2.2 Newtonian and non-Newtonian behaviour

Flow curve models used to rheologically characterise the fluids used in this thesis are the power law, Bingham plastic and Herschel-Bulkley models. Aqueous solutions of carboxymethyl cellulose ranging from 1.5% to 5.3% v/v exhibited shear-thinning behaviour which was well-described by the power law model. 3.5% to 6.8% v/v suspensions of bentonite in water exhibited Bingham plastic behaviour whereas 3.4% to 9.2% v/v suspensions of kaolin in water gave viscoplastic behavior that was well-described by the Herschel-Bulkley model. None of these fluids exhibited any significant time dependency.

2.2.1 Shear-thinning behaviour

These fluids are characterised by the viscosity (i.e. the ratio of shear stress to shear rate) decreasing non-linearly with increasing shear rate. The model used to describe this behaviour is the power law model given by:

$$\tau_{yx} = k \dot{\gamma}_{yx}^n \quad (2.2)$$

The empirical curve-fitting parameters k and n are the fluid consistency coefficient and the flow behaviour index respectively. It should be noted that if $n < 1$ in Eq. (2.2), the fluid will exhibit shear-thinning behaviour whereas if $n > 1$, the fluid will exhibit shear-thickening or dilatant behaviour. If $n = 1$, the equation reverts back to the Newtonian model given by Eq. (2.1) with $k = \mu$.

2.2.2 Viscoplastic fluid behaviour

This type of fluid behaviour is characterised by the presence of a yield stress which must be exceeded before the fluid will deform or flow. If the externally applied stress is smaller than the yield stress, the material will deform elastically (or flow in mass like a rigid body). This type of behaviour will give a

viscosity (i.e. the ratio of shear stress to shear rate) decrease with increasing shear rate once the yield stress has been exceeded.

The simplest model describing the viscoplastic behaviour of a fluid is the Bingham plastic model given by

$$\begin{aligned}\tau_{yx} &= \tau_{yB} + \mu_B \dot{\gamma}_{yx} \quad \text{for } \tau_{yx} > \tau_{yB} \\ \dot{\gamma}_{yx} &= 0 \quad \text{for } \tau_{yx} < \tau_{yB}\end{aligned}\tag{2.3}$$

where τ_{yB} and μ_B are the curve fitting constants which are known as Bingham yield stress and plastic viscosity respectively.

Here, the flow curve will give a straight line of slope μ_B once the yield stress given by the intercept τ_w has been exceeded.

A simple generalisation of the Bingham plastic model to embrace the non-linear flow curve when $\tau_{yx} > \tau_{yield}$ is the three-constant Herschel-Bulkley model given by

$$\begin{aligned}\tau_{yx} &= \tau_{yHB} + k \dot{\gamma}_{yx}^n \quad \text{for } \tau_{yx} > \tau_{yHB} \\ \dot{\gamma}_{yx} &= 0 \quad \text{for } \tau_{yx} < \tau_{yHB}\end{aligned}\tag{2.4}$$

With three curve-fitting parameters, this model may provide a better fit to the flow curve data than that with the Bingham Plastic model. The three curve-fitting constants τ_{yHB} , k and n are known as the Herschel-Bulkley yield stress, consistency coefficient and power law exponent respectively. This power law exponent will be different from the one used in the power law model.

It should be noted that this model can be reduced to three simpler models- the power law model, the Bingham plastic model and the Newtonian model.

If $\tau_{yHB} = 0$, Eq. (2.4) reverts to the power law model given by Eq. (2.2).

If $n = 1$, Eq. (2.4) becomes the Bingham plastic model given by Eq. (2.3).

If $n = 1$, and $\tau_{yHB} = 0$, Eq (2.4) describes the Newtonian model given by Eq. (2.1) with $k = \mu$.

There are other higher order models such as the Cross model which is appropriate to use at very high and very low shear rates and the Ellis model equation for low shear rates when there are significant deviations from the power law model. However, for pipe and open channel flow, the shear rate range of interest is between 1 and 1000 s^{-1} where Newtonian, power law, Bingham plastic and Herschel-Bulkley models are just as competent in describing the flow curve as the higher-order models (Heywood & Alderman, 2004 and Chhabra & Richardson, 2008).

2.2.3 Flow curve model selection and parameter estimation

The following procedure for flow curve model selection is presented; it is an extract from the paper presented by Alderman and Heywood (2004). It is not always obvious from the data which of the flow models presented in Table 2.1 should be used for design. Also it is customary to use τ rather than use τ_{yx} .

The following procedure is recommended:

1. Plot all the $(\tau, \dot{\gamma})$ data on linear axes and double logarithmic axes, separately. This is done to assess the suitability of the Newtonian, Bingham plastic and power-law models.
2. If there is considerable scatter in the data, decide by eye or from the correlation coefficient obtained by linear regression analysis whether a straight line through the linear or the log-log plot gives the better representation. Similarly, decide for the upper-bound curve. If one of these alternatives is acceptable, the use of the Herschel-Bulkley model is probably not warranted.
3. If neither of the above alternatives appears satisfactory because there is significant curvature of the data on both linear and log-log plots, then the following situations can arise.
 - If there is data curvature on the log-log plot, with the slope of the curve increasing with $\dot{\gamma}$, and in addition, if the linear plot does not produce a straight line, then the Herschel-Bulkley should adequately describe the data.
 - If there is data curvature on the log-log plot and the slope of the curve decreases with $\dot{\gamma}$, then the use of the Herschel-Bulkley model is inappropriate, as this implies a negative τ parameter. However, a curve fit is often possible and would result in a negative τ parameter. Either force-fit the Bingham plastic model or power law model to the data.

The parameters defined in the flow models given in Table 2.1 must be estimated. Since the Herschel-Bulkley model can be reduced to the Newtonian, power-law and Bingham plastic models, one can perform a least-squares regression analysis on the $(\tau, \dot{\gamma})$ data to obtain τ_{yHB} , k and n . It may then be possible to simplify the model by setting τ_{yHB} to zero if the estimate is close to zero and/or setting n to 1 if the estimate is close to unity.

Table 2.1 Flow curve models.

Flow curve description	Flow curve model
Newtonian	Newtonian model: $\tau = \mu_N \dot{\gamma}$
Shear-thinning or pseudoplastic	Power law model: ($n < 1$) $\tau = k \dot{\gamma}^n$
Shear-thickening or dilatant	Power law model: ($n > 1$) $\tau = k \dot{\gamma}^n$
Bingham plastic	Bingham plastic model: $\tau = \tau_{yB} + \mu_B \dot{\gamma}$
Viscoplastic	Generalised Bingham plastic or Herschel-Bulkley model $\tau = \tau_{yHB} + k \dot{\gamma}^n$

Two commonly used regression methods for fitting $(\tau, \dot{\gamma})$ data to the Herschel-Bulkley model are the non-linear least squares regression on unweighted data and the non-linear least squares regression on weighted data. In the first method it is assumed that the error, E lies in τ :

$$\tau = \tau_{yHB} + k \dot{\gamma}^m + E \quad (2.5)$$

where as in the second method, the error is assumed to lie in $\ln(\tau - \tau_{yHB})$:

$$\ln(\tau - \tau_{yHB}) = \ln k + m \ln \dot{\gamma} + E \quad (2.6)$$

Note m is used here instead of n as m in the Herschel-Bulkley model is not the same as n for the power law model.

Standard non-linear regression software packages can be used in either case. Both methods provide estimates of τ_{yHB} , k and n , which will predict viscometric data to within $\pm 2\%$ of the original data within the original $\dot{\gamma}$ range. Outside this $\dot{\gamma}$ range, the agreement can be poor (Brown and Heywood, 1991). Non-linear regression can also be performed using Microsoft Excel using the "Solver" tool (Roberts et al. 2001).

2.3 Open channel hydraulics

In this section the following topics will be covered:

- Wall shear stress expression;
- Non-Newtonian sheet flow down an inclined plain;
- The flow of a power law fluid down an inclined plane;
- The laminar flow of a Herschel–Bulkley fluid down an inclined plane;
- Combined expression for the flow in non-circular cross sections of arbitrary shape.

2.3.1 Determining the wall shear stress expression

The wall shear stress of a liquid in steady flow in an open channel of uniform cross section under the influence of gravity is determined by analysing the diagram shown in Figure 2.3.

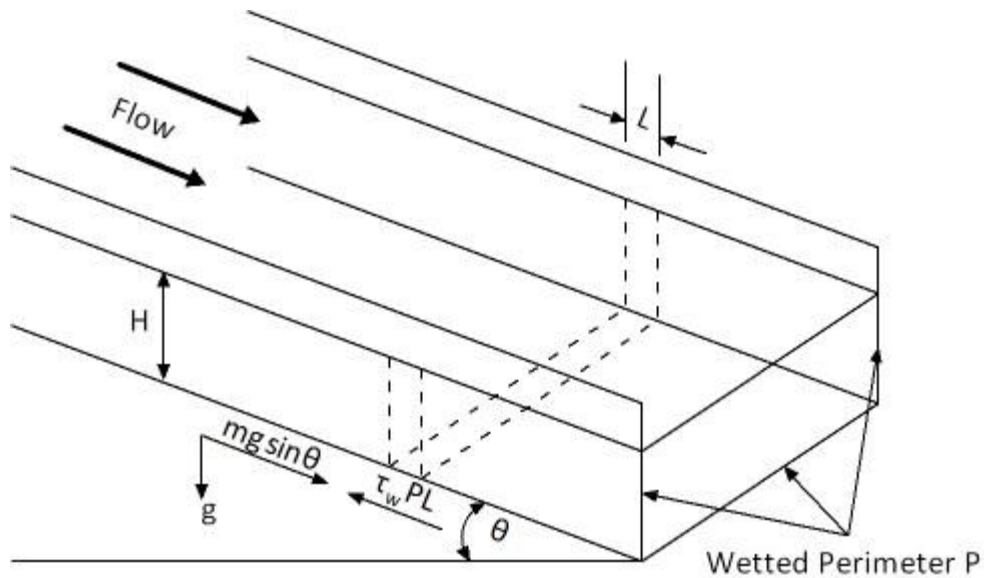


Figure 2.3. Open channel flow

A force balance between the downwards force, $mg \sin \theta$ causing flow parallel to the plane and the force opposing the flow is the wall shear stress τ_w times the area which gives

$$mg \sin \theta = \tau_w \cdot PL, \quad (2.7)$$

where m is the mass of fluid, θ is the angle of inclination of the channel to the horizontal plane, τ_w is the wall shear stress, P is the wetted perimeter due to the flow depth H , L is the channel length and g is the gravitational acceleration. Substituting for m gives:

$$AL\rho g \sin \theta = \tau_w PL \quad (2.8)$$

where A is the cross sectional flow area, L is the length and ρ is the density. Rearranging Eq. (2.8) gives:

$$\tau_w = \frac{A}{P} \rho g \sin \theta \quad (2.9)$$

Since the hydraulic diameter, R_h is defined as:

$$R_h = \frac{A}{P} \quad (2.10)$$

Eq. (2.9) can be rewritten as

$$\tau_w = R_h \rho g \sin \theta \tag{2.11}$$

Noting the Fanning friction factor is given by:

$$f = \frac{2 \tau_w}{\rho V^2} \tag{2.12}$$

Substituting for τ_w from equation (2.11) into equation (2.12) gives:

$$f = \frac{2R_h g \sin \theta}{V^2} \tag{2.13}$$

Equations for A and P as per equation (2.10) for each of the four different cross-sections can be found in Figure 2.4.

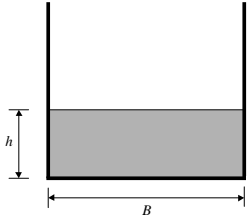
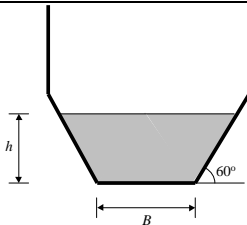
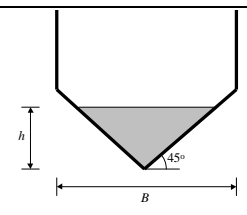
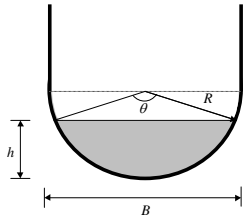
Section	Size	Cross-sectional area A	Wetted perimeter P	Surface width W
	B = 300 mm B = 150 mm	Bh	B + 2h	B
	B = 150 mm B = 75 mm	$h(B + xh)$ where $x = 1/\tan\theta$	$B + 2h\sqrt{1 + x^2}$ where $x = 1/\tan\theta$	$B + 2xh$ where $x = 1/\tan\theta$
	B = 300 mm	h^2	$2h\sqrt{2}$	2h
	B = 300 mm B = 150 mm	$\frac{D^2}{8}(\theta - \sin\theta)$ where θ $= 2\cos^{-1}\left(1 - \frac{2h}{D}\right)$	$D\left(\frac{1}{2}\theta\right)$ where θ $= 2\cos^{-1}\left(1 - \frac{2h}{D}\right)$	$D\left(\sin\frac{1}{2}\theta\right)$ where θ $= 2\cos^{-1}\left(1 - \frac{2h}{D}\right)$

Figure 2.4 Equations for cross-sectional area and wetted perimeter for the four channel shapes used in this research.

2.3.2 Non-Newtonian sheet flow down an inclined plane

It is possible to fundamentally derive the volumetric flow rate of a yield pseudoplastic fluid flowing as sheet flow down an inclined plane (Chhabra & Richardson, 2008).

The laminar flow of any fluid down an inclined plane where the flow is steady, incompressible, fully developed (no end effects) and there are no side walls is shown in Figure 2.5.

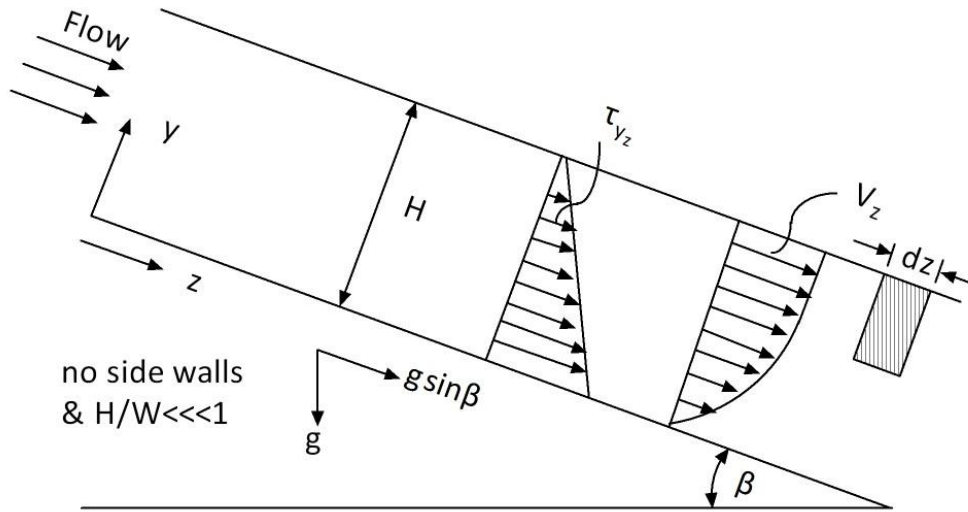


Figure 2.5 Flow on an inclined plane.

Writing a force balance on the differential element of the fluid as shown in Figure 2.5 gives:

$$W(H - y)dz\rho g \sin \beta = \tau_{yz}Wdz \quad (2.14)$$

let $dz \rightarrow 0$ and rearranging Eq.(2.14) yields

$$\tau_{yz} = \frac{W(H - y)\rho g \sin \beta}{W} = (H - y)\rho g \sin \beta \quad (2.15)$$

2.3.3 Flow of a power law fluid down an inclined plane

The flow of a power law fluid down an inclined plane with no side walls is given by:

$$\tau_{yz} = k \left(\frac{dV_z}{dy} \right)^n \quad (2.16)$$

where, k is the consistency coefficient and n is the flow behaviour index. Substituting Eq. (2.16) into Eq. (2.15) yields:

$$\frac{dV_z}{dy} = \left(\frac{\rho g \sin \beta}{k} \right)^{\frac{1}{n}} (H - y)^{\frac{1}{n}} \quad (2.17)$$

Integrating Eq. (2.17) with respect to y gives:

$$V_z = \left(\frac{\rho g \sin \beta}{k} \right)^{\frac{1}{n}} \left(\frac{n}{n+1} \right) H^{\frac{n+1}{n}} \left[1 - \left(1 - \frac{y}{H} \right)^{\frac{n+1}{n}} \right] \quad (2.18)$$

Since

$$Q = \int_0^H V_z W dy \quad (2.19)$$

Substituting for V_z and integrating gives:

$$Q = W \left(\frac{\rho g \sin \beta}{k} \right)^{\frac{1}{n}} \frac{n}{2n+1} H^{\frac{2n+1}{n}} \quad (2.20)$$

The full derivation for Eq. (2.20) can be found in Appendix C.

2.3.4 Laminar flow of a Herschel–Bulkley fluid down an inclined plane

The laminar flow of a Herschel–Bulkley fluid down an inclined plane is shown in Figure 2.6. The flow is considered to be steady, incompressible, fully developed (no end effects) with no side walls.

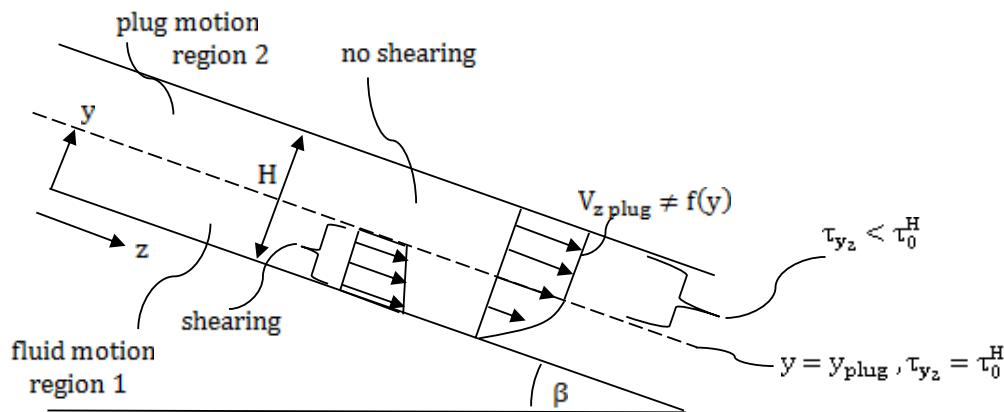


Figure 2.6 Flow of a Herschel–Bulkley fluid on an inclined plane.

The total flow is the sum of the flow in region 1 plus the flow in region2 giving

$$Q = \int_0^H W dy \cdot V_z = \int_0^{y_{plug}} W dy \cdot V_z + \int_{y_{plug}}^H W dy \cdot V_z \text{ plug} \quad (2.21)$$

where

$$V_z = \frac{k}{\rho g \sin \beta} \left(\frac{n}{n+1} \right) \left[\left(\frac{H \rho g \sin \beta - \tau_0^H}{k} \right)^{\frac{n+1}{n}} - \left(\frac{(H-y) \rho g \sin \beta - \tau_0^H}{k} \right)^{\frac{n+1}{n}} \right] \quad (2.22)$$

and

$$V_{zp} = V_{z_{y=y_{plug}}} = \frac{k}{\rho g \sin \beta} \left(\frac{n}{n+1} \right) \tau_w^{\frac{n+1}{n}} \left[\frac{1 - \frac{\tau_0^H}{\tau_w}}{k} \right]^{\frac{n+1}{n}} \quad (2.23)$$

The full derivation of equation (2.22) and equation (2.23) can be found in Appendix C

2.3.5 Combined expression for the flow in non-circular cross sections of arbitrary shape

Kozicki et al. (1986; 1967) proposed that the flow in non-circular cross sections can be expressed by combining the Rabinowitsch-Mooney equation for pipe flow given by equation (2.24) and the corresponding equation for slit flow given by equation (2.25) into a single equation given by equation (2.26).

The Rabinowitsch- Mooney equation for pipe flow is given by:

$$\dot{\gamma}_w = \frac{1}{4} \tau_w \frac{d \left(\frac{8V}{D} \right)}{d \tau_w} + \frac{3}{4} \left(\frac{8V}{D} \right) \quad (2.24)$$

The derivation of this equation can be found in various literature sources such as Kozicki and Tiu (1986), Holland and Bragg (1995) and Chhabra and Richardson (2008).

For flow between parallel plates or slit flow, the flow is assumed to be steady, laminar, incompressible, fully developed, with no-slip, no end effects and no side walls as shown in Figure 2.7.

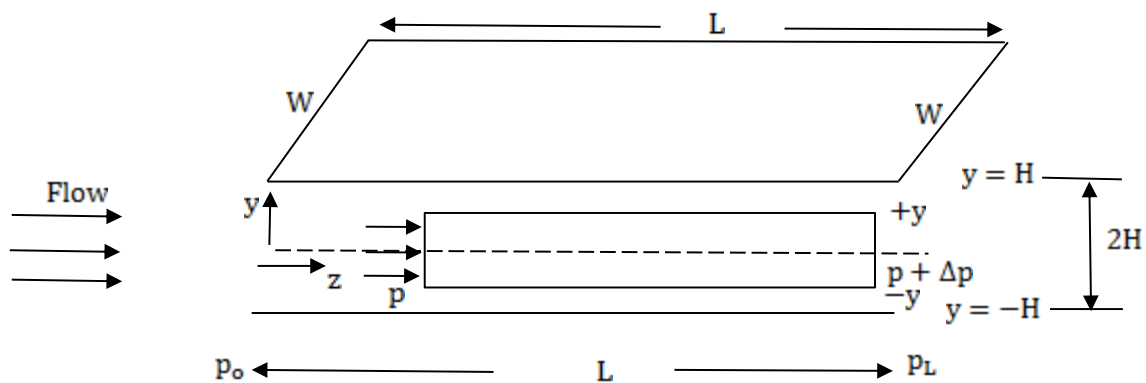


Figure 2.7. Slit flow.

The corresponding equation for slit flow to equation (2.24) is given by:

$$\dot{\gamma}_w = \frac{1}{2} \tau_w \frac{d}{d\tau_w} \left(\frac{8V}{D_h} \right) + \left(\frac{8V}{D_h} \right) \quad (2.25)$$

The full derivation of equation (2.25) for slit flow can be found in appendix C.

Due to the similarity between equations (2.24) and (2.25), Kozicki et al. (1986; 1967) proposed a combined equation for any arbitrary shape that is given by:

$$\dot{\gamma}_w = a\tau_w \frac{d}{d\tau_w} \left(\frac{8V}{D_h} \right) + b \left(\frac{8V}{D_h} \right) \quad (2.26)$$

where $a = 1/2$ and $b = 1$ for slit flow and $a = 1/4$ and $b = 3/4$ for pipe flow.

When side walls, as is the case for all open channels, have to be taken into account, this becomes much more complex and several semi-empirical and empirical derivations have been made. This will be discussed in the following sections.

2.4 Effect of shape on Newtonian open channel flow

Flow of water in a variety of open channels has been investigated by several researchers such as Straub et al. (1958) and Chow (1959). Along with experimental data as shown in Figure 2.8, Straub et al. (1958) presented a theory for laminar flow of Newtonian fluids in open channels with various cross-sections. They showed that the data in the laminar flow regime can be defined by a general relationship $f = K/Re$ where f is the Fanning friction factor and Re is the Newtonian Reynolds number and that K is “a purely numerical coefficient dependent on the channel shape”. Analytical and numerical solutions for K were provided for rectangular, semi-circular, elliptical, 60° , 90° and 120° triangular and trapezoidal channels.

The Darcy equation is the general expression for pressure drop of the flow of any liquid in laminar or turbulent flow in a pipe and is given by:

$$h_f = \frac{fLV^2}{2gD} \quad (2.27)$$

For the steady flow of a liquid in an open channel of uniform cross section, the depth of the liquid is uniform and the hydraulic slope of the free liquid surface is parallel to the slope of the channel bed, (Holland & Bragg, 1995). If the channel bed is at a small angle θ to the horizontal plane, the frictional head loss, h_f , per length, L , is equal to the slope of the channel and equal to $\sin \theta$. By replacing h_f/L with $\sin \theta$ and the diameter D with the hydraulic diameter $D = 4R_h$ for a pipe in Eq. (2.27), gives the Darcy friction factor as expressed by:

$$f_{\text{Darcy}} = \frac{4R_h 2g \sin \theta}{V^2} \quad (2.28)$$

The Fanning friction factor expression (Holland and Bragg, 1995), shows the relationship between the friction factor and the wall shear stress given as:

$$f_{\text{Fanning}} = \frac{2 \tau_w}{\rho V^2} \tag{2.12}$$

where, ρ is the fluid density, V the average velocity and $\tau_w = R_h \rho g \sin \theta$, giving:

$$f_{\text{Fanning}} = \frac{R_h 2g \sin \theta}{V^2} \tag{2.13}$$

From Eq. (2.13) and Eq. (2.28) it can be seen that the relationship between f_{Darcy} and f_{Fanning} is given by:

$$f_{\text{Darcy}} = 4f_{\text{Fanning}} \tag{2.29}$$

To compare the shape factor constants, the K values, found by Straub et al. (1958) depicted in Figure 2.8 to the shape factor K values for rectangular and triangular open channels established in this research, the Straub et al. (1958) values must be divided by four.

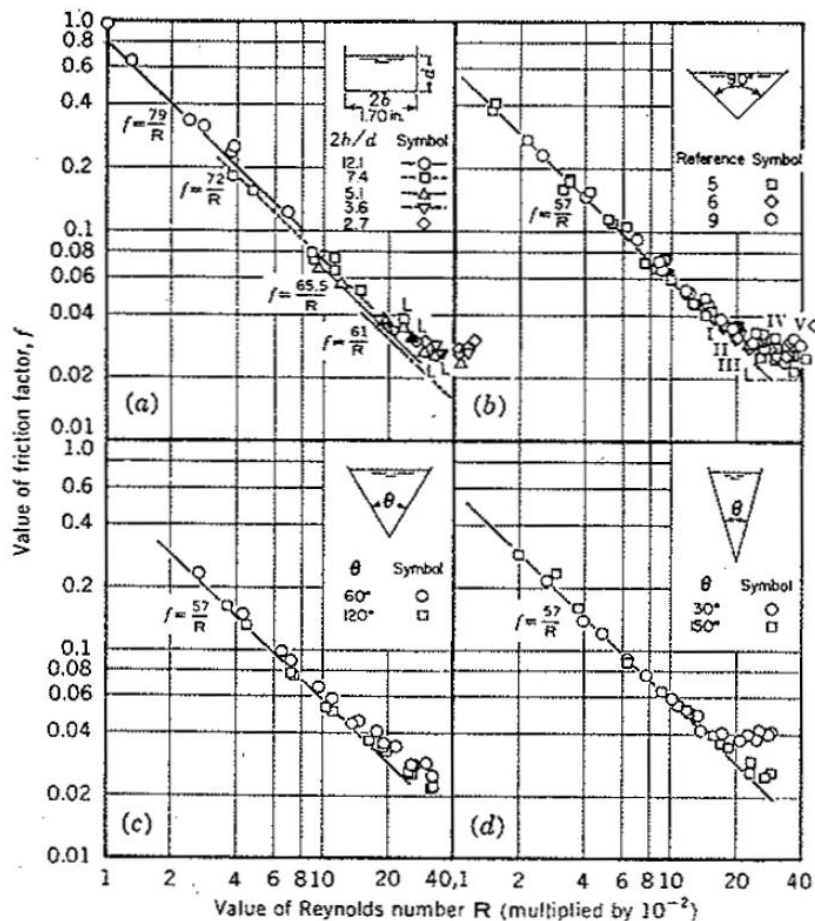


Figure 2.8. Friction factor vs. Reynolds number plots for smooth laminar flow in rectangular and triangular channels (Straub et al., 1958). The R used by Straub et al. (1958) is in fact Re .

Channel friction factors were evaluated by Straub et al. (1958) using the Darcy-Weisbach friction factor equation:

$$f_{Darcy} = \frac{S 4R_h 2g}{V^2} \tag{2.30}$$

where S is the channel slope ($S = \sin \theta$), V the average velocity, R_h the hydraulic radius and g the gravitational acceleration.

They established that the predicted f vs. Re line for smooth-walled, rectangular, triangular and semi-circular shaped channels to be coincident with the experimental data when plotted as an f vs. Re plot. For rectangular channels where the water height to channel width (h/W) ratios ranged from 0.08 to 0.37, K was found to vary from 19.75 to 15.25 compared with the corresponding analytical values of 21.5 to 16.25. For triangular channels where the vertex angle ranged from 30 degrees to 150 degrees, K was found to be 14.25 and independent of the vertex angle. This is in excellent agreement with the analytical value of 14.23 for a 90 degree channel and the numerical value of 14.15 for the other triangular channels. For semi-circular channels, they stated that the f vs. Re plot showed the data to be "grouped" about the $f = K/Re$ line where K was found analytically to be 16.

In his authoritative book on open channel flow, Chow (1959) produced an f vs. Re plot for flow of water in smooth-walled, rectangular and triangular channels based on the two datasets of Straub et al. (1958) Here, K was found to be approximately 24 for the rectangular channels and 14 for the triangular channels.

The simplest expression for the friction factor Reynolds number relationship for Newtonian turbulent flow in smooth pipes is given by the Blasius equation $f = 0.079Re^{-0.25}$ (Douglas, 1981), where f is the Fanning friction factor. This Blasius equation is valid for Reynolds numbers ranging from 3000 to 100000 (Holland & Bragg, 1995).

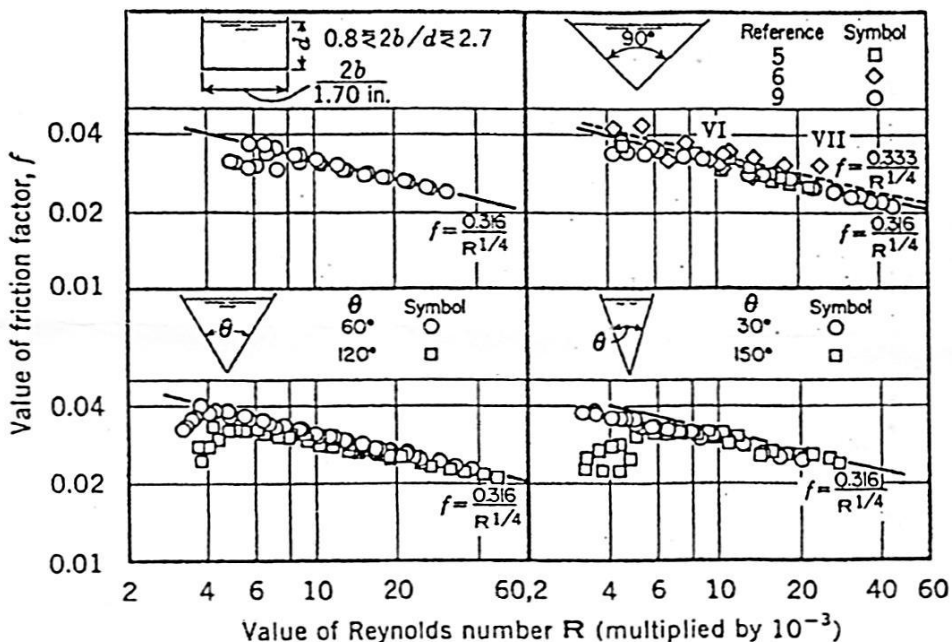


Figure 2.9. Friction factor vs. Reynolds number plots for smooth turbulent flow in rectangular and triangular channels Straub et al. (1958). The R used by Straub et al. (1958) is in fact Re .

Figure 2.9 depicts the friction factor Reynolds number relationship for Newtonian turbulent flow in rectangular and three different triangular channels (Straub et al., 1958). Using the Darcy friction factor the Blasius equation becomes

$f_{\text{Darcy}} = 0.316\text{Re}^{-0.25}$. They concluded that the channel shape have a relatively small effect on the frictional loss in turbulent flow of water in smooth open channels. They, however, had to rely on small datasets. The effect of shape on the Blasius equation for non-Newtonian fluids will be investigated in this work.

2.5 Effect of shape on non-Newtonian open channel flow

Very little has been reported in the literature for predicting non-Newtonian laminar flow in open channels of arbitrary cross-section.

The earliest model was that of Kozicki and Tiu (1967; 1986) who generalised the Rabinowitsch-Mooney equation for pipe flow and together with the corresponding expression for non-Newtonian flow between parallel plates (slit flow) proposed a single equation containing two factors a and b to account for different channel shapes. Kozicki and Tiu (1967; 1986) presented expressions for laminar flow of power law and Bingham fluids in rectangular, semi-circular and triangular open channels. Kozicki and Tiu did not experimentally verify their work.

From his work with clay-water suspensions, Coussot (1994) proposed shape factors for rectangular channels and trapezoidal shaped channels with 45° sides. Haldenwang et al. (2002; 2004) proposed a model for laminar flow of power law, Bingham plastic and Herschel-Bulkley fluids in rectangular, semi-circular, triangular and trapezoidal open channels.

Fitton (2007) provided a model for the prediction of tailings beach slopes and fundamental to the research approach was the acceptance that tailings flows across the beach were in self-formed channels and not in uniform ever-expanding sheets. Fitton (2008) proposed methods for the prediction of the state of flow and the depth of flow in open channels. He provided the following data: 49 data points of thickened tailings slurries 25 and 68% by weight tested in two semi-circular cross sections of 340 and 415 mm; 95 data points of CMC solutions of 11 different concentrations as well as two carbopol solutions of different concentrations in a 50 mm diameter semi-circular cross section. He also used datasets for rectangular channels collected by Haldenwang (2003) and a small dataset of 9 points for a rectangular channel published by Seckin et al. (2006) to validate his flow depth prediction procedure. His method for the prediction of the state of flow uses the Darcy friction factor as criterion. To predict the state of flow the Darcy friction factor is calculated using both the Hagen-Poiseuille equation and the Colebrook-White equation, if the Darcy friction factor calculated with the Hagen-Poiseuille equation is larger than that calculated with the Colebrook-White equation, the flow is laminar, if smaller, the flow is turbulent.

In this study, an investigation was made on the effect of channel shape on the friction factor-Reynolds Number relationship for laminar, open channel flow of non-Newtonian fluids. A check was also made on the validity of the pipe flow paradigm of $f = 16/\text{Re}$ used by Haldenwang et al. (2002), Haldenwang (2003) and Haldenwang et al. (2004) for open rectangular channels to other shaped channels.

During this research an investigation was also made on the effect of shape on the friction factor-Reynolds number relationship for turbulent non-Newtonian flow in rectangular, trapezoidal, semi-circular and triangular open channels. Five previously-published turbulent models, presented by Manning (1890), Torrance (1963), Wilson and

Thomas (1985), Slatter (1994) and Haldenwang (2003) were investigated. The Torrance (1963), Wilson and Thomas (1985) and Slatter (1994) pipe models were adapted for open channel flow by Haldenwang (2003).

2.5.1 Laminar flow models

The three previously-published laminar models reviewed are the Kozicki and Tiu (1967; 1986) model for laminar flow of power law and Bingham fluids in rectangular, semi-circular and triangular open channels; the Coussot (1994) model for laminar flow of a Herschel–Bulkley fluid in rectangular and trapezoidal open channels; the Haldenwang et al. (2002; 2004) model for laminar flow of power law, Bingham plastic and Herschel-Bulkley fluids in rectangular, semi-circular, triangular and trapezoidal open channels.

Kozicki & Tiu model

The earliest laminar flow model was that of Kozicki and Tiu (1967; 1986) who generalised the Rabinowitsch-Mooney equation for pipe flow (Cheremisinoff, (1988) and Holland & Bragg, (1995) where the wall shear rate is given by:

$$\dot{\gamma}_w = \frac{1}{4} \tau_w \frac{d\left(\frac{8V}{D}\right)}{d\tau_w} + \frac{3}{4} \left(\frac{8V}{D}\right) \quad (2.31)$$

and for flow between infinitely wide parallel plates (slit flow), where the wall shear rate is given by:

$$\dot{\gamma}_w = \frac{1}{2} \tau_w \frac{d\left(\frac{4V}{H}\right)}{d\tau_w} + 1 \left(\frac{4V}{H}\right) \quad (2.32)$$

By replacing the pipe diameter, D in Eq. (2.31) and the slit gap, H in Eq. (2.32) with the hydraulic radius R_h leads to two very similar looking equations representing the wall shear rate for pipe flow:

$$\dot{\gamma}_w = \frac{1}{4} \tau_w \frac{d\left(\frac{2V}{R_h}\right)}{d\tau_w} + \frac{3}{4} \left(\frac{2V}{R_h}\right) \quad (2.33)$$

and for slit flow:

$$\dot{\gamma}_w = \frac{1}{2} \tau_w \frac{d\left(\frac{2V}{R_h}\right)}{d\tau_w} + 1 \left(\frac{2V}{R_h}\right) \quad (2.34)$$

Kozicki and Tiu (1967; 1986) proposed a single equation that can be used for the estimation of the wall shear rate for laminar flow of various non-Newtonian fluids in different non-circular channels between the two limiting cases of pipe flow and slit flow. This is given by:

$$\dot{\gamma}_w = a\tau_w \frac{d\left(\frac{2V}{R_h}\right)}{d\tau_w} + b\left(\frac{2V}{R_h}\right) \quad (2.35)$$

where a and b are constants for various cross-sectional shapes. For pipe flow, $a=0.25$, $b=0.75$ and for slit flow, $a=0.5$ and $b=1.0$

They assumed that a generalisation of equation (2.35) for an arbitrary fluid flowing in a straight conduit of arbitrary cross sectional geometry can be given by:

$$\dot{\gamma}_w = f(\bar{\tau}_w) = a\bar{\tau}_w \frac{d\left(\frac{2V}{R_h}\right)}{d\bar{\tau}_w} + b\left(\frac{2V}{R_h}\right) \quad (2.36)$$

where $\bar{\tau}_w$ denotes the contour-integrated average values of τ_w , which are generally not constant along the wetted perimeter.

They also introduced a generalised Reynolds number, Re^* , such that the friction factor for fully-developed laminar flow through any constant cross-section duct is given by

$$f = \frac{16}{Re^*}, \quad (2.37)$$

where

$$Re^* = \frac{\rho V^{2-n^*} R_h^{n^*}}{2^{n^*-3} k^*} \quad (2.38)$$

with n^* and k^* are defined respectively by:

$$n^* = \frac{d \ln \bar{\tau}_w}{d \ln \left[\frac{2V}{R_h} \right]} \quad (2.39)$$

and

$$k^* = \frac{\bar{\tau}_w}{\left[\frac{2V}{R_h} \right]^{n^*}} \quad (2.40)$$

Through substitution of appropriate expressions for n^* and k^* , they obtained Re^* expressions for the power law and Bingham plastic fluids.

For the power law fluid

$$Re^*_p = \frac{R_h^n V^{2-n} \rho}{2^{n-3} k \left(\frac{a+bn}{n} \right)^n}, \quad (2.41)$$

with n^* and k^* are defined respectively by:

$$n^* = n \quad (2.42)$$

$$k^* = k \left(\frac{a+bn}{n} \right)^n \quad (2.43)$$

For Bingham plastic fluids

$$Re^*_{*B} = \frac{4R_h V \rho}{k^*} \left[\frac{1}{a+b} - \frac{\chi}{b} + \frac{a}{b(a+b)} \chi^{1+\frac{b}{a}} \right] \quad (2.44)$$

where a and b are the geometrical parameters relating to the shape of the flow geometry and χ is the ratio of Bingham yield stress to wall shear stress, $\tau_{yB}/\bar{\tau}_w$ with $\bar{\tau}_w = R_h \rho g \sin\theta$.

With n^* and k^* being defined respectively by:

$$n^* = \frac{a \left[\frac{1 - \chi^{1+\frac{b}{a}}}{a+b} - \frac{\chi \left(1 - \chi^{\frac{b}{a}} \right)}{b} \right]}{1 - \chi - b \left[\frac{1 - \chi^{1+\frac{b}{a}}}{a+b} - \frac{\chi \left(1 - \chi^{\frac{b}{a}} \right)}{b} \right]} \quad (2.45)$$

$$k^* = (a\beta)^{n^*} \bar{\tau}_w^{1+\frac{bn^*}{a}} \left[\left(\frac{a}{a+b} \right) \bar{\tau}_w^{1+\frac{b}{a}} - \frac{a}{b} \bar{\tau}_w^{\frac{b}{a}} \tau_y + \frac{a^2}{b(a+b)} \tau_y^{1+\frac{b}{a}} \right]^{-n^*} \quad (2.46)$$

where a and b are the geometrical parameters relating to the shape of the flow geometry, β is a parameter in the Bingham plastic model and χ is the ratio of Bingham yield stress to wall shear stress, $\tau_{yB}/\bar{\tau}_w$ with $\bar{\tau}_w = R_h \rho g \sin\theta$.

Noting $f = \frac{2\bar{\tau}_w}{\rho V^2}$ in Eq. (2.37), the average velocity expressions for the power law and Bingham plastic fluids

corresponding to Eq.'s (2.41) and (2.44) can be obtained. These are given respectively by:

$$V = \frac{R_h}{2} \left(\frac{\bar{\tau}_w}{K} \right)^{\frac{1}{n}} \left(\frac{n}{a + bn} \right) \quad (2.47)$$

and

$$V = \frac{R_h}{2} \frac{\bar{\tau}_w}{\mu_B} \left[\frac{1}{a + b} - \frac{\chi}{b} + \frac{a}{b(a + b)} \chi^{1 + \frac{b}{a}} \right] \quad (2.48)$$

Kozicki and Tiu (1967; 1986) did not provide expressions for Herschel-Bulkley fluids.

For open rectangular channels, the analytical solutions for Newtonian flow given by Straub et al. (1958) may be used for the evaluation of a and b.

$$a = 0.5 \left(\frac{\lambda}{1 + \lambda} \right)^2 \left(1 - \frac{32}{\pi^3} \sum_{n=0}^{\infty} \left(\frac{(-1)^n}{(2n+1)^3} \right) \left(\frac{1}{\cosh \left(\frac{(2n+1)\pi\lambda}{2} \right)} \right) \right)^{-1} \quad (2.49)$$

$$b = a [3\phi' - 1] \quad (2.50)$$

where

$$\phi' = \frac{\left(1 - \frac{32}{\pi^3} \sum_{n=0}^{\infty} \left(\frac{(-1)^n}{(2n+1)^3} \right) \left(\frac{1}{\cosh \left(\frac{(2n+1)\pi\lambda}{2} \right)} \right) \right)}{\left(1 - \frac{192}{\pi^5} \frac{1}{\lambda} \sum_{n=0}^{\infty} \left(\frac{1}{(2n+1)^5} \right) \tanh \left(\frac{(2n+1)\pi\lambda}{2} \right) \right)} \quad (2.51)$$

and

$$\lambda = \frac{W}{2h} \quad (2.52)$$

For open triangular channels, the analytical solutions for Newtonian flow given by Straub et al., (1958) was used for the evaluation of a and b. For a 90-degree symmetrical triangular open channel, a = 0.2122 and b = 0.6765 whereas for a 60-degree symmetrical triangular open channel, a = 0.2009 and b = 0.6831. For open semi-circular channels, the values of a and b used were those numerically obtained by Sestak (1974) as shown in Table 2.2.

Table 2.2 Values of a and b for open semi-circular channels, numerically obtained by Sestak (1974).

H/D	a	b
0.00	0.222	0.750
0.01	0.224	0.750
0.05	0.232	0.751
0.10	0.238	0.752
0.15	0.242	0.753
0.20	0.245	0.753
0.25	0.247	0.753
0.30	0.248	0.752
0.35	0.249	0.751
0.40	0.250	0.751
0.45	0.250	0.750
0.50	0.250	0.750
0.55	0.250	0.750
0.60	0.250	0.751
0.65	0.251	0.753
0.70	0.253	0.757
0.75	0.256	0.762
0.82	0.262	0.768
0.85	0.273	0.775
0.90	0.289	0.785
0.95	0.296	0.808
0.98	0.287	0.820
0.99	0.278	0.814
1.00	0.250	0.750

Coussot model

From his work with clay-water suspensions in rectangular and trapezoidal shaped channels, Coussot (1994) found that the flow behaviour of these suspensions over the range of concentrations studied were best described by the Herschel-Bulkley model with the power law exponent, n fixed at $1/3$. For these suspensions, he derived the expression for average wall shear stress in both channels to be

$$\tau_w = \tau_{yHB} \left(1 + \alpha (H_B)^{-0.9} \right) \quad (2.53)$$

where α is a shape factor for the open channel and HB is the Herschel-Bulkley number defined as:

$$H_B = \frac{\tau_{yHB}}{k} \left(\frac{h}{V} \right)^n \quad (2.54)$$

with h being the flow depth in the channel. From Equations (2.53) and (2.54), the average velocity can be obtained:

$$V = \frac{h}{\left[\frac{k}{\tau_{yHB}} \left\{ \frac{\alpha}{\left(\frac{\tau_w}{\tau_{yHB}} - 1 \right)} \right\}^{1.11} \right]^{\frac{1}{n}}} \quad (2.55)$$

The shape factor for the rectangular shaped channel was defined by Coussot (1994) as:

$$\alpha = 1.93 - 0.43 \left(\arctan \left(\left(\frac{10h}{W} \right)^{20} \right) \right) \quad \text{for } \frac{h}{W} < 1 \quad (2.56)$$

He claims that this is relevant for $h/W < 1$ where h is the flow depth and W is the width of the rectangular channel. Hence, for a 300 mm wide rectangular shaped channel, the shape factor is applicable for all values of h up to 300 mm. However, the value of α reaches a minimum value at a depth of approximately 60 mm indicating a h/W ratio of about 0.2. This contradicts the initial assumption of α being correct for an h/W ratio up to 1. The shape factor for the trapezoidal shaped channel with a base width W and an edge slope of 45° was found by Coussot (1994) to be:

$$\alpha = 1.93 - 0.6 \arctan \left(\left(\frac{0.4h}{W} \right)^{20} \right) \quad \text{for } \frac{h}{W} < 4 \quad (2.57)$$

Haldenwang et al (2002) model

By adapting the pipe flow paradigm for any open channel and introducing a new Reynolds number based on the Herschel-Bulkley model, Haldenwang et al. (2002; give2004) proposed an equation for the friction factor-Reynolds number relationship for laminar flow of non-Newtonian fluids in open channels. This is given by:

$$f = 16/Re_H \quad (2.58)$$

in which Re_H is the Haldenwang et al. (2002) Reynolds number given by:

$$Re_H = \frac{8\rho V^2}{\tau_y + k \left(\frac{2V}{R_h} \right)^n} \quad (2.59)$$

The Haldenwang et al. (2002) Reynolds number given by equation (2.59) was adapted for open channel flow from the Slatter (1994) Reynolds number for pipe flow by replacing the pipe diameter with 4 times the hydraulic radius. As the Slatter (1994) Reynolds number was not derived from dimensional analysis, that has traditionally played an important role in the formulation of Reynolds numbers, it deserves an explanation to why this was adopted in this study. Dimensional analysis is based on the general functional relationship between the problem variables being multiplicative (forming dimensionless products) and exponential. Dimensional analysis is therefore unable to resolve the additive nature of the fundamental rheological relationship needed for the Herschel-Bulkley model given in Table 2.1 (Slatter and Lazarus, 1993). Instead the excellent predicted versus experimental results obtained by Slatter, (1994) and Haldenwang, (2003) using their proposed Reynolds number expressions was considered here. Hence the Haldenwang et al. (2002) Reynolds number given by equation (2.59) for open channel flow was used in this research. While this may not satisfy the requirements of absolute scientific rigour, it has already produced workable engineering solutions (Haldenwang, 2003).

An advantage of using this Reynolds number is that it can also be used for fluids exhibiting Newtonian, power law and Bingham plastic behaviour. By substituting $n = 1$ and $\tau_y = 0$ in Eq. (2.59) will yield the Newtonian Reynolds number whereas by substituting $\tau_y = 0$ in Eq. (2.59) will give the power law Reynolds number. Finally, by substituting $n = 1$ in Eq. (2.59) will result in the Bingham plastic Reynolds number.

Noting $f = \frac{2\tau_w}{\rho V^2}$, it can be deduced from Equations (2.58) and (2.59) that the average velocity is given by:

$$V = \frac{R_h}{2} \left(\frac{\tau_w - \tau_{yHB}}{k} \right)^{\frac{1}{n}} \quad (2.60)$$

2.5.2 Turbulent flow models

The design of open channels transporting water in turbulent flow is well established. In 1769, Antoine Chézy, the hydraulic engineer of the water supply system in Paris, introduced his equation relating the mean velocity of steady turbulent flow of water to the hydraulic radius and the slope of the channel (Chow, 1959; Chanson, 1999). In 1890, Manning (1890) modified the Chezy equation, $V = C_{Chezy} \sqrt{R_h \sin \alpha}$ by replacing the Chezy coefficient, C with the Manning roughness coefficient, $n_{Manning}$.

Manning found by experiment that the Chezy coefficient, C , varied approximately as $(R_h)^{\frac{1}{6}}$ and the relationship between the Chezy coefficient, C and the Manning roughness coefficient, n is given by $C = (R_h)^{\frac{1}{6}} / n$ (Douglas, 1981). The Manning equation is still widely used for the design of open channels transporting mining tailings such as the flume at the Andina mine that is 87 km long operating at a flow rate of $0.9 \text{ m}^3/\text{s}$ (Fuentes, 2004).

Five previously-published turbulent models are reviewed.

- The Manning model, which was derived from the Chézy equation (Manning, 1890). This equation is valid for both uniform and non-uniform (gradually varied) flow of water.

- The Torrance (1963) turbulent model uses the Herschel-Bulkley model for the flow of non-Newtonian slurries exhibiting yield-shear thinning behaviour in smooth pipes.
- The Wilson and Thomas (1985) and Thomas and Wilson (1987) pipe flow model for yield-shear thinning fluids which predicts the thickening of the laminar sub-layer by an area ratio factor A_r was used by Wilson in 1991 for open channel flow.
- The Slatter (1994) turbulent pipe flow model for Herschel-Bulkley or yield shear thinning fluids.
- Haldenwang (2003) developed a turbulent open channel model based on the pipe flow model presented by Slatter (1994). By replacing the pipe diameter with four times the hydraulic radius the pipe flow model could be adapted for open channel flow.

Most of the non-Newtonian turbulent flow models described in this section have been derived from the pipe paradigm, the exception being the Newtonian Manning turbulent model.

Five previously published turbulent velocity models are now presented.

Manning

The Manning equation was derived from the Chézy equation (Manning, 1890) and is defined as:

$$V = \frac{1}{n_{\text{Manning}}} (R_h)^{\frac{2}{3}} \sqrt{\sin \theta} \quad (2.61)$$

with R_h being the hydraulic radius and θ the angle of the flume with the horizontal.

Manning experimentally determined that the Chezy coefficient, C varied approximately as $(R_h)^{\frac{1}{6}}$ (Douglas, 1981). The Manning equation is valid for both uniform and non-uniform (gradually varied) flow of water. The values of the Manning constant n_{Manning} vary from $n_{\text{Manning}} = 0,009$ for smooth plastic to $n_{\text{Manning}} = 0.025$ for cemented rubble surfaces. The unit for n_{Manning} in SI units is $\text{m}^{\frac{1}{3}} \text{s}^{-1}$. A comprehensive list of n_{Manning} -values has been published by Chow (1959).

Torrance pipe model adapted by Haldenwang (2003) for open channel flow

Torrance (1963) developed a turbulent flow model for non-Newtonian slurries exhibiting yield shear thinning behaviour in smooth pipes using the Herschel-Bulkley model. This model could be adapted to open channel flow by changing the pipe diameter to $4R_h$. The equation for the flow velocity is given by:

$$\frac{V}{V_*} = \frac{3.8}{n} + \frac{2.78}{n} \ln \left(1 - \frac{\tau_y}{\tau_w} \right) + \frac{2.78}{n} \ln \left(\frac{V_*^{2-n} \rho (2R_h)^n}{K} \right) - 4.17 \quad (2.62)$$

Wilson and Thomas pipe model adapted by Haldenwang (2003) for open channel flow

Wilson and Thomas (1985) and Thomas and Wilson (1987) presented a pipe flow model for viscoplastic fluids where the thickening of the laminar sub-layer is accounted for by the use of an area ratio factor, A_r . In 1991, Wilson proposed the use of this model for open channel flow provided that the pipe radius is replaced by the equivalent hydraulic radius of the open channel and the equivalent viscosity, μ_e is used instead of the Newtonian viscosity, μ_N . The average velocity V is given by:

$$V = V_* \left(\frac{V_N}{V_*} + 11.6(A_r - 1) - 2.5 \ln A_r - \Omega \right) \quad (2.63)$$

where

$$V_N = V_* \left(2.5 \ln \left(\frac{\rho V_*^2 R_h}{\mu_e} \right) + 1.75 \right) \quad (2.64)$$

The shear velocity is:

$$V_* = \sqrt{\frac{\tau_w}{\rho}} \quad (2.65)$$

and

$$\Omega = -2.5 \ln \left(1 - \frac{\tau_y}{\tau_w} \right) - 2.5 \frac{\tau_y}{\tau_w} \left(1 + 0.5 \frac{\tau_y}{\tau_w} \right). \quad (2.66)$$

The Ω factor accounts for the blunting of the velocity profile created by the yield stress of the fluid and the wall shear stress. The equivalent viscosity, μ_e is the viscosity that would be possessed by a Newtonian fluid giving the same smooth wall friction factor as that obtained with the non-Newtonian fluid.

Haldenwang model

Haldenwang (2003) developed a turbulent open channel model based on the pipe flow model presented by Slatter (1994). The average smooth wall turbulent velocity is as follows:

$$v = \sqrt{gh \sin \theta} \left(2.5 \ln \frac{2R_h}{e} - 76.86 \mu_{a(500)} - 9.45 \right) \quad (2.67)$$

with $\mu_{a(500)}$ being the point viscosity at a shear rate of 500 s^{-1} and the friction factor f is defined as:

$$f = \frac{0.66(2g h \sin \theta)}{(V_{\text{turb}})^2} \quad (2.68)$$

Haldenwang (2003) used his own as well as Naik (1983) turbulent data to verify his model.

Slatter pipe model adapted by Haldenwang (2003) for open channel flow

Slatter (1994) presented a turbulent pipe flow model for yield shear-thinning fluids. By replacing the pipe diameter with four times the hydraulic radius this was adapted for smooth wall open channel flow as follows:

$$V = V_* \left(2.5 \ln \left(\frac{2R_h}{d_{85}} \right) + 2.5 \ln Re_r + 1.75 \right). \quad (2.69)$$

For rough wall open channel flow

$$V = V_* \left(2.5 \ln \left(\frac{2R_h}{d_{85}} \right) + 4.75 \right), \quad (2.70)$$

with the roughness Reynolds number being

$$Re_r = \frac{8\rho(V_*)^2}{\tau_y + k \left(\frac{8V_*}{d_x} \right)^n}, \quad (2.71)$$

and d_x being the representative particle size of the solid particles. For the slurries tested, the d_{85} size was found to be a good representation of the turbulent roughness size effect of the solid particles in the slurry i.e. $d_x = d_{85}$ (Slatter 1994).

2.6 Composite Power law friction factor vs. Reynolds number modelling

To predict the friction factor covering both laminar and turbulent non-Newtonian flow in open channels, a logistic dose-response curve developed by Patankar et al. (2002) and Garcia et al. (2003) for pipe flow was used. This composite power law f vs. Re correlation equation is given by:

$$f = F_2 + \frac{(F_1 - F_2)}{\left(1 + \left(\frac{Re}{t} \right)^e \right)^f} \quad (2.72)$$

where, F_1 and F_2 are the power law relationships covering the laminar and turbulent flow regimes defined respectively as:

$$F_1 = aRe^b \quad (2.73)$$

and

$$F_2 = cRe^d \quad (2.74)$$

The parameters t , e and f are values for the transitional flow regime.

The modelling procedure of Garcia et al. (2003) used for pipe flow predictions was extended to the present work on non-Newtonian flow in open channels of various cross-sections.

2.7 Summary

Newtonian open channel flow is well researched, but the literature shows that for non-Newtonian flow in channels of various cross-sectional shapes that this is not the case. Coussot (1994) provided some data for the flow of a Herschel-Bulkley fluid in rectangular and trapezoidal channels. Fitton (2007; 2008) obtained data for flow of three different non-Newtonian fluids (carboxymethyl cellulose, carbopol and thickened tailings) in a semi-circular channel. A large experimental database for non-Newtonian flow in rectangular open channels was developed by Haldenwang (2003). There is therefore a need for a comprehensive database of the flow of non-Newtonian fluids flowing in triangular, rectangular, trapezoidal and semi-circular open channels.

Straub et al. (1958) provided analytical and numerical solutions for shape factor K values for open channel Newtonian laminar flow in rectangular, semi-circular, elliptical, 60° , 90° and 120° triangular and trapezoidal channels. Kozicki and Tiu (1967, 1986), provided shape factors a & b to accommodate for the shape effect of open channel flow of power law and Bingham plastic fluids, the shape factors they used were those evaluated from analytical solutions for rectangular and triangular channels and numerically for semi-circular channels for flow of Newtonian fluids in open channels of the same cross-section. They also provided friction factor, Reynolds number and velocity expressions for the flow of power law and Bingham plastic fluids in open channels of arbitrary cross sections. Their work was never experimentally verified and they did not provide expressions for Herschel-Bulkley fluids. Their models are also mathematically complex.

There is therefore a need to establish and experimentally verify the friction factor Reynolds number relationship to accommodate power law, Bingham plastic and Herschel-Bulkley fluids in open channels of different cross-sections. From this relationship new laminar models can be derived accommodating the effect of shape.

Haldenwang, (2003) adapted turbulent pipe flow velocity models of Torrance (1963), Wilson and Thomas (1985) and Slatter (1994) to open channel flow by replacing the pipe radius by the hydraulic radius of the open channel for rectangular channels. He also used the Naik (1983) mean velocity model which is based on a semi-circular channel, modified for a rectangular channel for the flow of a Bingham fluid. Comparing the Naik (1983) model with the other models, Haldenwang, (2003) found that it predicted the turbulent velocity the worst. Haldenwang (2003) used the Naik (1983) turbulent data to verify his model. There is very little in the literature on the effect of shape in turbulent flow of non-Newtonian fluids. Designers like Fuentes (2004) have used the Manning equation for open channel flow. The advantage of using this equation is that it is simple to use and it does include a roughness factor. For smooth pipe turbulent flow of water, the Blasius model is the simplest relation between friction factor and Reynolds number. By modifying the Blasius equation new turbulent velocity expressions could be derived for non-Newtonian flow in rectangular, trapezoidal, semi-circular and triangular open channels.

Garcia et al. (2003) applied a composite friction factor modelling technique to non-Newtonian flow in pipes. This technique could be applied to non-Newtonian flow in trapezoidal, rectangular, semi-circular and triangular open channels.

The literature review has revealed that there is sufficient evidence to prove that the effect of shape on non-Newtonian open channel flow has not been adequately studied.

2.8 References

Alderman, N.J. & Heywood, N.I. 2004. Improving Slurry Viscosity and Flow Curve Measurements. *Chemical Engineering Progress*, 100(4): 27-32, April.

Alderman, N.J. & Haldenwang, R. 2007. A review of Newtonian and non-Newtonian flow in rectangular open channels. *Hydrotransport 17, The Southern African Institute of Mining and Metallurgy and the BHR Group*, Cape Town, SA, 87-106.

Brown, N.P., & Heywood, N.I. 1991. *Slurry Handling: Design of Solid-Liquid Systems*. Dordrecht the Netherlands: Kluwer Publications.

Chanson, H. 1999. *The Hydraulics of Open Channel Flow*. London: Arnold. 69-74

Cheremisinoff, N.P. (ed.) 1988. *Encyclopaedia of Fluid Mechanics*, Volume 7, Texas: Gulf Publishing.

Chhabra, R.P & Richardson, J.F. 2008. *Non-Newtonian Flow and Applied Rheology*, 2nd edition. Oxford: Butterworth-Heinemann.

Chow, V.T. 1959. *Open Channel Hydraulics*. New York: McGraw-Hill. 9-12.

Coussot, P. 1994. Steady laminar flow of concentrated mud suspensions in open channels. *Journal of Hydraulic Research*, 4(32): 535-558.

Douglas, J.F. 1981. *Solution of Problems in Fluid Mechanics*. London: Pitman Publishing.

Fitton, T.G. 2007. Tailings beach slope prediction. Unpublished PhD thesis, Royal Melbourne Institute of Technology, University, Melbourne, Australia.

Fitton, T.G. 2008. Non-Newtonian Open Channel Flow – A Simple Method of Estimation of Laminar/Turbulent Transition and Flow Resistance. *Paste 2008*, Kasane, Botswana, 245-251.

Fuentes, R. (2004), Slurry flumes in Chile. (Keynote Address). *Hydrotransport 16: 16th International Conference on the Hydraulic Transport of Solids in Pipes*, Santiago, Chile, 325-333.

García, F., García, J.C., Padrino, J.C., Mata, C., Trallero, J.L. & Joseph, D.D. 2003. Power law and Composite Power law Friction Factor Correlations for Laminar and Turbulent Gas–liquid Flow in Horizontal Pipelines, *International Journal of Multiphase Flow*, 29: 1605–1624.

Govier, G.W & Aziz, K. 1972. *The flow of complex mixtures in pipes*. Van Nostrand Reinhold C. Florida, USA.

Guang, R., Rudman, M., Chryss, A., Slatter, P. & Bhattacharya, S. 2011. Direct Numerical Simulation Investigation of Turbulent Open Channel Flow of a Hershel-Bulkley Fluid. *14th International Seminar on Paste and Thickened Tailings (Paste 2011)*, 5-7 April 2011, Perth, Australia, 439-452.

Haldenwang, R., Slatter, P.T. & Chhabra, R.P. 2002. Laminar and Transitional Flow in Open Channels for Non-Newtonian Fluids. *Hydrotransport 15: 15th International Conference on the Hydraulic Transport of Solids in Pipes*. Banff, Canada, Organised by BHR Group, Cranfield, Bedfordshire, UK, 755-768.

Haldenwang, R. 2003. Flow of Non-Newtonian Fluids in Open Channels. Unpublished D. Tech. thesis. Cape Technikon, Cape Town SA.

Haldenwang, R., Slatter, P.T., Chhabra, R.P. 2004a. Prediction of Transition for Non-Newtonian Open Channel Flow. *11th International Conference on Transport and sedimentation of solid particles*, Prague Czech Republic, 387-396.

Haldenwang, R., Slatter, P.T., Vanayza, S., & Chhabra, R.P. 2004b. The Effect of Shape on Laminar Flow in Open Channels for Non-Newtonian Fluids. *16th International conference on Hydrotransport*, Santiago Chile, 311-324.

Haldenwang, R. & Slatter, P.T. 2006a. Experimental Procedure and Database for Non-Newtonian Open Channel Flow. *Journal Hydraulic Research*. 44(2): 283-287.

Haldenwang, R. & Slatter, P.T. 2006b. Turbulent Non-Newtonian Open Channel Flow. *12th International. Conference on Transport and sedimentation of solid particles*, Tbilisi, Georgia, 135-144.

Haldenwang, R & Slatter, P.T. 2006. Laminar Flow Models for Minerals Tailings Transport in Open Channels. *XXIIIth International Mineral Processing Congress*, Istanbul, Turkey, 3-8 Sept. 1759-1764.

Haldenwang, R. Kotze, R. & Chhabra, R.P. 2012. Determining the Viscous Behaviour of Non-Newtonian Fluids in a Flume Using a Laminar Sheet Flow Model and Ultrasonic Velocity Profiling (UVP) System. *Journal of the Brazilian Society of Mechanical Science & Engineering*, 34 (3): 276-284.

Hanks, R.W. 1979. Course notes hydraulic design of complex fluids. *1981 Richard Hanks Associates, Inc. Orem, Utah. USA.*

-
- Heywood N.I., & Alderman, N.J. 2004. Fundamentals of Rheological Classification and Measurement of High Solids Concentration Slurries and Pastes. *16th International conference on Hydrotransport*, Santiago, Chile, 675-699.
- Holland, F.A & Bragg, R. 1995. Fluid Flow for Chemical Engineers. 2nd edition, Oxford: Butterworth-Heinemann.
- Kozicki, W. & Tiu, C. 1967. Non-Newtonian Flow Through Open Channels. *Canadian Journal of Chemical Engineers*, 45: 127-134.
- Kozicki, W. & Tiu, C. 1986. Parametric Modelling of Flow Geometries in Non-Newtonian Flows. *Encyclopaedia of Fluid Mechanics, Vol 7, N.P. Cheremisinoff (ed)*.. Houston: Gulf Publishing Co, 199 – 252.
- Manning, R. 1890. On the Flow of Water in Open Channels and Pipes. *Institute of Civil Engineers Ireland*, 20: 161-207.
- Naik, B. 1983. Mechanics of Mudflow Treated as the Flow of a Bingham Fluid. Unpublished PhD thesis. Washington State University.
- Patankar, N.A., Joseph, D.D., Wang, J., Barree, R.D., Conway, M. & Asadi, M. 2002. Power Law Correlations for Sediment Transport in Pressure Driven Channel Flows. *International Journal of Multiphase Flow*, 28: 1269–1292.
- Roberts, G.P., Barnes, H.A & Mackie, C. 2001. Using the Microsoft Excel ‘solver’ Tool to Perform Non-Linear Curve Fitting, Using a Range of Non-Newtonian Flow Curves as Examples. *Applied Rheology, Kerschensteiner Verlag GmbH, Lappersdorf, Germany* 11(5): 271-276.
- Seckin, G., Seckin, N. & Yurtal, R. 2006. Boundary shear stress analysis in smooth rectangular channels. *Canadian Journal of Civil Engineering*, 33(3): 336-342.
- Sestak, J. 1974. Flow of non-Newtonian fluids in open circular channels, *Canadian Journal of Chemical Engineering*, 52: 670-672.
- Slatter, P.T. 1994. Transitional and Turbulent Flow of Non-Newtonian Slurries in Pipes. Unpublished PhD thesis. University of Cape Town, Cape Town SA.
- Spelay, R., Sumner, R.J., Sanders, R.S. & Gillies, R.G. 2006. Laminar Open Channel Flow of Kaolin Clay Slurries Containing Sand. *13th International Conference Transport and sedimentation of solid particles*, Tbilisi Georgia, 300-317.
- Spelay, R. 2007. Solids Transport in Laminar, Open Channel Flow of Non-Newtonian Slurries. Unpublished PhD thesis. University of Saskatchewan, Saskatoon CA.

Straub, L.G., Silberman, E. & Nelson, H.C. 1958. Open Channel Flow at Small Reynolds Numbers. *American Society of Civil Engineers*, 123: 685–713.

Thomas, A.D., Wilson, K.C. 1987. New Analysis of Non-Newtonian Turbulent Flow: Yield Power Law Fluids. *Canadian Journal of Chemical Engineers*, 65(2): 335-338.

Torrance, B. McK. 1963. Friction Factors for Turbulent Non-Newtonian Flow in Circular Pipes, *South African Mechanical Engineers*, 13: 89-91.

Wilson, K.C. & Thomas, A.D. 1985. A New Analysis of the Turbulent Flow of Non-Newtonian Fluids. *Canadian Journal of Chemical Engineers*, 63: 539-546.

Wilson, K.C. 1991. Flume Design for Homogeneous Slurry Flow, *Particulate Science and Technology*, 9, 149-159.

CHAPTER 3

RESULTS

Research method

Published as

Burger, J.H. Haldenwang, R. and Alderman, N.J. (2010), Experimental database for non-Newtonian flow in four channel shapes. *Journal of Hydraulic Research*. Vol. 48, No. 3 (2010), pp. 363–370.

Chapter 3 Research method

3.1 Abstract

The database for non-Newtonian flow in rectangular open channels developed by the Flow Process Research Centre at the Cape Peninsula University of Technology was recently extended to include the test work on non-Newtonian flow in open channels of semi-circular, triangular and trapezoidal cross-sections. As for flow in rectangular open channels, the flow of carboxymethyl cellulose solutions and aqueous kaolin and bentonite suspensions was investigated in these open channels at angles varying from 1° to 5°. The flow curve data for these three fluids was best represented by the power law, Bingham plastic and Herschel-Bulkley models, respectively. The research methodology in the use of this extended database to study laminar, transitional and turbulent non-Newtonian open channel flow is described. It is hoped that this database will be a useful resource to researchers working in the field of non-Newtonian open channel flow.

Keywords: Cross-sectional shape, experimental database, non-Newtonian fluid, open channel flow, rheology

3.2 Introduction

The effect of channel shape on non-Newtonian, open channel flow design has not yet been fully investigated. Channels of rectangular, semi-circular and trapezoidal cross-sections are often found in the minerals industry where tailings are transported from the mine to the disposal facilities Haldenwang and Slatter (2006a). Non-Newtonian flow in various channel cross-sections also occurs in the wastewater and food processing industries Fitton (2008). Fluids exhibiting non-Newtonian behaviour are not easy to characterise and changes in fluid concentration and other physical properties affect its rheological behaviour, which in turn affects fluid flow. This is especially true for fluids exhibiting yield/shear thinning behaviour.

A large experimental database for non-Newtonian flow in rectangular open channels was developed by the Flow Process Research Centre, Cape Peninsula University of Technology Haldenwang (2003) and Haldenwang & Slatter (2006a). Prior to the publication of this database, only limited studies were available. Coussot (1994) provided data for the flow of kaolin suspensions of varying concentrations in rectangular and trapezoidal channels, whereas Naik (1983) obtained data for turbulent flow of kaolin suspensions in a rectangular flume. Wang and Plate (1996) and Wang (2002) carried out experimental studies on the flow of clay suspensions in rectangular channels. Fitton (2007, 2008) obtained data for flow of three different non-Newtonian fluids in semi-circular channels.

The database for non-Newtonian flow in rectangular channels Haldenwang (2003) and Haldenwang & Slatter (2006a) was recently extended to include non-Newtonian flow in open channels of semi-circular, triangular and trapezoidal cross-sections. The objective of this research is to present open channel flow data for these shapes. The database previously reported for non-Newtonian flow in rectangular channels Haldenwang and Slatter (2006a) was used by Fitton (2007, 2008), Spelay et al. (2006) and Spelay (2007) for verification purposes.

3.3 Fundamentals

Non-Newtonian open channel flow data can be presented in the form of a Moody chart where the Fanning friction factor f is plotted against Reynolds number, allowing laminar, transitional or turbulent flow regions to be identified (Chow 1959). The factor f for pipe-flow can be adapted for open channel flow by replacing the pipe diameter D with 4 times the hydraulic radius ($D = 4R_h$) as:

$$f = \frac{2R_h g \sin \theta}{V^2} \quad (2.13)$$

$$R_h = \frac{A}{P} \quad (2.10)$$

where A = cross-sectional flow area and P = wetted perimeter of channel.

Haldenwang et al. (2002) defined a new Reynolds number Re_H , based on the Herschel-Bulkley model that was adapted from the pipe Reynolds number presented by Slatter (1994) as Eq.(2.59)

$$Re_H = \frac{8\rho V^2}{\tau_y + k \left(\frac{2V}{R_h} \right)^n} \quad (2.59)$$

where τ_y , k and n are the yield stress, consistency coefficient and flow behaviour index as defined by the Herschel-Bulkley model. This Reynolds number can also be used for fluids exhibiting Newtonian, power law and Bingham plastic behaviour.

3.4 Research method

Flume tests were carried out in a 10 m long, rectangular flume designed at the Flow Process Research Centre. This flume can be tilted up to 5° from the horizontal. By placing a partition insert, the flume width was changed from 300 mm to 150 mm. By inserting appropriate cross-sectional inserts, the rectangular flume can be changed into a triangular, semi-circular or trapezoidal cross-section Figure 3.1

The flow, provided by a 100 mm progressive cavity, positive displacement pump and a Warman® 4x3 centrifugal slurry pump, was monitored by an electromagnetic flow meter. The discharge capacity was 45 l/s. Flow depths were measured using digital depth gauges of ±5% accuracy fitted at the 5 m and 6 m positions from the flume entrance. These two positions were found to be optimum for depth measurement (Haldenwang 2003). Since the difference in fluid height between these two positions was found to be minimal, the flow in the region can therefore be taken as steady. A data logger was used to record the various outputs as a function of time. All data were then fed to a PC so that a Moody chart resulted as output. For each of the cross sectional shapes, datasets were collected for each test material at various concentrations, slopes and flow rates. A summary of test materials is given in Table 3.1.

Flow curve measurements of the test material were also made in-situ using an inline tube viscometer fitted with three tubes of diameters 13, 28 and 80 mm. Each tube was fitted with an electromagnetic flow meter and two differential pressure transducers of different measuring ranges were used to obtain the pressure drop across a fixed tube length. From these measurements, the wall shear stress τ_w and the nominal wall shear rate $8V/D$ were calculated. Error propagation analysis indicated errors of 0.5% and 0.6% in τ_w and $8V/D$, respectively. These data were then transformed by the Rabinowitsch-Mooney method to obtain the flow curve. Since three different tube diameters over a fixed tube length were used, a check for the presence of wall slip was made. If all the flow curves obtained for the three tube diameters collapsed onto a single curve, this indicated non-presence of wall slip. Various model fits were then made to the flow curve data whilst ensuring the shear stress range used for the model fit was similar to that covered by the flume. It was found that the 1.5 to 5.3 % vol carboxymethyl cellulose solutions, 3.5 to 6.8 % vol bentonite in water suspensions and 3.4 to 9.2% vol kaolin in water suspensions were best represented by the power law, Bingham plastic and Herschel-Bulkley models, respectively. The correlation coefficient was used as the criterion for determining the best model fit. The variation of the model parameters τ_y , k and n with solids concentration for each fluid are given in Table 1.

3.4.1 Data

The data for flow of three different non-Newtonian fluids in four channel shapes are summarised in a database available at http://www.cput.ac.za/flowpro/flumedata_2010.pdf. An example dataset is given in Table 3.2 and as a Moody chart in Fig.3.2.

A detailed analysis of this database has been carried out Burger et al. (2010a; 2010b), Haldenwang et al. (2004a; 2004b), Alderman and Haldenwang (2007), and Haldenwang & Slatter (2006b). The main findings are summarised below.

3.5 Laminar flow

Data in the laminar flow regime can be represented by a straight line of -1 slope in the Moody chart defined by (Burger et al. 2010a)

$$f = \frac{K}{Re_H} \quad (3.1)$$

where K = numerical coefficient depending on channel shape. Plots of f versus Re_H for flow of three non-Newtonian fluids of varying concentrations listed in Table 3. 1 in rectangular, triangular, semi-circular and triangular flumes was obtained by Burger et al. (2010a) together with their corresponding $f \times Re_H$ versus Re_H plots. Example plots are given in Figure 3.3 (a) and (b), respectively

The average K values for the four channel shapes were obtained using Burger et al. (2010a)

$$K = \frac{16\rho g(A/P) \sin \theta}{\tau_y + k \left(\frac{2VP}{A} \right)^n} \quad (3.2)$$

The K values found were 14.6 for triangular flumes with a vertex angle of 90°, 16.2 for semi-circular flumes, 16.4 for rectangular flumes and 17.6 for trapezoidal flumes with 60° sides. These values agree well with those found by Straub et al. (1958) and Chow (1959) for open channel flow of Newtonian fluids except for the trapezoidal flume, for which $K = 15$ resulted from numerical analysis. Because of this close agreement, Eqs. (2.59) and (3.1) provide a general basis for predicting laminar flow of Newtonian and non-Newtonian fluids in open channels of various cross-sections provided that the K value for the channel slope and the fluid properties are known.

The various models available for predicting the laminar flow of the power law, Bingham plastic and Herschel-Bulkley fluids in open channels were compared using data from this database (Burger et al., 2010a, 2010b, Alderman and Haldenwang, 2007). These various non-Newtonian, laminar flow models were summarised by Burger et al. (2010b). The comparison was done using two different approaches:

- (1) Comparison of measured wall shear stresses with model wall shear stresses where $\tau_w = R_h \rho g \cdot \sin\theta$ and the model wall shear stress is given by an appropriate equation using measured values of R_h and V .
- (2) Comparison of actual velocities with model velocities with the actual velocity is simply the volumetric discharge divided by the flow cross-sectional area and the model velocity is given by the appropriate equation for the model using measured values of R_h and τ_w .

Figures 3.4 and 3.5 compare Eqs. (2.59) and (3.1) with the Kozicki and Tiu (1967), and Coussot (1994) models for predicting laminar flow of a power law fluid in the triangular flume using shear stress and velocity, respectively, as a basis. Despite excellent agreement is observed from the three models, the present approach gave the best fit (Burger et al. 2010b). Although similar conclusions were also found for laminar flow of power law fluids in other flume shapes, this was not the case for laminar, open channel flow of Bingham and Herschel-Bulkley fluids. Figures 3.6 and 3.7 are similar to Figs.3.4 and 3.5 but for laminar flow of a Herschel-Bulkley fluid in the trapezoidal flume. Although the model shear stresses from the three models were found to fall within $\pm 15\%$ of the measured values, the present model gave again the best fit (Burger et al. 2010b). Despite the scatter in Fig. 3.7, this model was found to be the best for estimating velocities. The scatter was ascribed to the introduction of the yield stress as a parameter in the velocity calculation (Burger et al., 2010b).

3.6 Laminar-turbulent transition

The transition from laminar to turbulent flow of Newtonian fluids in open channels has been reported to occur at Reynolds numbers between 2,000 and 3,000 (Straub et al. 1958). Few attempts were made to predict the laminar-turbulent transition of non-Newtonian fluids in open channels. The methods for predicting this transition was reviewed by Alderman and Haldenwang (2007). Of these, Haldenwang's transition model (Haldenwang 2003, Alderman and Haldenwang 2007) is the only available model applicable for power law, Bingham plastic and Herschel-Bulkley fluids. This model was developed for rectangular open channels based on the Froude number and the point viscosity at a shear rate of 100 s^{-1} . In plotting R_H against the Froude number $F = V/(gh)^{0.5}$, a trend similar for all test materials was observed such that the onset of transition is distinguishable for each slope. With the transition onset for each slope deemed to be the point of deflection of the appropriate R_H versus F curve, he found that this point corresponded always to the deviation from the $16/R_H$ line on the Moody chart. It was found that the transition

occurred at much lower Reynolds numbers than that for Newtonian fluids. Work is currently in progress to extend this work to other channel shapes.

3.7 Turbulent flow

A review of the various models for predicting turbulent flow of non-Newtonian fluids in rectangular open channels was given by Alderman and Haldenwang (2007). This included Manning's equation for turbulent open channel water flow (Chow 1959) since it is still used in the minerals industry. The relevance of Manning's equation for non-Newtonian open channel flow was investigated by Haldenwang (2003), Burger et al. (2010b), and Haldenwang & Slatter (2006b). A comparison of Manning's equation with the four different models, three of which were adapted from pipe flow, indicated good agreement despite the lack of rheological parameters in the equation. Figure 3.8 shows that the Manning, Torrance (1963) and Slatter (1994) models predict velocities higher than the actual. Despite the scatter, both the Wilson-Thomas (Wilson and Thomas 1985, Thomas and Wilson 1987), and Haldenwang (2003) models appear to predict velocities close to the actual used. Of these two models, the Haldenwang model for turbulent flow has the least scatter. Work is currently in progress to extend this work to other channel shapes.

3.8 Conclusions

The database published herein was used to expand work originally published by Haldenwang (2003) and Haldenwang & Slatter (2006a) from rectangular channels to other-shaped channels. It was found for laminar, non-Newtonian open channel flow, that the relationship $f = K/R_e$ is applicable provided the appropriate flow curve model is used to describe the non-Newtonian material property. The K value was found to depend on the channel shape. Further research is needed to extend the work done on transitional and turbulent flow in rectangular channels to other shapes.

3.9 Notation

A	cross-sectional area (m ²)
B	flume width (m)
D	pipe diameter (m)
<i>f</i>	Fanning friction factor (-)
F	Froude number (-)
g	gravitational acceleration (m/s ²)
h	flow depth (m)
k	fluid consistency coefficient (Pa.s ⁿ)
K	laminar flow constant (-)
n	flow behaviour index (-)
P	wetted perimeter (m)
R _h	hydraulic radius (m)
R _H	Haldenwang Reynolds number (-)
V	average velocity (m/s)
W	width (m)

θ	slope angle from the horizontal (degrees)
ρ	density (kg/m^3)
τ_w	wall shear stress (Pa)
τ_y	yield stress (Pa)

3.10 References

Alderman, N.J. & Haldenwang, R. 2007. A review of Newtonian and non-Newtonian flow in rectangular open channels. *Hydrotransport 17, The Southern African Institute of Mining and Metallurgy and the BHR Group*, Cape Town, SA, 87-106.

Burger J.H., Haldenwang R., Alderman N.J. 2010. Friction factor-Reynolds number relationship for laminar flow of non-Newtonian fluids in open channels of different cross-sectional shapes. *Chemical Engineering Science*, 65(11): 3549-3556.

Burger J.H., Haldenwang R., Alderman N.J. (2010b). Laminar flow of non-Newtonian fluids in open channels of different cross-sectional shapes. *J. South African Inst. Min. Metall.* (submitted).

Chow, V.T. 1959. *Open Channel Hydraulics*. New York: McGraw-Hill. 9-12.

Coussot, P. 1994. Steady laminar flow of concentrated mud suspensions in open channels. *Journal of Hydraulic Research*, 4(32): 535-558.

Fitton, T.G. 2007. Tailings beach slope prediction. Unpublished PhD thesis, Royal Melbourne Institute of Technology, University, Melbourne, Australia.

Fitton, T.G. 2008. Non-Newtonian Open Channel Flow – A Simple Method of Estimation of Laminar/Turbulent Transition and Flow Resistance. *Paste 2008*, Kasane, Botswana, 245-251.

Haldenwang, R., Slatter, P.T. & Chhabra, R.P. 2002. Laminar and Transitional Flow in Open Channels for Non-Newtonian Fluids. *Hydrotransport 15: 15th International Conference on the Hydraulic Transport of Solids in Pipes*. Banff, Canada, Organised by BHR Group, Cranfield, Bedfordshire, UK, 755-768.

Haldenwang, R. 2003. Flow of Non-Newtonian Fluids in Open Channels. Unpublished D. Tech. thesis. Cape Technikon, Cape Town SA.

Haldenwang, R., Slatter, P.T., Chhabra, R.P. 2004a. Prediction of Transition for Non-Newtonian Open Channel Flow. *11th International Conference on Transport and sedimentation of solid particles*, Prague Czech Republic, 387-396.

Haldenwang, R., Slatter, P.T., Vanayza, S., & Chhabra, R.P. 2004b. The Effect of Shape on Laminar Flow in Open Channels for Non-Newtonian Fluids. *16th International conference on Hydrotransport*, Santiago Chile, 311-324.

Haldenwang, R. & Slatter, P.T. 2006a. Experimental Procedure and Database for Non-Newtonian Open Channel Flow. *Journal Hydraulic Research*. 44(2): 283-287.

Haldenwang, R. & Slatter, P.T. 2006b. Turbulent Non-Newtonian Open Channel Flow. *12th International. Conference on Transport and sedimentation of solid particles*, Tbilisi, Georgia, 135-144.

Kozicki, W. & Tiu, C. 1967. Non-Newtonian Flow Through Open Channels. *Canadian Journal of Chemical Engineers*, 45: 127-134.

Naik, B. 1983. Mechanics of Mudflow Treated as the Flow of a Bingham Fluid. Unpublished PhD thesis. Washington State University.

Slatter, P.T. 1994. Transitional and Turbulent Flow of Non-Newtonian Slurries in Pipes. Unpublished PhD thesis. University of Cape Town, Cape Town SA.

Spelay, R., Sumner, R.J., Sanders, R.S. & Gillies, R.G. 2006. Laminar Open Channel Flow of Kaolin Clay Slurries Containing Sand. *13th International Conference Transport and sedimentation of solid particles*, Tbilisi Georgia, 300-317.

Spelay, R. 2007. Solids Transport in Laminar, Open Channel Flow of Non-Newtonian Slurries. Unpublished PhD thesis. University of Saskatchewan, Saskatoon CA.

Straub, L.G., Silberman, E. & Nelson, H.C. 1958. Open Channel Flow at Small Reynolds Numbers. *American Society of Civil Engineers*, 123: 685–713.

Thomas, A.D., Wilson, K.C. 1987. New Analysis of Non-Newtonian Turbulent Flow: Yield Power Law Fluids. *Canadian Journal of Chemical Engineers*, 65(2): 335-338.

Torrance, B. McK. 1963. Friction Factors for Turbulent Non-Newtonian Flow in Circular Pipes, *South African Mechanical Engineers*, 13: 89-91.

Wang, Z.-Y. & Plate, E.J. 1996. A Preliminary Study on the Turbulence Structure of Flows of Non-Newtonian Fluid. *Journal Hydraulic Research*, 34(3): 345-361.

Wang, Z.-Y. 2002. Free Surface Instability of Non-Newtonian Laminar Flows. *Journal Hydraulic Research*, 40(4): 449-460.

Wilson, K.C. & Thomas, A.D. 1985. A New Analysis of the Turbulent Flow of Non-Newtonian Fluids. *Canadian Journal of Chemical Engineers*, 63: 539-546.

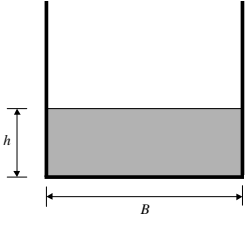
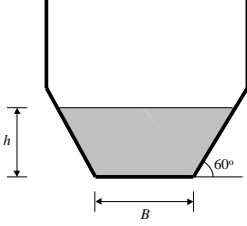
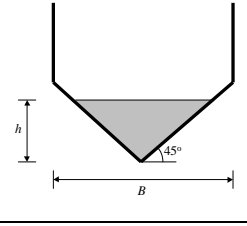
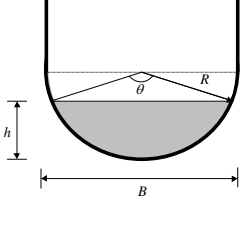
Section	Size	Cross-sectional area A	Wetted perimeter P	Surface width W
	$B = 300 \text{ mm}$ $B = 150 \text{ mm}$	Bh	$B + 2h$	B
	$B = 150 \text{ mm}$ $B = 75 \text{ mm}$	$h(B + xh)$ where $x = 1/\tan\theta$	$B + 2h\sqrt{1 + x^2}$ where $x = 1/\tan\theta$	$B + 2xh$ where $x = 1/\tan\theta$
	$B = 300 \text{ mm}$	h^2	$2h\sqrt{2}$	$2h$
	$B = 300 \text{ mm}$ $B = 150 \text{ mm}$	$\frac{D^2}{8}(\theta - \sin\theta)$ where $\theta = 2\cos^{-1}\left(1 - \frac{2h}{D}\right)$	$D\left(\frac{1}{2}\theta\right)$ where $\theta = 2\cos^{-1}\left(1 - \frac{2h}{D}\right)$	$D\left(\sin\frac{1}{2}\theta\right)$ where $\theta = 2\cos^{-1}\left(1 - \frac{2h}{D}\right)$

Figure 3.1 Various flume shapes used in experiments for area and perimeter for channel shapes used in this research

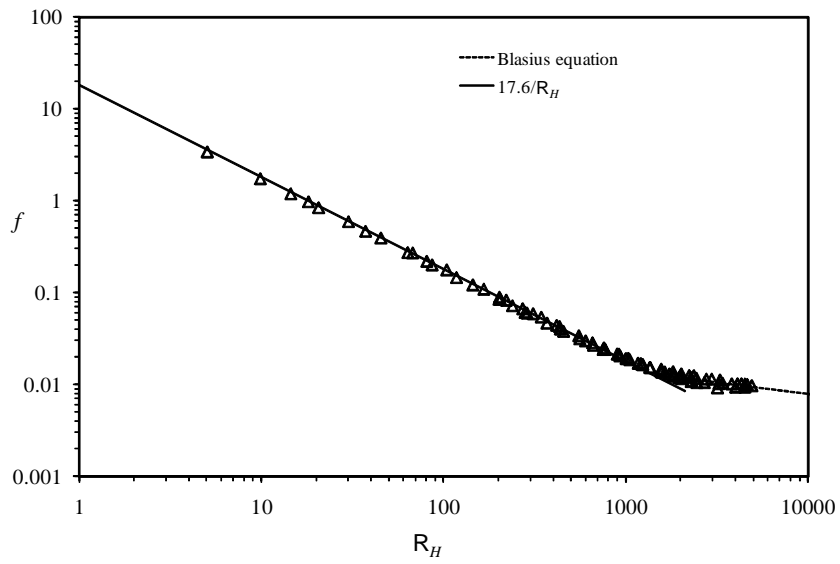
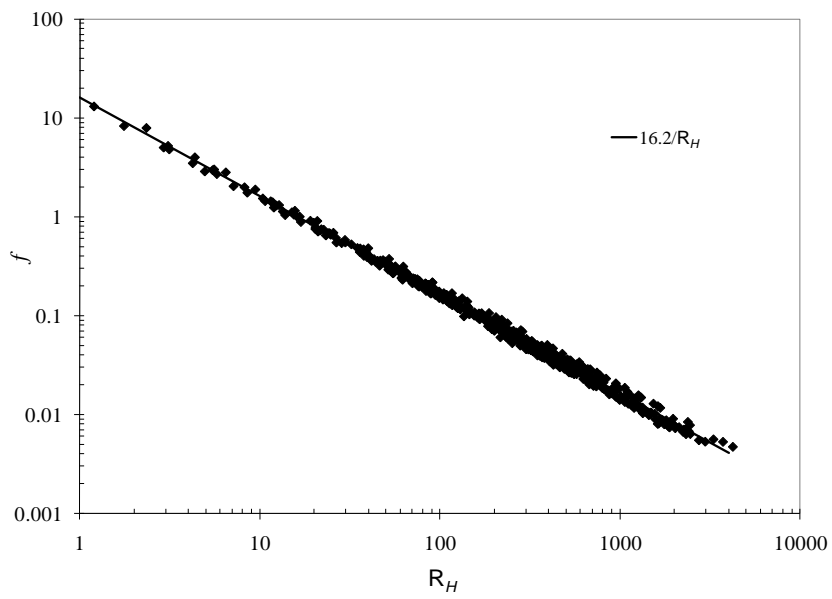
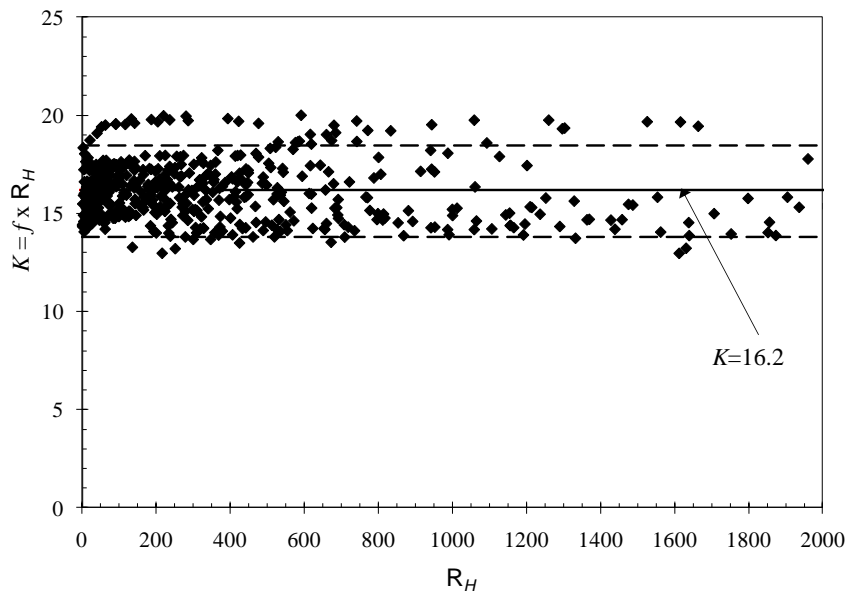


Figure 3.2 Moody diagram with $f = 17.6/R_H$ for 7.1% kaolin suspension in 150 mm trapezoidal flume



(a)



(b)

Figure 3.3 Plots of (a) f versus R_H and (b) $f \times R_H$ versus R_H for laminar flow of three different non-Newtonian fluids in semi-circular flume at angles of 1° to 5°

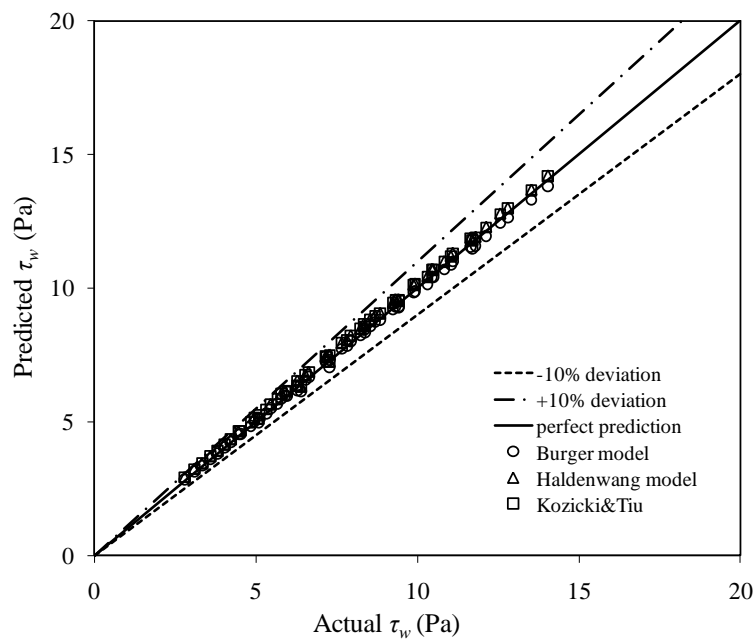


Figure 3.4 Model comparison based on shear stress for laminar flow of 4.89% CMC solution in 300 mm triangular flume

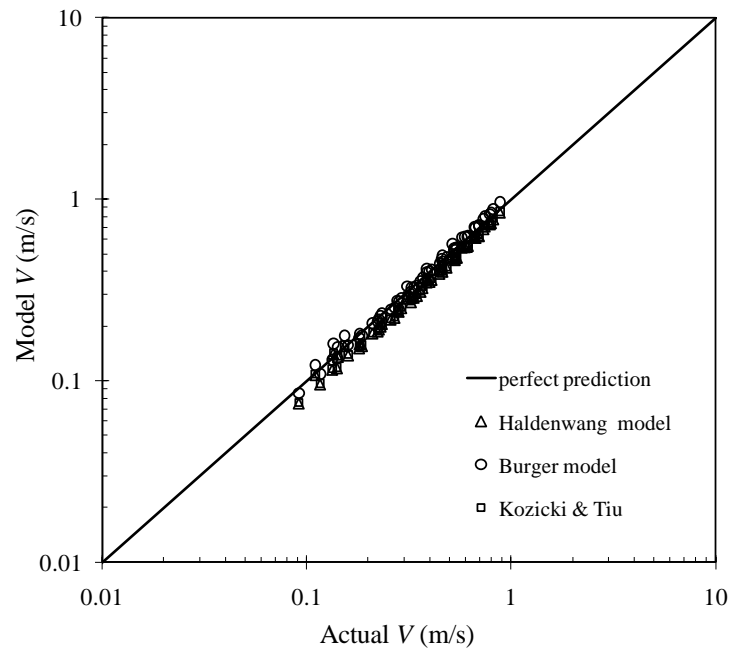


Figure 3.5 Model comparison based on velocity for laminar flow of 4.89% CMC solution in 300 mm triangular flume

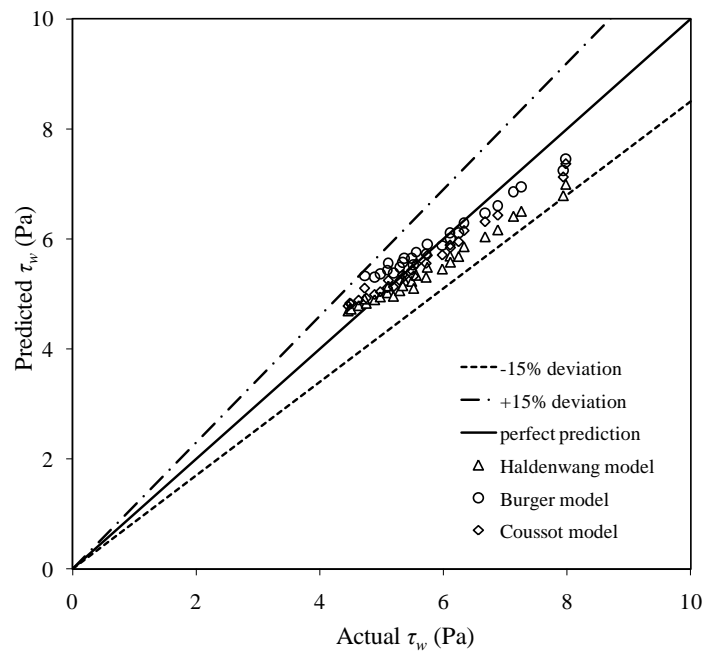


Figure 3.6 Model comparison based on shear stress for laminar flow of 5.4% kaolin suspension in 75 mm trapezoidal flume

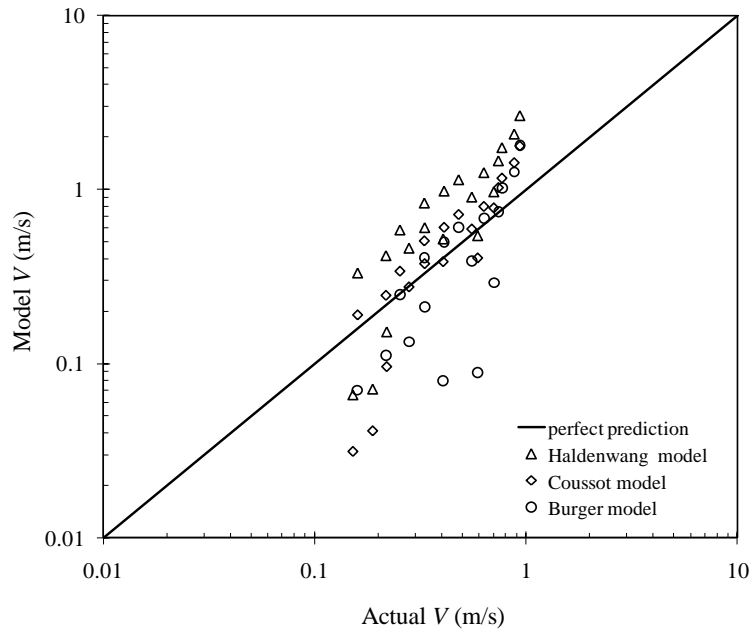


Figure 3.7 Model comparison based on velocity for laminar flow of 5.4% kaolin suspension in 75 mm trapezoidal flume

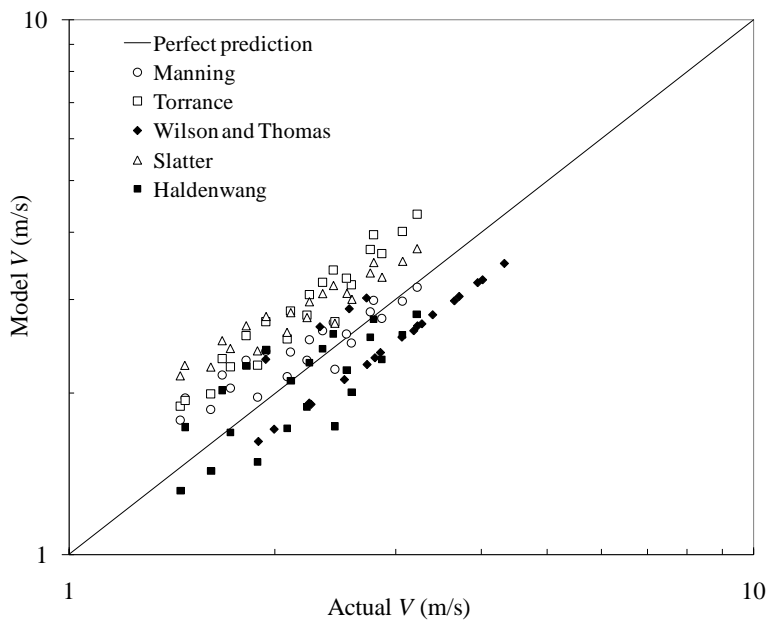


Figure 3.8 Comparison of Herschel-Bulkley models for turbulent flow of 6% kaolin suspension ($\tau_y = 6.8 \text{ Pa}$, $K = 0.149 \text{ Pa s}^n$, $n = 0.52$) in 150 mm smooth rectangular flume

Table 3.1 Materials tested

CMC solutions				
Concentration (%vol.)	Density (kg/m ³)	τ_y (Pa)	k (Pa.s ⁿ)	n
1.5	1008	-	0.014	0.944
2.0	1013	-	0.035	0.776
3.0	1018	-	0.145	0.788
3.1	1018	-	0.091	0.823
4.0	1023	-	0.330	0.727
4.9	1028	-	0.599	0.690
5.3	1028	-	0.920	0.678
Bentonite in water suspensions				
3.5	1022	3.00	0.0036	1
4.5	1027	4.30	0.0036	1
4.8	1029	5.66	0.0036	1
4.9	1030	5.20	0.0040	1
5.4	1033	7.25	0.0038	1
6.2	1038	15.78	0.0064	1
6.8	1042	18.34	0.0078	1
Kaolin in water suspensions				
3.4	1056	1.30	0.051	0.568
3.5	1058	0.50	0.061	0.560
5.0	1082	3.58	0.060	0.630
5.4	1089	4.40	0.084	0.582
7.0	1115	8.18	0.142	0.570
7.1	1117	11.6	0.148	0.557
9.0	1148	19.0	0.210	0.616
9.2	1152	18.9	0.194	0.550

Table 3.2 Flume data for flow of 7.1% kaolin suspension in a 150 mm trapezoidal flume

Material:	Kaolin
Concentration (% vol)	7.1
Density (kg/m ³)	1118.0
τ_y (Pa)	11.56
K (Pa.s ⁿ)	0.148
n	0.557
Flume width (mm)	150
Flume Shape	Trapezoidal

Slope flume (deg)	Flow Q (l.s ⁻¹)	Depth h (m)	Slope flume (deg)	Flow Q (l.s ⁻¹)	Depth h (m)	Slope flume (deg)	Flow Q (l.s ⁻¹)	Depth h (m)	Slope flume (deg)	Flow Q (l.s ⁻¹)	Depth h (m)	Slope flume (deg)	Flow Q (l.s ⁻¹)	Depth h (m)
1	0.545	0.0688	2	0.500	0.0386	3	0.636	0.0261	4	1.014	0.0211	5	1.502	0.0176
1	0.826	0.0712	2	0.730	0.0397	3	0.860	0.0270	4	1.317	0.0218	5	1.800	0.0180
1	1.041	0.0726	2	0.918	0.0408	3	1.089	0.0276	4	1.710	0.0221	5	2.122	0.0187
1	2.051	0.0784	2	1.126	0.0416	3	1.522	0.0284	4	2.044	0.0227	5	2.428	0.0189
1	2.566	0.0811	2	1.595	0.0431	3	2.119	0.0291	4	2.501	0.0232	5	2.848	0.0195
1	3.267	0.0826	2	2.175	0.0444	3	2.566	0.0293	4	3.006	0.0238	5	3.521	0.0203
1	4.191	0.0868	2	2.596	0.0450	3	3.037	0.0294	4	4.045	0.0251	5	4.080	0.0213
1	5.077	0.0904	2	3.072	0.0453	3	4.110	0.0313	4	4.422	0.0252	5	4.439	0.0217
1	6.017	0.0939	2	4.181	0.0464	3	5.103	0.0328	4	5.055	0.0265	5	5.092	0.0226
1	8.041	0.0997	2	4.686	0.0474	3	6.160	0.0345	4	6.161	0.0280	5	6.263	0.0244
1	10.057	0.1044	2	5.251	0.0481	3	7.147	0.0362	4	7.066	0.0296	5	7.148	0.0257
1	15.411	0.1135	2	6.102	0.0489	3	7.998	0.0377	4	8.111	0.0315	5	8.046	0.0273
1	20.825	0.1209	2	6.960	0.0498	3	9.338	0.0402	4	9.146	0.0333	5	9.182	0.0291
1	24.689	0.1249	2	8.056	0.0515	3	10.199	0.0416	4	10.251	0.0349	5	10.170	0.0309
1	28.576	0.1293	2	9.106	0.0530	3	12.533	0.0459	4	12.653	0.0392	5	13.860	0.0363
1	33.534	0.1363	2	10.093	0.0548	3	14.379	0.0491	4	16.005	0.0450	5	22.048	0.0497
1	37.774	0.1424	2	13.102	0.0603	3	16.291	0.0529	4	22.258	0.0554	5	27.985	0.0581
1	40.948	0.1463	2	16.086	0.0660	3	20.038	0.0597	4	24.767	0.0596	5	35.189	0.0681
			2	22.680	0.0787	3	22.484	0.0639	4	30.657	0.0680			
			2	28.563	0.0892	3	28.507	0.0739	4	35.975	0.0754			
			2	33.090	0.0962	3	33.039	0.0812	4	39.918	0.0805			
			2	38.588	0.1044	3	40.076	0.0910	4	43.345	0.0846			
			2	44.308	0.1136				4	45.820	0.0874			

CHAPTER 4

RESULTS

Friction factor-Reynolds number relationship for laminar flow of non-Newtonian fluids in open channels of different cross-sectional shapes

Published as

Burger, J.H., Haldenwang, R. and Alderman, N.J. (2010), Friction factor-Reynolds number relationship for laminar flow of non-Newtonian fluids in open channels of different cross-sectional shapes. *Chemical Engineering Science*.

Vol 6, No 11, 3549–3556.

Chapter 4 Friction factor-Reynolds number relationship for laminar flow of non-Newtonian fluids in open channels of different cross-sectional shapes

4.1 Abstract

The effect of channel shape on the friction factor-Reynolds number relationship for laminar, open channel flow of three non-Newtonian fluids was investigated. For each channel shape, the data can be described by a general relationship, $f = K/Re_H$ where f is the Fanning friction factor and Re_H is the appropriate Haldenwang et al. (2002) Reynolds number corresponding to the flow curve model used to describe the non-Newtonian behaviour exhibited by the test fluid. The K values were found to be 14.6 for triangular channels with a vertex angle of 90° , 16.2 for semi-circular channels, 16.4 for rectangular channels and 17.6 for trapezoidal channels with 60° sides. These K values were found to be in line with those reported by Straub et al. (1958) and Chow (1969) for open channel flow of Newtonian fluids as opposed to the assumption made by Haldenwang et al. (2002, 2004) of using a constant value of 16 based on the pipe flow paradigm for all channel shapes.

Keywords: Open channel, Cross sectional shape, Non-Newtonian fluid, Friction factor, Reynolds number, Rheology, Laminar flow.

4.2 Introduction

The effect of cross sectional shape on non-Newtonian open channel flow design has not been fully investigated and understood. Although datasets are available for non-Newtonian flow in rectangular open channels Coussot (1994), Haldenwang (2003) and Haldenwang & Slatter (2006) and in semi-circular open channels Fitton (2007; 2008), there were none available for non-Newtonian flow in other cross-sectional shaped channels. However, the Flow Process Research Centre at the Cape Peninsula University of Technology have recently extended the experimental database created by Haldenwang (2003) to include the test work carried out on the flow of three non-Newtonian fluids in five tilting flumes of various cross-sectional shapes.

In this study, an investigation was made on the effect of channel shape on the friction factor-Reynolds Number relationship for laminar, open channel flow of non-Newtonian fluids. A check was also made on the validity of the pipe flow paradigm of $f = 16/Re_H$ used by Haldenwang et al. (2002), Haldenwang (2003) and Haldenwang et al. (2004) for open rectangular channels to other shaped channels.

4.3 Background

The effect of channel shape on laminar flow of Newtonian and non-Newtonian fluids in open channels is of interest for a variety of industrial applications. Channels with rectangular, semi-circular and trapezoidal cross-sections are often encountered in the minerals industry where the tailings are transported from the mine to the disposal

facilities (Haldenwang and Slatter, 2006). Non-Newtonian flow in channels with various cross-sections also occurs in the wastewater and food processing industries (Fitton, 2008).

Flow of water in a variety of open channels has been investigated by several researchers Straub et al. (1958) and Chow (1959). Along with experimental data, Straub et al. (1958) presented a theory for laminar flow of Newtonian fluids in open channels with various cross-sections. They showed that the data in the laminar flow regime can be defined by a general relationship $f = K/Re$ where f is the Fanning friction factor and Re is the Newtonian Reynolds number and that K is “a purely numerical coefficient dependent on the channel shape”. Analytical and numerical solutions for K were provided for rectangular, semi-circular, elliptical, 60° , 90° and 120° triangular and trapezoidal channels.

They found that the predicted f vs. Re line for smooth-walled, rectangular, triangular and semi-circular-shaped channels to be coincident with the experimental data when plotted as a f vs. Re plot. For rectangular channels where the water height to channel width (h/W) ratios ranged from 0.08 to 0.37, K was found to vary from 19.75 to 15.25 compared with the corresponding analytical values of 21.5 to 16.25. For triangular channels where the vertex angle ranged from 30° to 150° , K was found to be 14.25 and independent of the vertex angle. This is in excellent agreement with the analytical value of 14.23 for 90° channel and the numerical value of 14.15 for the other triangular channels. For semi-circular channels, they stated that the f vs. Re plot showed the data to be “grouped” about the $f = K/Re$ line where K was found analytically to be 16.

In his authoritative book on open channel flow, Chow (1959) produced a f vs. Re plot for flow of water in smooth-walled, rectangular and triangular channels based on the two datasets of Straub et al. (1958) and Lansford & Robertson (1958). Here, K was found to be approximately 24 for the rectangular channels and 14 for the triangular channels.

Very little has been reported in the literature for predicting non-Newtonian laminar flow in open channels of arbitrary cross-section. The only method available was that proposed by Kozicki and Tiu (1967, 1986). In developing their model, the Rabinowitsch-Mooney equation applicable to pipe and slit flow was generalised to obtain the fully-developed laminar friction factors of non-Newtonian fluids in non-circular channels. They introduced a generalised Reynolds number, Re^* such that the friction factor for fully-developed laminar flow through any constant cross-section channel is given by

$$f = \frac{16}{Re^*} \quad (2.37)$$

where

$$Re^* = \frac{\rho V^{2-n^*} R_h^{n^*}}{2^{n^*-3} k^*} \quad (2.38)$$

where n^* and k^* are defined by

$$n^* = \frac{d \ln \bar{\tau}_w}{d \ln \left[\frac{2V}{R_h} \right]} \quad (2.39)$$

and

$$k^* = \frac{\bar{\tau}_w}{\left[\frac{2V}{R_h} \right]^{n^*}} \quad (2.40)$$

They concluded that Re^* can be used as “a criterion for the existence of laminar flow in the general case involving a non-Newtonian fluid and arbitrary cross section”. Through substitution of appropriate expressions for n^* and k^* , they obtained Re^* expressions for the power law and Bingham plastic fluids. These are given respectively by

$$Re_p^* = \frac{R_h^n V^{2-n} \rho}{2^{n-3} k \left(\frac{a + bn}{n} \right)^n} \quad (2.34)$$

and

$$Re_B^* = \frac{4R_h V \rho}{\eta_B} \left[\frac{1}{a+b} - \frac{\chi}{b} + \frac{a}{b(a+b)} \chi^{\frac{b}{a}+1} \right] \quad (2.37)$$

where a and b are the geometrical parameters relating to the shape of the flow geometry and χ is the ratio of Bingham yield stress to wall shear stress, τ_{yB}/τ_w with $\tau_w = R_h \rho g \sin \theta$.

Following the approach of Kozicki and Tiu (1967, 1986), Coussot (1994) derived an expression for Re^* for the Herschel-Bulkley fluid. Unfortunately, this was found to be erroneous since it did not contain the power law exponent anywhere within the expression.

The shape factors used by Kozicki and Tiu (1967, 1986) in Eq.'s (2.34) and (2.37) were those evaluated from analytical solutions for flow of *Newtonian* fluids in the open channel of the same cross-section. Values of a and b for various open channels can be found in the paper by Kozicki and Tiu (1986). No experimental work was carried out by Kozicki and Tiu (1967, 1986) to validate their model.

Few experimental studies have been made on the effect of shape on flow of non-Newtonian flow in open channels. Coussot (1994) provided some data for the flow of a Herschel-Bulkley fluid in rectangular and trapezoidal channels.

Fitton (2007, 2008) obtained data for flow of three different non-Newtonian fluids (carboxymethylcellulose, carbopol and thickened tailings) in semi-circular channels.

Haldenwang (2003) and Haldenwang & Slatter (2006) provided an extensive database for non-Newtonian flow in rectangular open channels. As a means of collapsing the laminar flow data for three different non-Newtonian fluids (kaolin, bentonite and carboxymethylcellulose) onto a single master curve on the f vs. Re plot, Haldenwang et al. (2002) defined a new Reynolds number based on the Herschel-Bulkley model that was adapted from the pipe Reynolds number presented by Slatter (1994). This is given by

$$Re_H = \frac{8\rho V^2}{\tau_y + k\left(\frac{2V}{R_h}\right)^n} \quad (2.59)$$

An advantage of using this Reynolds number is that it can also be used for fluids exhibiting Newtonian, power law and Bingham plastic behaviour. Through the use of Eq. (2.59) for Re , they found the laminar flow data for three non-Newtonian fluids did collapse onto the $f = K/Re_H$ line where $K = 16$. Furthermore, Alderman and Haldenwang (2007) found the model developed by Haldenwang et al. (2002) for laminar flow of power law, Bingham plastic and Herschel-Bulkley fluids in rectangular channels to be the most reliable in terms of predicting actual velocities as well as aligning to the $f = 16/Re_H$ line.

The database for non-Newtonian flow in rectangular channels was extended by Haldenwang et al. (2004) to include their limited study on non-Newtonian flow in semi-circular and trapezoidal channels. They looked at the efficiency of the definitions of the Reynolds number due to Haldenwang et al. (2002) and those of Kozicki and Tiu (1967) in correlating the laminar flow data on the f vs. Re plot for these channel shapes. For the range of shapes and fluids studied, they concluded the $f = K/Re_H$ line using the simpler Reynolds number proposed by Haldenwang et al. (2002) adequately predicts their experimental data in the laminar flow regime, provided the correct flow curve model is used to take account of the rheology of the test fluid used. Here, the pipe flow paradigm of $K = 16$ was used. Moreover, they found the Reynolds number defined by Kozicki and Tiu (1967, 1986) consisting of two shape factors did not predict their experimental data in the laminar flow regime as accurately. This was attributed to the yield stress having a significant effect that was not adequately taken into account.

In this study, the database used by Haldenwang (2003) for rectangular channels was extended to include non-Newtonian flow in semi-circular, trapezoidal and triangular channels. Using the Haldenwang et al. (2002) definition of Re , the effect of shape on the f vs. Re relationship for laminar, open channel flow of non-Newtonian fluids was investigated in some depth. Furthermore, a check was also made on the validity of the pipe flow paradigm of $f = 16/Re_H$ used by Haldenwang et al. (2002,2004) and Haldenwang (2003) for open rectangular channels to other shaped channels.

4.4 Materials and Methods

The tests were carried out in a 10 m long tilting flume designed and built by the Flow Process Research Centre at the Cape Peninsula University of Technology. Further details of this flume shown in Figure 4.1 can be found in Haldenwang (2003). This flume can be hydraulically tilted at various angles up to 5° from the horizontal. The width of this rectangular flume can be changed from 300 mm to 150 mm by placing a partition mid-section lengthways down the flume. By inserting an appropriate cross sectional insert, the rectangular flume can be changed into a flume with a triangular, semi-circular or trapezoidal cross-section. The various flume shapes with its dimensions used in this study are shown in Figure 4.3.

Flow curve measurements of the test material were also made in-situ during the flume test using an in-line tube viscometer shown in Figure 4.2 fitted with three tubes of different diameters, 13, 28 and 80 mm. Each of the three tubes was fitted with an electromagnetic flow meter and two differential pressure transducers across a fixed length. Calibration with water gave an error of less than 10% for both the flow rate and the pressure drop (Haldenwang, 2003).

A summary of the materials tested is given in Table 4.1. For these materials, the flow curve data from the three different tube diameters were found to collapse onto a single curve thus confirming the non-presence of wall-slip during the flow curve measurement. Various model fits were then made to the flow curve data. It was found that the 1.5 to 5.3% v/v carboxymethyl cellulose solutions, 3.5 to 6.2% v/v bentonite in water suspensions and 3.4 to 9.2% v/v kaolin in water suspensions was best represented by the power law, Bingham plastic and Herschel-Bulkley models respectively. The correlation coefficient was used here as the criterion for determining the best model fit. Also observed in Table 4.1 is the expected systematic variation of τ_w , k and n with solids concentration for each of the three fluids studied. This analysis also showed errors in the wall shear stress and wall shear rate to be very small (typically 0.1% and 0.6% of the wall shear stress and the wall shear rate values respectively). These findings are consistent with those found by Slatter (1994) who used the same range of materials in his pipe flow studies.

The flow rate of the material flowing down the flume was monitored using an electromagnetic flow meter whilst the flow depth at various channel slopes from 1° to 5° was made using digital depth gauges fitted at 5 and 6 m positions from the flume entrance. These positions were found to be the optimal positions for depth measurement (Haldenwang, 2003). Since the difference in fluid height between these two points was found to be minimal, the flow in the region can therefore be taken as steady flow. A data logger was used to record the various data outputs as a function of time. All of this data was then fed into a PC so that a f vs. Re_H plot can be generated as output.

4.5 Results and Discussions

The laminar flow data obtained for the three different non-Newtonian fluids in open channels of four different cross-sections were analysed using the approach of Haldenwang et al. (2002) for collapsing the data onto a single master curve on the f vs. Re_H plot. Here, the Fanning friction factor is given by

$$f = \frac{2R_h g \sin \theta}{V^2} \quad (2.13)$$

in which the hydraulic radius, R_h is defined as

$$R_h = \frac{A}{P} \quad (2.10)$$

where A is the cross-sectional area for flow and P is the wetted perimeter of the channel. Equations for A and P for each of the four different cross-sections can be found in Figure 4.3. For the Reynolds number, the Haldenwang et al. (2002) Reynolds number defined by Eq. (2.59) was used. Care was taken to ensure the data was indeed in the laminar flow regime by rejecting all data points where Re was greater than 2100 in addition to those which deviated from the K/Re line.

A f vs. Re_h plot for a selection of six different non-Newtonian fluid/open channel shape combinations is shown in Figure 4.4 together with the $f=16/Re$ line for laminar flow. Comparison of the experimental data in the laminar flow region with the pipe flow paradigm of $f=16/Re_h$ used by Haldenwang et al. (2002) appears to be reasonable. However, a closer examination of the f vs. Re_h data of all fluid/shape combinations revealed that the pipe flow paradigm of $f=16/Re_h$ did not always fit the data well. Figures 4.5 to 4.8 show the individual f vs. Re_h plots for the four of the six fluid/shape combinations used in Figure 4.4. Least square fits to each of these plots revealed an $f = K/Re_h$ relationship with the value of K dependent on the cross-sectional shape of the channel.

Substitution of Eq.'s (2.59), (2.13) and (2.10) into the $f = K/Re_h$ relationship leads to an expression for K in terms of the channel parameters and the fluid flow properties.

$$K = \frac{16\rho g(A/P) \sin \theta}{\tau_y + k\left(\frac{2VP}{A}\right)^n} \quad (3.2)$$

Although this equation is for fluids exhibiting Herschel-Bulkley behaviour, it can also be used for fluids exhibiting Newtonian, power law and Bingham plastic behaviour provided appropriate values for τ_y , k and n are used. For all of these fluids, it can be deduced from this equation that for a fluid of known flow properties flowing in an open channel of a fixed slope at a given velocity, K will be solely dependent on the channel shape through A/P . This general conclusion ties in with the same conclusion made by Straub et al. (1958) for Newtonian fluids. Error propagation analysis performed on all the measured and derived variables in Eq. (3.2) showed the maximum error in K for any fluid in any channel shape did not exceed +/-1.

The average K value in each of the four channel shapes was obtained using the approach of Judy et al. (2002). Using all of the experimental data for flow of three different non-Newtonian fluids of varying concentrations in each of the four channels of varying dimensions and slopes, an f vs. Re_h plot was obtained. These "combination" plots are

shown respectively in Figures 4.9, 4.11, 4.13 and 4.15 for rectangular, semi-circular, triangular and trapezoidal open channels. Together with these “combination” plots, the corresponding $f \cdot Re_H$ vs. Re_H plots were also obtained, Figures 4.10, 4.12, 4.14 and 4.16. The average K value quoted in Figures 4.9, 4.11, 4.13, and 4.15 was obtained by taking the mean of all the K values given in Figures 4.10, 4.12, 4.14 and 4.16. It can be seen from these plots that most of the experimental data lies within 1.2 to 1.6 SD (standard deviation) of the average K value.

For rectangular channels, K ranged from 12.5 to 20 giving an average value of 16.4. This was based on 647 data points of which 90% lie within 1.5 SD of the average K value. Hence, a 95% confidence level gave a upper limit of 16.5 and a lower limit of 16.3 based on the average K value. The range of K values found is broadly similar to the Straub et al. (1958) experimental values of 15.25 to 19.75 and analytical values of 16.25 to 21.5 for Newtonian flow. It is fortuitous that the pipe flow paradigm of $f = 16/Re_H$ used by Haldenwang et al. (2002) was found to be applicable in the earlier work carried out by Haldenwang (2003) on non-Newtonian flow in rectangular channels.

In the case of semi-circular channels, K ranged from 13.0 to 20 giving an average value of 16.2. This was based on 485 data points of which 89.7% lie within 1.5 SD of the average K value. Hence, a 95% confidence level dataset gave a upper limit of 16.3 and a lower limit of 16 based on the average K value. The value of 16.2 compared well with the value of 16 found analytically by Straub et al. (1958) for Newtonian flow. Given its similar geometry, it is perhaps not surprising that the pipe flow paradigm of $f = 16/Re_H$ (Haldenwang et al. 2002) was found to be applicable here.

For triangular channels with a vertex angle of 90° , K ranged from 11.9 to 18 giving an average value of 14.6. This was based on 326 data points of which 93% lie within 1.2 SD of the average K value. Hence, a 95% confidence level gave an upper limit of 14.7 and a lower limit of 14.4 based on the average K value. The value of 14.6 ties in well with the experimental value of 14.25 and the analytical value of 14.23 found by Straub et al. (1958) for Newtonian flow.

In the case of trapezoidal channels with 60° sides, K ranged from 14.7 to 21 giving an average value of 17.6. This was based on 460 data points of which 85.2% lie within 1.6 SD of the average K value. Hence, a 95% confidence level gave a upper limit of 17.7 and a lower limit of 17.4 based on the average K value. The value of 17.6 did not compare too well with the numerical value of 15 found by Straub et al. (1958) for Newtonian flow. For these two types of open channels, the pipe flow paradigm of $f = 16/Re_H$ was found not to be applicable.

Comparison of $f = K/Re$ lines using two different Re definitions were also made for a range of fluid/shape combinations. Here, the $f = K/Re_H$ line based on the Kozicki and Tiu (1967) Re definition for a power law or a Bingham plastic fluid, Eq. (2.41) or Eq. (2.44) was compared with the one based the Haldenwang et al. (2002) Re definition, Eq. (2.59). A representative f vs. Re_H plot for a CMC solution flowing in a semi-circular channel is given in Figure 4.17. This plot was found to show excellent agreement between the two $f = K/Re_H$ lines. This was also observed for the other CMC solutions/shape combinations. Hence, the K values using the Haldenwang et al.(2002) Re definition given above are equally applicable to those based on the Kozicki and Tiu (1967) Re definition for a power law fluid. However, this conclusion could not be said for bentonite suspensions for each of the four different channels since agreement between the two $f = K/Re_H$ lines was not obtained. Figure 4.18 gives an example plot

showing the large deviation between the two datasets. This discrepancy can be largely explained by the effect of the yield stress parameter which is not properly accounted for when calculating the Kozicki and Tiu (1967) Reynolds number for a Bingham plastic fluid.

For the range of fluids and channel shapes studied, it is clear from the “combination” plots that the $f = K/Re_H$ line using Eq. (2.59) for the calculation of Re adequately predicts the laminar flow data to within 1.2 to 1.6 SD of the average K value, provided that the correct flow curve model is used to describe the rheology of the test fluid. Apart from the incorrect assumption of $K = 16$, these findings do corroborate those made by Haldenwang et al. (2004) in their initial work with non-Newtonian flow in semi-circular and trapezoidal channels.

4.6 Conclusions

Detailed analysis on laminar flow of three non-Newtonian fluids in open channels of four different cross-sectional shapes revealed that open channel flow does differ from pipe flow and that the pipe flow paradigm of $f = 16/Re_H$ used previously by Haldenwang et al. (2002, 2004) for non-Newtonian laminar flow in open channels of different cross sectional shapes was found to be incorrect. With the Haldenwang et al. (2002) definition for Re in the f vs. Re_H relationship, it was found that $f = K/Re_H$ was more appropriate in describing non-Newtonian flow in open channels provided the appropriate flow curve model was used to describe the non-Newtonian property of the fluid. Due to the inability of properly accounting for the presence of yield stress in the calculation of Re when using the Kozicki and Tiu (1967) definition in the f vs. Re relationship, the Haldenwang et al. (2002) Re definition was found to be the better of the two.

For the three non-Newtonian fluids in four different channel shapes studied, it was found that the overall average K value was found to be 14.6 for triangular channels with a vertex angle of 90° , 16.2 for semi-circular channels, 16.4 for rectangular channels and 17.6 for trapezoidal channels with 60° sides. All of these K values were found to be similar to those found by Straub et al. (1958) and Chow (1969) for open channel flow of Newtonian fluids. Because of this close agreement, $f = K/Re_H$ using Eq. (2.59) for Re does provide us with a general equation for predicting laminar flow of Newtonian and non-Newtonian fluids in open channels of various cross-sections provided the K value for the channel shape and the flow properties of the fluid are known.

4.7 Acknowledgements

The authors would like to acknowledge the National Research Foundation of South Africa and the Cape Peninsula University of Technology for funding this research.

4.8 Notation

Symbol	Description	Units
a	shape factor constant Eq. (2.35)	-
A	cross-sectional area of flow	m^2
b	shape factor constant Eq. (2.35)	-

Symbol	Description	Units
f	Fanning friction factor	-
g	acceleration due to gravity	m/s^2
K	laminar flow constant in the f vs. Re relationship Eq. (3.1)	-
k	consistency coefficient	$Pa \cdot s^n$
k^*	consistency coefficient as defined by Eq. (2.40)	$Pa \cdot s^n$
k'	apparent consistency coefficient, Eq. (7.4)	$Pa \cdot s$
n	flow behaviour index	-
n^*	flow behaviour index as defined by Eq. (2.39)	-
P	Wetted perimeter	m
Re	Reynolds number	-
Re^*	generalised Reynolds number, Eq. (2.38)	-
Re^*_B	Kozicki and Tiu Bingham Reynolds number, Eq. (2.44)	-
Re^*_p	Kozicki and Tiu power law Reynolds number, Eq. (2.41)	-
Re_H	Haldenwang et al Reynolds number, Eq. (2.59)	-
R_h	hydraulic radius	m
V	average velocity	m/s
W	channel width	m
μ_B	Bingham plastic viscosity	$Pa \cdot s$
θ	slope angle from the horizontal	degrees
ρ	density	Kg/m^3
τ_w	wall shear stress	Pa
τ_y	yield stress	Pa
χ	ratio of Bingham yield stress to wall shear stress	-

4.9 References

Alderman, N.J. & Haldenwang, R. 2007. A review of Newtonian and non-Newtonian flow in rectangular open channels. *Hydrotransport 17, The Southern African Institute of Mining and Metallurgy and the BHR Group*, Cape Town, SA, 87-106.

Chow, V.T. 1959. *Open Channel Hydraulics*. New York: McGraw-Hill. 9-12.

Coussot, P. 1994. Steady laminar flow of concentrated mud suspensions in open channels. *Journal of Hydraulic Research*, 4(32): 535-558.

Fitton, T.G. 2007. Tailings beach slope prediction. Unpublished PhD thesis, Royal Melbourne Institute of Technology, University, Melbourne, Australia.

Friction factor-Reynolds number relationship for laminar flow of non-Newtonian fluids in open channels of different cross-sectional shapes

Fitton, T.G. 2008. Non-Newtonian Open Channel Flow – A Simple Method of Estimation of Laminar/Turbulent Transition and Flow Resistance. *Paste 2008*, Kasane, Botswana, 245-251.

Haldenwang, R., Slatter, P.T. & Chhabra, R.P. 2002. Laminar and Transitional Flow in Open Channels for Non-Newtonian Fluids. *Hydrotransport 15: 15th International Conference on the Hydraulic Transport of Solids in Pipes*. Banff, Canada, Organised by BHR Group, Cranfield, Bedfordshire, UK, 755-768.

Haldenwang, R. 2003. Flow of Non-Newtonian Fluids in Open Channels. Unpublished D. Tech. thesis. Cape Technikon, Cape Town SA.

Haldenwang, R., Slatter, P.T., Vanayza, S., & Chhabra, R.P. 2004. The Effect of Shape on Laminar Flow in Open Channels for Non-Newtonian Fluids. *16th International conference on Hydrotransport*, Santiago Chile, 311-324.

Haldenwang, R. & Slatter, P.T. 2006. Experimental Procedure and Database for Non-Newtonian Open Channel Flow. *Journal Hydraulic Research*. 44(2): 283-287.

Haldenwang, R & Slatter, P.T. 2006. Laminar Flow Models for Minerals Tailings Transport in Open Channels. *XXIIIth International Mineral Processing Congress*, Istanbul, Turkey, 3-8 Sept. 1759-1764.

Judy, J., Maynes, D. & Webb, B.W. 2002. Characterisation of Frictional Pressure Drop for Liquid Flows Through Microchannels. *International Journal Heat Mass Transfer*, 45 (17) 3477-3489.

Kozicki, W. & Tiu, C. 1967. Non-Newtonian Flow Through Open Channels. *Canadian Journal of Chemical Engineers*, 45: 127-134.

Kozicki, W. & Tiu, C. 1986. Parametric Modelling of Flow Geometries in Non-Newtonian Flows. *Encyclopaedia of Fluid Mechanics, Vol 7, (ed) N.P. Cheremisinof*. Houston: Gulf Publishing Co, 199 – 252.

Lansford, W.M. & Robertson, J.M. 1958. Discussion of Open Channel Flow at Small Reynolds Numbers by Straub, L.G., Silberman, E. & Nelson, H.C. *Transactions American Society of Civil Engineers*, 123: 707–712.

Slatter, P.T. 1994. Transitional and Turbulent Flow of Non-Newtonian Slurries in Pipes. Unpublished PhD thesis. University of Cape Town, Cape Town SA.

Straub, L.G., Silberman, E. & Nelson, H.C. 1958. Open Channel Flow at Small Reynolds Numbers. *American Society of Civil Engineers*, 123: 685–713.

Table 4.1 Summary of materials used

CMC solutions				
Concentration (%vol)	Density (kg/m ³)	τ_y (Pa)	k (Pa.s ⁿ)	n
1.5	1008	-	0.014	0.94
2.0	1013	-	0.035	0.78
3.0	1018	-	0.145	0.79
3.1	1018	-	0.091	0.82
4.0	1023	-	0.330	0.73
4.9	1028	-	0.599	0.69
5.3	1028	-	0.920	0.68
Bentonite in water suspensions				
Concentration (% vol)	Density (kg/m ³)	τ_y (Pa)	k (Pa.s ⁿ)	n
3.5	1022	3.0	0.0036	1
4.6	1028	5.7	0.0043	1
5.4	1033	7.5	0.0048	1
6.2	1038	15.8	0.0064	1
6.8	1042	18.3	0.0078	1
Kaolin in water suspensions				
Concentration (% vol)	Density (kg/m ³)	τ_y (Pa)	k (Pa.s ⁿ)	n
3.4	1056	1.3	0.051	0.57
3.5	1058	0.5	0.061	0.56
5.0	1082	3.6	0.060	0.63
5.3	1089	5.0	0.061	0.60
7.0	1115	8.2	0.142	0.57
7.1	1117	8.1	0.140	0.57
9.0	1148	20.4	0.267	0.53
9.2	1152	18.9	0.194	0.55

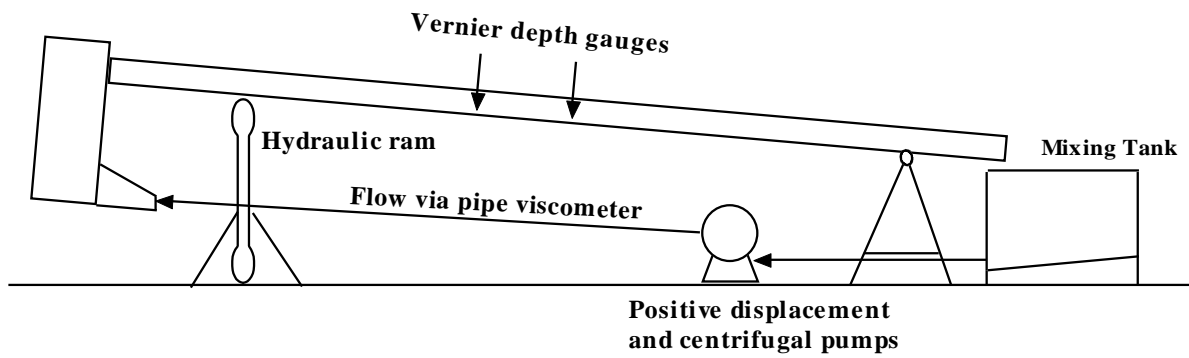


Figure 4.1 10 m flume rig

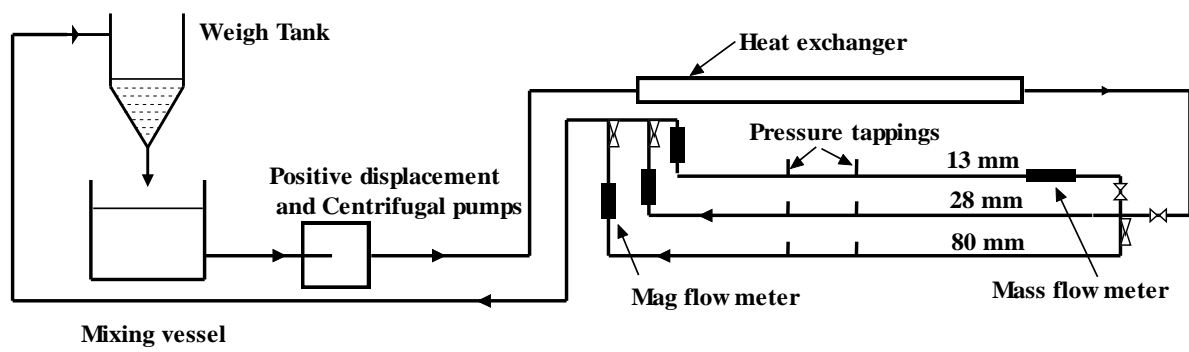


Figure 4.2 In-line pipe viscometer

Friction factor-Reynolds number relationship for laminar flow of non-Newtonian fluids in open channels of
different cross-sectional shapes

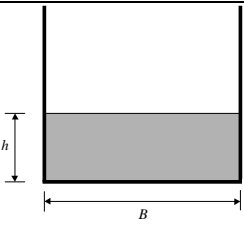
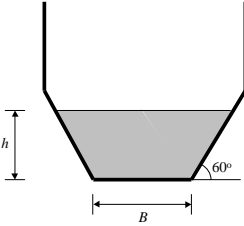
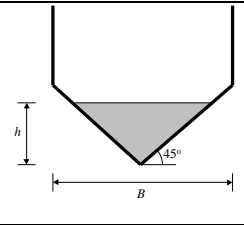
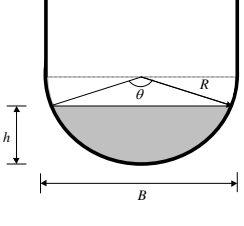
Section	Size	Cross-sectional area A	Wetted perimeter P	Surface width W
	$B = 300 \text{ mm}$ $B = 150 \text{ mm}$	Bh	$B + 2h$	B
	$B = 150 \text{ mm}$ $B = 75 \text{ mm}$	$h(B + xh)$ where $x = 1/\tan\theta$	$B + 2h\sqrt{1 + x^2}$ where $x = 1/\tan\theta$	$B + 2xh$ where $x = 1/\tan\theta$
	$B = 300 \text{ mm}$	h^2	$2h\sqrt{2}$	$2h$
	$B = 300 \text{ mm}$ $B = 150 \text{ mm}$	$\frac{D^2}{8}(\theta - \sin\theta)$ where θ $= 2\cos^{-1}\left(1 - \frac{2h}{D}\right)$	$D\left(\frac{1}{2}\theta\right)$ where θ $= 2\cos^{-1}\left(1 - \frac{2h}{D}\right)$	$D\left(\sin\frac{1}{2}\theta\right)$ where θ $= 2\cos^{-1}\left(1 - \frac{2h}{D}\right)$

Figure 4.3 Open channel shapes used in this study

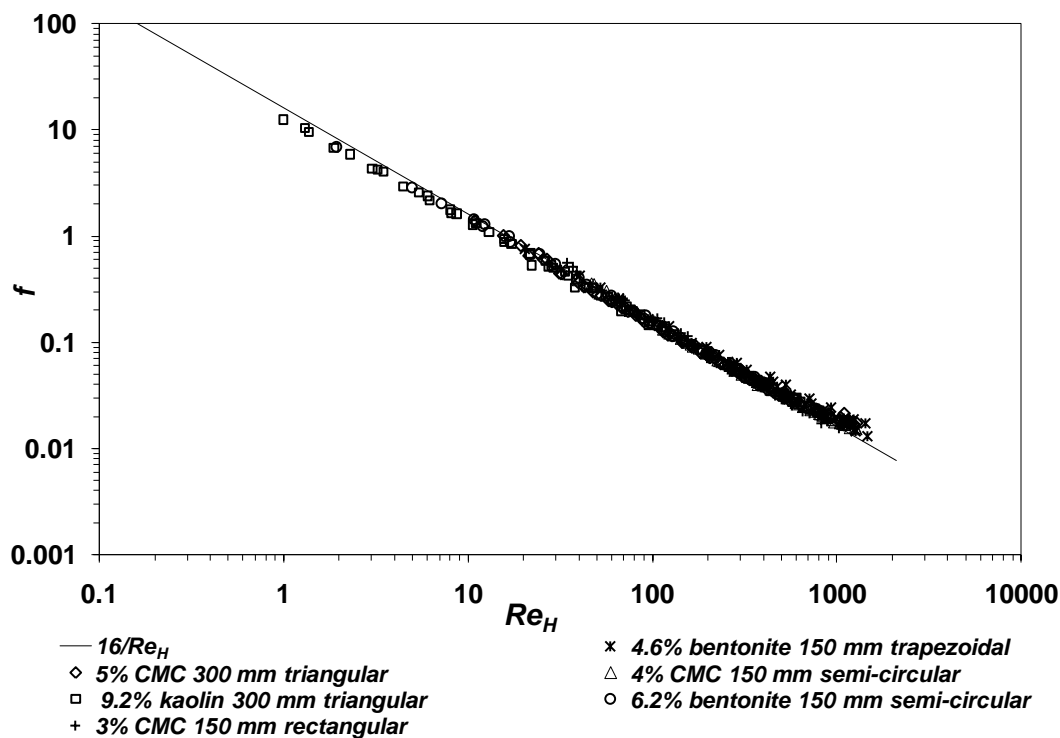


Figure 4.4 A f vs. Re_H plot for 4.6%, 6.2% bentonite, 3.1% CMC and 5.3%, 7.1% kaolin flowing in various cross sectional shape flumes at slope angles of 1 to 5 degrees.

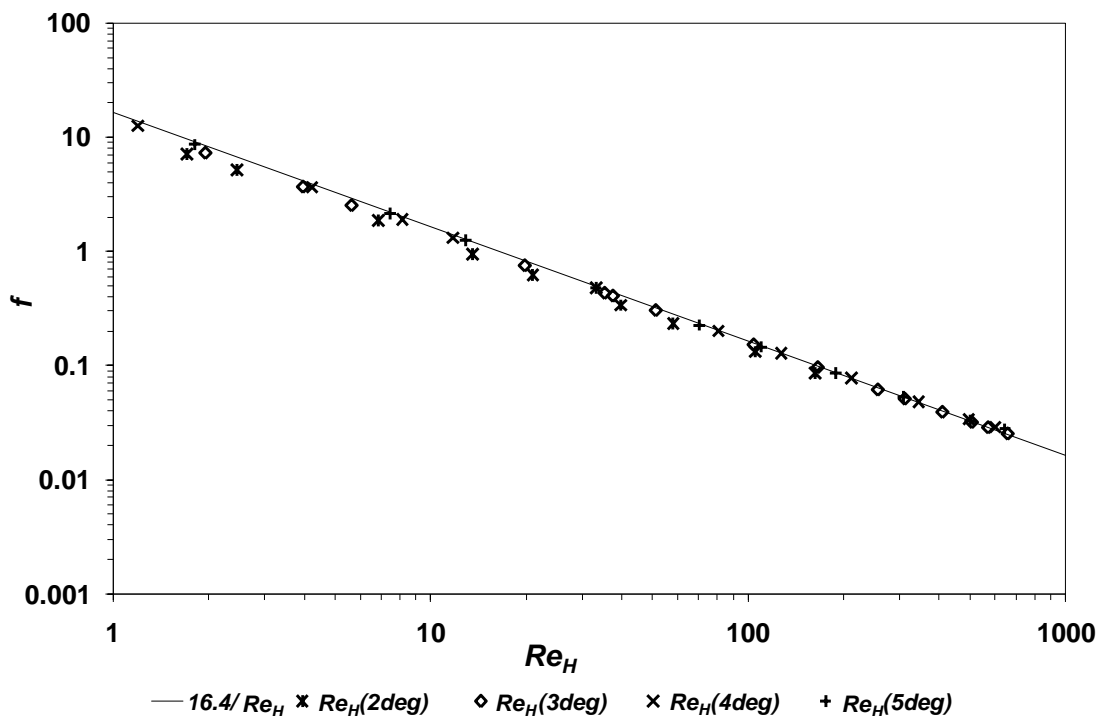


Figure 4.5 A f vs. Re_H plot for 10% kaolin in 150 mm rectangular flume with a best line fit of $f = 16.4/Re$

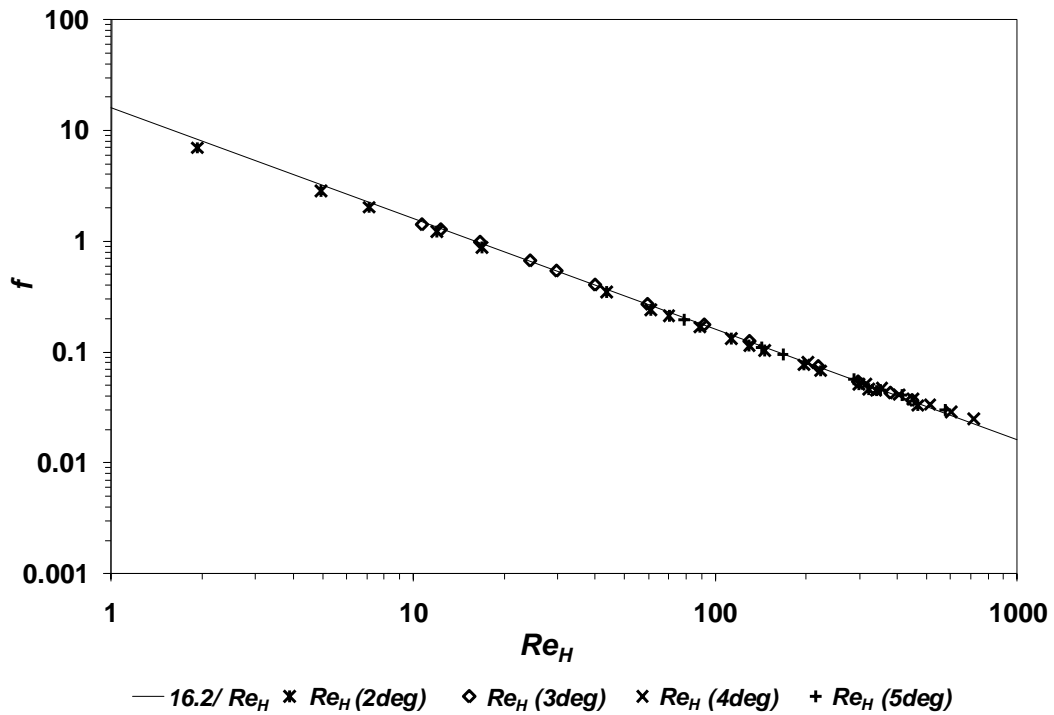


Figure 4.6 A f vs. Re_H plot for 6.2% bentonite in 150 mm semi-circular flume with a best line fit of $f = 16.2/Re$

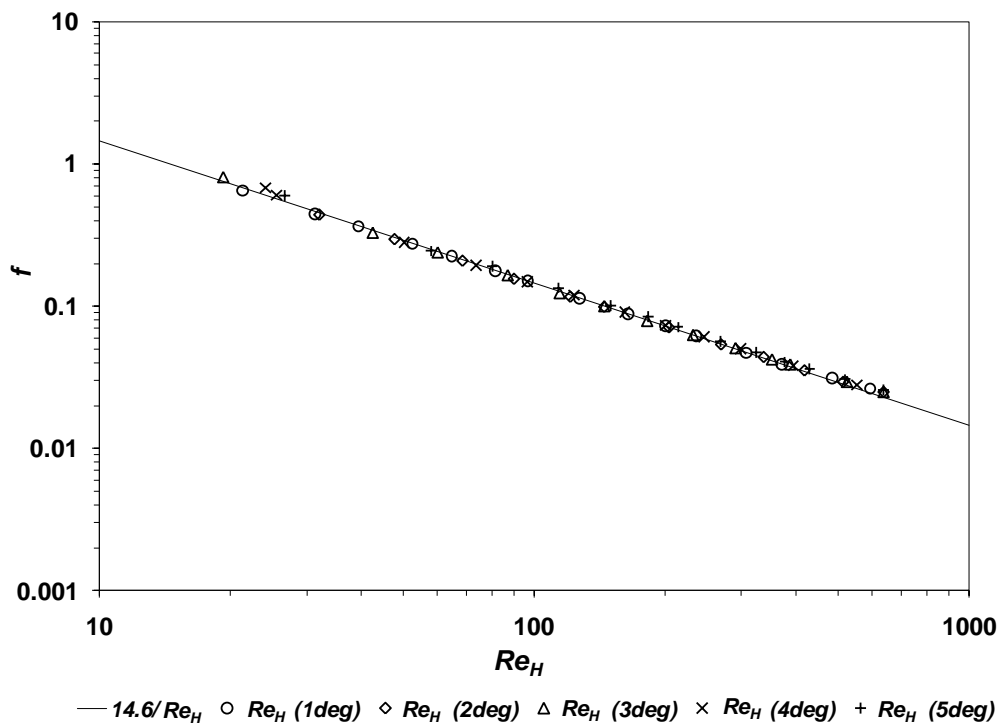


Figure 4.7 A f vs. Re_H plot for 4.89% CMC in 300 mm triangular shape flume with a best line fit of $f = 14.6/Re$

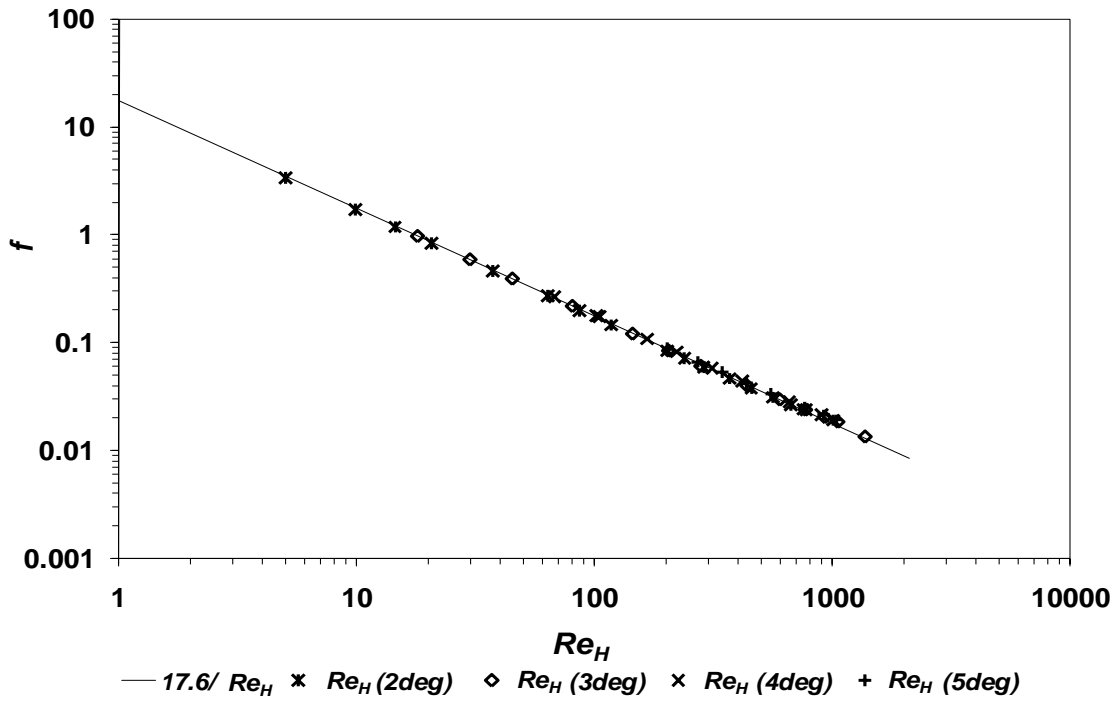


Figure 4.8 A f vs. Re_H plot for 7.1% kaolin in a 150 mm trapezoidal shape flume with a best line fit of $f = 17.6/Re$

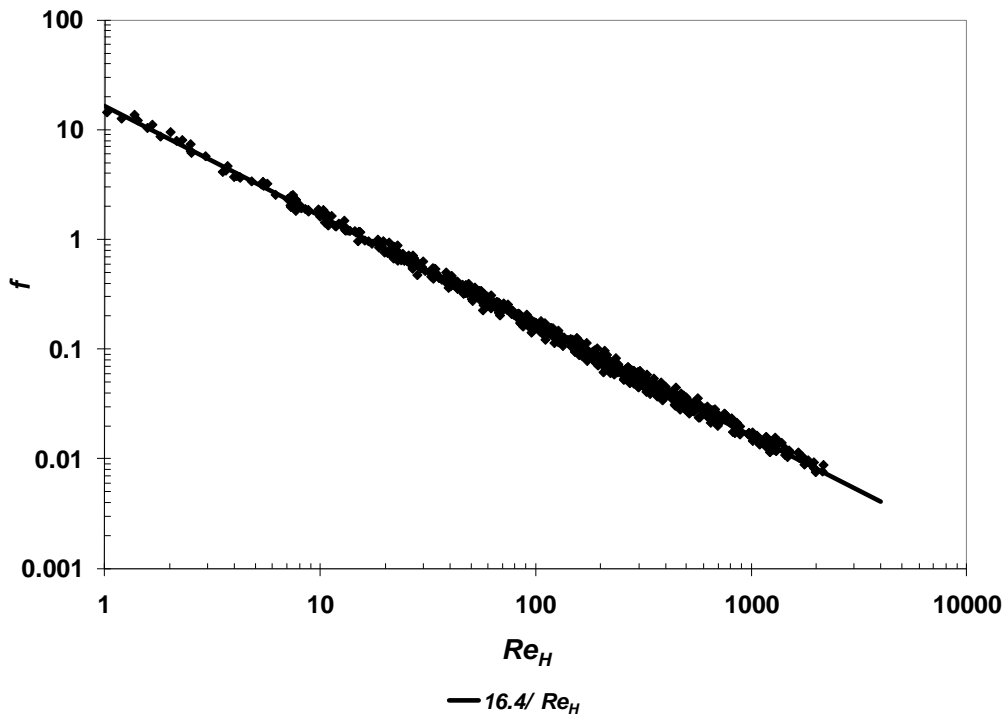


Figure 4.9 A f vs. Re_H plot for three different non-Newtonian fluids flowing in a rectangular flume at slope angles of 1 to 5 degrees.

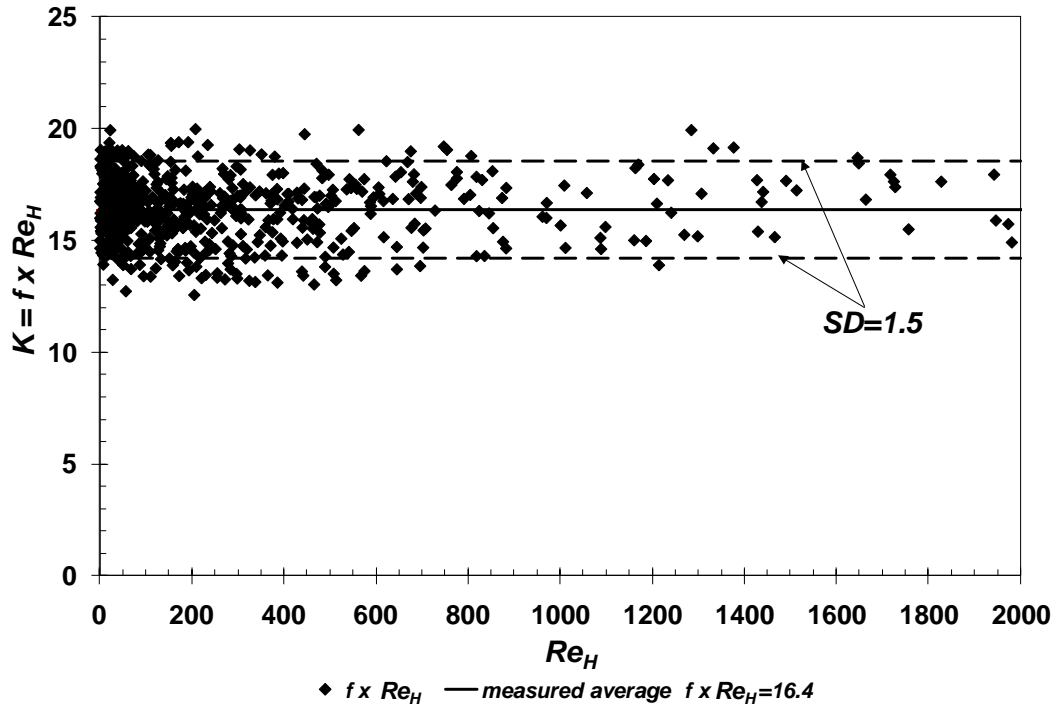


Figure 4.10 Measured $f \times Re_H$ versus Re_H corresponding to Figure 4.9.

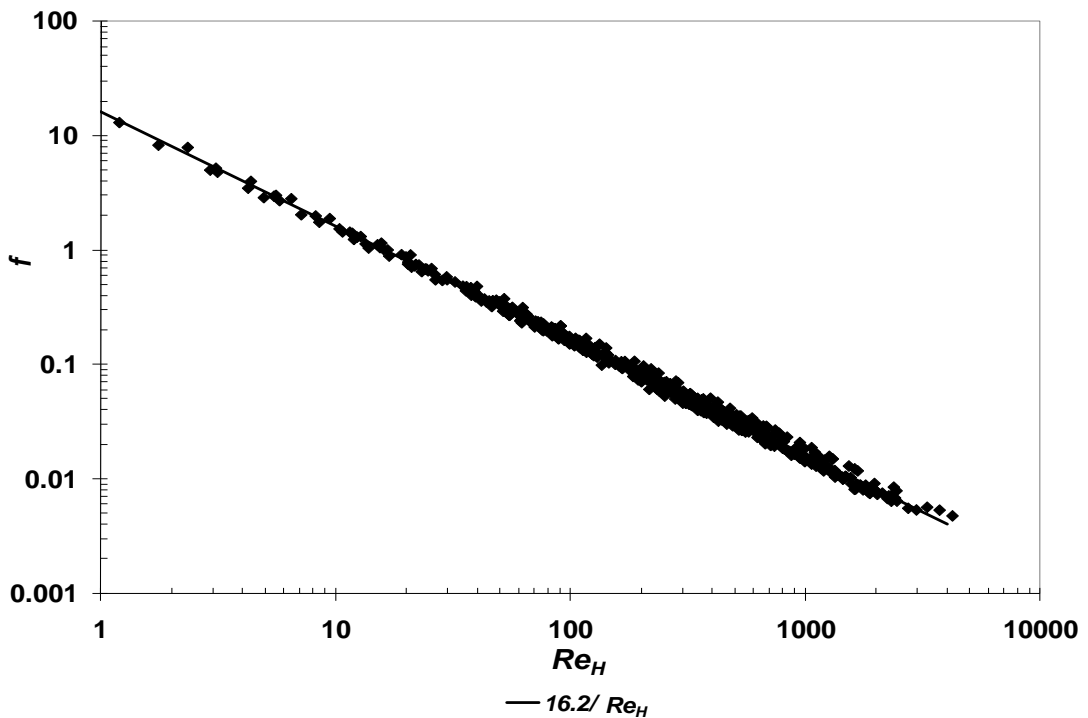


Figure 4.11 A f vs. Re_H plot for three different non-Newtonian fluids flowing in a semi-circular flume at slope angles of 1 to 5 degrees.

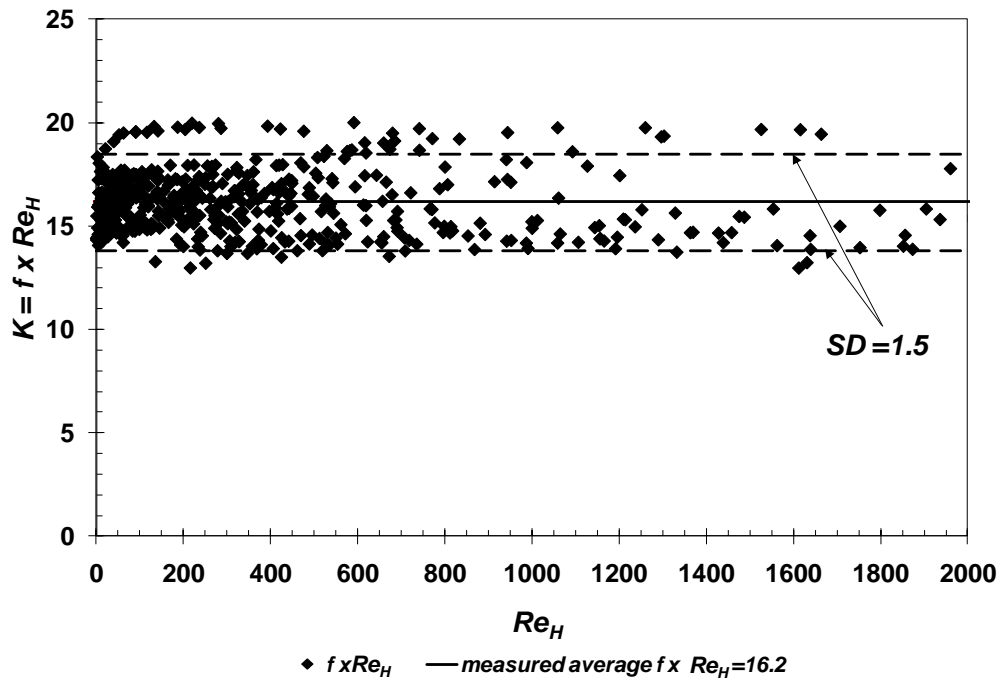


Figure 4.12 Measured $f \times Re_H$ versus Re_H plot corresponding to Figure 4.11.

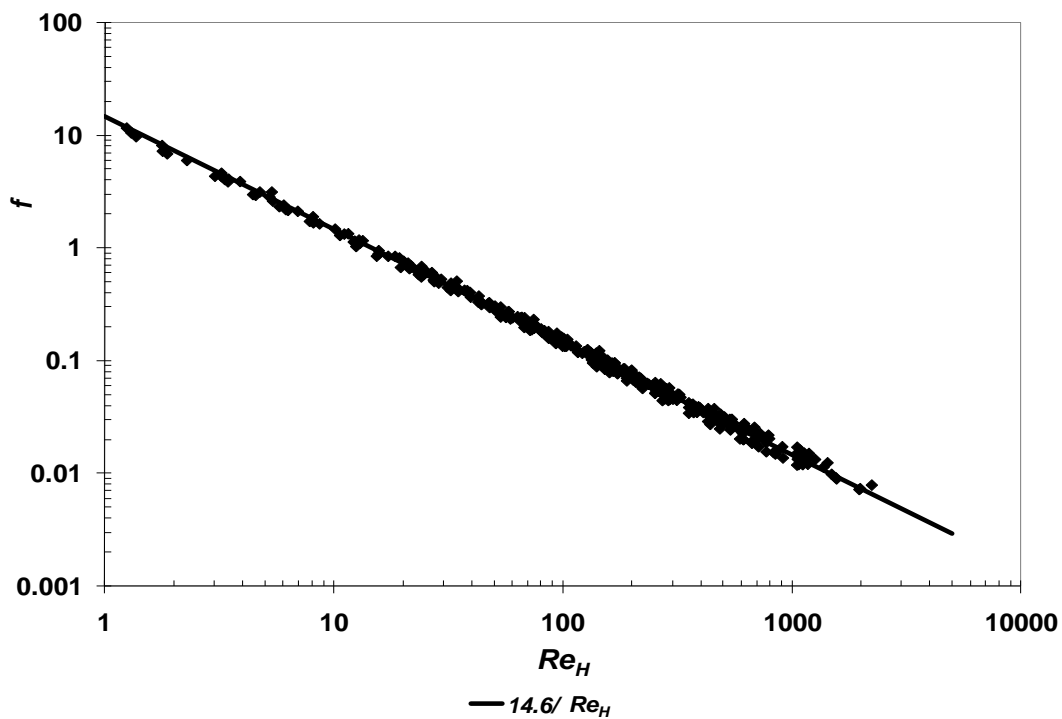


Figure 4.13 A f vs. Re_H plot for three different non-Newtonian fluids flowing in a triangular flume at slope angles of 1 to 5 degrees

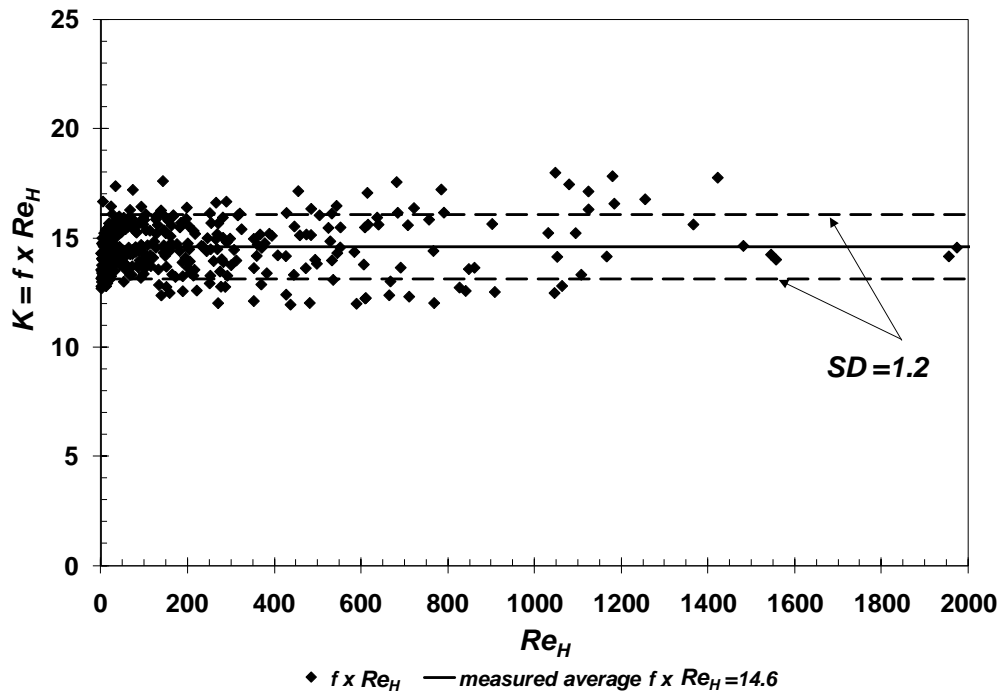


Figure 4.14 Measured $f \times Re_H$ versus Re_H plot corresponding to Figure 4.13.

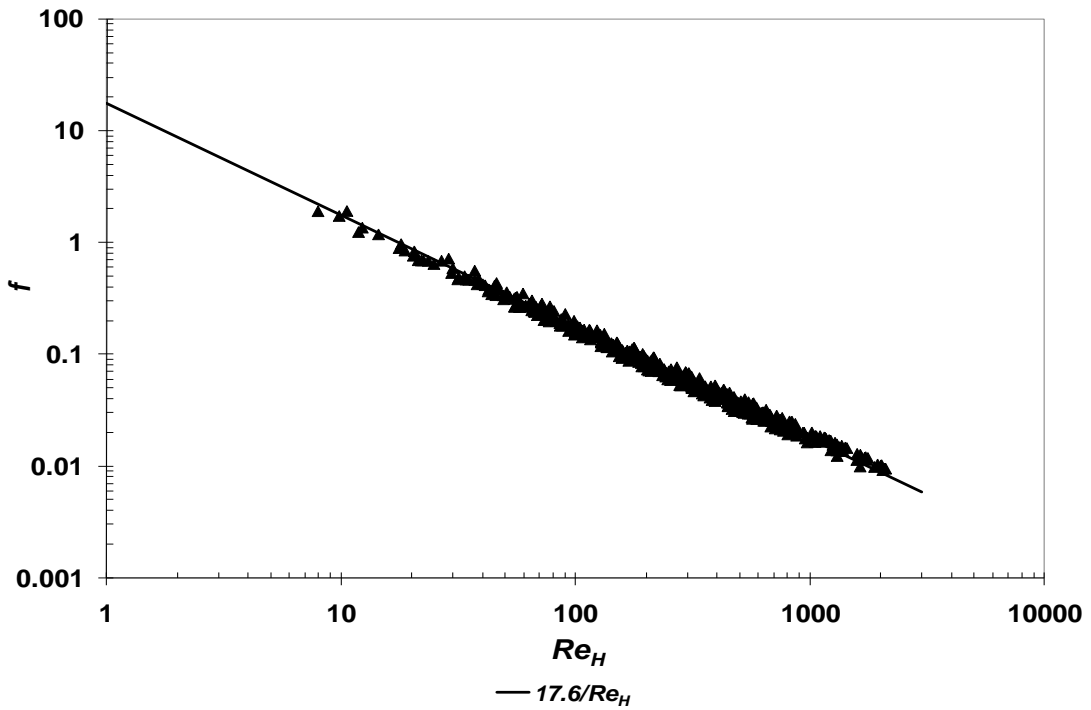


Figure 4.15 A f vs. Re_H plot for three different non-Newtonian fluids flowing in a trapezoidal flume at slope angles of 1 to 5 degrees

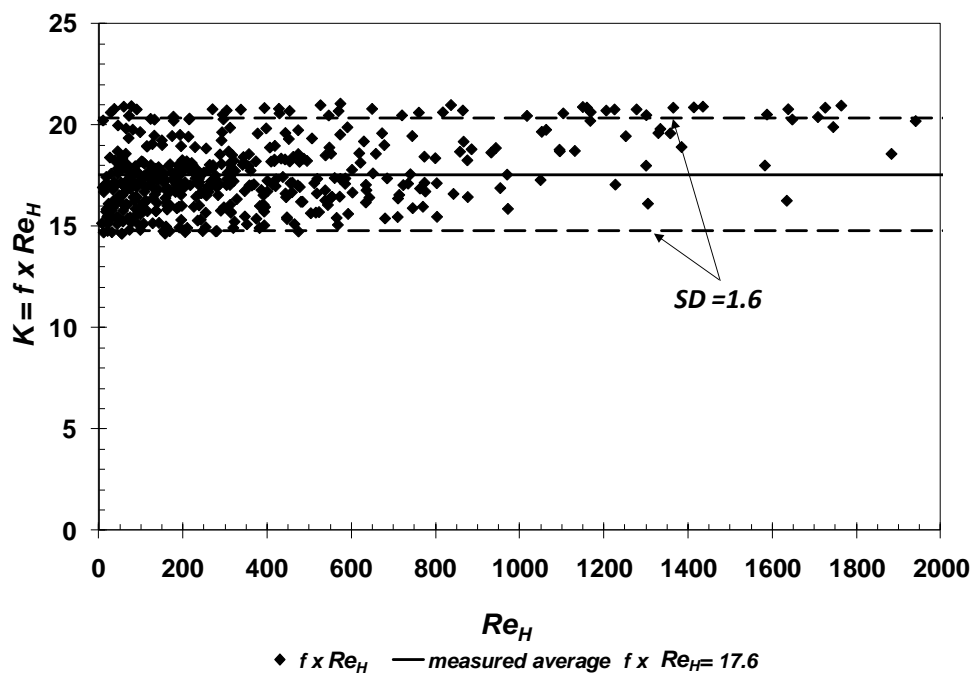


Figure 4.16 Measured $f \times Re_H$ versus Re_H plot corresponding to Figure 4.15.

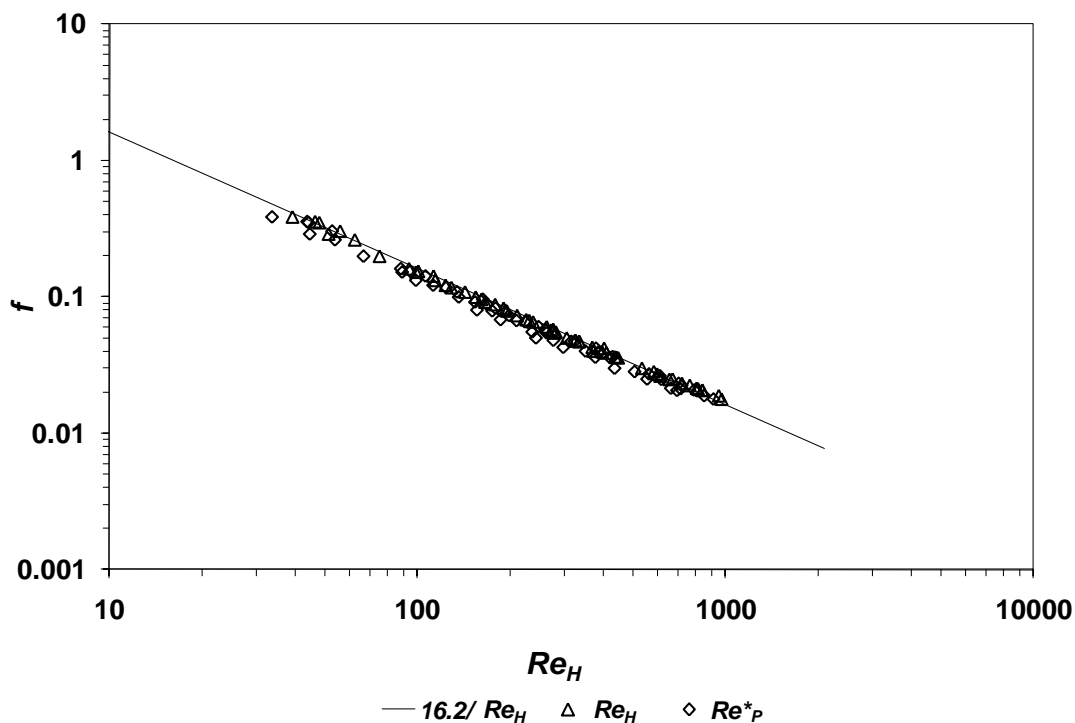


Figure 4.17 A f vs. Re_H plot comparing the use of Re_H and Re^*_P for 4% CMC in 150 mm semi-circular shaped flume at slope angles of 1 to 5 degrees

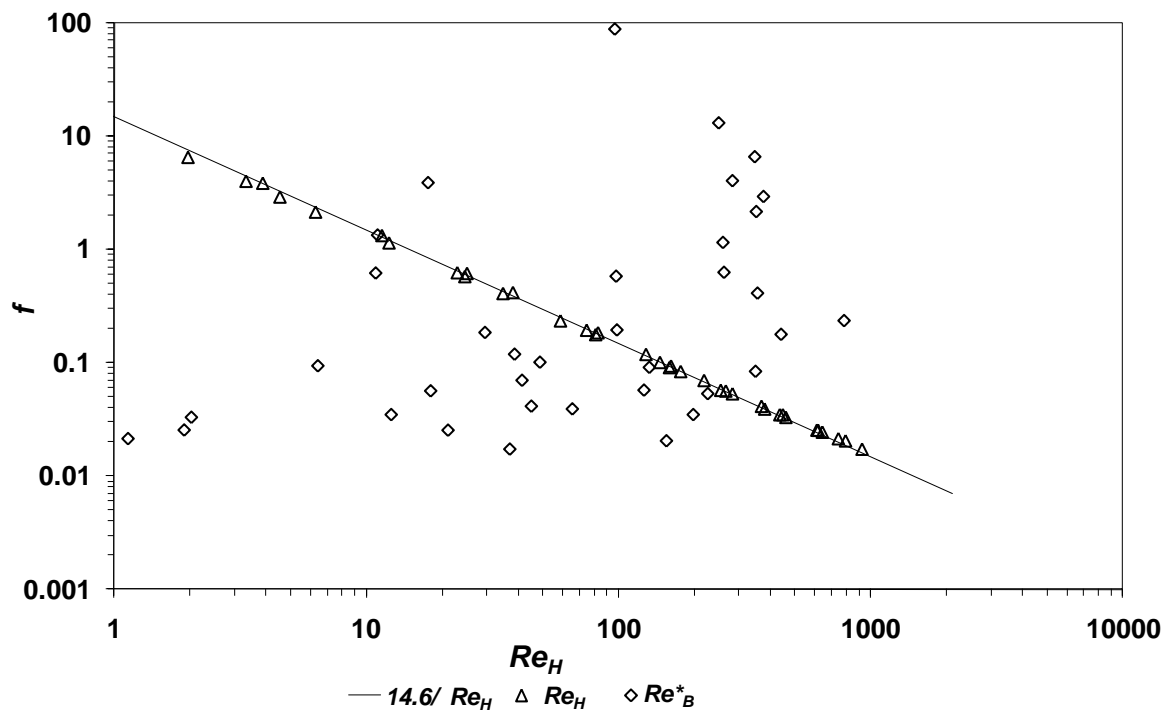


Figure 4.18 A f vs. Re_H plot comparing the use of Re_H and Re^*_B for 5.4% bentonite in 300 mm triangular shaped flume at slope angles of 1 to 5 degrees

CHAPTER 5

RESULTS

Laminar and Turbulent Flow of non-Newtonian Fluids in Open Channels for Different Cross-sectional Shapes

Manuscript Submitted

Burger, J.H., Haldenwang, R. and Alderman, N.J. 2014. Laminar and Turbulent flow of non-Newtonian fluids in open channels for different cross-sectional shapes. (ASCE Journal of Hydraulic Engineering).

Chapter 5 Laminar and Turbulent Flow of non-Newtonian Fluids in Open Channels for Different Cross-sectional Shapes

5.1 Abstract

New models for the prediction of laminar and turbulent flow of non-Newtonian fluids in open channels of different cross-sectional shapes are proposed. These models are compared with three previously-published models for laminar flow and five previously-published models for turbulent flow using our recently extended experimental database for non-Newtonian flow in open channels of different cross-sectional shapes. Flow of three different fluids (aqueous carboxymethyl cellulose solutions and kaolin and bentonite suspensions) was investigated in open channels of four different cross-sections (rectangular, semi-circular, trapezoidal and triangular) at slopes varying from 1 to 5 degrees. The new laminar model gave a closer fit to the data than those from the previously-published models. However, the presence of the yield stress still presents a problem which makes the flow prediction in laminar flow for such fluids not very accurate. The new model for turbulent flow gave the best fit to the flow data compared to the five previously-published models which fell within a 30% error margin. A particular advantage of both new models is that it is applicable for all the different fluids tested and for all the four open channel cross-sectional shapes.

Subject headings: Tailings, open channel, cross-sectional shape, non-Newtonian fluid, rheology, laminar, turbulent.

5.2 Introduction

Open channels, flumes or launders are used in the mining industry to transport non-Newtonian slurries to tailings areas. The design of these flumes is not straightforward mainly due to the changes in the material properties affecting the rheology and the differences in the channel shape. Although datasets are available for non-Newtonian flow in rectangular open channels Coussot, (1994); Haldenwang, (2003); Haldenwang & Slatter, (2006) and Burger et al. (2010a) and in semi-circular open channels Fitton, (2007; 2008), there were none available for non-Newtonian flow in triangular and trapezoidal open channels.

The Flow Process Research Centre at the Cape Peninsula University of Technology have recently extended their experimental database for non-Newtonian flow in rectangular open channels (Haldenwang 2003) to include the test work on the flow of three non-Newtonian fluids in five tilting flumes of semi-circular, triangular and trapezoidal cross-sections (Burger et al., 2010b). The channel width ranged from 150 mm to 300 mm. The three fluids studied were aqueous carboxymethyl cellulose solutions and kaolin and bentonite suspensions at various concentrations. During the flow measurement, rheological characterisation of these fluids was also conducted using an in-line tube viscometer with three different tube diameters. The flow curves for each of three tube diameters were found to be coincident which indicated no wall slip for the three fluids at the various concentrations studied. Curve fits to these flow curves were made as appropriate using the Power law, Bingham plastic and Herschel-Bulkley models given respectively by

$$\tau_{yx} = k \dot{\gamma}_{yx}^n \quad (2.2)$$

$$\tau_{yx} = \tau_{yB} + \mu_B \dot{\gamma}_{yx} \quad (2.3)$$

$$\tau_{yx} = \tau_{yHB} + k \dot{\gamma}_{yx}^n \quad (2.4)$$

where k is the consistency coefficient, n is the flow behaviour index, μ_B is the plastic viscosity, τ_{yB} is the Bingham yield stress and τ_{yHB} is the Herschel-Bulkley yield stress.

Non-Newtonian open channel flow data can be presented in the form of a Moody chart where the Fanning friction factor f is plotted against the appropriate Reynolds number allowing laminar, transitional or turbulent flow regions to be identified (Burger et al 2010a, 2010b). If the Haldenwang et al. (2002) Reynolds number, Re_H is used as the appropriate Reynolds number for open channel flow of three non-Newtonian fluids in four different cross-sectional shapes, Re_H was found to range approximately from 5 to 15000. By taking the onset of transitional flow to be the deviation away from the laminar line on the f vs Re_H plot, it could start at $Re_H = 500$ (Haldenwang, 2003).

5.3 Laminar flow

In this study, a new model is proposed for the prediction of laminar flow of power law, Bingham plastic and Herschel-Bulkley fluids in rectangular, semi-circular, triangular and trapezoidal open channels. This model was compared with three previously-published models, namely:

- The Kozicki & Tiu, (1967, 1986) model for laminar flow of power law and Bingham fluids in rectangular, semi-circular and triangular open channels.
- The Coussot, (1994) model for laminar flow of a Herschel–Bulkley fluid in rectangular and trapezoidal open channels.
- The Haldenwang et al. (2002, 2004) model for laminar flow of power law, Bingham plastic and Herschel-Bulkley fluids in rectangular, semi-circular, triangular and trapezoidal open channels.

The model comparison was made using velocity as a basis.

5.4 Turbulent flow

A new model is also proposed for the prediction of turbulent flow of power law, Bingham plastic and Herschel-Bulkley fluids in rectangular, semi-circular, triangular and trapezoidal open channels. This model was compared with five previously-published models, namely:

- The Manning model which was derived from the Chézy equation (Manning, 1890). This equation is valid for both uniform and non-uniform (gradually varied) flow of water.
- The model developed by Torrance, (1963) for turbulent flow of non-Newtonian slurries exhibiting viscoplastic behaviour in smooth pipes using the Herschel-Bulkley model.
- The model presented by Wilson & Thomas, (1985) and Thomas & Wilson, (1987) for pipe flow of viscoplastic fluids based on the thickening of the laminar sub-layer by an area ratio factor, A_r . Wilson, (1991) proposed the use of this model for open channel flow.

- Slatter, (1994) proposed a turbulent pipe flow model for viscoplastic fluids which has been adapted for open channel flow by replacing the pipe diameter with four times the hydraulic radius.
- The model presented by Haldenwang, (2003) for turbulent open channel flow which was derived from the pipe flow model presented by Slatter, (1994).

The model comparison was made using velocity as a basis.

5.5 Literature and theory

The effect of channel shape on laminar flow of non-Newtonian fluids in open channels is of interest for a variety of industrial applications. Channels with rectangular, semi-circular and trapezoidal cross-sections are often encountered in the minerals industry where tailings are transported from the mine to the disposal facilities (Haldenwang & Slatter, 2006). Non-Newtonian flow in channels with various cross-sectional shapes is also found in the wastewater and food processing industries (Fitton, 2008). To date, methods for predicting non-Newtonian laminar flow in open channels of arbitrary cross-section are limited in the literature.

Most of the non-Newtonian models for turbulent flow have been derived from the pipe paradigm with the exception being the Manning equation which was developed for channel flow of water. The proposed new turbulent velocity model is also based on the pipe paradigm through the modified Blasius equation with the Reynolds number being defined by the (Haldenwang et al., 2002) Reynolds number. The shape effect on open channel flow is accounted for by using the appropriate K value in the $f = K/Re$ relationship for laminar flow and the appropriate a and b values in the modified Blasius equation $f = aRe^b$ for turbulent flow.

These models are briefly discussed below together with a description of the new laminar and turbulent velocity models.

5.5.1 Laminar flow models

The four methods for predicting non-Newtonian laminar flow in open channels of arbitrary cross-sections are summarised below.

Kozicki & Tiu model.

The earliest model was that of Kozicki & Tiu (1967, 1986), who generalised the Rabinowitsch-Mooney equation for pipe and slit flow to obtain expressions for the average velocity for fully-developed laminar flow of various non-Newtonian fluids in non-circular channels. They also introduced a generalised Reynolds number, Re^* such that the friction factor for fully-developed laminar flow through any constant cross-section duct is given by

$$f = \frac{16}{Re^*} \quad (2.37)$$

where

$$Re^* = \frac{\rho V^{2-n^*} R_h^{n^*}}{2^{n^*-3} k^*} \quad (2.38)$$

and n^* and k^* are defined respectively by

$$n^* = \frac{d \ln \bar{\tau}_w}{d \ln \left[\frac{2V}{R_h} \right]} \quad (2.39)$$

$$k^* = \frac{\bar{\tau}_w}{\left[\frac{2V}{R_h} \right]^{n^*}} \quad (2.40)$$

in which the average shear stress, $\bar{\tau}_w$ is given by $\bar{\tau}_w = R_h \rho g \sin \theta$

where θ is the channel slope to the horizontal.

The hydraulic radius, R_h in Eqs (2.37) to (2.40) is given by

$$R_h = \frac{A}{P} \quad (2.10)$$

where A is the cross-sectional area for flow and P is the wetted perimeter of the channel. Expressions for A and P for the four open channel shapes used in this study can be found in Table 5.1.

Through substitution of appropriate expressions for n^* and k^* , Kozicki et al. (1966) obtained Re^* expressions for the power law and Bingham plastic fluids. For power law fluids, this is given by

$$Re_p^* = \frac{R_h^n V^{2-n} \rho}{2^{n-3} k \left(\frac{a + bn}{n} \right)^n} \quad (2.41)$$

since

$$n^* = n \quad (5.1)$$

and

$$k^* = k \left(\frac{a + bn}{n} \right)^n \quad (5.2)$$

For Bingham plastic fluids, this is given by

$$Re_{*B} = \frac{4R_h V \rho}{\mu_B} \left[\frac{1}{a+b} - \frac{\chi}{b} + \frac{a}{b(a+b)} \chi^{1+\frac{b}{a}} \right] \quad (2.44)$$

since

$$n^* = \frac{a \left[\frac{1 - \chi^{1+\frac{b}{a}}}{a+b} - \frac{\chi \left(1 - \chi^{\frac{b}{a}} \right)}{b} \right]}{1 - \chi - b \left[\frac{1 - \chi^{1+\frac{b}{a}}}{a+b} - \frac{\chi \left(1 - \chi^{\frac{b}{a}} \right)}{b} \right]} \quad (5.3)$$

and

$$k^* = (a \mu_p)^{n^*} \bar{\tau}_w^{1+\frac{bn^*}{a}} \left[\left(\frac{a}{a+b} \right) \bar{\tau}_w^{1+\frac{b}{a}} - \frac{a}{b} \bar{\tau}_w^{\frac{b}{a}} \tau_{yB} + \frac{a^2}{b(a+b)} \tau_{yB}^{1+\frac{b}{a}} \right]^{-n^*} \quad (5.4)$$

where a and b are the geometrical parameters relating to the shape of the flow geometry, μ_p is the plastic viscosity and χ is the ratio of Bingham yield stress to wall shear stress, $\tau_{yB}/\bar{\tau}_w$, with $\bar{\tau}_w = R_h \rho g \sin \theta$.

Noting $f = \frac{2\bar{\tau}_w}{\rho V^2}$ in Equation (2.37), the average velocity expressions for the power law and Bingham plastic

fluids corresponding to Equations (2.41) and (2.44) can be obtained. These are given respectively by

$$V = \frac{R_h}{2} \left(\frac{\bar{\tau}_w}{K} \right)^{\frac{1}{n}} \left(\frac{n}{a+bn} \right) \quad (2.47)$$

and

$$V = \frac{R_h}{2} \frac{\bar{\tau}_w}{\mu_B} \left[\frac{1}{a+b} - \frac{\chi}{b} + \frac{a}{b(a+b)} \chi^{1+\frac{b}{a}} \right] \quad (2.48)$$

For open rectangular channels, the analytical solutions for Newtonian flow given by Straub et al. (1958) may be used for the evaluation of a and b .

$$a = 0.5 \left(\frac{\lambda}{1+\lambda} \right)^2 \left(1 - \frac{32}{\pi^3} \sum_0^{\infty} \left(\frac{(-1)^n}{(2n+1)^3} \right) \left(\frac{1}{\cosh \frac{(2n+1)\pi\lambda}{2}} \right) \right)^{-1} \quad (2.49)$$

$$b = a[3\phi' - 1] \quad (2.50)$$

where

$$\varphi' = \frac{\left(1 - \frac{32}{\pi^3} \sum_0^{\infty} \left(\frac{(-1)^n}{(2n+1)^3} \right) \left(\frac{1}{\cosh\left(\frac{(2n+1)\pi\lambda}{2}\right)} \right) \right)}{\left(1 - \frac{192}{\pi^5} \frac{1}{\lambda} \sum_0^{\infty} \left(\frac{1}{(2n+1)^5} \right) \tanh\left(\frac{(2n+1)\pi\lambda}{2}\right) \right)} \quad (2.51)$$

and

$$\lambda = \frac{W}{2h} \quad (2.52)$$

where W is the rectangular channel width and h is the flow depth.

For open triangular channels, the analytical solutions for Newtonian flow given by (Straub et al. 1958) were used for the evaluation of a and b. For a 90-degree symmetrical triangular open channel, a = 0.2122 and b = 0.6765 whereas for a 60-degree symmetrical triangular open channel, a = 0.2009 and b = 0.6831. For open semi-circular channels, the values of a and b used were those numerically obtained by Sestak, (1974).

Coussot model

From his work with clay-water suspensions in rectangular and trapezoidal shaped channels, Coussot, (1994) found that the flow behaviour of these suspensions over the range of concentrations studied were best described by the Herschel-Bulkley model given by Eq. (2.4) with the power law exponent, n fixed at $\frac{1}{3}$. For these suspensions, he derived the expression for average wall shear stress in both channels to be

$$\tau_w = \tau_{yHB} \left(1 + \alpha (H_B)^{-0.9} \right) \quad (2.53)$$

where α is a shape factor for the open channel and H_B is the Herschel-Bulkley number defined as

$$H_B = \frac{\tau_{yHB}}{k} \left(\frac{h}{V} \right)^n \quad (2.54)$$

with h being the flow depth in channel.

From Equations (2.53) and (2.54), the average velocity can be obtained:

$$V = \frac{h}{\left[\frac{k}{\tau_{yHB}} \left\{ \frac{\alpha}{\left(\left(\tau_w / \tau_{yHB} \right) - 1 \right)} \right\}^{1.11} \right]^{\frac{1}{n}}} \quad (2.55)$$

The shape factor for the rectangular shaped channel was defined by Coussot, (1994) as

$$\alpha = 1.93 - 0.43 \left(\arctan \left(\left(\frac{10h}{W} \right)^{20} \right) \right) \quad \text{for } \frac{h}{W} < 1 \quad (2.56)$$

He claims that this is valid for $h/W < 1$. Hence, for a 300 mm wide rectangular shaped channel, the shape factor is applicable for all values of h up to 300 mm. However, the value of α reaches a minimum value at a depth of approximately 60 mm indicating a h/W ratio of about 0.2. This contradicts the initial assumption of α being correct for h/W ratios up to 1.

The shape factor for the trapezoidal shaped channel with a base width B and a slope of 45° for the two sides was defined by Coussot, (1994) as

$$\alpha = 1.93 - 0.6 \arctan \left(\left(\frac{0.4h}{W} \right)^{20} \right) \quad \text{for } \frac{h}{W} < 4 \quad (2.57)$$

Haldenwang model

By adapting the pipe flow paradigm for any open channel and introducing a new Reynolds number based on the Herschel-Bulkley model, (Haldenwang et al. 2002) proposed an equation for the friction factor-Reynolds number relationship for laminar flow of non-Newtonian fluids in open channels. This is given by

$$f = 16/\text{Re}_H \quad (2.58)$$

in which Re_H is the (Haldenwang et al. 2002) Reynolds number given by

$$\text{Re}_H = \frac{8\rho V^2}{\tau_y + k \left(\frac{2V}{R_h} \right)^n} \quad (2.59)$$

A particular advantage of using the (Haldenwang et al. 2002) Reynolds number is that it can be equally applicable for fluids exhibiting power law and Bingham plastic behaviour in addition to fluids exhibiting yield-shear-thinning

behaviour. Noting $f = \frac{2\tau_w}{\rho V^2}$ where τ_w is the average wall shear stress, it can be deduced from Equations (2.58)

and (2.59) that the average velocity is given by

$$V = \frac{R_h}{2} \left[\frac{\tau_w - \tau_{yHB}}{k} \right]^{1/n} \quad (2.60)$$

New model

A recent study by (Burger et al. 2010b) revealed the pipe flow paradigm adopted by (Haldenwang et al. 2002, 2004) for laminar, non-Newtonian flow in open channels of different cross-sectional shapes was found to be invalid. Instead of Eq. (2.58), it is proposed that the friction-factor versus Reynolds number relationship is replaced by

$$f = K/Re_H \quad (3.1)$$

where K is the laminar flow constant for the open channel cross-sectional shape. Noting $f = \frac{2\tau_w}{\rho V^2}$ where τ_w is the average wall shear stress, it can be deduced from Equations (2.59) and (3.1) that the average velocity for a Herschel-Bulkley fluid is given by

$$V = \frac{R_h}{2} \left[\frac{(16/K)\tau_w - \tau_{yHB}}{k} \right]^{1/n} \quad (5.5)$$

The K values to be used in Equation (5.5) were those experimentally found by (Burger et al. 2010b). Hence, K = 14.6 for a 90° symmetrical triangular channel, 16.2 for a semi-circular channel, 16.4 for a rectangular channel and 17.6 for trapezoidal channel with 60° sides.

A summary of all the laminar flow models can be found in Table 5.2.

5.5.2 Turbulent flow models

The six different methods for predicting non-Newtonian turbulent flow in open channels of arbitrary cross-sections are summarised below. Most of these models have been derived from the pipe paradigm, the exception being the Manning equation. The proposed new turbulent velocity model is also based on the pipe paradigm through the modified Blasius equation with the Reynolds number being defined by the (Haldenwang et al. 2002) Reynolds number.

Manning equation

The Manning equation was derived from the Chézy equation (Manning, 1890) and is defined as:

$$V = \frac{1}{n_{\text{Manning}}} (R_h)^{2/3} \sqrt{\sin\theta} \quad (2.61)$$

with R_h being the hydraulic radius as defined by Eq. (2.10) and θ the angle of the flume from the horizontal. This equation is valid for both uniform and non-uniform (gradually varied) flow of water. The Manning constant, n_{Manning} varies from 0.010 s/m^{1/3} for smooth plastic surfaces to 0.025 s/m^{1/3} for cemented rubble surfaces (Chow, 1959). This equation was found to be 'reasonably reliable' when predicting fully rough turbulent flow of water in open channels (Chanson, 1999).

Despite no research being reported on the applicability of Eq. (2.61) for open channel flow of Newtonian and non-Newtonian fluids other than water, this equation has been adopted in the minerals industry for open channel

design. For example, (Fuentes et al. 2004) reported on the use of this equation to design flumes for the transportation of mine tailings in South America.

Torrance pipe model adapted

Torrance, (1963) developed a model for turbulent flow of fluids exhibiting viscoplastic behaviour in smooth pipes using the Herschel-Bulkley model. Haldenwang, (2003) used the same adaption method proposed by Wilson and Thomas, (1985) in applying this pipe flow model for open channel flow. By changing the pipe diameter to $4R_h$, the flow velocity based on this model is given by

$$\frac{V}{V_*} = \frac{3.8}{n} + \frac{2.78}{n} \ln\left(1 - \frac{\tau_y}{\tau_w}\right) + \frac{2.78}{n} \ln\left(\frac{V_*^{2-n} \rho (2R_h)^n}{K}\right) - 4.17 \quad (2.62)$$

where V_* is the shear velocity given by

$$V_* = \sqrt{\frac{\tau_w}{\rho}} \quad (2.65)$$

Wilson and Thomas pipe model adapted

Wilson & Thomas, (1985) and (Thomas & Wilson, 1987) presented a pipe flow model for viscoplastic fluids where the thickening of the laminar sub-layer is accounted for by the use of an area ratio factor, A_r . Wilson, (1991) proposed the use of this model for open channel flow provided that the pipe radius is replaced by the equivalent hydraulic radius of the open channel and the equivalent viscosity, μ_e is used in place of the Newtonian viscosity, μ_N

The average velocity is given by

$$V = V_* \left(\frac{V_N}{V_*} + 11.6(A_r - 1) - 2.5 \ln A_r - \Omega \right) \quad (2.63)$$

where V_* is the shear velocity given by Eq. (2.65) and V_N is the Newtonian mean velocity for smooth pipe flow given by

$$V_N = V_* \left(2.5 \ln \left(\frac{\rho V_* 2R_h}{\mu_e} \right) + 1.75 \right) \quad (2.64)$$

The equivalent viscosity μ_e is the viscosity that would be possessed by a Newtonian fluid giving the same smooth wall friction factor as that obtained with the non-Newtonian fluid.

The term Ω in Eq. (2.66) accounts for the blunting of the velocity profile created by the presence of a yield stress of the viscoplastic fluid. This is given by

$$\Omega = -2.5 \ln \left(1 - \frac{\tau_y}{\tau_w} \right) - 2.5 \frac{\tau_y}{\tau_w} \left(1 + 0.5 \frac{\tau_y}{\tau_w} \right) \quad (2.66)$$

where τ_y is the yield stress of the viscoplastic fluid and τ_w is the average wall shear stress.

Slatter pipe model adapted

Slatter, (1994) presented a turbulent pipe flow model for yield shear-thinning fluids. Haldenwang, (2003) used the same adaption method proposed by Wilson and Thomas, (1985) in applying this pipe flow model for open channel flow. By replacing the pipe diameter with four times the hydraulic radius, the average velocity is given by

$$V = V_* \left(2.5 \ln \left(\frac{2R_h}{d_{85}} \right) + 2.5 \ln \text{Re}_r + 1.75 \right) \quad (2.69)$$

for smooth wall open channel flow and

$$V = V_* \left(2.5 \ln \left(\frac{2R_h}{d_{85}} \right) + 4.75 \right) \quad (2.70)$$

for rough wall open channel flow with the roughness Reynolds number being

$$\text{Re}_r = \frac{8\rho(V_*)^2}{\tau_y + k \left(\frac{8V_*}{d_x} \right)^n} \quad (2.71)$$

and d_x being the representative particle size of the solid particles. For the slurries tested, the d_{85} size was found to give a good representation of the turbulent roughness size effect of the solid particles in the slurry, i.e. $d_x = d_{85}$ (Slatter, 1994).

Haldenwang pipe model adapted

Haldenwang, (2003) developed a turbulent open channel model based on the pipe flow model presented by (Slatter, 1994). The average smooth wall turbulent velocity is given by

$$V = \sqrt{gh \sin \theta} \left(2.5 \ln \frac{2R_h}{e} - 76.86 \mu_{a(500)} - 9.45 \right) \quad (2.67)$$

with $\mu_{a(500)}$ being the point or apparent viscosity at a shear rate of 500 s^{-1} and h being the flow height in the channel.

New model

In this study, it was found that the turbulent data did not collapse onto the line given by the Blasius equation $f = 0.079\text{Re}^{-0.25}$. However, by using the modified Blasius equation given by Eq. (5.6) where different values for a and b were obtained for the different channel shapes given in Table 5.3, the data was found to collapse onto a single line.

$$f_{mB} = a\text{Re}_H^b \quad (5.6)$$

where f is the friction factor and Re_H is the Haldenwang et al. (2002) Reynolds number. Substituting $f = \frac{2\tau_w}{\rho V^2}$ into

Eq. (5.6), the velocity is given by:

$$V = \sqrt{\frac{2\tau_w}{\rho a(\text{Re}_H)^b}} \quad (5.7)$$

A summary of all the turbulent flow models is presented in Table 5.4.

5.6 Experimental

The test work was carried out in a 10 m long tilting flume designed and built by the Flow Process and Rheology Centre at the Cape Peninsula University of Technology. Further details of this flume can be found in (Haldenwang, 2003). This flume can be hydraulically tilted at various angles up to 5° from the horizontal. The width of this rectangular flume can be changed from 300 mm to 150 mm by placing a partition mid-section lengthways down the flume. By inserting an appropriate cross-sectional insert, the rectangular flume can be changed into a flume with a triangular, semi-circular or trapezoidal cross-section. The flume shapes with its dimensions used in this study are shown in Table 5.1.

A summary of the materials tested in the flume is given in Table 5.5. These were prepared by the gradual addition of the required amount of the polymer (carboxymethyl cellulose) or clay (kaolin and bentonite) in tap water in the 2000 litre mixing tank of the flume rig using a 4-bladed, stainless steel, pitched blade impeller driven by an electrical motor to produce a homogeneous solution or suspension. Since bentonite in water suspensions can exhibit significant thixotropic (time-dependent) behaviour (e.g. Alderman et al. 1989), this was minimised by first pre-shearing the suspension by agitation in the mixing tank and then recirculating this suspension through the flow loop as shown in Figure 5.1 for 60 minutes before the flume test was undertaken. The suction of the suspension to the flume entrance is taken from the mixing tank through the supply pump, the flow meter and the tube viscometer to the flume inlet reservoir rising into the flume. The discharge from the flume exit is returned back into the mixing tank.

Flow curve measurements were made using an in-line tube viscometer fitted with three tubes of different diameters, 13, 28 and 80 mm. Each of these three tubes was fitted with a Krohne magnetic flow meter (with a maximum error of 4%) and a Fuji differential pressure transducer gauge (where the accuracy stated by the

manufacturer is within 0.1% of full scale). This means for the high range differential pressure transducer, the differential pressure error is ± 25 Pa and for the low range differential pressure transducer, the differential pressure error is ± 4 Pa. For bentonite in water suspensions, the flow curves measured before and after the flume test confirmed that there was no discernible change between the two flow curves on account of thixotropy. Various model fits were then made to the flow curve data over the measured shear rate range. It was found that the 1.5 to 5.3% v/v carboxymethyl cellulose in water solutions, 3.5 to 6.8% v/v bentonite in water suspensions and 3.4 to 9.2% v/v kaolin in water suspensions were well represented by the power law, Bingham plastic, and Herschel-Bulkley models respectively. The correlation coefficient was used here as the criterion for determining the best model fit.

The volumetric flow rate of the material flowing down the flume, Q was monitored using a Krohne magnetic flow meter whilst the flow depth at various channel slopes from 1° to 5° was made with a $\pm 5\%$ accuracy using Mitutoyo digital depth gauges (having a 0.01 mm accuracy from 0 to 100 mm and 0.02 mm accuracy from 100 mm to 250 mm) located at 5 and 6 m positions from the flume entrance. These positions were found to be the optimal positions for depth measurement. Since the difference in fluid height between these two points was found to be minimal, the flow in the region can therefore be taken as steady flow. From the measured flow depth, the cross-sectional area for flow, A can be then calculated according to the appropriate equation for the channel shape given in Table 5.1. Dividing Q by A allows the calculation of the velocity of the material flowing down the flume, V . A data logger was used to record the various data outputs as a function of time. All of this data was then fed into a PC so that an f vs. Re plot can be generated as output.

5.6.1 Results and Discussion

A comparison of the various previously-published models outlined in the laminar flow section for the prediction of laminar flow of power law, Bingham plastic and Herschel-Bulkley fluids in trapezoidal, rectangular, semi-circular and triangular smooth wall, open channels was made with our new model using representative data from our newly compiled experimental database.

To obtain an objective measure of comparison between the different models, the log standard error (LSE) was used. The lower the LSE, the better is the model fit to the experimental data. This approach was found by Lazarus and Nielson, (1978) to be a useful guide for ranking models. In addition to the LSE values, the correlation coefficient (R^2) values were also obtained.

The five previously-published models summarised in the turbulent flow section for the prediction of turbulent flow of power law, Bingham plastic and Herschel-Bulkley fluids in trapezoidal, rectangular, semi-circular and triangular smooth wall, open channels were all compared with the proposed new model using representative data from our newly compiled experimental database.

Laminar flow of a power law fluid

An example plot given in Figure 5.2 gives a comparison of our model with the experimental data for laminar flow of a power law fluid in a 300 mm triangular channel using velocity as a basis. There is an excellent agreement between the predicted velocities from the three models and the measured velocity according to Table 5.6 the LSE values for the three models in Figure 5.2 suggest that our model gives the best fit.

A similar plot to Figure 5.2 is given in Figure 5.3 for 150 and 300 mm rectangular channels, in Figure 5.4 for a 150 mm trapezoidal channel and in Figure 5.5 for 150 and 300 mm semi-circular channels. As observed for laminar flow of a

power law fluid in the 300 mm triangular channel, these three plots showed excellent agreement between the predicted velocities obtained from the new model and the other models with the measured velocities. The LSE values given in Table 5.6 suggested that the new model gave the best fit for the triangular and trapezoidal channels whereas the Kozicki and Tiu model gave a better fit for the rectangular channel. For the semi-circular channel, there was very little difference between the new model and the one proposed by Haldenwang. Here, the prediction of velocities can either be done using the new model or the Haldenwang et al. (2002) model.

Laminar flow of a Bingham plastic fluid

Plots for laminar flow of a Bingham plastic fluid in 300 mm triangular and semi-circular channels are shown in Figures 5.6 and 5.7 respectively. Both of these plots show significant scatter between the measured and the model velocities. Similar scatter was also observed in the velocity comparison plots for laminar flow of a Bingham plastic fluid in 150 and 300 mm rectangular and 150 mm trapezoidal channels. The introduction of the yield stress as a parameter in the calculation of the model velocities is thought to be the main cause of the scatter observed in these plots. The LSE values in Table 5.6 show that for the new model gave the best fit for triangular and trapezoidal channels whereas the Kozicki and Tiu model gave the better fit for rectangular and semi-circular channels.

Laminar flow of a Herschel-Bulkley fluid

Plots for laminar flow of a Herschel-Bulkley fluid in 150 and 300 mm rectangular and 75 and 150 mm trapezoidal channels again show significant scatter between the measured and the model velocities as shown respectively in Figures 5.8 and 5.9. Similar scatter was also observed in the velocity comparison plots for laminar flow of a Herschel-Bulkley fluid in 300 mm triangular and semi-circular channels. As previously observed for laminar flow of Bingham plastic fluids in open channels of different cross-sections, the introduction of the yield stress as a parameter in the calculation of the model velocities is thought to be the main cause of the scatter observed in these plots. However, the LSE values in Table 5.6 for these plots seem to indicate that the new model is the best one while noting there was very little difference between the new model and the one proposed by Haldenwang for the semi-circular channel.

Turbulent flow of non-Newtonian fluids in various channel shapes

Five previously-published models for predicting turbulent flow of three different non-Newtonian fluids (carboxymethyl cellulose solutions and aqueous kaolin and bentonite suspensions) in open channels of four different cross-sections (trapezoidal, rectangular, semi-circular, and triangular) were compared with the new model.

Figures 5.10 to 5.13 give velocity model comparison plots for the turbulent flow of three above-mentioned non-Newtonian fluids in a trapezoidal, rectangular, semi-circular and triangular open channel respectively. It can be seen from all of these plots that the new model does give a much tighter fit to the experimental data. This is further supported by Table 5.7, where the new model gives the lowest LSE values or highest R^2 values when compared with the other five previously-published models. Of these five previously-published models, only the turbulent flow of the three non-Newtonian fluids in a semi-circular channel fitted to the Haldenwang model give a comparable R^2 value to that fitted to the new model.

5.7 Conclusions

The new model for predicting laminar flow of power law fluids in open channels of different cross-sectional shapes gave good agreement between measured and predicted values when compared on a velocity basis. It was shown from the various comparison plots that our model was either better or equivalent to the three previously-published models. Here, the incorporation of the effect of shape into our model by using the appropriate K value for the actual cross-section enhances the accuracy in the prediction of velocity.

However, it was found that the new model was not always to be better than the other three previously-published models for the prediction of laminar flow of Bingham plastic and Herschel-Bulkley fluids in open channels of different cross-sectional shapes. Given the level of scatter found in the velocity comparison plots, this seems to suggest that the introduction of the yield stress for the calculation of model velocities in our model is the main cause for the scatter. Further work is still needed to underpin the underlying causes for this scatter.

The new model for predicting turbulent flow of non-Newtonian fluids in channels of different cross-sectional shapes gave excellent fits to the experimental data. Moreover, it was found to be consistently the better model as observed from Figures 5.10 to 5.13 and the results in Table 5.7. This new model predicted data well within the accepted error margin of 30% as shown by the model comparison plots. Also noted in Table 5.7, is that the LSE values is consistently the lowest when the new model is compared with the experimental data. The reason for the success of the new model can be attributed to the yield stress not having much effect when in turbulent flow compared with laminar flow.

A particular advantage of both new models for laminar and turbulent open channel flow is that they are applicable for all the non-Newtonian fluids tested and for the four cross-sectional shapes.

5.8 Acknowledgements

The financial support of this work from the National Research Foundation (NRF) and the Cape Peninsula University of Technology (CPUT) is very much appreciated.

5.9 Notation

The following symbols are used in this paper:

Symbol	Description	Units
A	cross-sectional area for flow	m ²
A _r	area ratio Eq. (2.63)	-
a	shape factor constant (laminar)	-
a	shape factor constant (turbulent) Eqs. (5.6) & (5.7)	-
b	shape factor constant (laminar)	-
b	shape factor constant (turbulent) Eqs. (5.6) & (5.7)	-
d _x	representative particle size of the solid particles	μm

Symbol	Description	Units
e	hydraulic roughness	m
f	Fanning friction factor	-
g	acceleration due to gravity	m/s^2
H_B	Herschel-Bulkley number	-
h	flow depth	m
K	laminar flow constant in the f vs. Re relationship	-
k	consistency coefficient	$Pa \cdot s^n$
k^*	consistency coefficient as defined by Eq. (2.40)	$Pa \cdot s^n$
n	flow behaviour index	-
n^*	flow behaviour index as defined by Eq. (2.39)	-
$n_{Manning}$	Manning constant	$s/m^{1/3}$
Re	Reynolds number	-
Re^*	generalised Reynolds number, Eq. (2.38)	-
Re_B^*	Kozicki and Tiu Bingham Reynolds number, Eq. (2.44)	-
Re_p^*	Kozicki and Tiu power law Reynolds number, Eq. (2.41)	-
Re_H	Haldenwang et al Reynolds number, Eq. (2.59)	-
Re_r	roughness Reynolds number, Eq. (2.71)	-
R_h	hydraulic radius	m
V	average velocity	m/s
V^*	shear velocity Eq. (2.65)	m/s
V_N	Newtonian mean velocity, Eq. (2.64)	m/s
W	channel width	m
α	Coussot shape factor, Eq. (2.56) & (2.57)	-
β	subtended angle of semi-circular cross-section, Table 5.1	radians
$\mu_{a(500)}$	apparent viscosity at shear rate of 500 s^{-1}	$Pa \cdot s$
μ_B	Bingham plastic viscosity	$Pa \cdot s$
μ_e	equivalent viscosity	$Pa \cdot s$
μ_N	Newtonian viscosity	$Pa \cdot s$
θ	angle of flume from horizontal	degrees
λ	flow width to depth ratio, Eq. (2.52)	-
ρ	density	Kg/m^3
τ_w	average wall shear stress	Pa
$\bar{\tau}_w$	contour-integrated average values of wall shear stress.	Pa
τ_y	yield stress	Pa
τ_{yB}	Bingham yield stress	Pa
τ_{yHB}	Herschel-Bulkley yield stress	Pa
ϕ'	defined by Eq.(2.51)	-
χ	ratio of Bingham yield stress to wall shear stress	-

Symbol	Description	Units
Ω	blunting effect of velocity profile, Eq. (2.66)	-

5.10 References

Alderman, N.J., Ram Babu, D., Hughes, T.L. and Maitland, G.C. (1989), The rheological properties of water-based drilling fluids - Effect of bentonite chemistry. *Speciality Chemicals*, 9(5), 314-326.

Burger, J.H. Haldenwang, R. and Alderman, N.J. (2010a), Experimental database for non-Newtonian flow in four channel shapes. *Journal of Hydraulic Research*. 48(3), 363–370.

Burger, J.H. Haldenwang, R. and Alderman, N.J. (2010b), Friction factor-Reynolds number relationship for laminar flow of non-Newtonian fluids in open channels of different cross-sectional shapes. *Chemical Engineering Science*. 6(11), 3549–3556.

Burger, J., Haldenwang, R., Chhabra, R.P. and Alderman, N.J. (2014), Power law and composite power law friction factor correlations for laminar and turbulent non-Newtonian open channel flow. *J. Braz. Soc. Mech. Sci. Eng.* DOI 10.1007/S40430-014-0188-1.

Coussot, P. (1994), Steady laminar flow of concentrated mud suspensions in open channels. *Journal of Hydraulic Research*, 32(4), 535-558.

Chanson, H. (1999), *The Hydraulics of Open Channel Flow*. London: Arnold.

Chow, Ven T. (1959), *Open Channel Hydraulics*. New York: McGraw-Hill.

Fitton, T.G. (2007), Tailings beach slope prediction. PhD thesis, RMIT University, Melbourne, Australia.

Fitton, T.G., (2008), Non-Newtonian open channel flow – A simple method of estimation of laminar/turbulent transition and flow resistance. In: *Paste 2008, Kasane, Botswana* (A.B. Fourie, R.J. Jewell, A. Paterson and P. Slatter, eds) pp. 245-251.

Fuentes, R. (2004), Slurry flumes in Chile. (Keynote Address). *Hydrotransport 16: 16th International Conference on the Hydraulic Transport of Solids in Pipes*, Santiago, Chile.

Haldenwang, R. (2003). Flow of non-Newtonian fluids in open channels. Unpublished D.Tech thesis. Cape Technikon, Cape Town, South Africa.

Haldenwang, R. and Slatter, P.T. (2006), Experimental procedure and database for non-Newtonian open channel flow. *Journal of Hydraulic Research*, 44(2), 283-287.

Haldenwang, R. Slatter, P.T. and Chhabra, R.P. (2002), Laminar and transitional flow in open channels for non-Newtonian fluids, In: Hydrotransport 15: 15th International Conference on the Hydraulic Transport of Solids in Pipes. Banff, Canada, pp 755-768.

Haldenwang, R. Slatter, P.T. Vanyaza, S. and Chhabra, R.P. (2004), The effect of shape on laminar flow in open channels for non-Newtonian fluids, In: Proc of Hydrotransport 16, 16th International Conference on Hydrotransport, Santiago, Chile, 26-28 April, pp 311-325.

Kozicki, W., Chou, C.H. and Tiu, C. (1966), Non-Newtonian flow in ducts of arbitrary cross-sectional shape. Chemical Engineering Science, 21, 665–679.

Kozicki, W. and Tiu, C. (1967), Non-Newtonian flow through open channels. Canadian Journal of Chemical Engineering, 45, 127-134.

Kozicki, W. and Tiu, C. (1986), Parametric modelling of flow geometries in non-Newtonian flows, In: Encyclopedia of Fluid Mechanics, Vol 7, ed N.P. Chermisinoff, Gulf Publishing Co, Houston, 199 – 252.

Lazarus, J.H. and Nielson, I.D. (1978),. A generalised correlation for friction head losses of settling mixtures in horizontal smooth pipelines, 5th Int. Conf. on the hydraulic transport of solids in pipes, Hydrotransport 5, Paper B1.

Manning, R. (1890), On the flow of water in open channels and Pipes, Trans. Inst. Civil Eng. Ireland, 20, 161-207.

Slatter, P.T. (1994), Transitional and Turbulent flow of non-Newtonian slurries in pipes. Unpublished PhD thesis. University of Cape Town. Cape Town.

Sestak, J. (1974), Flow of non-Newtonian fluids in open circular channels, Can. J. Chem. Eng., 52, 670-672.

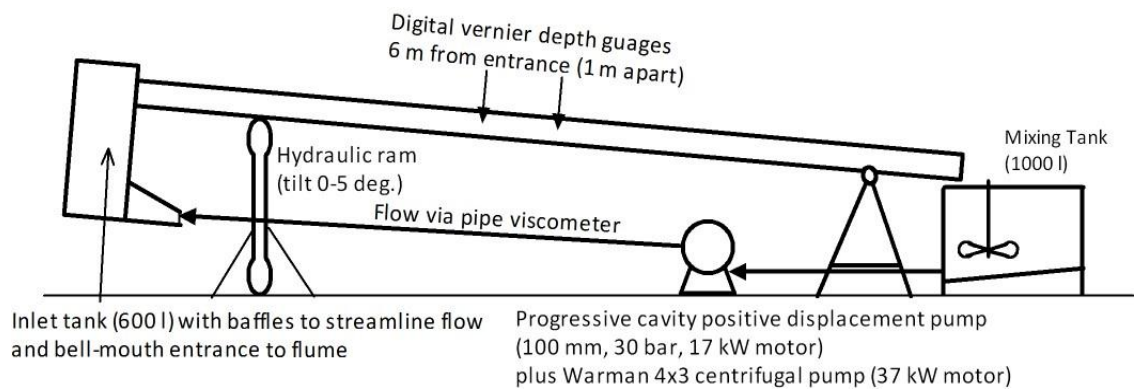
Straub, L.G., Silberman, E., and Nelson, H.C. (1958), Open channel flow at small Reynolds numbers, Trans ASCE, 123, 685 – 706.

Thomas, A.D. and Wilson, K.C. (1987), New analysis of non-Newtonian turbulent flow-yield power law fluids. Can. J. Chem. Eng., 65, 335-338.

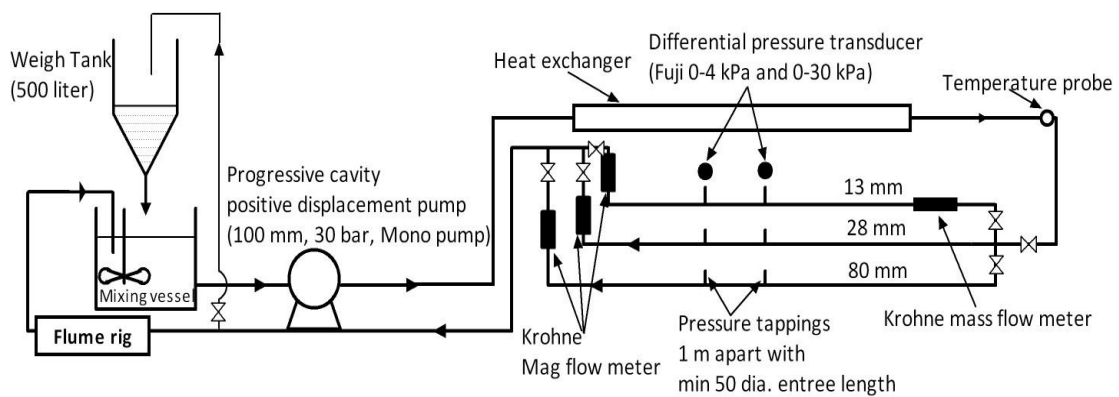
Torrance, B. McK. (1963), Friction factors for turbulent non-Newtonian flow in circular pipes, South African Mech. Eng., 13, 89-91.

Wilson, K.C. and Thomas, A.D. (1985), A new analysis of the turbulent flow of non-Newtonian fluids. Can. J. Chem. Eng., 63, 539-546.

Wilson, K.C. (1991), Flume design for homogeneous slurry flow, Particulate Science and Technology, 9, 149-159.



(a)



(b)

Figure 5.1(a) 10 m rectangular tilting flume linked to (b) 3-tube in-line viscometers

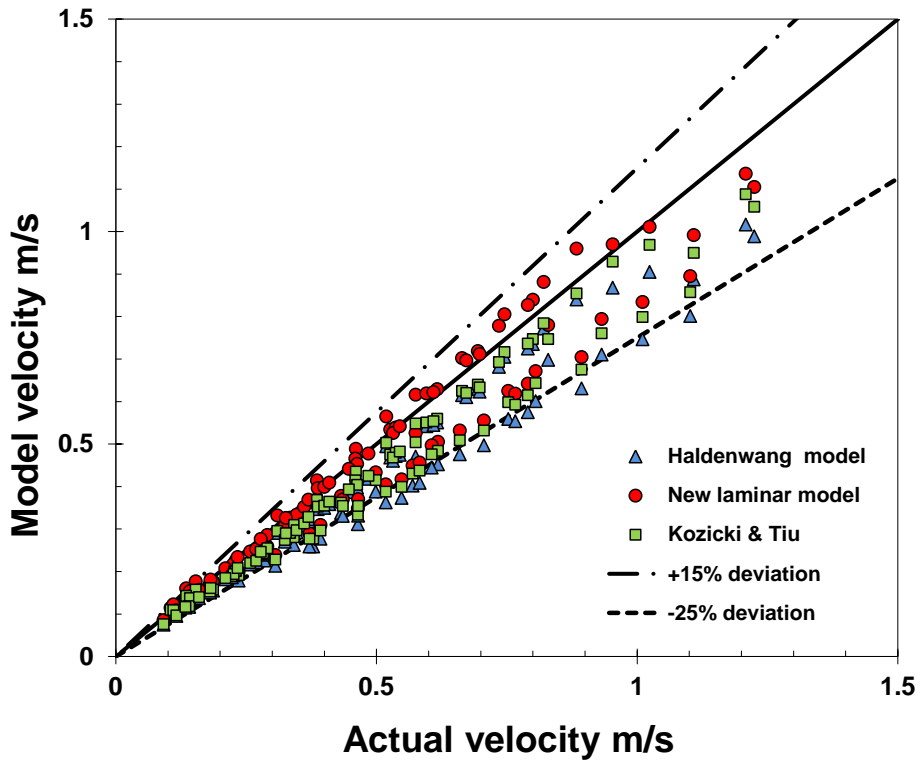


Figure 5.2 Model comparison based on velocity of 3.1 and 4.9% CMC solution flowing in a 300 mm triangular shape channel.

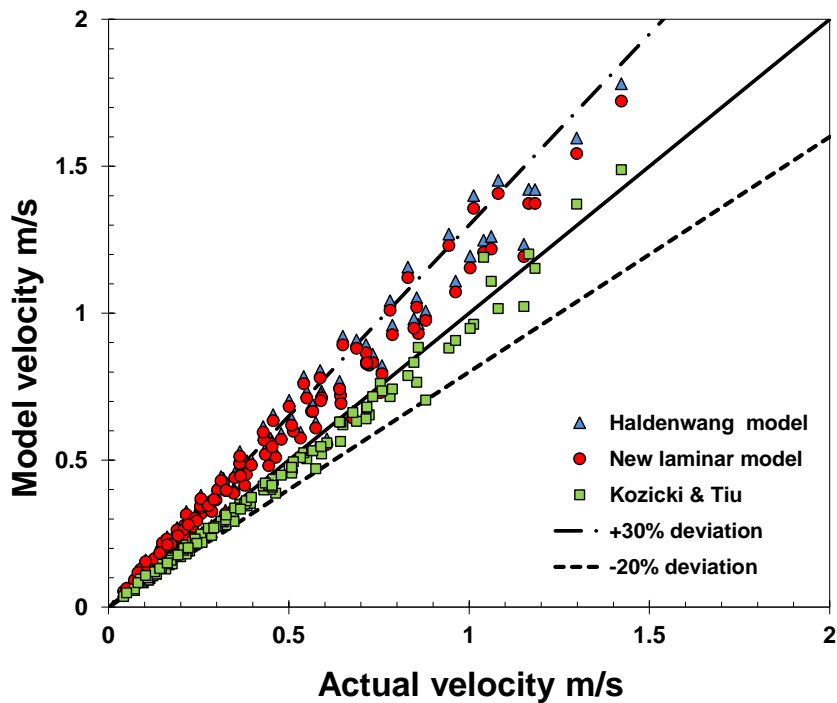


Figure 5.3 Model comparison based on velocity of 3% and 4% CMC solution flowing in a 150 and 300 mm rectangular channel.

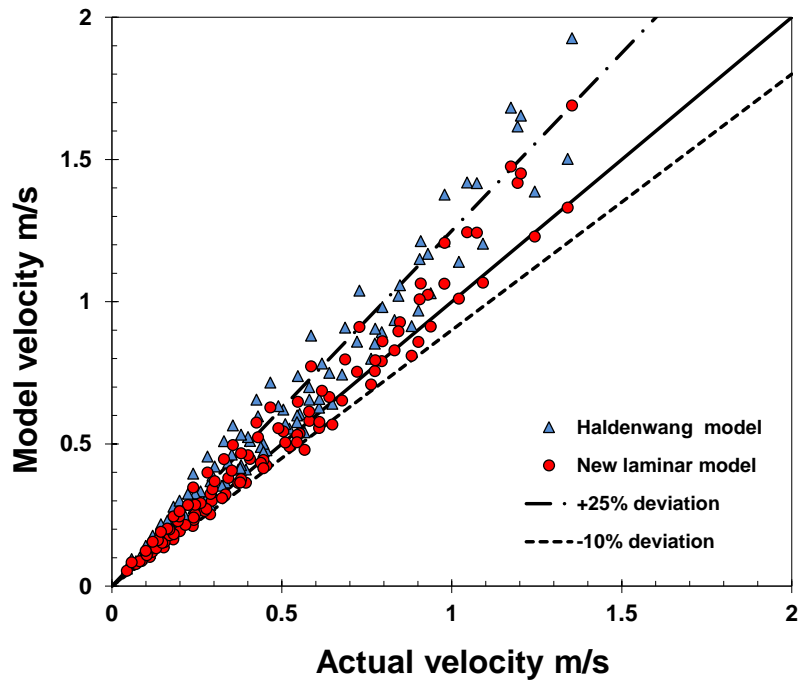


Figure 5.4 Model comparison based on velocity of 3 and 4% CMC solution flowing in a 150 mm trapezoidal channel.

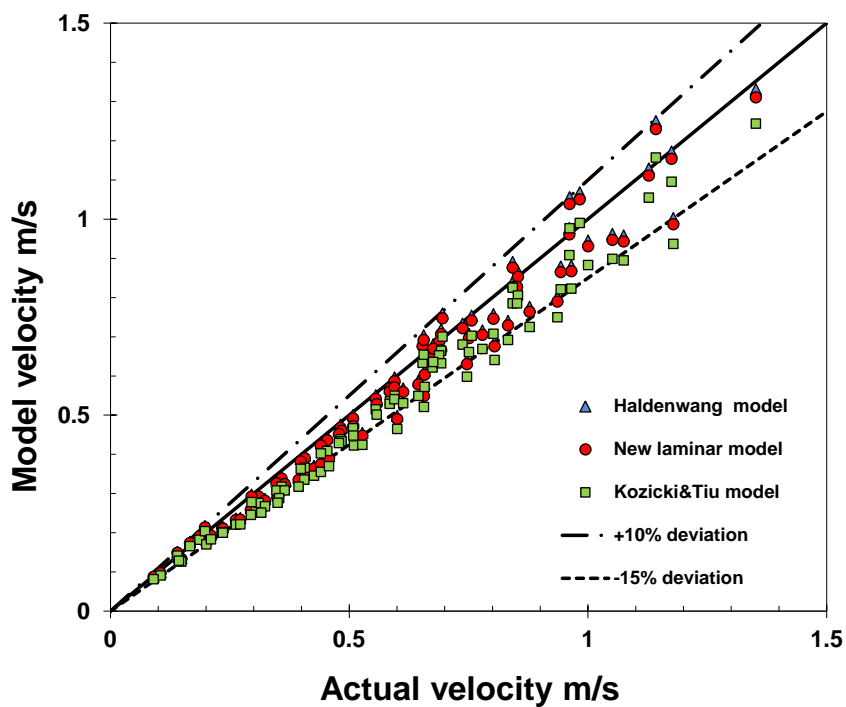


Figure 5.5 Model comparison based on velocity of 3 and 4% CMC solution flowing in a 150 mm and 300 mm semi-circular channel.

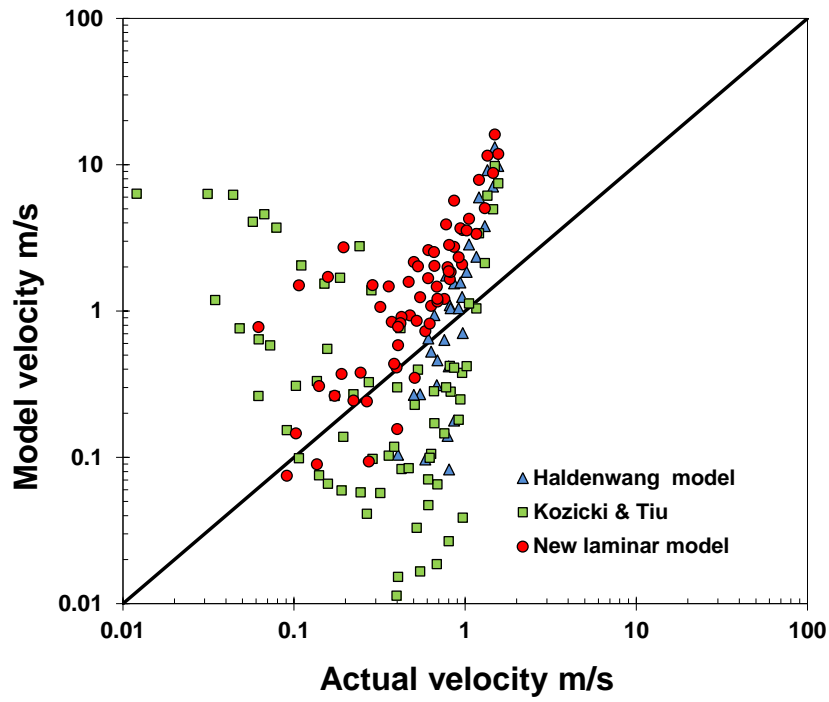


Figure 5.6 Model comparison based on velocity of 4.86 and 5.38% bentonite suspension flowing in a 300 mm triangular shaped channel.

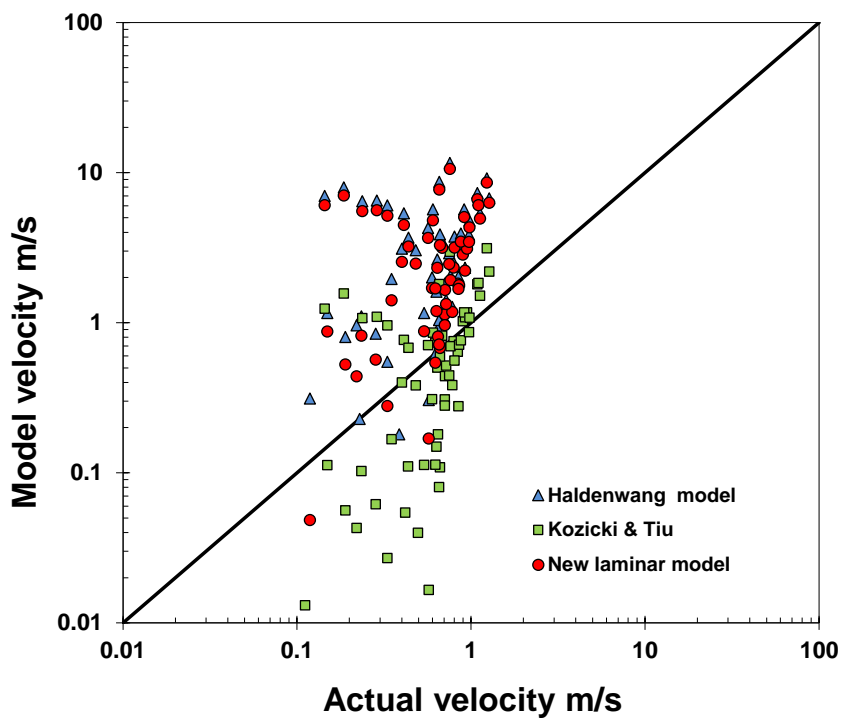


Figure 5.7 Model comparison based on velocity of 4.6 and 6.2% bentonite suspension flowing in a 300 mm semi-circular channel

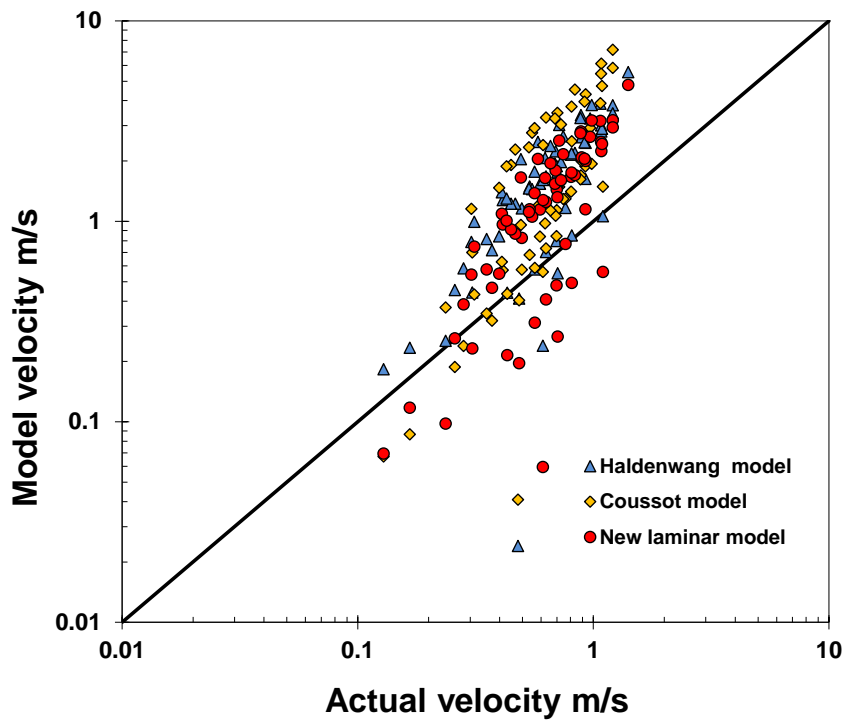


Figure 5.8 Model comparison based on velocity of 7.1 and 9% kaolin suspension flowing in a 150 and 300 mm rectangular channel.

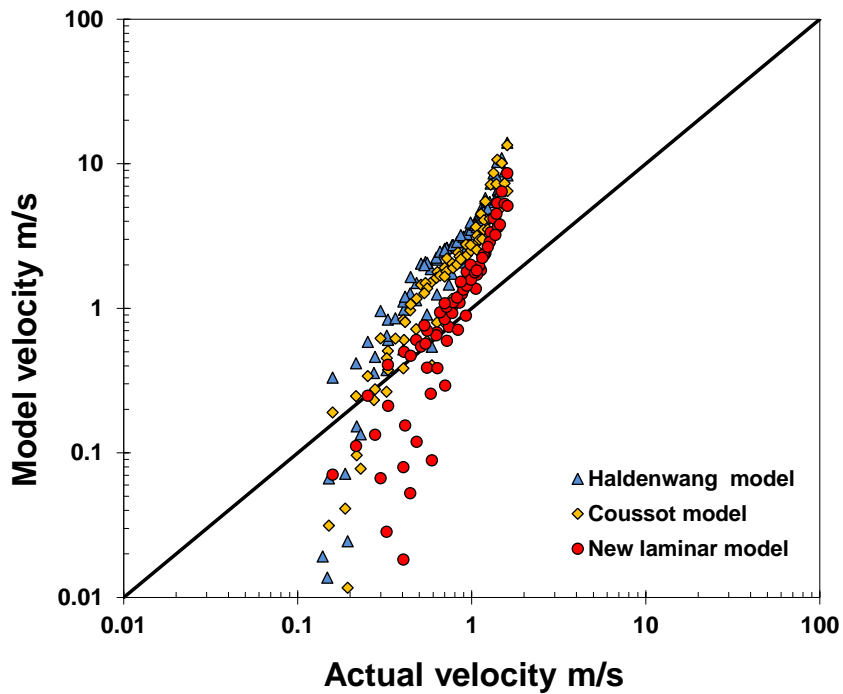


Figure 5.9 Model comparison based on velocity of 5.4 and 9% kaolin suspension flowing in a 75 and 150 mm trapezoidal channel.

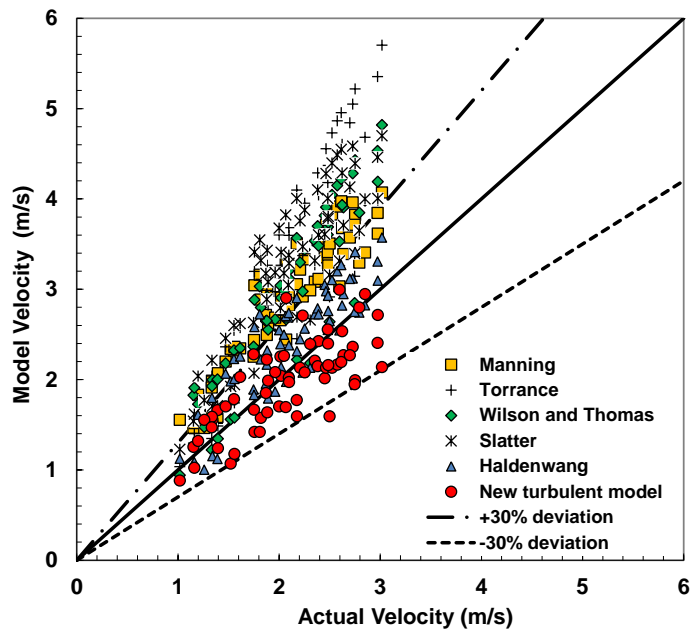


Figure 5.10 Model velocity comparisons for turbulent flow of three different non-Newtonian fluids in a 150 mm trapezoidal open channel.

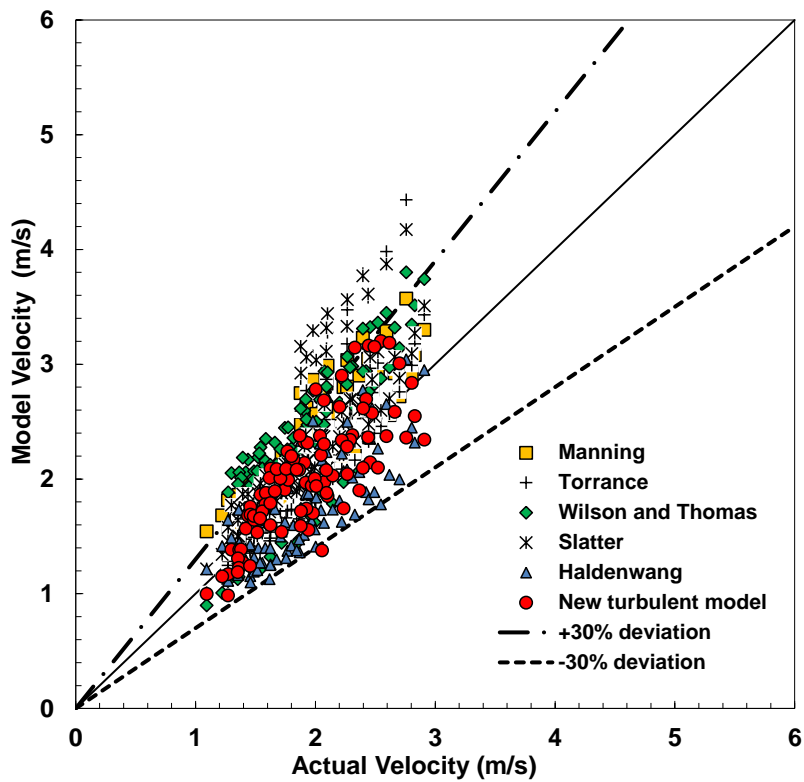


Figure 5.11 Model velocity comparisons for turbulent flow of three different non-Newtonian fluids in a 150 and 300 mm rectangular open channels.

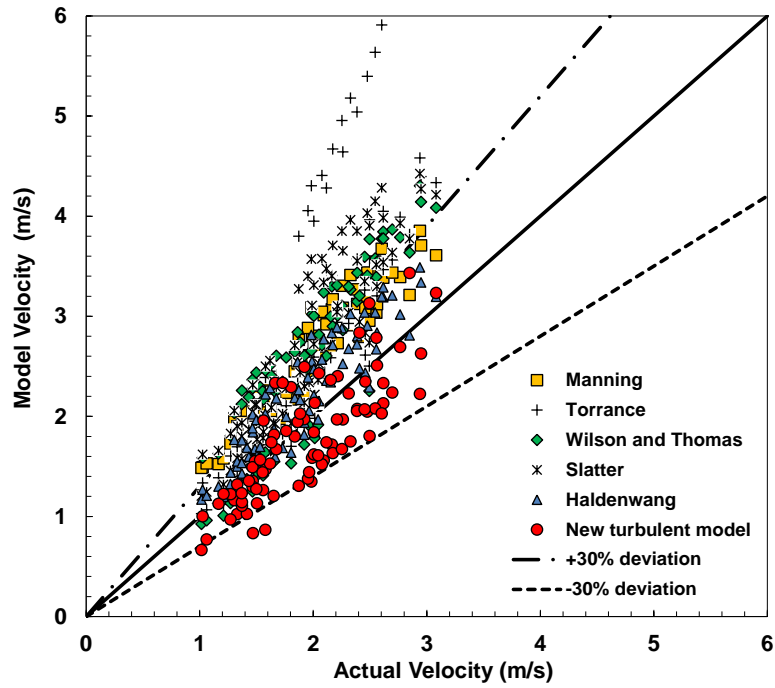


Figure 5.12 Model velocity comparison for turbulent flow of three different non-Newtonian fluids in a 150 and 300 mm semi-circular open channels.

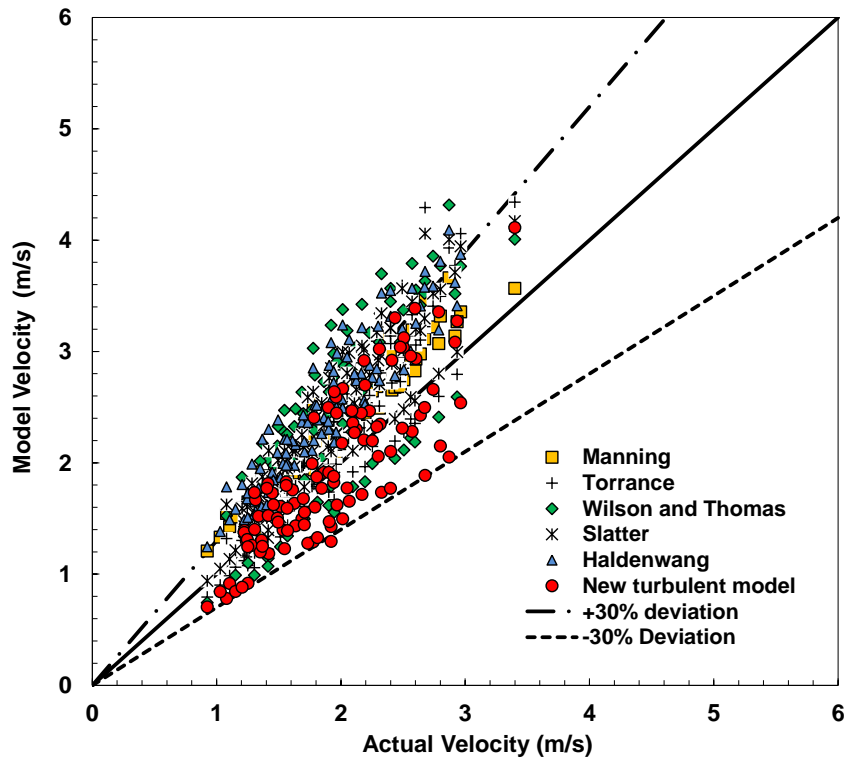


Figure 5.13 Model velocity comparison for turbulent flow of three different non-Newtonian fluids in a 300 mm triangular open channel.

Table 5.1 Open channel shapes used in this study

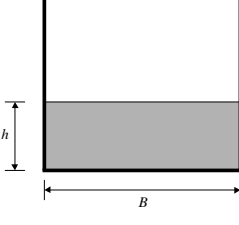
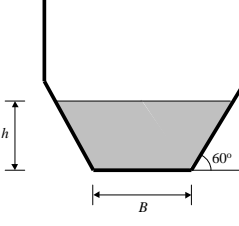
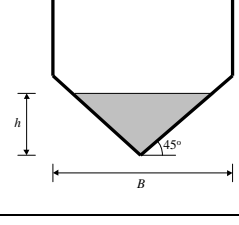
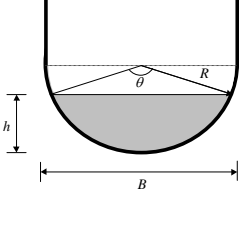
Section	Size	Cross-sectional area A	Wetted perimeter P	Surface width W
	$B = 300 \text{ mm}$ $B = 150 \text{ mm}$	Bh	$B + 2h$	B
	$B = 150 \text{ mm}$ $B = 75 \text{ mm}$	$h(B + xh)$ where $x = 1/\tan\theta$	$B + 2h\sqrt{1 + x^2}$ where $x = 1/\tan\theta$	$B + 2xh$ where $x = 1/\tan\theta$
	$B = 300 \text{ mm}$	h^2	$2h\sqrt{2}$	$2h$
	$B = 300 \text{ mm}$ $B = 150 \text{ mm}$	$\frac{D^2}{8}(\theta - \sin\theta)$ where θ $= 2\cos^{-1}\left(1 - \frac{2h}{D}\right)$	$D\left(\frac{1}{2}\theta\right)$ where θ $= 2\cos^{-1}\left(1 - \frac{2h}{D}\right)$	$D\left(\sin\frac{1}{2}\theta\right)$ where θ $= 2\cos^{-1}\left(1 - \frac{2h}{D}\right)$

Table 5.2 Summary of non-Newtonian, laminar flow models for open channels

Author	Year	Shape	BP	PL	HB	Average velocity	Reynolds number
Kozicki & Tiu	1967	Rectangular		•		$V = \frac{R_h}{2} \left(\frac{\bar{\tau}_w}{k} \right)^{\frac{1}{n}} \left(\frac{n}{a + bn} \right)$	$Re^*_{p} = \frac{R_h^n V^{2-n} \rho}{2^{n-3} k \left(\frac{a + bn}{n} \right)^n}$
		Triangular Semicircular	•			$V = \frac{R_h \bar{\tau}_w}{2 \eta_B} \left[\frac{1}{a + b} - \frac{\chi}{b} + \frac{a}{b(a + b)} \chi^{\frac{b}{a} + 1} \right]$	$Re^*_{B} = \frac{4 R_h V}{\eta_B} \left[\frac{1}{a + b} - \frac{\chi}{b} + \frac{a}{b(a + b)} \chi^{\frac{b}{a} + 1} \right]$
Coussot	1994	Rectangular Trapezoidal			•	$V = \frac{h}{\left[\frac{k}{\tau_{yHB}} \left\{ \frac{\alpha}{((\tau_w/\tau_{yHB}) - 1)} \right\}^{1.11} \right]^{\frac{1}{n}}}$ with $n = 1/3$	
Haldenwang	2002	Rectangular Triangular Semicircular	•	•	•	$V = \frac{R_h}{2} \left[\frac{\tau_w - \tau_{yHB}}{k} \right]^{1/n}$	$Re_{2(YPP)} = \frac{8\rho V^2}{\tau_{yHB} + k \left(\frac{2V}{R_h} \right)^n}$
Burger et al.	2014	Rectangular Triangular Semicircular Trapezoidal	•	•	•	$V = \frac{R_h}{2} \left[\frac{(16/K)\tau_w - \tau_{yHB}}{k} \right]^{1/n}$	$Re_{2(YPP)} = \frac{8\rho V^2}{\tau_{yHB} + k \left(\frac{2V}{R_h} \right)^n}$

Table 5.3 Turbulent Constants a and b used in the modified Blasius equation.

Shape	Rectangular	Semi-circular	Trapezoidal	Triangular
a	0.1200	0.0480	0.0851	0.0415
b	-0.3297	-0.2049	-0.2655	-0.2022

Table 5.4 Summary of non-Newtonian, turbulent flow models for open channels

Author	Year	BP	PL	HB	Average velocity	Reynolds number
Manning or Gauckler- Manning	1890 1867				$V = \frac{1}{n_{\text{Manning}}} (R_h)^{\frac{2}{3}} \sqrt{\sin \theta}$	
Torrance	1963	•	•	•	$\frac{V}{V_*} = \frac{3.8}{n} + \frac{2.78}{n} \ln \left(1 - \frac{\tau_y}{\tau_w} \right) + \frac{2.78}{n} \ln \left(\frac{V_*^{2-n} \rho (2R_h)^n}{K} \right) - 4.17$	$Re = \frac{8\rho V^2}{K \left(\frac{2V}{R_h} \right)^n}$
Wilson and Thomas	1985	•	•	•	$V = V_* \left(\frac{V_N}{V_*} + 11.6(A_r - 1) - 2.5 \ln A_r - \Omega \right) \quad V_* = \sqrt{\frac{\tau_w}{\rho}}$ $A_r = 2 \frac{1 + (\tau_y/\tau_w)^n}{1+n} \quad V_N = V_* \left(2.5 \ln \left(\frac{\rho V_* 2R_h}{\eta_e} \right) + 1.75 \right)$ $\Omega = -2.5 \ln \left(1 - \frac{\tau_y}{\tau_w} \right) - 2.5 \frac{\tau_y}{\tau_w} \left(1 + 0.5 \frac{\tau_y}{\tau_w} \right)$	$Re = \frac{4R_h V \rho}{\eta_e}$
Slatter	1994	•	•	•	$V = V_* \left(2.5 \ln \left(\frac{2R_h}{d_{85}} \right) + 2.5 \ln Re_r + 1.75 \right)$ provided $Re_r \leq 3.32$	$Re_r = \frac{8\rho V_*^2}{\tau_y + K \left(\frac{8V_*}{d_{85}} \right)^n}$
Haldenwang	2003	•	•	•	$V_{\text{turb}} = \sqrt{g h \sin \theta} \left(2.5 \ln \frac{2R_h}{e} - 76.86\eta_{500} - 9.45 \right)$	$Re_H = \frac{8\rho V^2}{\tau_{yHB} + K \left(\frac{2V}{R_h} \right)^n}$
New model	2014	•	•	•	$V_T = \sqrt{\frac{2\tau_w}{\rho a (Re_H)^b}}$	$Re_H = \frac{8\rho V^2}{\tau_{yHB} + K \left(\frac{2V}{R_h} \right)^n}$

Table 5.5 Summary of test materials

CMC solutions				
Concentration (%vol)	Density (kg/m ³)	τ_y (Pa)	k (Pa.s ⁿ)	n
1.5	1008	-	0.014	0.944
2.0	1013	-	0.035	0.776
3.0	1018	-	0.145	0.788
3.1	1018	-	0.091	0.823
4.0	1023	-	0.330	0.727
4.9	1028	-	0.599	0.690
5.3	1028	-	0.920	0.678
Bentonite in water suspensions				
Concentration (% vol)	Density (kg/m ³)	τ_y (Pa)	k (Pa.s ⁿ)	n
3.5	1022	3.0	0.0036	1
4.5	1027	4.3	0.0036	1
4.8	1029	5.7	0.0036	1
4.9	1030	5.2	0.0040	1
5.4	1033	7.3	0.0038	1
6.2	1038	15.8	0.0064	1
6.8	1042	18.3	0.0078	1
Kaolin in water suspensions				
Concentration (% vol)	Density (kg/m ³)	τ_y (Pa)	k (Pa.s ⁿ)	n
3.4	1056	1.3	0.051	0.568
3.5	1058	0.5	0.061	0.560
5.0	1082	3.6	0.060	0.630
5.4	1089	4.4	0.084	0.582
7.0	1115	8.2	0.142	0.570
7.1	1118	11.6	0.148	0.557
9.0	1148	19.0	0.210	0.616
9.2	1152	18.9	0.194	0.550

Table 5.6 Log square error values for laminar model velocities compared with measured velocities for models tested.

Material	Concentration %vol	Shape	Size(mm)	Model				Figure
				New	Haldenwang	Cousot	Kozicki&Tiu	
CMC	3.1& 4.9	Triangular	300	0.00550	0.00926	-	0.00744	2
	3 & 4	Rectangular	150 & 300	0.00814	0.00921	-	0.00398	3
	3 & 4	Trapezoidal	150	0.00610	0.00996	-	-	4
	3 & 4	Semi-circular	150 & 300	0.00463	0.00415	-	0.00662	5
Bentonite	4.86 & 5.38	Triangular	300	0.06806	0.10362	-	0.15487	6
	4.6 & 6.8	Rectangular	150 & 300	0.09641	0.10939	-	0.07359	
	4.5 & 6.8	Trapezoidal	150	0.07498	0.08790	-	-	
	4.6 & 6.2	Semi-circular	300	0.09348	0.09756	-	0.08266	7
Kaolin	6.99 & 9.23	Triangular	300	0.05862	0.16401	-	-	
	7.1 & 9	Rectangular	150 & 300	0.04708	0.05339	0.05853	-	8
	5.4 & 9	Trapezoidal	75 & 150	0.04610	0.06314	0.05632	-	9
	7.1 & 9	Semi-circular	300	0.06828	0.06043	-	-	

Table 5.7 Turbulent velocity model comparison for the flow of bentonite, CMC and kaolin in channel shapes tested based on log squared error (LSE) and correlation coefficient (R^2).

Shape	Model	R^2	LSE
Trapezoidal	New model	0.97	0.0098
	Haldenwang	0.97	0.0103
	Manning	0.92	0.0190
	Wilson-Thomas	0.90	0.0205
	Slatter	0.88	0.0241
	Torrance	0.86	0.0248
Rectangular	New model	0.98	0.0069
	Manning	0.97	0.0078
	Haldenwang	0.97	0.0082
	Torrance	0.96	0.0090
	Slatter	0.95	0.0098
	Wilson-Thomas	0.95	0.0121
Semi-circular	Haldenwang	0.97	0.0083
	New model	0.96	0.0104
	Manning	0.94	0.0141
	Wilson-Thomas	0.92	0.0152
	Slatter	0.91	0.0164
	Torrance	0.86	0.0183
Triangular	Manning	0.97	0.0078
	New model	0.97	0.0081
	Torrance	0.96	0.0082
	Slatter	0.95	0.0099
	Haldenwang	0.94	0.0122
	Wilson-Thomas	0.93	0.0126

CHAPTER 6

RESULTS

Laminar non-Newtonian open channel flow: Investigating velocity, wall shear stress and fluid depth

Published as

Burger, J.H., Haldenwang, R. and Alderman, N.J. 2010. Laminar non-Newtonian open channel flow: Investigating velocity, wall shear stress and fluid depth. 18th International Conference on Hydrotransport, Rio de Janeiro, Brazil; 22-24 September 2010.

Chapter 6 Laminar non-Newtonian open channel flow:

Investigating velocity, wall shear stress and fluid depth

Data for laminar non-Newtonian flow in various non-circular open channels can be described by a general relationship, $f = K/Re_H$ where f is the friction factor and Re_H is the appropriate Haldenwang et al. (2002) Reynolds number corresponding to the flow curve model used to describe the non-Newtonian behaviour exhibited by the test fluid. The K values were found to range from 14.6 to 17.6 depending on the channel shape used and to be similar to those reported for Newtonian flow Burger et al. (2010).

Despite the excellent alignment of $f = K/Re_H$ line with the data found for each channel shape, this paper outlines the concerns regarding the comparison of actual and model velocities, the comparison of measured and model wall stresses and the flow depth sensitivity. In terms of velocity, wall shear stress and flow depth prediction, the Haldenwang et al. (2002) model was found to hold reasonably well for power law fluids. However, this was not the case for Bingham plastic and Herschel-Bulkley fluids largely due to the failure of including the contribution of the yield stress in the calculation of the wall shear stress.

6.1 Introduction

Open channels, flumes or launders are used in the mining industry to transport mineral ore slurries or tailings to waste disposal sites. With open channel flow being a gravity driven process, the design of these channels is highly dependent on the available slope for flow. Mountainous terrain such as the Andes in Chile and Peru often provide ample gradient for channel flow over large distances. In these locations, the transportation of tailings is usually performed in turbulent flow where the flow depth is reasonably constant.

However, with water becoming a scarce and expensive resource, there has been a demand for significant reduction of water used in tailings preparation. With the requirement of tailings being transported at higher concentrations, this causes the slurry to become more non-Newtonian in nature to the extent that the flow in the channel is no longer turbulent. In this laminar flow regime, the flow depth can change dramatically depending on the slurry rheological properties. If the slurry exhibits viscoplastic behaviour, the impact on the flow depth is further complicated by the presence of a yield stress that must be overcome for slurry flow.

6.2 Laminar non – Newtonian open channel flow

Laminar flow of non-Newtonian flow in open channels of various cross-sectional shapes is of interest to several industries including the mining and minerals, paper and pulp, wastewater and food industries. The database for non-Newtonian flow in rectangular open channels developed by the Flow Process Research Centre (FPRC) at the Cape Peninsula University of Technology Haldenwang (2003) and Haldenwang & Slatter (2006) was recently extended to include non-Newtonian flow in open channels of semi-circular, triangular and trapezoidal cross-sections (Burger et al. 2010). Prior to the publication of this database, only limited experimental datasets were available. Coussot (1994) provided data for the flow of kaolin suspensions in rectangular and trapezoidal channels whereas

Naik (1983) obtained data for flow of kaolin suspensions in a rectangular flume. Wang and Plate (1996) and Wang (2002) carried out experimental studies on the flow of clay suspensions in rectangular channels. Fitton (2007, 2008) obtained data for flow of three different non-Newtonian fluids in semi-circular channels. Fitton (2007), (2008); Spelay et al. (2006) and Spelay (2007) used the FPRC database for verification purposes in their work.

As for pipe flow, open channel flow data can be presented in the form of a Moody chart where the Fanning friction factor, f is plotted against Reynolds number, Re allowing laminar, transitional or turbulent flow regimes to be identified (13,14), Here, f is given by

$$f = \frac{2R_h g \sin \theta}{V^2} \quad (2.13)$$

with Re being the Newtonian Reynolds number given by

$$Re = \frac{\rho V 4R_h}{\eta} \quad (6.1)$$

in which the hydraulic radius, R_h is defined as

$$R_h = \frac{A}{P} \quad (2.10)$$

where A is the cross-sectional area for flow and P is the wetted perimeter of the channel.

Along with the experimental data, Straub et al. (1958) presented a theory for laminar flow of Newtonian fluids in open channels with various cross-sections. They showed that the data in the laminar flow regime is defined by a general relationship

$$f = \frac{K}{Re} \quad (6.2)$$

where K is a numerical constant dependent on the channel shape. Analytical and numerical solutions for K were provided for a range of different cross-sectional shapes.

Very little has been reported in the literature for predicting non-Newtonian laminar flow in open channels of arbitrary cross-section. The earliest method was that proposed by Kozicki and Tiu (1967, 1986) who generalised the Rabinowitsch-Mooney equation applicable to pipe and slit flow for laminar flow of power law and Bingham plastic fluids in non-circular channels. Following the approach of by Kozicki & Tiu (1967, 1986) and Coussot (1994) derived expressions for laminar flow of a Herschel-Bulkley fluid in rectangular and trapezoidal channels. Unfortunately, these expressions were found to be erroneous since they did not contain the power law exponent anywhere within the expressions. By introducing a new Reynolds number based on the Herschel-Bulkley model adapted from the pipe Reynolds number presented by Slatter (1994) and Haldenwang et al. (2002) proposed an equation for the

friction factor-Reynolds number relationship for laminar flow of non-Newtonian fluids in non-circular open channels. This was given by

$$f = \frac{16}{\text{Re}_H} \quad (2.58)$$

where Re_H is given by

$$\text{Re}_H = \frac{8\rho V^2}{\tau_y + k \left(\frac{2V}{R_h} \right)^n} \quad (2.59)$$

An advantage of using this Reynolds number is that it can also be used for fluids exhibiting Newtonian, power law and Bingham plastic behaviour. Through the use of equation (2.58), they found the laminar flow data of three different non-Newtonian fluids in rectangular open channels did collapse onto the $f = 16/\text{Re}_H$ line. However, Burger et al. (2010) found the pipe flow paradigm of $f = 16/\text{Re}_H$ used by Haldenwang et al. (2002, 2004) for non-Newtonian flow in open channels of different cross-sectional shapes was incorrect. Instead, they found the use of Haldenwang et al. (2002) definition for Re given by equation (2.59) in the f vs. Re relationship as defined by equation (3.1) was more appropriate in describing non-Newtonian flow in non-circular open channels. This relationship is given by

$$f = \frac{K}{\text{Re}_H} \quad (3.1)$$

For the three non-Newtonian fluids in four different channels studied, they found the K values to be 14.6 for triangular channels with a vertex angle of 90° , 16.2 for semi-circular channels, 16.4 for rectangular channels and 17.6 for trapezoidal channels with 60° sides. All of these K values were found to be in line with those reported by Straub et al. (1958) and Chow (1959) for open channel flow of Newtonian fluids.

Alderman and Haldenwang (2007) carried out a limited comparative study between the various models for the prediction of laminar flow of power law, Bingham plastic and Herschel-Bulkley fluids in rectangular open channels using the data from the FPRC database. They concluded that the Haldenwang et al. (2002) model was the better model of the available models. Despite the excellent alignment of this model with the $16/\text{Re}_H$ line for all three non-Newtonian fluids, they found that this model only gave a good agreement between the model and actual velocities for power law fluids. The large scatter observed between the model and actual velocities for Bingham plastic and Herschel-Bulkley fluids were attributed to the yield stress as a parameter in the velocity calculation. Since Burger et al. (2010) found the use of the Haldenwang et al. (2002) model to be inappropriate for non-Newtonian flow in open channels of different cross-sectional shapes, this paper reports on the comparison of actual and model velocities and the comparison of measured and model wall shear stresses based on the f vs. Re relationship as defined by Eq. (3.1). In addition, the influence of the measured flow depth on these comparisons will be commented upon.

6.3 Experimental

The tests were carried out in a 10 m long tilting flume designed and built by the Flow Process Research Centre at the Cape Peninsula University of Technology. Further details of this flume can be found in Haldenwang (2003). This flume can be hydraulically tilted at various angles up to 5 degrees from the horizontal. The width of this rectangular flume can be changed from 300 to 150 mm by placing a partition mid-section lengthways down the flume. By inserting an appropriate cross sectional insert, the rectangular flume can be changed into a flume with a triangular, semi-circular or trapezoidal cross-section. The various flume shapes with its dimensions used in this study are shown in Figure 6.1.

Flow curve measurements of the test material were also made in-situ during the flume test using an in-line tube viscometer fitted with three tubes of different diameters, 13, 28 and 80 mm. Each of the three tubes was fitted with an electromagnetic flow meter and two differential pressure transducers across a fixed length. Calibration with water gave an error of less than 10% for both the flow rate and the pressure drop (Haldenwang, 2003).

A summary of the test materials can be found in Burger et al. (2010). For these materials, the flow curve data from the three different tube diameters were found to collapse onto a single curve thus confirming the non-presence of wall-slip during the flow curve measurement. Various model fits were then made to the flow curve data. It was found that the 1.5 to 5.3% v/v carboxymethyl cellulose (CMC) solutions, 3.5 to 6.2% v/v bentonite in water suspensions and 3.4 to 9.2% v/v kaolin in water suspensions was best represented by the power law, Bingham plastic and Herschel-Bulkley models respectively. The correlation coefficient was used here as the criterion for determining the best model fit. This analysis also showed errors in the wall shear stress and wall shear rate to be very small (typically 0.1% and 0.6% of the wall shear stress and the wall shear rate values). These findings are consistent with those found by Slatter (1994) who used the same range of materials in his pipe flow studies.

The flow, provided by a 100 mm progressive cavity, positive displacement pump and a Warman 4x3 centrifugal slurry pump, was monitored by an electromagnetic flow meter. The maximum flow rate achieved was 45 l/s. Flow depths were measured with digital depth gauges of $\pm 5\%$ accuracy fitted at the 5 and 6 m positions from the flume entrance. These two positions were found to be the optimum for depth measurement (Haldenwang, 2003). Since the difference in fluid depth between these two points was found to be minimal, the flow in this region can therefore be taken as steady. A data logger was used to record the various data outputs as a function of time. All data were then fed to a PC so that a Moody chart can be generated as output.

6.4 Results

Using all of the experimental data for laminar flow of three different non-Newtonian fluids of varying concentrations in each of the four channels of varying dimensions and slopes, an f vs. Re_H plot was obtained for each channel shape (Burger et al. 2010). These plots are reproduced in Figures 6.2 to 6.5 for rectangular, semi-circular, triangular and trapezoidal open channels respectively.

It can be seen from these plots that the most of the experimental data does collapse onto a master curve to within 1.2 to 1.6 SD (standard deviation) of the average K value. Burger et al. (2010) also concluded these K values to be in line with those reported for open channel Newtonian flow Straub et al. (1958) and Chow (1959) as opposed to the Haldenwang et al. (2002, 2004) assumption of using a constant value of 16 for all channel shapes.

This paper expands the work of Burger et al. (2010) to report on the comparison of actual and model velocities where the actual velocity is simply the volumetric flow rate divided by the flow cross-sectional area and the model velocity is given by the appropriate equation for the model given by Eq. (3.1) using measured values of R_h and $(\tau_w = R_h \rho g \sin \theta)$. Comparison of measured and model wall shear stresses where the measured wall stress is given by $(\tau_w = R_h \rho g \sin \theta)$ and the model wall shear stress is given by the appropriate equation for the model given by Eq. (3.1) using measured values of R_h and V . Good agreement between the velocity and wall shear stress comparisons will reaffirm the validity of the model given by Eq. (3.1) for predicting non-Newtonian flow in open channels of various cross-sectional shapes. Putting aside the different model given by Eq. (2.58) and (2.59) used for flow of three different non-Newtonian fluids in rectangular open channels, Alderman and Haldenwang (2007) did demonstrate that the velocity comparison did not always hold well despite the excellent alignment of the model with the $16/Re_H$ line. This was especially true for Bingham and Herschel-Bulkley fluids. In addition, the sensitivity of the flow depth measurement on open channel flow is discussed.

6.4.1 Comparison of actual and model velocities

Using the datasets for flow of 4 to 5% v/v CMC solutions in four different shaped channels, the actual and model velocities for a typical power law fluid are compared in Figure 6.6 This comparison shows that there is a $\pm 20\%$ variation between the actual and model velocities. Similar levels of variation were also observed for the other CMC solutions studied.

For fluids exhibiting yield stress behaviour, a similar plot to Figure 6.6 was obtained using a selected range of datasets for flow of kaolin and bentonite suspensions in four different shaped channels. This is given in Figure 6.7 where it can be seen that there is a vast deviation between the actual and model velocities. Here, the error is in the region of $\pm 1000\%$. This poor agreement is in spite of the excellent alignment of the K/Re_H line found by Burger et al. (2010). A possible cause of the large variation observed in Figure 6.7 is the introduction of the yield stress as a parameter in the calculation of the model velocities. Here, the contribution of the yield stress is ignored in the calculation of the wall shear stress that is used in the model velocity calculation.

6.4.2 Comparison of measured and model wall shear stresses

Using the same dataset used for Figure 6.6, the actual and model wall shear stresses for a typical power law fluid are compared in Figure 6.8. This comparison shows that there is a $\pm 10\%$ variation between the actual and model wall shear stresses. Similar levels of variation were also observed for the other CMC solutions studied.

Using the same datasets in Figure 6.7, the actual and model wall shear stresses for a range of fluids exhibiting yield stress behaviour are compared in Figure 6.9. This comparison shows that there is a $\pm 20\%$ variation between the actual and model wall shear stresses, which can be regarded to be within experimental error. However, a closer

inspection of Figure 6.9 seem to suggest that none of the individual datasets show a one-to-one agreement between model and actual wall shear stresses suggesting that the contribution of yield stress in the calculation of the wall shear stress should not be ignored.

6.4.3 Flow depth sensitivity

During the experimental test work, it was observed that the flow depth is a very sensitive parameter especially when the flow depth was small. Plots of flow depth as a function of velocity and volume concentration were obtained for the three different non-Newtonian fluids flowing in four different shaped channels at slopes varying from 1 to 5°. Figure 6.10 depicts the variation of the initial flow depth with volume concentration at slope angles of 2° and 4°. It can be seen from this plot that for a given slope, this variation appears to be independent of the channel shape at low concentrations and dependent of the channel shape at higher concentrations. Taking the worst case, there is an overall increase in the flow depth of ~2700% and ~1200% when the channel slope is 2° and 4° respectively.

A similar plot to Figure 10 for the variation of flow depth with volume concentration at the onset of transition flow is given in Figure 6.11. Here, similar conclusions for Figure 6. 10 can be applied for this plot except that for the worst case, there is an overall increase in the flow depth of ~2000% and ~880% when the channel slope is 2° and 4° respectively.

Comparison between measured and model flow depths at the start of flow and at the onset of transition flow are shown in Figures 6.12 and 6.13 for power law and yield stress fluids respectively. It can be seen that that there is a ± 5% and ± 20% variation between the measured and model flow depths for power law and yield stress fluids respectively. The larger scatter observed in Figure 6.11 can be attributed to the failure to include the contribution of the yield stress in the calculation of the wall shear stress when calculating the model flow depth.

6.5 Conclusions

Despite the excellent alignment of the $f = K/Re_H$ line with the data found for rectangular, semi-circular, triangular and trapezoidal open channels shown in Figures 6.2 to 6.5 respectively, a closer inspection of the data revealed the following observations.

- For power law fluids, there is a ±20% variation between the actual and model velocities, a ±10% variation between the actual and model wall shear stresses and a ± 5% variation between the measured and model flow depths.
- For Bingham and Herschel Bulkley fluids, there is a ±1000% variation between the actual and model velocities and a ±20% variation between the actual and model wall shear stresses and the measured and model flow depths. The scatter was attributed to the failure to the contribution of yield stress in the calculation of the wall shear stress when calculating model velocities/wall shear stresses/flow depths.

These observations would suggest a satisfactory design of open channels for laminar flow of power law fluids will be gained when using the Haldenwang et al. (2002) Reynolds number. However, this will not be the case for Bingham and Herschel-Bulkley fluids. Further research is needed to generalise the wall shear stress equation ($\tau_w = R_h \rho g \sin \theta$) to incorporate the contribution of the yield stress. This will require a better understanding of the shear stress distribution of the Bingham and Herschel-Bulkley fluids flowing in the open channel. An attempt at arriving at such an equation has been initially made for flow in rectangular channel but this will be reported only when a detailed analysis of the data has been completed.

NOTATION

Symbol	Description	Units
A	cross-sectional area of flow	m ²
B	channel width	m
<i>f</i>	Fanning friction factor	-
g	acceleration due to gravity	m/s ²
h	flow depth	m
K	laminar flow constant in the <i>f</i> vs. Re relationship Eq. (3.1)	-
k	consistency coefficient	Pa.s ⁿ
n	flow behaviour index	-
P	wetted perimeter	m
Re	Reynolds number	-
Re _H	Haldenwang et al Reynolds number, Eq. (2.59)	-
R _h	hydraulic radius	m
V	average velocity	m/s
μ _N	Newtonian viscosity	Pa.s
θ	slope angle from the horizontal	degrees
ρ	density	Kg/m ³
τ _w	wall shear stress	Pa
τ _y	yield stress	Pa

6.6 References

Alderman, N.J. & Haldenwang, R. 2007. A review of Newtonian and non-Newtonian flow in rectangular open channels. *Hydrotransport 17, The Southern African Institute of Mining and Metallurgy and the BHR Group, Cape Town, SA*, 87-106.

Burger, J.H., Haldenwang, R. & Alderman, N.J. 2010. Friction factor-Reynolds number relationship for laminar flow of non-Newtonian fluids in open channels of different cross-sectional shapes, *Chemical Engineering Science*, 65(11):3549-3556.

Burger, J.H., Haldenwang, R. & Alderman, N.J. 2010. Experimental procedure and database for non-Newtonian flow in different channel shapes, *Journal of Hydraulic Research*, 48(3): 363–370.

Chow, V.T. 1959. *Open Channel Hydraulics*. New York: McGraw-Hill. 9-12.

Coussot, P. 1994. Steady laminar flow of concentrated mud suspensions in open channels. *Journal of Hydraulic Research*, 4(32): 535-558.

Fitton, T.G. 2007. Tailings beach slope prediction. Unpublished PhD thesis, Royal Melbourne Institute of Technology, University, Melbourne, Australia.

Fitton, T.G. 2008. Non-Newtonian Open Channel Flow – A Simple Method of Estimation of Laminar/Turbulent Transition and Flow Resistance. *Paste 2008*, Kasane, Botswana, 245-251.

Haldenwang, R., Slatter, P.T. & Chhabra, R.P. 2002. Laminar and Transitional Flow in Open Channels for Non-Newtonian Fluids. *Hydrotransport 15: 15th International Conference on the Hydraulic Transport of Solids in Pipes*. Banff, Canada, Organised by BHR Group, Cranfield, Bedfordshire, UK, 755-768.

Haldenwang, R. 2003. Flow of Non-Newtonian Fluids in Open Channels. Unpublished D. Tech. thesis. Cape Technikon, Cape Town SA.

Haldenwang, R., Slatter, P.T., Vanayza, S., & Chhabra, R.P. 2004b. The Effect of Shape on Laminar Flow in Open Channels for Non-Newtonian Fluids. *16th International conference on Hydrotransport*, Santiago Chile, 311-324.

Haldenwang, R. & Slatter, P.T. 2006a. Experimental Procedure and Database for Non-Newtonian Open Channel Flow. *Journal Hydraulic Research*. 44(2): 283-287.

Kozicki, W. & Tiu, C. 1967. Non-Newtonian Flow Through Open Channels. *Canadian Journal of Chemical Engineers*, 45: 127-134.

Kozicki, W. & Tiu, C. 1986. Parametric Modelling of Flow Geometries in Non-Newtonian Flows. *Encyclopaedia of Fluid Mechanics, Vol 7, N.P. Cheremisinoff. (ed)*. Houston: Gulf Publishing Co, 199 – 252.

Naik, B. 1983. Mechanics of Mudflow Treated as the Flow of a Bingham Fluid. Unpublished PhD thesis. Washington State University.

Slatter, P.T. 1994. Transitional and Turbulent Flow of Non-Newtonian Slurries in Pipes. Unpublished PhD thesis. University of Cape Town, Cape Town SA.

Spelay, R., Sumner, R.J., Sanders, R.S. & Gillies, R.G. 2006. Laminar Open Channel Flow of Kaolin Clay Slurries Containing Sand. *13th International Conference Transport and sedimentation of solid particles*, Tbilisi Georgia, 300-317.

Spelay, R. 2007. Solids Transport in Laminar, Open Channel Flow of Non-Newtonian Slurries. Unpublished PhD thesis. University of Saskatchewan, Saskatoon CA.

Straub, L.G., Silberman, E. & Nelson, H.C. 1958. Open Channel Flow at Small Reynolds Numbers. *American Society of Civil Engineers*, 123: 685–713.

Wang, Z.-Y. & Plate, E.J. 1996. A Preliminary Study on the Turbulence Structure of Flows of Non-Newtonian Fluid. *Journal Hydraulic Research*, 34(3): 345-361.

Wang, Z.-Y. 2002. Free Surface Instability of Non-Newtonian Laminar Flows. *Journal Hydraulic Research*, 40(4): 449-460.

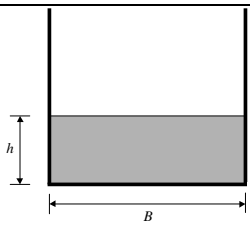
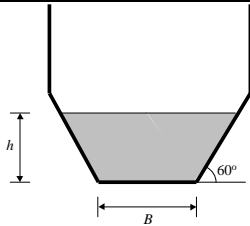
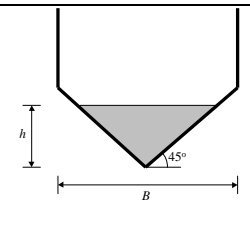
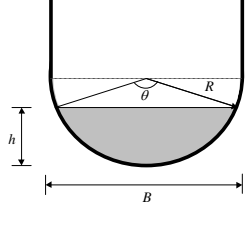
Section	Size	Cross-sectional area A	Wetted perimeter P	Surface width W
	B = 300 mm B = 150 mm	Bh	B + 2h	B
	B = 150 mm B = 75 mm	$h(B + xh)$ where $x = 1/\tan\theta$	$B + 2h\sqrt{1 + x^2}$ where $x = 1/\tan\theta$	$B + 2xh$ where $x = 1/\tan\theta$
	B = 300 mm	h^2	$2h\sqrt{2}$	2h
	B = 300 mm B = 150 mm	$\frac{D^2}{8}(\theta - \sin\theta)$ where $\theta = 2\cos^{-1}\left(1 - \frac{2h}{D}\right)$	$D\left(\frac{1}{2}\theta\right)$ where $\theta = 2\cos^{-1}\left(1 - \frac{2h}{D}\right)$	$D\left(\sin\frac{1}{2}\theta\right)$ where $\theta = 2\cos^{-1}\left(1 - \frac{2h}{D}\right)$

Figure 6.1 Various flume shapes used in this study

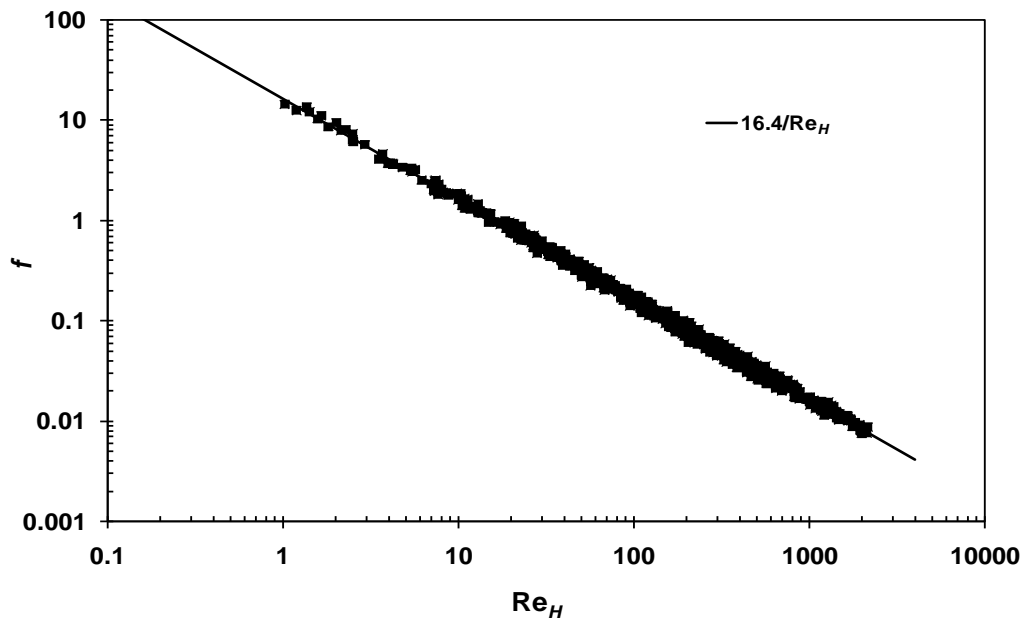


Figure 6.2 A f vs. Re plot showing 647 data points for laminar flow of three different non-Newtonian fluids in a rectangular flume at slope angles of 1 to 5°.

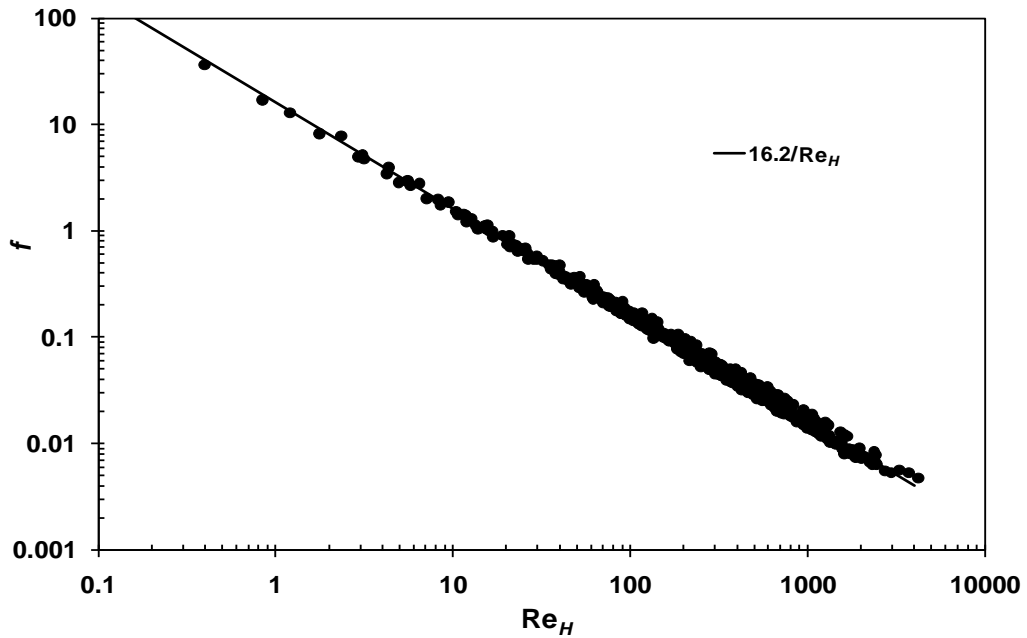


Figure 6.3 A f vs. Re plot showing 485 data points for laminar flow of three different non-Newtonian fluids in a semi-circular flume at slope angles of 1 to 5°

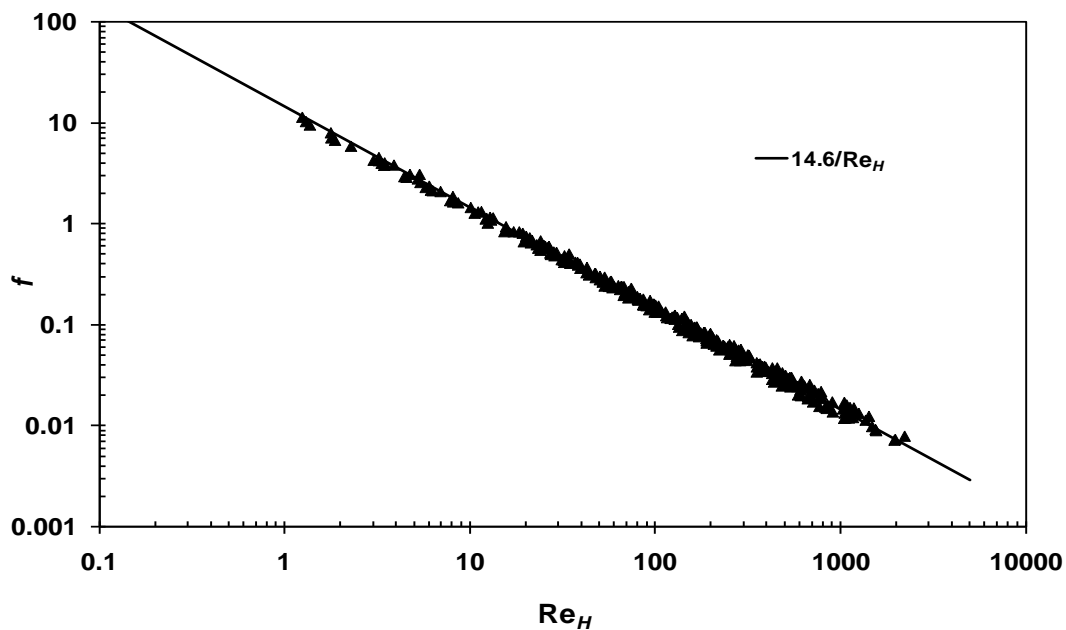


Figure 6.4 A f vs. Re plot showing 326 data points for laminar flow of three different non-Newtonian fluids flowing in a triangular flume at slope angles of 1 to 5°.

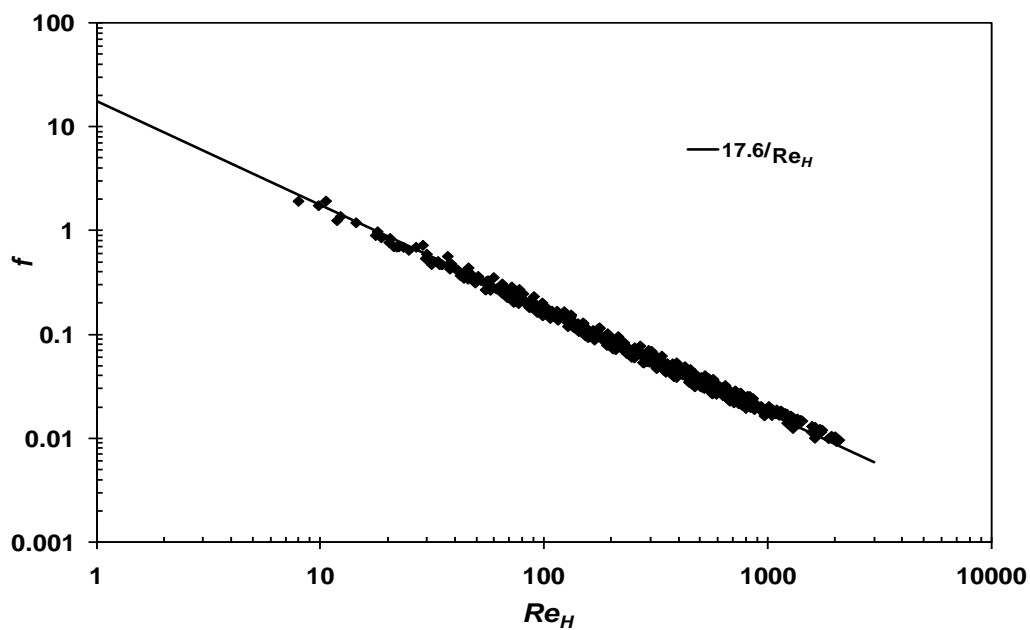


Figure 6.5 A f vs. Re plot showing 460 data points for laminar flow of three different non-Newtonian fluids flowing in a trapezoidal flume at slope angles of 1 to 5°.

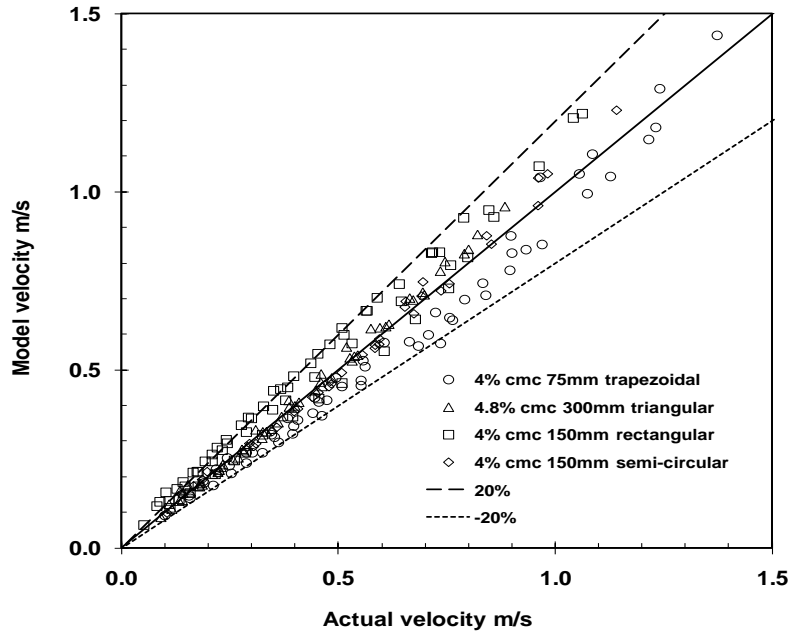


Figure 6.6 Velocity comparison for a typical power law fluid flowing in four different shaped channels.

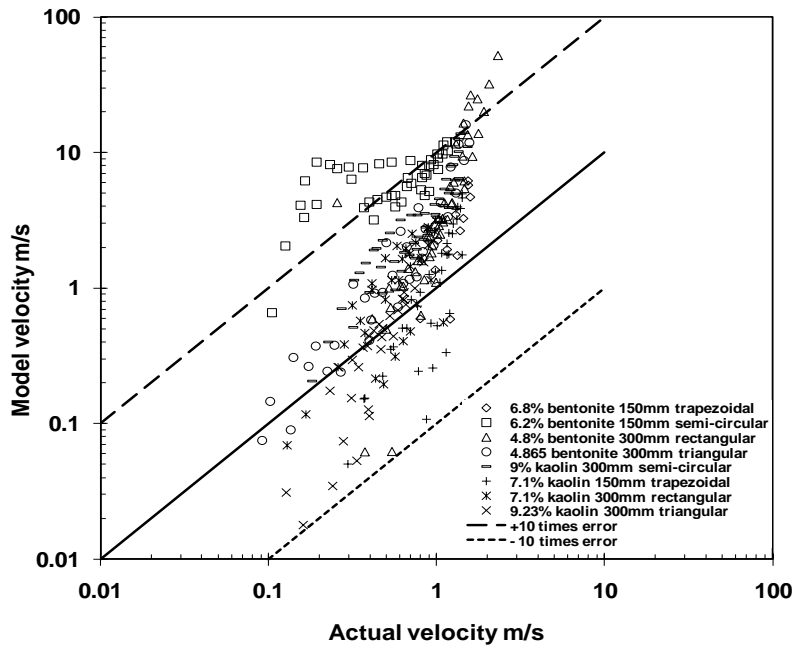


Figure 6.7 Velocity comparison for a range of yield stress fluids flowing in four different shaped channels.

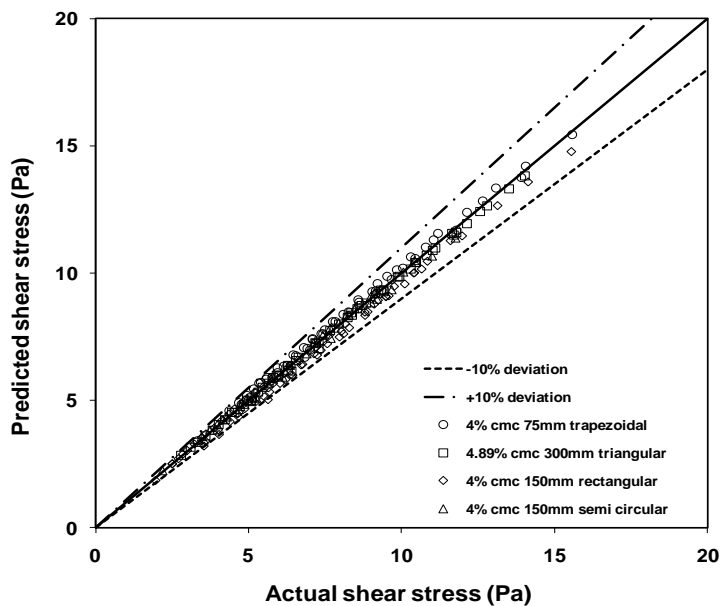


Figure 6.8 Wall shear stress comparison for a typical power law fluid flowing in four different shaped channels.

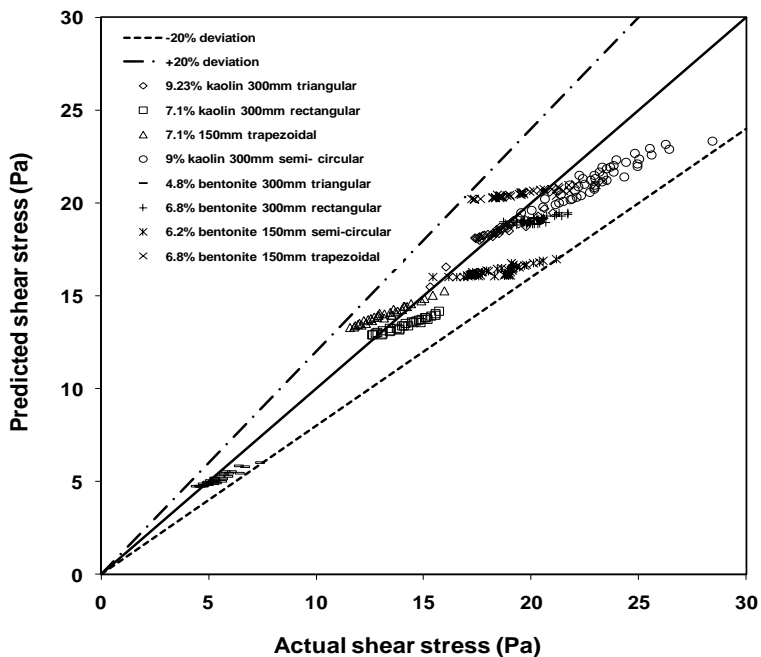


Figure 6.9 Wall shear stress comparison for a range of yield stress fluids flowing in four different shaped channels.

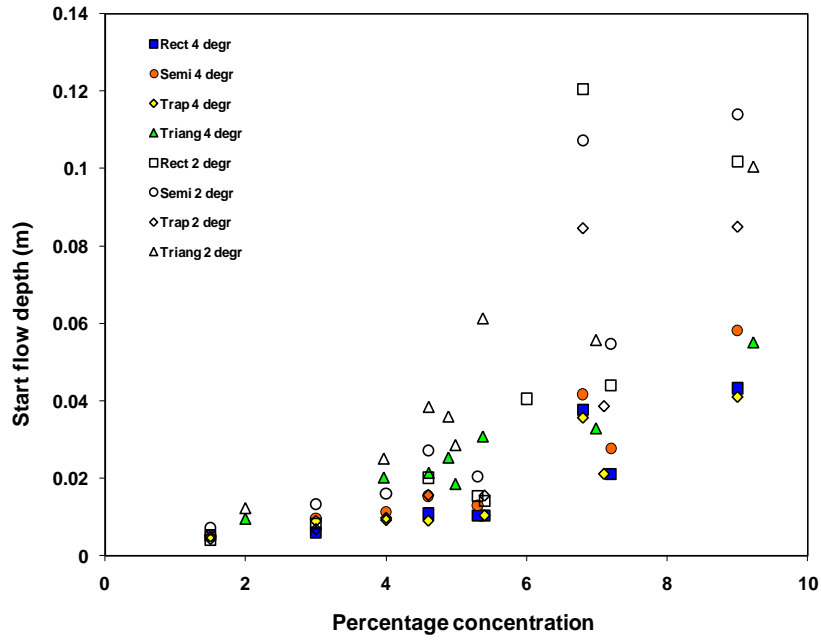


Figure 6.10 Initial flow depth versus volume concentration of three different non-Newtonian fluids flowing in four different shaped channels at slopes of 2° and 4°.

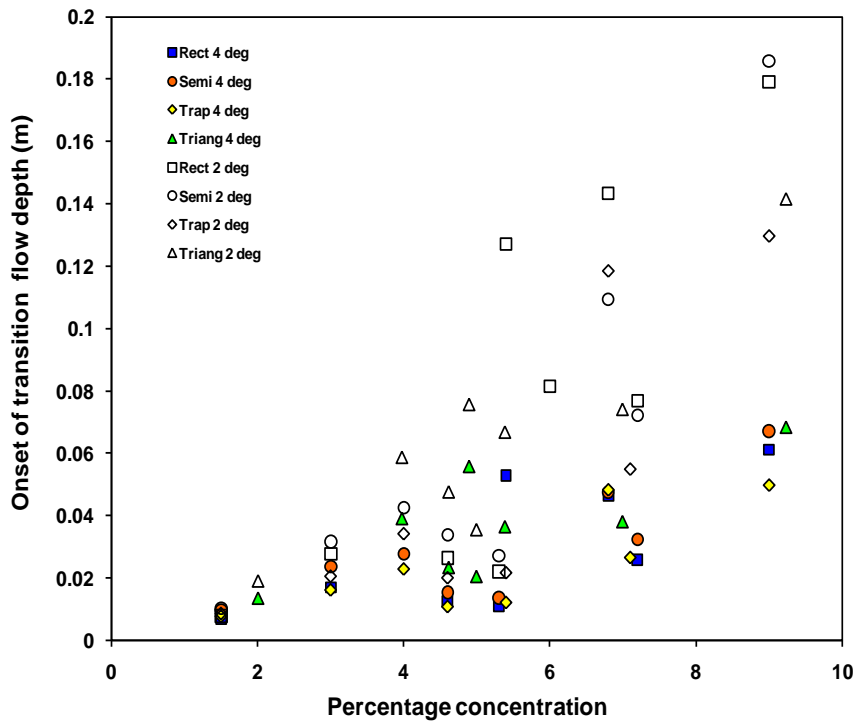


Figure 6.11 Onset of transition flow depth versus volume concentration of three different non-Newtonian fluids flowing in four different shaped channels at slopes of 2° and 4°.

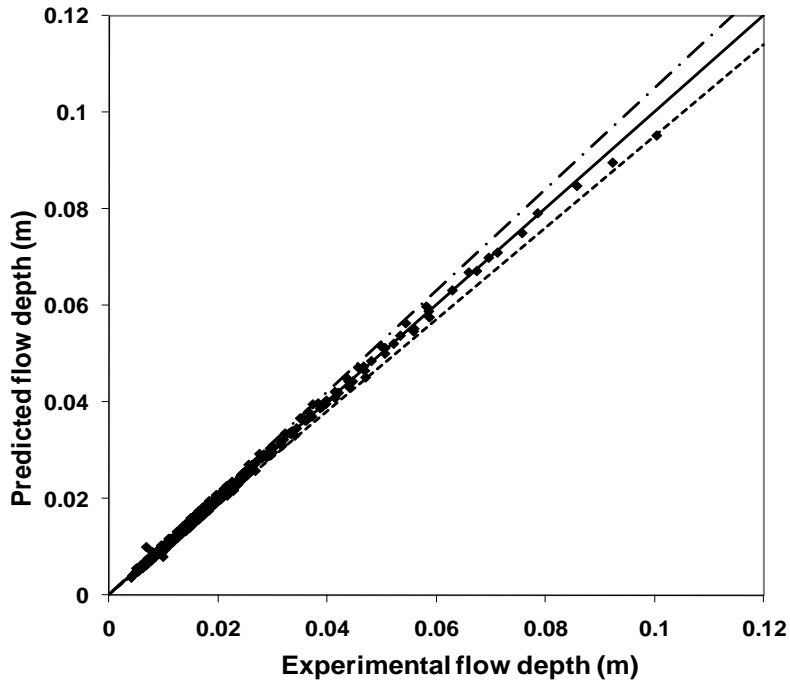


Figure 6.12 Predicted versus measured flow depth at start and end of laminar flow for CMC solutions flowing in four different shaped channels.

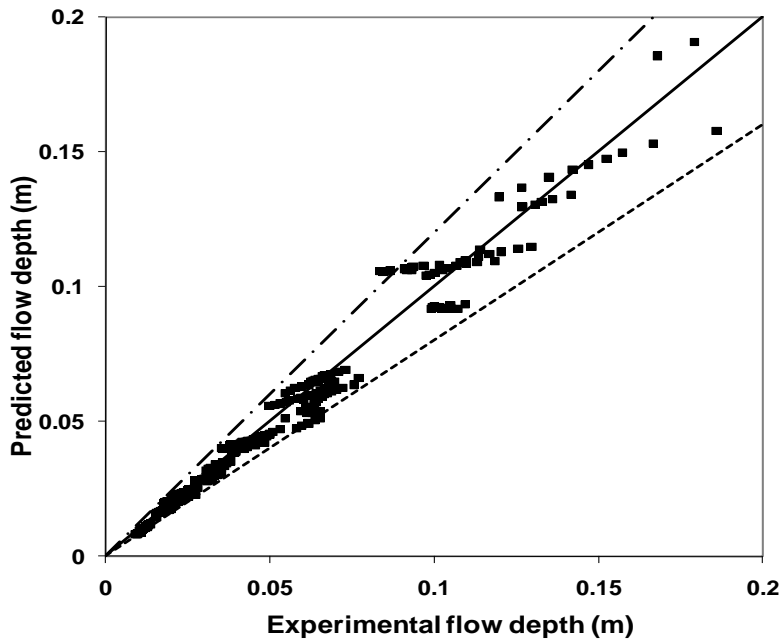


Figure 6.13 Predicted versus measured flow depth at start and end of laminar flow for kaolin and bentonite suspensions flowing in four different shaped channels.

CHAPTER 7

RESULTS

Power law and composite power law friction factor correlations for laminar and turbulent non-Newtonian open channel flow

Accepted for Publication as

Burger, J.H., Haldenwang, R., Chhabra, R.P. and Alderman, N.J. 2013. Power law and composite power law friction factor correlations for laminar and turbulent non-Newtonian open channel flow J. Braz. Soc. Mech. Sci. Eng.

DOI 10.1007/S40430-014-0188-1

Chapter 7 Power law and composite power law friction factor correlations for laminar and turbulent non-Newtonian open channel flow

Abstract

Extensive experimental results conducted in a 10 m flume for various types of non-Newtonian fluids spanning a range of cross-sectional open channel shapes are presented and analysed in depth in this work. Open channel flow of non-Newtonian slurries is relevant in mining and chemical engineering applications. This database coupled with the literature data is used to develop the generalized friction factor-Reynolds number correlations in a unified fashion. Much confusion still exists in the literature regarding the definition of non-Newtonian Reynolds numbers. This difficulty is circumvented by considering two widely accepted definitions of the Reynolds number, namely due to Haldenwang et al. (2002) for open channel flow and the modified Metzner-Reed pipe flow Reynolds number adapted for open channel flow. Three different types of purely viscous non-Newtonian fluids in rectangular, trapezoidal, triangular and semi-circular channel shapes were tested. The modelling procedure of Garcia et al. (2003) used for pipe flow predictions was extended to the present work. The logistic dose curves based on the Reynolds number proposed by Haldenwang et al. (2002) performed better than those based on the adapted Metzner-Reed Reynolds number. Correlations developed can be used for the design of open channels of various shapes to transport non-Newtonian fluids.

Keywords: open channel, non-Newtonian fluid, friction factor, Reynolds number, laminar and turbulent flow.

7.1 Introduction

The design of open channels for transporting water in turbulent flow has been successfully done for millennia (Chow, 1959). For non-Newtonian fluids, this is, however, not the case. Although several studies have been conducted in the past few decades (e.g., Kozicki and Tiu, 1967, 1986; Coussot, 1994; Naik, 1983; Haldenwang, 2003; Haldenwang and Slatter, 2006; Fuentes, 2004; Fitton, 2007, 2008 and Burger et al., 2010), this is still largely an empirical process depending very much on the accurate measurement of the non-Newtonian properties of the fluid especially in laminar flow. In turbulent flow the yield stress and shear thinning properties have been found to have a much less of an influence than that for laminar flow. Here, models for Newtonian channel flow have been found to predict non-Newtonian channel flow reasonably well with acceptable levels of accuracy. As for Newtonian fluids, the cross-sectional channel shape undoubtedly affects the flow characteristics; the corresponding work with non-Newtonian fluids in open channel flow has been rather limited. There are a few studies available for flow of non-Newtonian fluids in rectangular open channels (Coussot, 1994; Haldenwang, 2003; Haldenwang and Slatter, 2006 and Burger et al., 2010), in semi-circular open channels (Fitton, 2007, 2008 and Burger et al., 2010) and in trapezoidal and triangular open channels (Burger et al., 2010).

Work on dam-break channel flows with non-Newtonian fluids was extensively reviewed by Minussi et al. (2012). They also investigated the dam-break flow behaviour of aqueous Carbopol 940 solutions (characterised by the

Herschel-Bulkley model) in a 320 mm rectangular shaped channel. These abrupt releases of fluid results were then compared with different numerical simulations. They found the numerical code based on complete momentum equations gave the best agreement.

In several industrial applications, non-Newtonian fluids are transported in open channels of different cross-sectional shapes. In the mining industry, open channels with rectangular, semi-circular and trapezoidal cross-sections are used to transport tailings from the mine to the disposal facilities (Haldenwang and Slatter, 2006). Other applications include wastewater and food processing industries where different shapes of channels are used (Fitton, 2008).

Open channel flow data, as for pipe flow data, are often expressed in the dimensionless form as a Fanning friction factor versus Reynolds number f vs. Re plot which is often referred to as the Moody diagram. This form of representation not only reconciles results for the open channel flow of Newtonian and non-Newtonian fluids, but also facilitates the delineation of the laminar, transitional and turbulent flow regimes. In laminar flow, the f vs. Re plot is influenced by the rheology of the non-Newtonian fluid flowing through the channel and by adopting Re_H , the Haldenwang et al. (2002) Reynolds number, as Re , to account for this non-Newtonian behaviour, the f vs. Re plot in laminar flow collapses onto a single line with the slope being influenced by the channel shape through the friction factor Reynolds number relationship, $f = K/Re_H$ where K is a constant specific to a channel shape (Burger et al., 2010). As for pipe flow of non-Newtonian fluids, it is far more difficult to analyse the data for open channel non-Newtonian flow operating in the transitional and turbulent flow regimes than that in the laminar flow regime. This study endeavours to fill this gap in the literature.

The aim of this study is to develop a composite model covering both laminar and turbulent flow regimes for different types of non-Newtonian fluids flowing in four different channel shapes. A composite power law friction factor modelling technique introduced by Garcia et al. (2003) for the estimation of pressure drop in both the laminar and turbulent flow regimes in pipes is explored here for the analogous case in open channels.

7.2 Dimensional Considerations

The friction factor versus Reynolds number f vs. Re correlations for the flow of water in rectangular and triangular shaped open channels has been reported by Chow (1959) where he used the data of Straub et al. (1958) to develop the correlations. These, as well as the other studies are summarized in standard textbooks (e.g. Chow, 1959; Chanson, 1999; Chhabra, & Richardson, 2008). Using a Reynolds number based on a paradigm of the pipe Reynolds number (Slatter, 1994), Haldenwang et al. (2002) collapsed rectangular channel data onto a single f vs. Re plot (Haldenwang et al., 2002). This analysis was subsequently extended using additional rectangular channel data by Haldenwang and Slatter (2006).

The Fanning friction factor is given by

$$f = \frac{2gR_h \sin\theta}{V^2} \quad (2.13)$$

in which the hydraulic radius, R_h is defined as

$$R_h = \frac{A}{P} \quad (2.10)$$

where A is the cross-sectional area for flow and P is the wetted perimeter of the channel. Expressions for A and P for the different open channel shapes tested can be found in Table 7.1. In its most general form, the appropriate Reynolds number to be used for the f vs. Re relationship is given by

$$Re_H = \frac{8\rho V^2}{\tau_y + k \left(\frac{2V}{R_h} \right)^n} \quad (2.59)$$

where τ_y , k and n are yield stress, consistency coefficient and power law index as defined by the Herschel-Bulkley model respectively (Haldenwang et al., 2002). An advantage of using this Reynolds number is that it can also be used for fluids exhibiting Newtonian, power law and Bingham plastic behaviour. By putting $n = 1$ and $\tau_y = 0$ in Eq. (59) will yield the Newtonian Reynolds number whereas by putting $\tau_y = 0$ in Eq. (59) will give the power law Reynolds number. Finally, by putting $n = 1$ in Eq. (59) will result in the Bingham plastic Reynolds number.

The volumetric flow rate of the fluid flowing down the channel, Q and the flow depth, h are both experimentally measured. Since $Q = VA$ where A is the cross-sectional area for flow, the velocity V required for Eqn. (59) can then be obtained.

Burger et al. (2010) extended the database to include data for semi-circular, trapezoidal and triangular channels using the same set of non-Newtonian fluids that was previously used. The effect of channel shape in the laminar flow using the extended database was studied by Burger et al (2010). A distinct characteristic of the laminar flow region is the constancy of $K = f Re_H$ which is only dependent on the shape of the flow passage. The resulting values of the K for the shapes studied thus far are summarised in Table 7.3.

It is worthwhile to add here that the literature is inundated with several other definitions of the Reynolds numbers and some of these were compared with Eq. (59) in a review by Alderman and Haldenwang (2007). From this study, they concluded that the Reynolds number given by Eq. (59) adequately accommodates the flow curve characteristics for all the fluids studied in open channels over a wide range of Reynolds numbers. This Reynolds number with the addition of the K -values given in Table 7.3 can also take into account the contribution of the different channel shapes used. Therefore, this definition of the Reynolds number was also used in this work.

The friction factor-Reynolds number relationship for open channel turbulent flow of non-Newtonian fluids was also investigated by Burger et al. (2014). Five empirical turbulent flow models (most of these were adapted from pipe flow) were compared and a modified Blasius type relationship incorporating the effect of channel shape was developed for the friction factor for the range of fluids and shapes tested. This modified Blasius equation takes the form of:

$$f_{mB} = cRe^d \quad (7.1)$$

with the constants c and d given in Table 7.4.

As far as it can be ascertained, the Metzner-Reed (M-R) Reynolds number for pipe flow has never been used for the prediction of open channel flow of Herschel-Bulkley fluids, but the generalised form has been used for power law and Bingham fluids. The M-R Reynolds number for pipe flow of power law fluids is given by:

$$Re_{MR} = \frac{\rho V^{2-n'} D^{n'}}{k' 8^{n'-1}} \quad (7.2a)$$

Equation (7.2a) is adapted for open channel flow by replacing D with $4R_h$ giving:

$$Re_{MR} = \frac{\rho V^{2-n'} 4R_h^{n'}}{k' 8^{n'-1}} \quad (7.2b)$$

For pipe flow of a Bingham fluid, it can be shown that τ_y and μ_b can be linked to the apparent power-law constants k' and n' evaluated from the laminar flow data (Chhabra and Richardson, 2008). These relations are of the following form:

$$n' = \frac{1 - \frac{4}{3}\xi + \frac{\xi^4}{3}}{1 - \xi^4} \quad (7.3)$$

$$k' = \tau_w \left[\frac{\mu_B}{\tau_w \left(1 - \frac{4}{3}\xi + \frac{\xi^4}{3} \right)} \right]^{n'} \quad (7.4)$$

in which

$$\xi = \frac{\tau_0^B}{\tau_w} \quad (7.5)$$

where τ_0^B is the Bingham yield stress.

For a Herschel-Bulkley fluid in pipe flow, the k' and n' values according to Kazadi (2005) are given by

$$k' = \frac{\tau_0}{\left\{ \frac{4n}{k^n \tau_0^3} (\tau_0 - \tau_y)^{1+n} \left[\frac{(\tau_0 - \tau_y)^2}{1+3n} + \frac{2\tau_y(\tau_0 - \tau_y)}{1+2n} + \frac{\tau_y^2}{1+n} \right] \right\}^{n'}} \quad (7.6)$$

$$n' = \frac{1}{-3 + \left(\frac{1+n}{n} \right) \left(\frac{\tau_0}{\tau_0 - \tau_y} \right) + \frac{2\tau_0(1+n)(\tau_0 + 2n\tau_0 + n\tau_y)}{(1+n)(1+2n)(\tau_0 - \tau_y)^2 + 2(\tau_0 - \tau_y)(1+n)(1+3n) + \tau_y^2(1+2n)(1+3n)}} \quad (7.7)$$

For the different channel shapes, all the data was grouped together and f vs. Re plots were generated for various fluids, slopes and flume sizes. To predict the friction factor over the whole range of Reynolds numbers, a logistic dose-response curve was used by Patankar et al. (2002) and Garcia et al. (2003). This composite power law f vs. Re correlation equation is given by

$$f = F_2 + \frac{(F_1 - F_2)}{\left(1 + \left(\frac{Re}{t} \right)^e \right)^f} \quad (2.72)$$

where F_1 and F_2 are the power law relationships covering the laminar and turbulent flow regimes defined respectively as:

$$F_1 = aRe^b \quad (2.73)$$

and

$$F_2 = cRe^d \quad (2.74)$$

In laminar flow for the channel shapes tested the constant 'a' in Eqn. (2.73) is the same as the K values given in Table 7.3 whereas the constant 'b' has the numerical value of -1. In turbulent flow, the constants 'c' and 'd' are the constants obtained for the modified Blasius equation (7.1) and values are given in Table 7.4. With these values determined, the parameters 't', 'e' and 'f' were then obtained by fitting Eqn. (2.72) to all the data points of the f vs. Re plot by a non-linear curve fit so that the transitional flow region can be defined.

The correlation coefficient (R^2) values and the log standard error (LSE) (Lazarus and Nielson, 1978) for the composite power law f vs. Re curve fit to the data were determined as

$$R^2 = \frac{\sum (f_{pred} - ave(f_{exp}))^2}{\sum (f_{exp} - f_{pred})^2 + \sum (f_{pred} - ave(f_{exp}))^2} \quad (7.8)$$

$$\text{LSE} = \frac{\sqrt{\sum (\log(f_{\text{exp}}) - \log(f_{\text{pred}}))^2}}{N - 1} \quad (7.9)$$

Two additional data sets, one in laminar flow of kaolin suspensions of 20.5 to 27.4% v/v in water having densities of 1328 to 1438 kg/m³ in a rectangular flume by Coussot (1994) and the other in turbulent flow of kaolin suspension of 8.57 to 22.1% v/v in water having densities of 1150 to 1360 kg/m³ in a rectangular flume by Naik (1984) were also used to check the effectiveness of the model given by Eq. (2.72). For the Coussot (1994) and the Naik (1983) data sets, 113 and 95 data points were used respectively.

7.3 Experimental methods and materials

All the tests, apart from the Coussot (1994) and Naik (1984) data sets were conducted at the Cape Peninsula University of Technology in a 10 m long tilting flume shown in Figure 7.1 (Burger et al. 2010). This hydraulically tilting flume, as described by Haldenwang (2003), can be tilted at various angles from the horizontal to 5°. This rectangular flume, which is 300 mm wide, can be fitted with a partition to change the width to 150 mm. These two flumes can then be fitted with triangular, trapezoidal and semi-circular inserts to create flumes of the other shapes studied herein. An in-line tube viscometer with three tubes with 13, 28 and 80 mm tubes was used to obtain flow curve measurements. Each tube was fitted with a magnetic flow meter and a differential pressure transducer which when calibrated with water gave errors of less than 10% for flow rate and pressure drop Haldenwang (2003).

The fluid depth in the flume was measured at two positions, 5 and 6 m from the inlet with digital depth gauges, which was established by Haldenwang (2003) to be the optimum for position for steady flow as the difference in fluid height was always less than 2.9%. The flow rate of the fluid flowing in the flume was measured using the magnetic flow meter in each of the three tube viscometers installed as part of the flume rig.

The test fluids used were 1.5 to 5.3% v/v carboxymethyl cellulose (CMC) solutions, having densities of 1008 to 1028 kg/m³, 3.5 to 6.8% v/v bentonite in water suspensions having densities of 1022 to 1042 kg/m³ and 3.4 to 9.2% v/v kaolin in water suspensions having densities of 1056 to 1152 kg/m³. These were found to be best represented by the power law, Bingham plastic and Herschel-Bulkley models respectively. A summary of the test fluids used can be found in Table 7.2.

The test fluids were prepared by the gradual addition of the required amount of the polymer or clay in tap water using an electrical motor mixer fitted with a 4 bladed, 250mm blade length stainless steel impeller as agitator to produce a homogeneous solution or suspension. It is known that carboxymethyl cellulose (CMC) solutions do undergo biodegradation with time (Clark, 1993). Flow curve measurements of the CMC solution made before and after the flume test showed that there was no discernible change detected in the flow curves over the period of testing (maximum of one day). It is also known that bentonite suspensions can exhibit significant thixotropic (time-dependent) behaviour during shear. To minimize this effect, the bentonite suspension was first pre-sheared by vigorously mixing the suspension and recirculating this suspension through the flow loop (Figure 7.1) for 60 minutes

before the flume test was undertaken. The suction to the flume entrance is taken from the mixing/reservoir vessel fitted with an electrical motor mixer and a stainless steel, 4 bladed impeller through the supply pumps, the flow meter and the tube viscometer to the flume inlet reservoir rising into the flume. The discharge from the flume exit is returned back into the mixing/reservoir vessel. Flow curve measurements of the bentonite suspension made before and after the flume test confirmed that there was no discernible change in the flow curves measured before and after each test on account of thixotropy.

7.4 Results and Discussion

The f vs. Re data was analysed separately for the four different channel shapes with Re being the Haldenwang Reynolds number, Re_H and alternatively, the adapted Metzner-Reed Reynolds number, Re_{MR} . The f vs. Re data for all the fluids studied for a given channel shape was combined and then a curve fit was made to Eq. (2.72) to determine the parameters 't', 'e' and 'f' for the transitional flow region by optimisation. The 'a' constant values corresponding to the K values given in Table 7.3 and the 'b' value as -1 for the laminar flow region and the 'c' and 'd' values given in Table 7.4 for the turbulent flow region were used in Eq. (2.72) before the optimisation process for the determination of 't', 'e' and 'f' values for the transitional flow regime was carried out. The resulting parameters are given in Table 7.5, using Re_H and Table 7.6, using Re_{MR} for the four channel shapes investigated.

Figures 7.2 to 7.9 show the f vs. Re plots with their composite power law fits and the corresponding parity plots, f_{exp} vs. f_{pred} for the four channel shapes studied where the Reynolds number is that defined by Haldenwang (2002), Eq. (2.59). Figures 7.10 to 7.17 show a similar set of plots to those given by Figures 7.2 to 7.9 but with the Reynolds number being defined by the adapted Metzner-Reed Reynolds number, Eq. (7.2b). Separately Figure 7.18 depicts the f vs. Re_H plot together with the composite power law correlation for non-Newtonian flow in a rectangular flume using the datasets published by Coussot (1994) and Naik (1983). Figure 7.19 gives the corresponding parity plot, f_{exp} vs. f_{pred} for Figure 7.18.

The values of R^2 and LSE for the composite power law fits to the f vs. Re_H and f vs. Re_{MR} data for the four channel shapes are given in Table 7.7. Lower LSE values were obtained for the f vs. Re_H fits for 3 of the four channel shapes than for the corresponding f vs. Re_{MR} fits, the LSE value for the triangular channel using Re_{MR} had a lower value. Higher R^2 values were obtained for the f vs. Re_H plots for the rectangular and triangular channels than those for the corresponding f vs. Re_{MR} plots whereas the R^2 values for the f vs. Re_H plots for the semi-circular and trapezoidal channels were found to be comparable to those for the corresponding f vs. Re_{MR} plots.

The R^2 and LSE values for the composite power law fits to the combined 113 data points obtained by Coussot (1994) and 95 data points obtained by Naik (1983) for non-Newtonian flow in rectangular channels as shown in Figure 7.18 was found to be 0.98 and 0.006 respectively.

The comparison expressed as a percentage where the predicted friction factor differed from the experimental values by more than +/-30% using the Haldenwang (2002) Reynolds number and the adapted Metzner - Reed Reynolds number in the f_{exp} vs. f_{pred} plots are given in Table 7.8. The lower this percentage is, the better the predicted fit to the experimental values. It can be concluded that for all channel shapes used, the use of the

Haldenwang (2002) Reynolds number in the f_{exp} vs. f_{pred} plots gave a closer fit than those based the adapted Metzner - Reed Reynolds number.

7.5 Conclusions

The results show that the composite power law friction factor modelling technique used by Garcia et al. (2003) for pipe flow can be used to adequately predict flow in an open channel of a given cross-sectional shape provided that an appropriate Reynolds number is used to take into account the non-Newtonian behaviour of the test fluid. It was found that the results using the Haldenwang et al. (2002) Reynolds number yielded better results than those based the adapted Metzner-Reed Reynolds number.

Two independent data sets, one from Coussot (1994) in laminar flow and the second from Naik (1983) in turbulent flow, both for a rectangular channel, were used to test the friction factor prediction given by Eq. (2.72). The correlation coefficient for the fit to the combined data set was 0.98 indicating the appropriateness of the proposed composite power law friction factor equation.

This work will bring greater awareness to those dealing with the design of open channels in the mining and chemical engineering on the impact of concentrating up slurries in open channels of different cross-sections due to the lack of water availability.

7.6 Acknowledgements

The authors would like to acknowledge the National Research Foundation of South Africa and the Cape Peninsula University of Technology for funding this research.

7.7 Notation

Symbol	Description	Units
a	channel shape factor constant for laminar flow, Eq. (2.73)	-
A	cross-sectional area of flow	m^2
b	power law exponent taken as -1, Eq. (2.73)	-
c	"Blasius" power law constant for turbulent flow, Eq. (2.74)	-
d	"Blasius" power law exponent for turbulent flow, Eq. (2.74)	-
D	pipe diameter	m
e	composite power law friction factor exponent, Eq. (2.72)	-
f	composite power law friction factor exponent, Eq. (2.72)	-
f	Fanning friction factor	-
F_1	laminar flow power law friction factor	-
F_2	turbulent flow power law friction factor	-
f_{mB}	modified Blasius friction factor, Eq. (5.2)	-
f_{pred}	predicted Fanning friction factor based on Eq. (7.8)	-
f_{exp}	experimental Fanning friction factor Eq. (7.8)	-
$f_{exp(ave)}$	averaged experimental Fanning friction factor Eq. (7.8)	-

Symbol	Description	Units
g	acceleration due to gravity	m/s^2
K	laminar flow constant in the f vs Re relationship Eq. (3.1)	-
k	consistency coefficient	$Pa \cdot s^n$
k'	apparent consistency coefficient, Eq. (7.4)	$Pa \cdot s$
n	flow behaviour index	-
N	number of points, Eq. (7.9)	-
n'	apparent Power law index, Eq. (7.3)	-
P	wetted perimeter	m
Q	volumetric flow rate	M^3/s
R^2	correlation coefficient	-
Re	Reynolds number	-
Re_H	Haldenwang et al Reynolds number, Eq. (2.59)	-
Re_{MR}	Metzner-Reed Reynolds number adapted for open channel flow, Eq.(7.2)	-
R_h	hydraulic radius	m
t	composite power law friction factor exponent, Eq. (2.72)	-
V	average velocity	m/s
μ_B	Bingham plastic viscosity	$Pa \cdot s$
θ	channel angle from the horizontal	degrees
ξ	ratio of wall shear stress to Bingham yield stress	-
ρ	density	Kg/m^3
τ_0	wall shear stress Eqns. (7.6) & (7.7)	Pa
τ_w	wall shear stress	Pa
τ_y	yield stress	Pa

7.8 References

Alderman, N.J. & Haldenwang, R. 2007. A review of Newtonian and non-Newtonian flow in rectangular open channels. *Hydrotransport 17, The Southern African Institute of Mining and Metallurgy and the BHR Group, Cape Town, SA*, 87-106.

Burger, J.H., Haldenwang, R. & Alderman, N.J. 2010. Friction factor-Reynolds number relationship for laminar flow of non-Newtonian fluids in open channels of different cross-sectional shapes, *Chemical Engineering Science*, 65(11): 3549–3556.

Burger, J.H., Haldenwang, R. & Alderman, N.J. 2010. Experimental procedure and database for non-Newtonian flow in different channel shapes, *Journal of Hydraulic Research*, 48(3): 363–370.

Burger, J.H., Haldenwang, R. & Alderman, N.J. 2014. Laminar and turbulent flow of non-Newtonian fluids in open channels for different cross-sectional shapes, Submitted to *ASCE Journal of Hydraulic Engineering*.

Chanson, H. 1999. *The Hydraulics of Open Channel Flow*. London: Arnold. 69-74

Chhabra, R.P & Richardson, J.F. 2008. *Non-Newtonian Flow and Applied Rheology*, 2nd edition. Oxford: Butterworth-Heinemann.

Chow, V.T. 1959. *Open Channel Hydraulics*. New York: McGraw-Hill. 9-12.

Clark, M.T. 1993. Rheological additives in Rheological Properties of Cosmetics and Toiletries. New York: Laba.D. (ed), Marcel Dekker, Inc . Ch. 4.

Coussot, P. 1994. Steady laminar flow of concentrated mud suspensions in open channels. *Journal of Hydraulic Research*, 4(32): 535-558.

Fitton, T.G. 2007. Tailings beach slope prediction. Unpublished PhD thesis, Royal Melbourne Institute of Technology, University, Melbourne, Australia.

Fitton, T.G. 2008. Non-Newtonian Open Channel Flow – A Simple Method of Estimation of Laminar/Turbulent Transition and Flow Resistance. *Paste 2008*, Kasane, Botswana, 245-251.

Fuentes, R. (2004), Slurry flumes in Chile. (Keynote Address). *Hydrotransport 16: 16th International Conference on the Hydraulic Transport of Solids in Pipes*, Santiago, Chile, 325-333

García, F., García, J.C., Padrino, J.C., Mata, C., Trallero, J.L. & Joseph, D.D. 2003. Power law and Composite Power law Friction Factor Correlations for Laminar and Turbulent Gas–liquid Flow in Horizontal Pipelines, *International Journal of Multiphase Flow*, 29: 1605–1624.

Haldenwang, R., Slatter, P.T. & Chhabra, R.P. 2002. Laminar and Transitional Flow in Open Channels for Non-Newtonian Fluids. *Hydrotransport 15: 15th International Conference on the Hydraulic Transport of Solids in Pipes*. Banff, Canada, Organised by BHR Group, Cranfield, Bedfordshire, UK, 755-768.

Haldenwang, R. 2003. Flow of Non-Newtonian Fluids in Open Channels. Unpublished D. Tech. thesis. Cape Technikon, Cape Town SA.

Haldenwang, R. & Slatter, P.T. 2006a. Experimental Procedure and Database for Non-Newtonian Open Channel Flow. *Journal Hydraulic Research*. 44(2): 283-287.

Haldenwang, R., Slatter, P.T. & Chhabra, R.P. 2010. An Experimental Study of non-Newtonian Fluid Flow in Rectangular Flumes in Laminar, Transition and Turbulent Flow Regimes. *Journal of the South African Institution of Civil Engineering*.52(1): 11-19

Kazadi D.M. 2005. Non-Newtonian Losses Through Diaphragm Valves, MTech thesis. CPUT Theses & Dissertations. Paper 190. http://dk.cput.ac.za/td_cput/190

Kozicki, W. & Tiu, C. 1967. Non-Newtonian Flow Through Open Channels. *Canadian Journal of Chemical Engineers*, 45: 127-134.

Kozicki, W. & Tiu, C. 1986. Parametric Modelling of Flow Geometries in Non-Newtonian Flows. *Encyclopaedia of Fluid Mechanics, Vol 7, (ed) N.P. Cheremisinof*. Houston: Gulf Publishing Co, 199 – 252.

Lazarus, J.H. & Nielson, I.D. 1978. A Generalised Correlation for Friction Head Losses of Settling Mixtures in Horizontal Smooth Pipelines. *Hydrotransport 5, 5th International conference on the hydraulic transport of solids in pipes*. Paper B1.

Minussi, R.B., Maciel, G., (2012), “Numerical Experimental Comparison of Dam Break Flows with non-Newtonian Fluids”, *J.Braz. Soc. Mech. Sci & Eng.*, Vol. XXXIV, No2, pp. 167–178.

Naik, B. 1983. Mechanics of Mudflow Treated as the Flow of a Bingham Fluid. Unpublished PhD thesis. Washington State University.

Patankar, N.A., Joseph, D.D., Wang, J., Barree, R.D., Conway, M. & Asadi, M. 2002. Power Law Correlations for Sediment Transport in Pressure Driven Channel Flows. *International Journal of Multiphase Flow*, 28: 1269–1292

Straub, L.G., Silberman, E. & Nelson, H.C. 1958. Open Channel Flow at Small Reynolds Numbers. *American Society of Civil Engineers*, 123: 685–713.

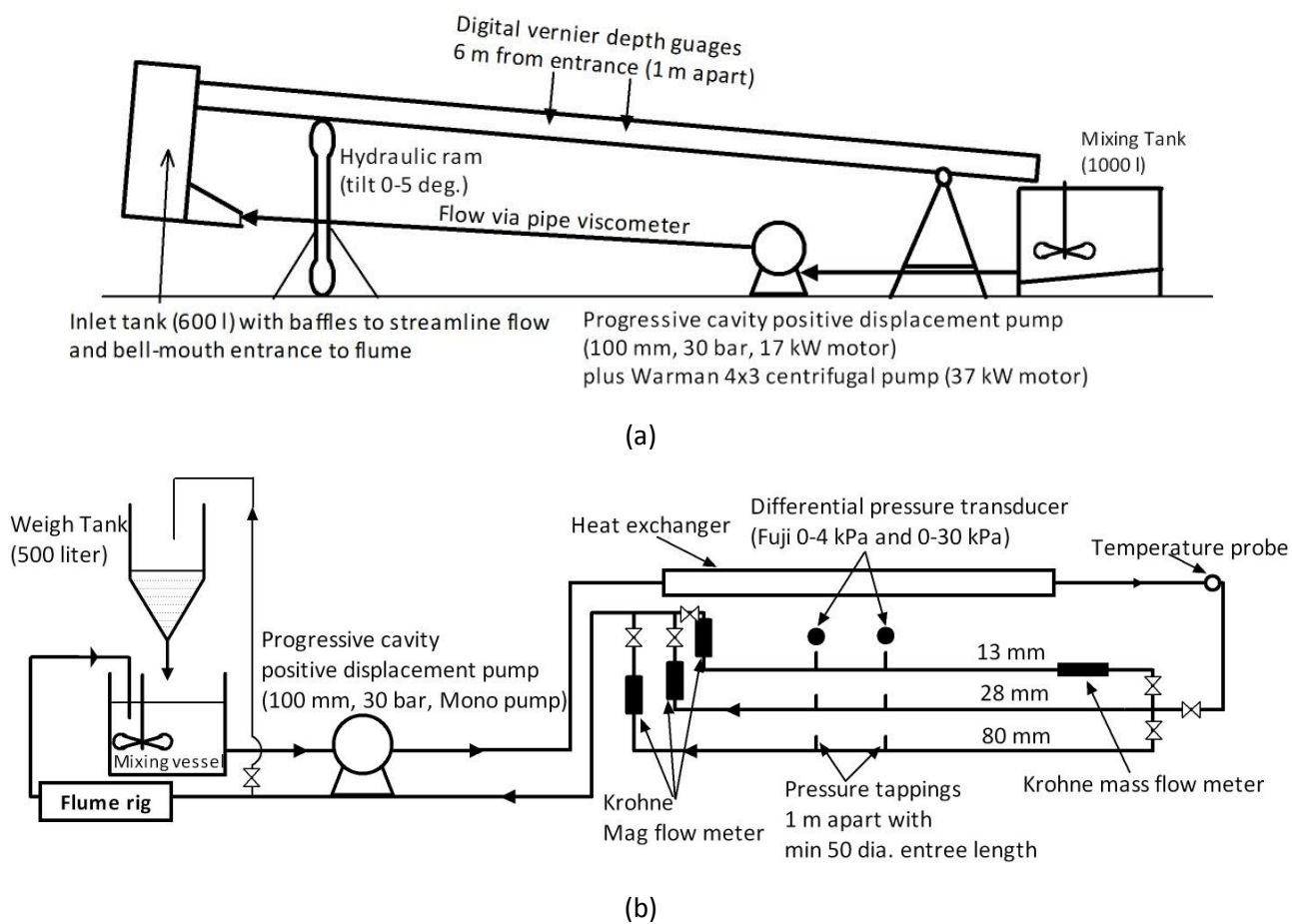


Figure 7.1 (a) 10 m rectangular tilting flume linked to (b) 3 in-line tube viscometers

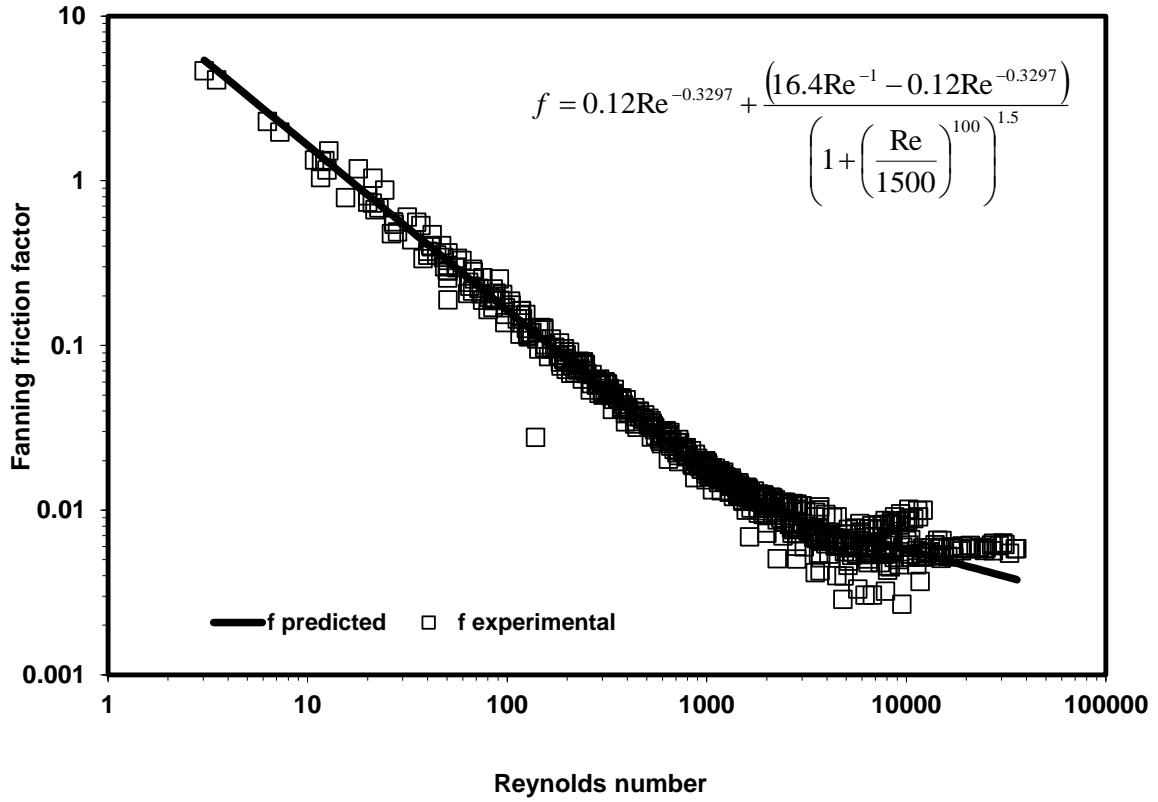


Figure 7.2 f vs. Re relationship for rectangular flume using Re_H (all materials)

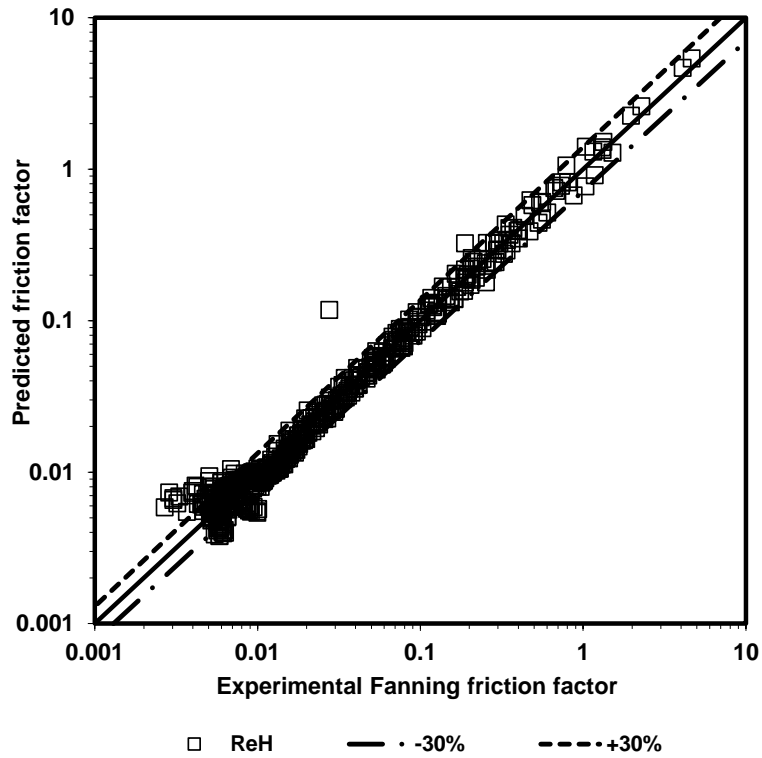


Figure 7.3 f_{pred} vs. f_{exp} for rectangular flume using Re_H (all materials)

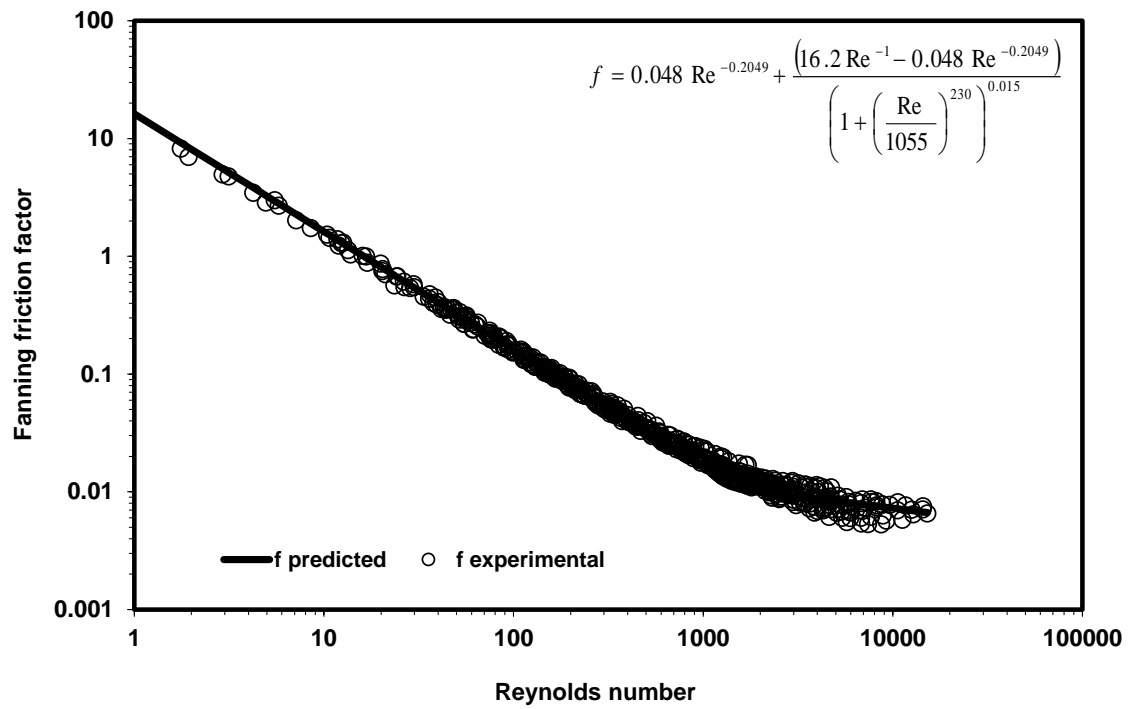


Figure 7.4 f vs. Re relationship for semi-circular flume using Re_H (all materials)

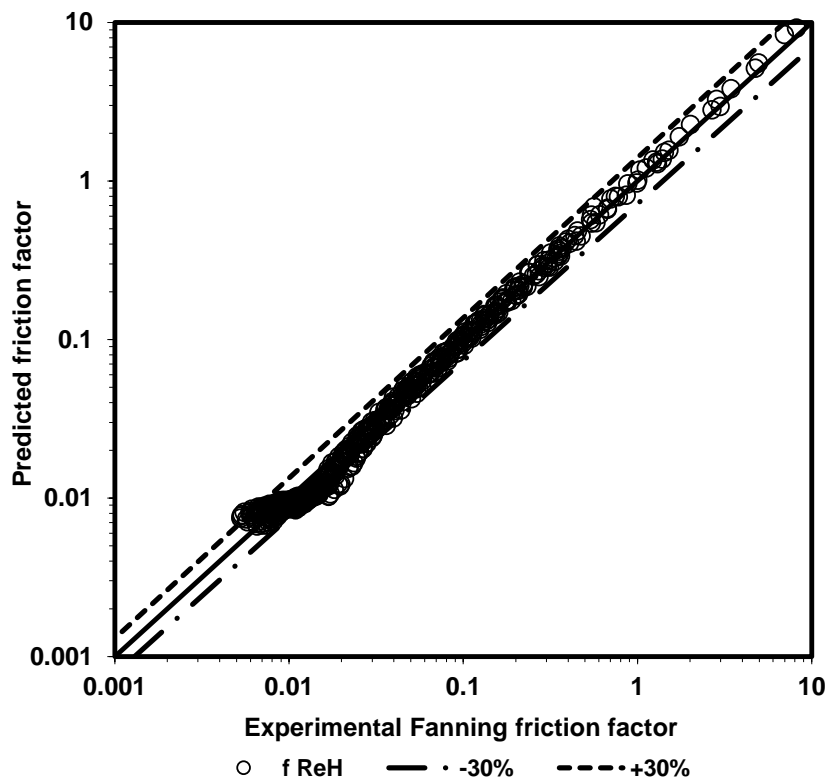


Figure 7.5 f_{pred} vs. f_{exp} for semi-circular flume using Re_H (all materials)

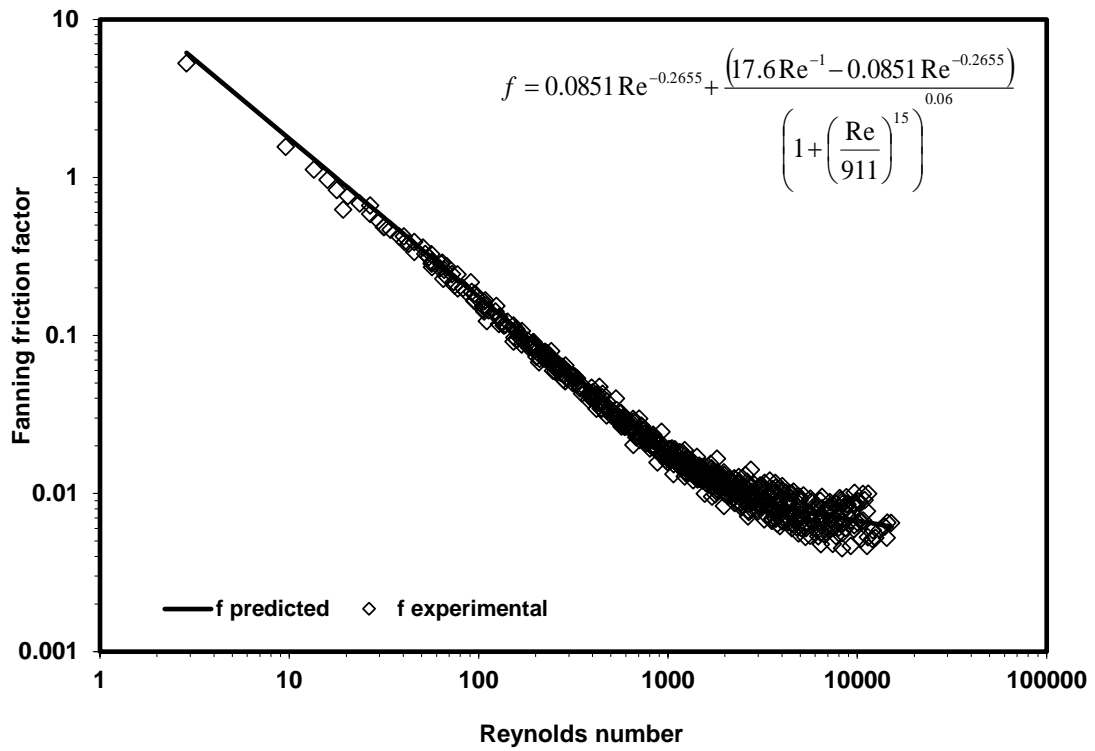


Figure 7.6 f vs. Re relationship for trapezoidal flume using Re_H (all materials)

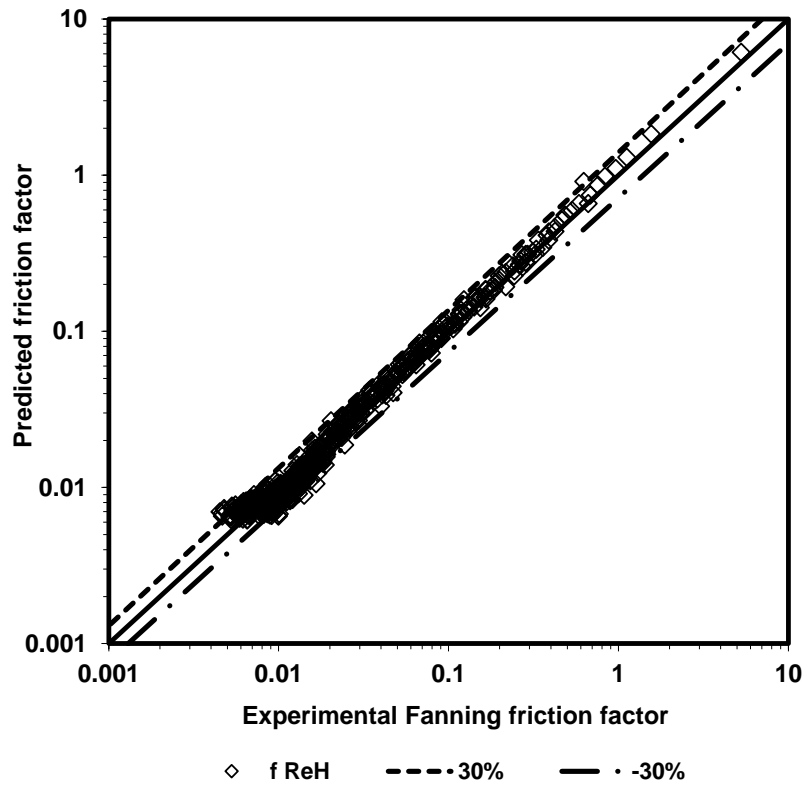


Figure 7.7 f_{pred} vs. f_{exp} for trapezoidal flume using Re_H (all materials)

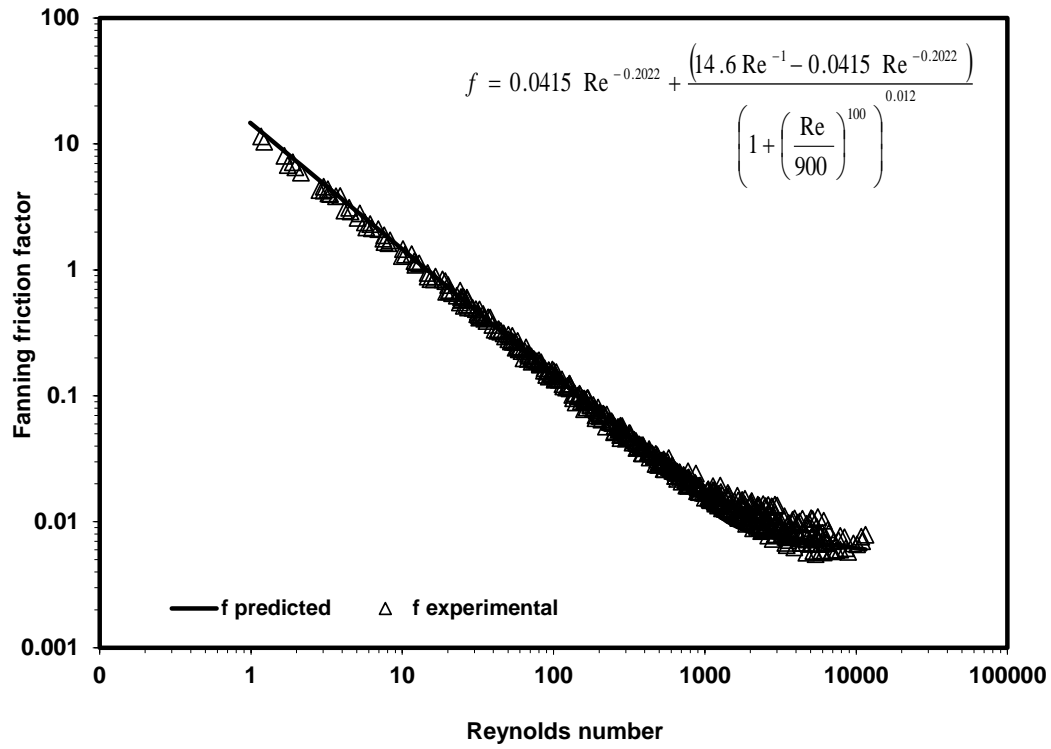


Figure 7.8 f vs. Re relationship for triangular flume using Re_H (all materials)

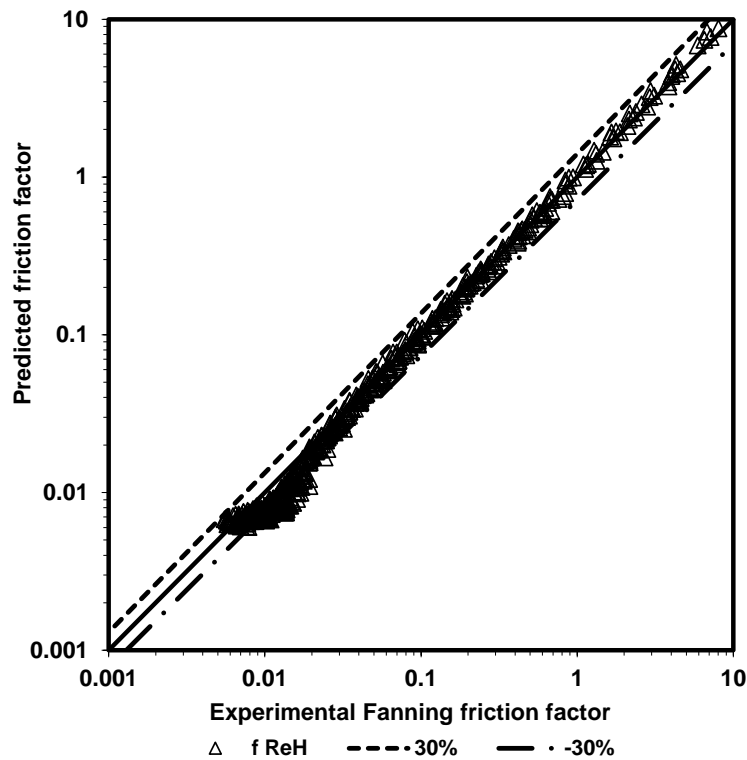


Figure 7.9 f_{pred} vs. f_{exp} for triangular flume using Re_H (all materials)

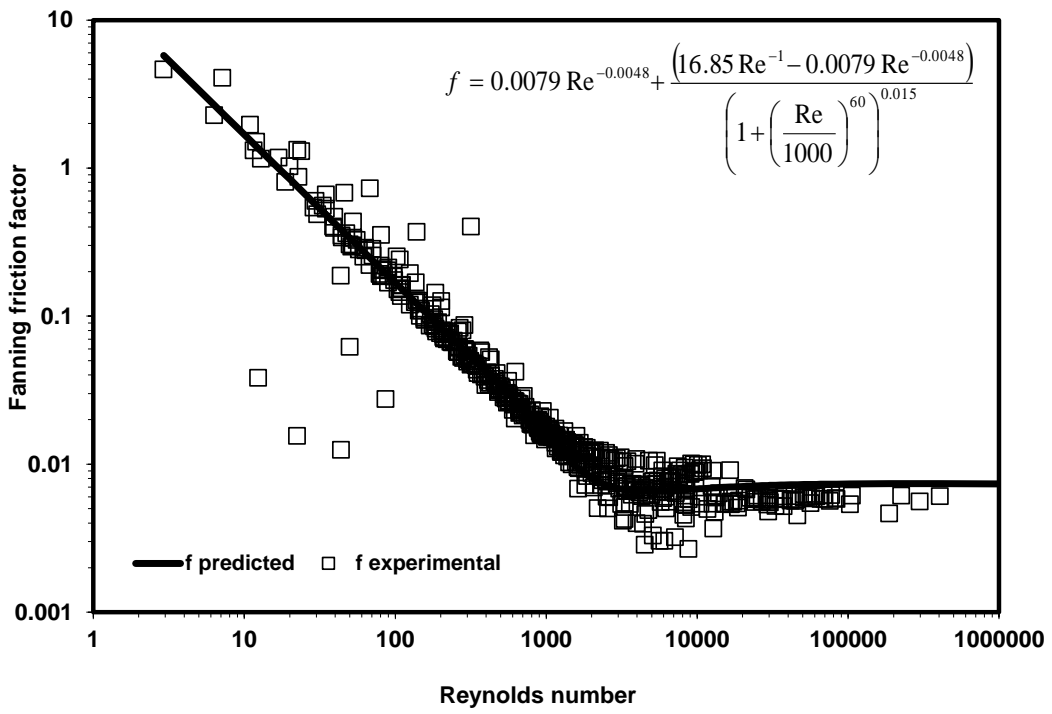


Figure 7.10 f vs. Re relationship for rectangular flume using Re_{MR} (all materials)

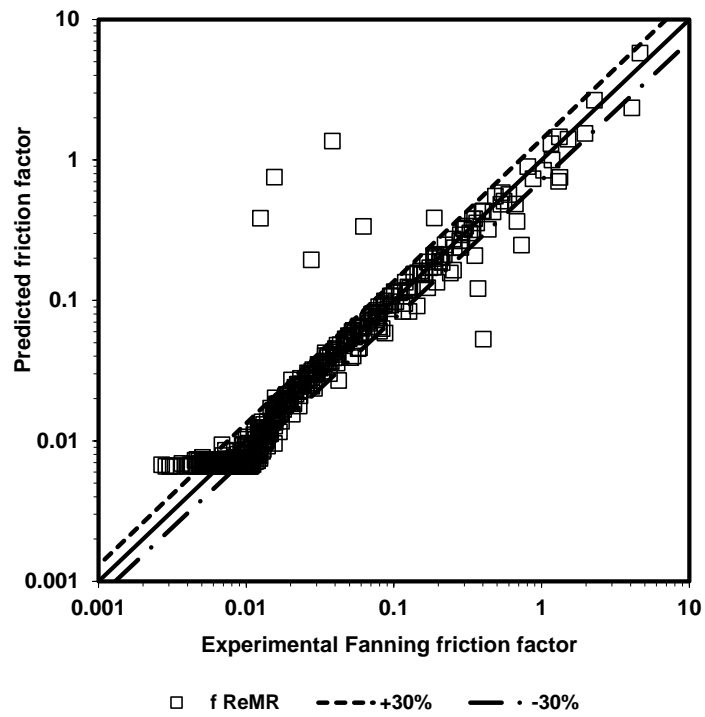


Figure 7.11 f_{pred} vs. f_{exp} for rectangular flume using Re_{MR} (all materials)

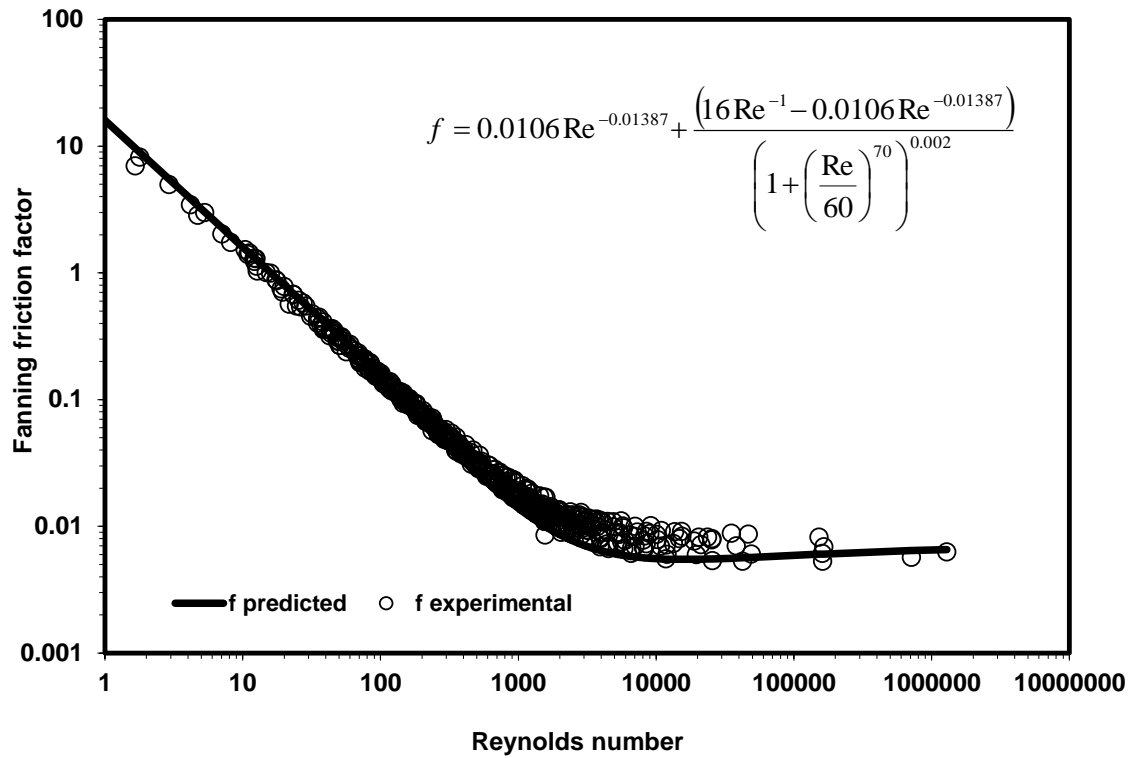


Figure 7.12 f vs. Re relationship for semi-circular flume using Re_{MR} (all materials)

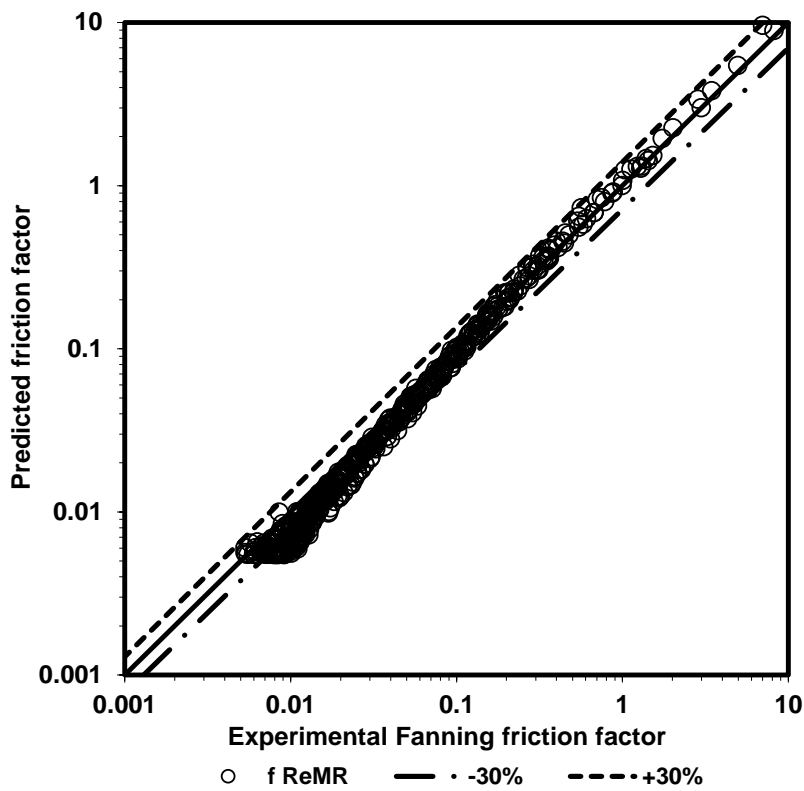


Figure 7.13 f_{pred} vs. f_{exp} for semi-circular flume using Re_{MR} (all materials)

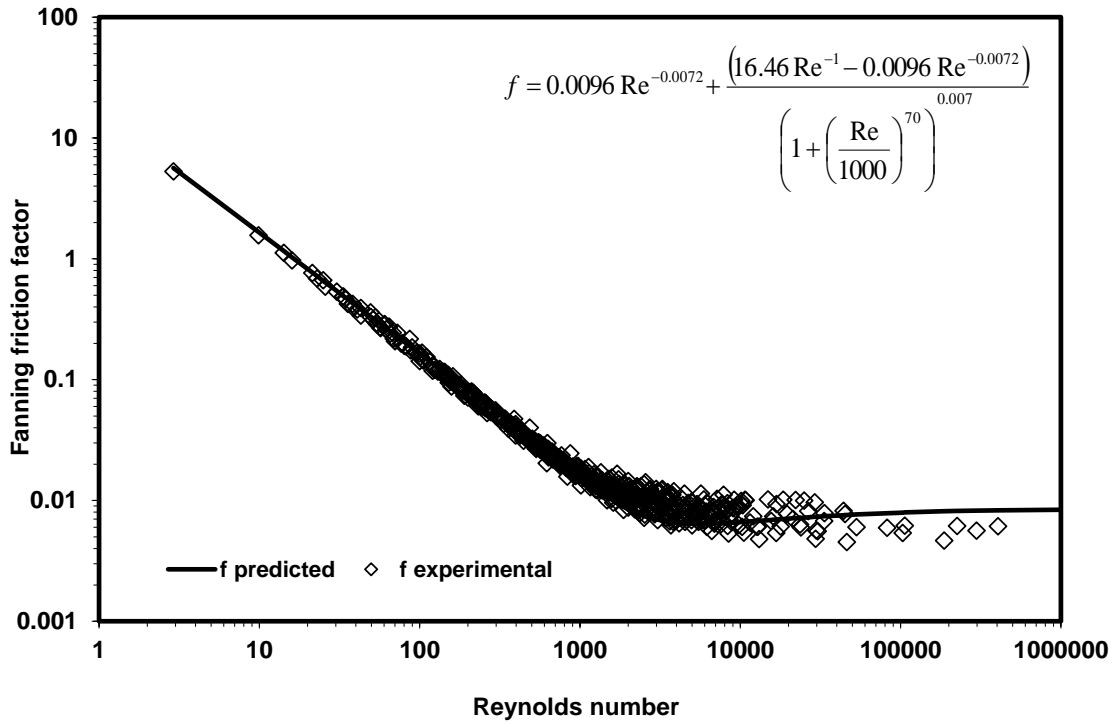


Figure 7.14 f vs. Re relationship for trapezoidal flume using Re_{MR} (all materials)

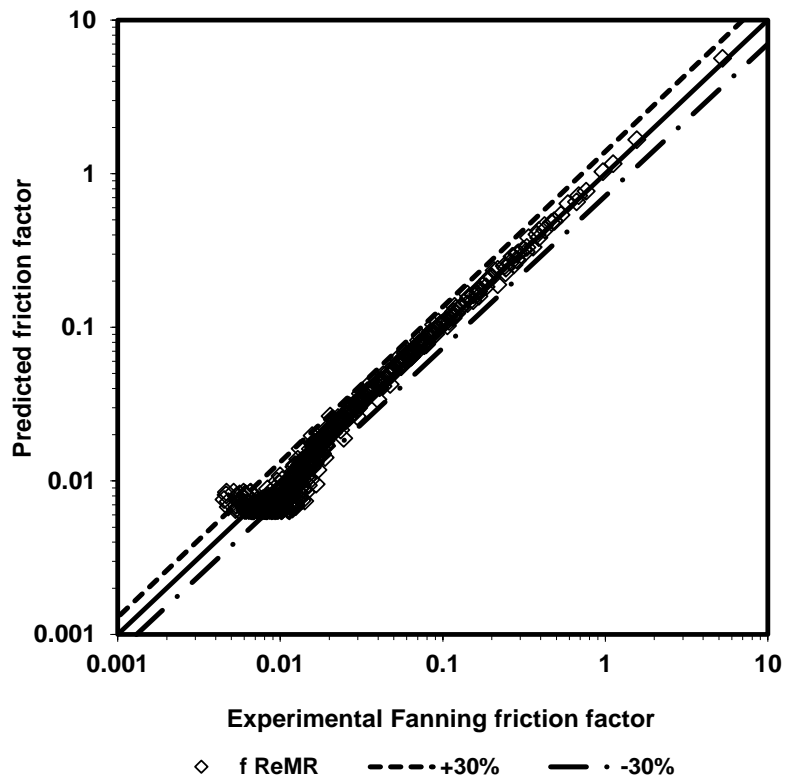


Figure 7.15 f_{pred} vs. f_{exp} for trapezoidal flume using Re_{MR} (all materials)

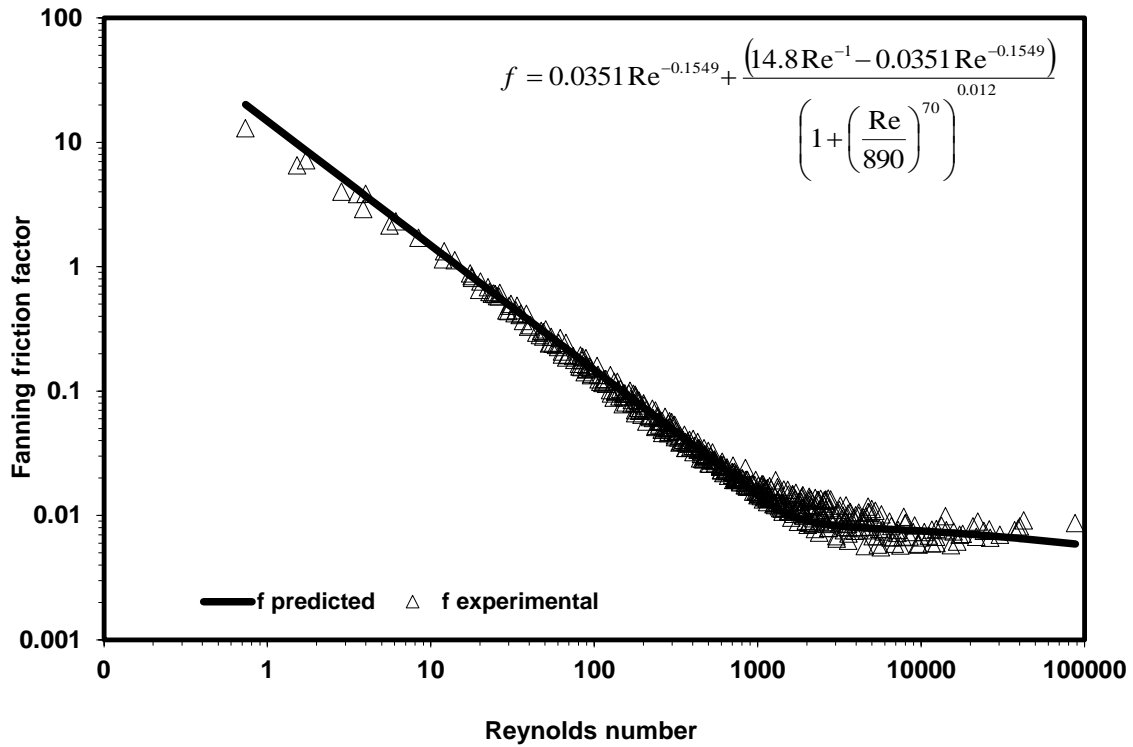


Figure 7.16 f vs. Re relationship for triangular flume using Re_{MR} (all materials)

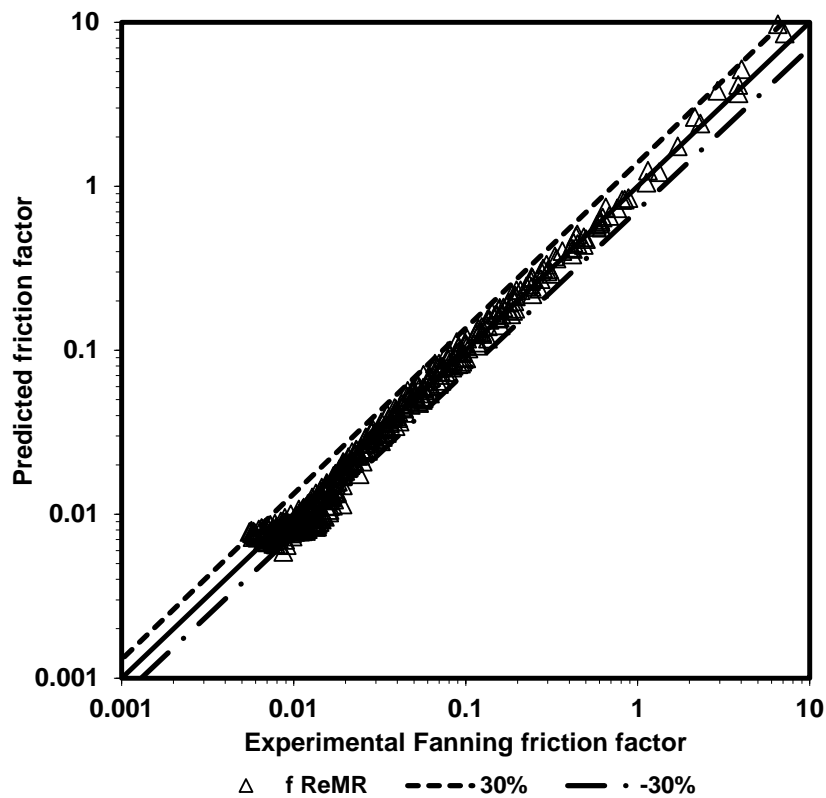


Figure 7.17 f_{pred} vs. f_{exp} for triangular flume using Re_{MR} (all materials)

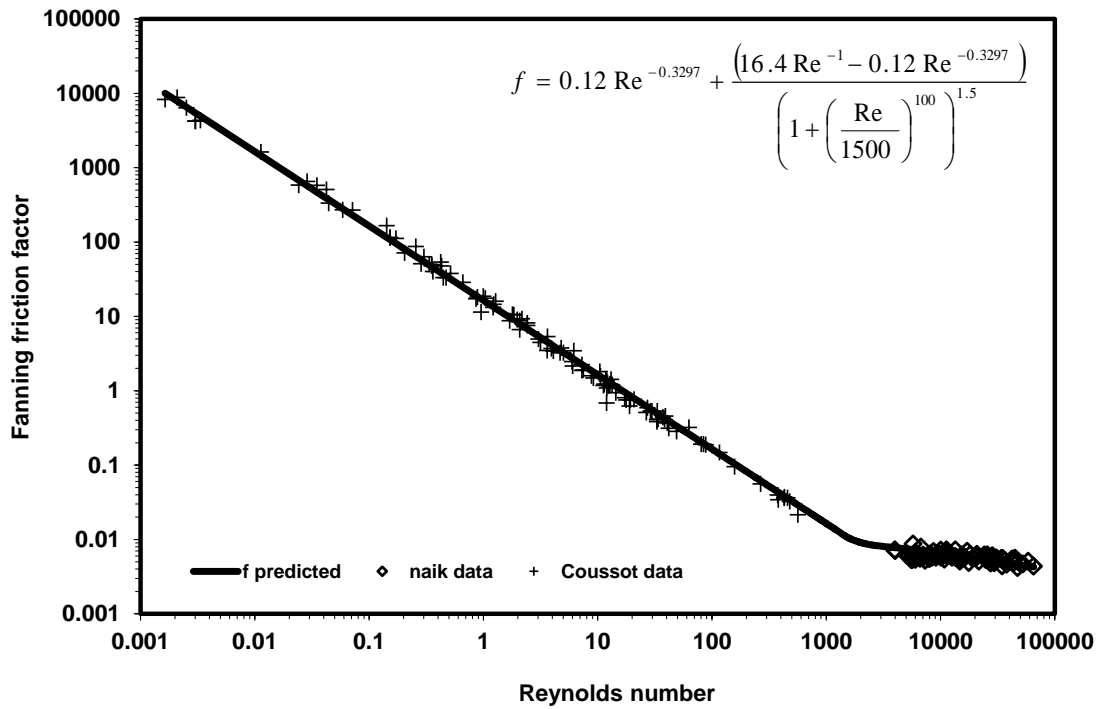


Figure 7.18 f vs. Re relationship for rectangular flume using Re_H (Coussot and Naik data)

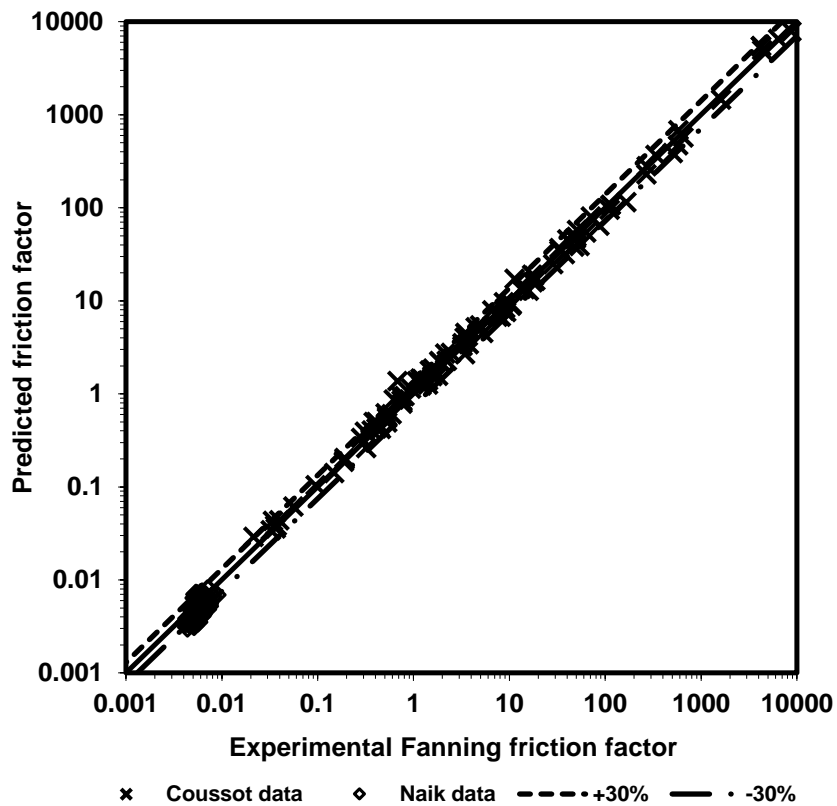


Figure 7.19 f_{pred} vs. f_{exp} for rectangular flume using Re_H (Coussot and Naik data)

Table 7.1 Open channel shapes used in this study.

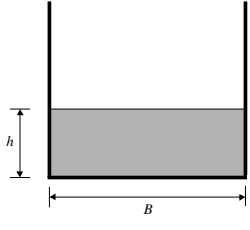
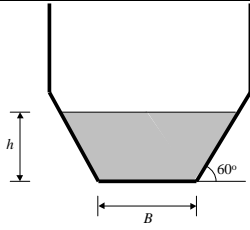
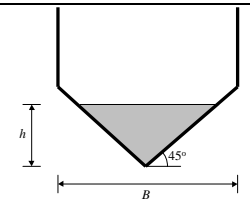
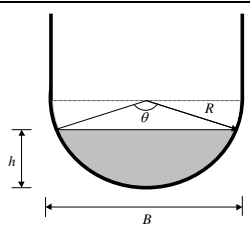
Section	Size	Cross-sectional area A	Wetted perimeter P	Surface width W
	B = 300 mm B = 150 mm	Bh	B + 2h	B
	B = 150 mm B = 75 mm	$h(B + xh)$ where $x = 1/\tan\theta$	$B + 2h\sqrt{1 + x^2}$ where $x = 1/\tan\theta$	$B + 2xh$ where $x = 1/\tan\theta$
	B = 300 mm	h^2	$2h\sqrt{2}$	2h
	B = 300 mm B = 150 mm	$\frac{D^2}{8}(\theta - \sin\theta)$ where θ $= 2\cos^{-1}\left(1 - \frac{2h}{D}\right)$	$D\left(\frac{1}{2}\theta\right)$ where θ $= 2\cos^{-1}\left(1 - \frac{2h}{D}\right)$	$D\left(\sin\frac{1}{2}\theta\right)$ where θ $= 2\cos^{-1}\left(1 - \frac{2h}{D}\right)$

Table 7.2 Summary of materials used.

CMC solutions				
Concentration (%vol.)	Density (kg/m ³)	τ_y (Pa)	k (Pa.s ⁿ)	n
1.5	1008	-	0.014	0.944
2.0	1013	-	0.035	0.776
3.0	1018	-	0.145	0.788
3.1	1018	-	0.091	0.823
4.0	1023	-	0.330	0.727
4.9	1028	-	0.599	0.690
5.3	1028	-	0.920	0.678
Bentonite in water suspensions				
3.5	1022	3.00	0.0036	1
4.5	1027	4.30	0.0036	1
4.8	1029	5.66	0.0036	1
4.9	1030	5.20	0.0040	1
5.4	1033	7.25	0.0038	1
6.2	1038	15.78	0.0064	1
6.8	1042	18.34	0.0078	1
Kaolin in water suspensions				
3.4	1056	1.30	0.051	0.568
3.5	1058	0.50	0.061	0.560
5.0	1082	3.58	0.060	0.630
5.4	1089	4.40	0.084	0.582
7.0	1115	8.18	0.142	0.570
7.1	1117	11.6	0.148	0.557
9.0	1148	19.0	0.210	0.616
9.2	1152	18.9	0.194	0.550

Table 7.3 K-values of different shape channels (Burger et al., 2010)

Shape	Rectangular	Semi-circular	Trapezoidal with 60 ^o angle sides	Triangular with 90 ^o angle sides
K	16.4	16.2	17.6	14.6
No of data points	647	485	460	326

Table 7.4 Modified Blasius c and d values for different shape channels (Burger et al., 2014)

Shape	Rectangular	Semi-circular	Trapezoidal with 60° sides	Triangular with 90° Angle sides
c	0.1200	0.0480	0.0851	0.0415
d	-0.3297	-0.2049	-0.2655	-0.2022

Table 7.5 Parameters in composite power law correlation for each shape, (based on Re_H)

Shape	a	b	c	d	e	f	t
Rectangular	16.4	-1	0.1200	-0.3297	100	1.5	1500
Semi-circular	16.2	-1	0.0480	-0.2049	230	0.015	1055
Trapezoidal	17.6	-1	0.0851	-0.2655	15	0.06	911
Triangular	14.6	-1	0.0415	-0.2022	100	0.012	900

Table 7.6 Parameters in composite power law correlation for each shape, (based on Re_{MR})

Shape	a	b	c	d	e	f	t
Rectangular	16.85	-1	0.0079	-0.0048	60	0.015	1000
Semi-circular	16.0	-1	0.0106	-0.0139	70	0.002	60
Trapezoidal	16.46	-1	0.0096	-0.0072	70	0.007	1000
Triangular	14.8	-1	0.0351	-0.1549	70	0.012	890

Table 7.7 Statistical ranking of different friction factor vs. Re correlations

Reynolds number	R^2	LSE
Rectangular Re_H	0.980	0.0039
Rectangular Re_{MR}	0.883	0.0052
Semi-circular Re_H	0.987	0.0029
Semi-circular Re_{MR}	0.993	0.0045
Trapezoid Re_H	0.981	0.0026
Trapezoid Re_{MR}	0.996	0.0038
Triangular Re_H	0.987	0.0037
Triangular Re_{MR}	0.910	0.0034

Table 7.8 Percentage of f_{pred} values differing by more than $\pm 30\%$ from f_{exp} values

Reynolds number and shape	Percentage of f prediction differing by $> \pm 30\%$ from experimental values
Rectangular Re_H	10.3
Rectangular Re_{MR}	28.9
Semi-circular Re_H	3.2
Semi-circular Re_{MR}	15.6
Trapezoid Re_H	6.2
Trapezoid Re_{MR}	12.1
Triangular Re_H	11.3
Triangular Re_{MR}	8.0

Chapter 8 Conclusions and recommendations

8.1 Conclusions

The comprehensive database compiled during this research of the homogeneous flow of shear-thinning, Bingham plastic and yield shear-thinning fluids in rectangular, triangular, semi-circular and trapezoidal cross sectional shaped open channels is by itself a major contribution. From this database, the following significant contributions are made:

Shape factor for open channels

Open channel flow does differ from pipe flow and the pipe flow paradigm of $f = 16/Re$ used previously by Haldenwang et al. (2002, 2004) for non-Newtonian laminar flow in open channels of different cross sectional shapes was found to be incorrect. The relationship $f = K/Re_H$ was found to be more appropriate in describing non-Newtonian flow in open channels of differing cross-sections. Here, Re_H is the Haldenwang et al. (2002) Reynolds number which also accounted for the flow curve behaviour of the fluid flowing in an open channel and K is a shape factor constant given by:

$$K = \frac{16\rho g(A/P) \sin \theta}{\tau_y + k\left(\frac{2VP}{A}\right)^n} \quad (3.2)$$

This equation is for fluids exhibiting Herschel-Bulkley behaviour, but it can also be used for fluids exhibiting Newtonian, power law and Bingham plastic behaviour provided appropriate values for τ_y , k and n are used. Error propagation analysis on all experimental equipment and measurements during this research showed that the max error in K was ± 1 . The overall average K value was found to be 14.6 for triangular channels with a vertex angle of 90 degrees, 16.2 for semi-circular channels, 16.4 for rectangular channels and 17.6 for trapezoidal channels with 60 degree sides. The shape factor K values for non-Newtonian flow in open channels found in this research compared well with K values found by Straub et al. (1958) for Newtonian flow in open channels of different cross sectional shapes. It was also established that most of the experimental data lie within 1.2 to 1.6 SD (standard deviation) from the average K value.

For all of these fluids, it can be deduced from Eq. (3.2) that for a fluid of known flow properties flowing in an open channel of a fixed slope at a given velocity, K will be solely dependent on the channel shape through the ratio of channel area to channel perimeter, A/P (Burger et al. 2010).

This general conclusion ties in with the same conclusion made by Straub et al. (1958) for Newtonian fluids.

Due to the inability of properly accounting for the presence of yield stress in the calculation of Re when using the Kozicki and Tiu (1967) definition in the f vs. Re relationship, the Haldenwang et al. (2002) Re definition was found to be the better of the two (Burger et al. 2010).

Laminar flow velocity prediction

A new average velocity equation for laminar flow of non-Newtonian flow in open channels given by:

$$V = \frac{R_h}{2} \left(\frac{(16/K) \tau_w - \tau_{yHB}}{k} \right)^{\frac{1}{n}} \quad (5.5)$$

where R_h is the hydraulic radius, K is the channel shape factor, τ_{yHB} is the yield stress, τ_w is the wall shear stress, k is the fluid consistency coefficient and n is the flow behaviour index.

The new model was either better or equivalent to the three previously-published laminar flow models as given in Section 2.5.1. The incorporation of the effect of shape into Eq. (5.1) by using the appropriate K value for the actual cross-section enhances the accuracy in the prediction of velocity. However, it was found that the new model was not always to be better than the other three previously-published models for the prediction of laminar flow of Bingham plastic and Herschel-Bulkley fluids in open channels of different cross-sectional shapes.

Turbulent flow velocity prediction

Shape does have an effect in turbulent flow of non-Newtonian fluids flowing in open channels. From this research, it was found that the turbulent data did not collapse onto the line given by the Blasius equation given by $f = 0.079Re^{-0.25}$. Instead, the data collapsed onto the line given by the modified Blasius equation given by $f_{mB} = aRe^b$ where different values for the constants a and b were obtained for the different channel shapes tested as given in Table 5.2 in Chapter Five. A new average velocity equation for turbulent flow of non-Newtonian flow in open channels is given by:

$$V_T = \sqrt{\frac{2\tau_w}{\rho a (Re_H)^b}} \quad (5.7)$$

where τ_w is the wall shear stress, ρ the fluid density, Re_H the Haldenwang et al. (2002) Reynolds number and a & b are the shape factors determined from the modified Blasius equation. Values of a & b for a rectangular channel were found to be 0.12 and -0.3297, for a semi-circular channel 0.048 and -0.2049, for a trapezoidal channel with 60° sides, 0.0851 and -0.2655 and for a triangular channel with vertex angle of 90°, values of a & b were found to be 0.0415 and -0.2022.

The new expression for predicting turbulent flow of non-Newtonian fluids in channels of different cross-sectional shapes predicted the experimental data very well and was found to be consistently the better model as can be seen from the (LSE) and (R^2) values in Table 5.7. The predicted data from the new velocity model fell within the accepted research error margin of 30%, as shown in the model comparison plots, Figure 5.10, Figure 5.11, Figure 5.12 and Figure 5.13.

The positive results obtained with the new velocity equation are partly due to the fact that the yield stress has less of an effect in turbulent flow.

Composite power law friction factor modelling

Validating the application to non-Newtonian open channel flow, the composite power law friction factor modelling technique used by Garcia et al. (2003) for pipe flow where the composite friction factor is given by:

$$f = F_2 + \frac{(F_1 - F_2)}{\left(1 + \left(\frac{Re}{t}\right)^e\right)^f} \quad (2.72)$$

where F_1 and F_2 are the power law relationships covering the laminar and turbulent flow regimes defined respectively as:

$$F_1 = aRe^b \quad (2.73)$$

and

$$F_2 = cRe^d \quad (2.74)$$

The Reynolds number range was from 5 to 15000 for the flow of the three non-Newtonian fluids tested in four different cross sectional shapes.

The composite power law friction factor modelling technique used by Garcia et al. (2003) for pipe flow can be used to adequately predict flow in an open channel of a given cross-sectional shape provided that an appropriate Reynolds number is used to take into account the non-Newtonian behaviour of the test fluid. It was found that the results using the Haldenwang et al. (2002) Reynolds number yielded better results than those based on the adapted Metzner-Reed Reynolds number, (Burger et al. 2013).

Two independent data sets, one from Coussot (1994) in laminar flow with the Reynolds number range up to 564 and the second from Naik (1984) in turbulent flow with the Reynolds number range from 4000 up to 65000 both for a rectangular channel, were used to test the friction factor prediction given by Eq. (2.72).

The correlation coefficient for the fit to the combined data set was 0.98 indicating the appropriateness of the proposed composite power law friction factor equation, however it is important to note that constants a & b in Eq. (2.73) and c & d in Eq. (2.74), the laminar and turbulent constants must be determined independently before constants e , f and t , the transition constants are determined.

The contributions made and the results obtained from this research have gone a long way in improving our understanding of non-Newtonian open channel flow.

8.2 Recommendations

From the outcomes achieved during this research the following recommendations can be made.

- The large experimental database compiled during this research can be used by future researchers to further increase the understanding of non-Newtonian open channel flow.
- The new laminar and turbulent velocity expressions can be used in the prediction of flow of non-Newtonian flow during the design of open channels when the fluid properties are known as well as the channel cross sectional shape application.
- The shape factor K values in the $f = K/Re_H$ relationship for non-Newtonian laminar flow in rectangular, triangular, trapezoidal and semi-circular open channels determined in this research can be used for the design of open channels.
- The composite power law friction factor modelling technique used by Garcia et al. (2003) for pipe flow can be applied to non-Newtonian open channel flow.

Despite the excellent alignment of the $f = K/Re_H$ line with the data found for rectangular, semi-circular, triangular and trapezoidal open channels, further work is still needed to underpin the underlying effect of the yield stress in causing the large scatter of research data depicted in the laminar model velocity comparison plots of both the laminar model presented in this work as well as the previously published models in homogeneous yield shear-thinning and Bingham plastic flow.

To take the understanding of open channel flow of non-Newtonian fluids to the next level, one would have to measure not only the average flow but map the cross-sectional velocity profiles and wall shear stress distributions. This can then be used to verify CFD modelling. A first attempt to measure velocity profiles of non-Newtonian fluids in a rectangular open channel using Ultrasound Velocity Profiling (UVP) has been made by Haldenwang et al. (2012). The application of real time in-line UVP measurements in the supply line and or in the flume could be used to obtain the rheology for each depth measurement. This would enable one to ascertain the sensitivity of the flow to changes in rheology which up to now has been nearly impossible.

The effect of yield stress on the prediction of velocity needs to be investigated further.

Appendices

Appendix A. Database for non-Newtonian flow in different channel shapes

The following section contains all the flume data which was used in this research. The data sets are for tests in the rectangular flumes of width 150 mm and 300 mm, 90 degree triangular flume of 300 mm width, 60 degree trapezoidal flumes of 150 mm and 300 mm width and semi-circular shaped flume with diameter 150 mm and 300 mm width. The channel slope, flow and flow depth as well as the rheological parameters are presented in tabular form for each of the tests. The test fluids are kaolin and bentonite suspensions and carboxymethyl cellulose (CMC) solutions.

Material:	Bentonite
Concentration/vol:	4.8%
Density kg/m³:	1029.0
T_y (Pa):	5.66
K (Pa.sⁿ):	0.0036
n:	1.000
Flume width (mm):	150
Flume Shape	Semicircular

SLOPE	FLOW	DEPTH	SLOPE	FLOW	DEPTH	SLOPE	FLOW	DEPTH	SLOPE	FLOW	DEPTH	SLOPE	FLOW	DEPTH
FLUME	Q	h	FLUME	Q	h	FLUME	Q	h	FLUME	Q	h	FLUME	Q	h
(degrees)	(l.s ⁻¹)	(m)	(degrees)	(l.s ⁻¹)	(m)	(degrees)	(l.s ⁻¹)	(m)	(degrees)	(l.s ⁻¹)	(m)	(degrees)	(l.s ⁻¹)	(m)
1	1.319	0.0620	2	0.504	0.0271	3	0.623	0.0186	4	0.631	0.0154	5	0.652	0.0133
1	0.936	0.0637	2	0.822	0.0292	3	0.934	0.0203	4	1.035	0.0175	5	1.003	0.0152
1	2.413	0.0641	2	1.365	0.0308	3	1.505	0.0228	4	1.496	0.0201	5	1.563	0.0183
1	0.451	0.0644	2	1.760	0.0307	3	2.055	0.0259	4	2.088	0.0229	5	2.101	0.0207
1	0.690	0.0648	2	2.256	0.0331	3	2.650	0.0291	4	2.585	0.0249	5	2.495	0.0220
1	1.715	0.0656	2	2.735	0.0338	3	3.009	0.0292	4	3.004	0.0249	5	2.987	0.0221
1	3.009	0.0679	2	3.023	0.0351	3	3.615	0.0310	4	3.517	0.0266	5	3.534	0.0242
1	3.509	0.0693	2	3.656	0.0391	3	4.117	0.0329	4	4.109	0.0288	5	4.487	0.0271
1	4.662	0.0705	2	4.409	0.0418	3	4.976	0.0359	4	5.344	0.0325	5	5.143	0.0293
1	5.551	0.0726	2	5.587	0.0455	3	6.054	0.0394	4	6.115	0.0354	5	6.230	0.0324
1	6.583	0.0758	2	7.403	0.0517	3	8.074	0.0459	4	8.134	0.0414	5	6.280	0.0324
1	7.599	0.0786	2	9.068	0.0572	3	10.232	0.0519	4	10.202	0.0470	5	8.205	0.0380
1	8.891	0.0811	2	10.168	0.0613	3	14.448	0.0641	4	14.487	0.0577	5	10.187	0.0433
1	10.162	0.0847	2	14.123	0.0723	3	21.963	0.0824	4	20.079	0.0707	5	14.389	0.0532
1	11.943	0.0873	2	21.573	0.0933				4	25.261	0.0804	5	19.619	0.0645
1	11.909	0.0906												
1	13.162	0.0935												
1	17.664	0.1071												
1	20.065	0.1143												

Material:	CMC
Concentration/vol:	1.5%
Density kg/m³:	1009.2
T_y (Pa):	0.00
K (Pa.sⁿ):	0.014
n:	0.944
Flume width (mm):	150
Flume Shape	Semicircular

SLOPE	FLOW	DEPTH	SLOPE	FLOW	DEPTH	SLOPE	FLOW	DEPTH	SLOPE	FLOW	DEPTH	SLOPE	FLOW	DEPTH
FLUME	Q	h	FLUME	Q	h	FLUME	Q	h	FLUME	Q	h	FLUME	Q	h
(degrees)	(l.s ⁻¹)	(m)	(degrees)	(l.s ⁻¹)	(m)	(degrees)	(l.s ⁻¹)	(m)	(degrees)	(l.s ⁻¹)	(m)	(degrees)	(l.s ⁻¹)	(m)
1	0.172	0.0099	2	0.124	0.0072	3	0.105	0.0060	4	0.088	0.0050	5	0.117	0.0054
1	0.212	0.0103	2	0.172	0.0079	3	0.199	0.0073	4	0.133	0.0059	5	0.142	0.0057
1	0.257	0.0111	2	0.219	0.0085	3	0.225	0.0076	4	0.177	0.0064	5	0.212	0.0065
1	0.343	0.0122	2	0.266	0.0090	3	0.261	0.0079	4	0.217	0.0068	5	0.254	0.0069
1	0.433	0.0131	2	0.323	0.0094	3	0.318	0.0083	4	0.271	0.0071	5	0.362	0.0076
1	0.518	0.0141	2	0.414	0.0103	3	0.426	0.0092	4	0.318	0.0076	5	0.455	0.0083
1	0.637	0.0154	2	0.506	0.0112	3	0.520	0.0100	4	0.358	0.0081	5	0.634	0.0092
1	0.729	0.0161	2	0.621	0.0120	3	0.630	0.0110	4	0.424	0.0085	5	0.755	0.0097
1	0.818	0.0168	2	0.818	0.0139	3	0.764	0.0119	4	0.512	0.0092	5	0.923	0.0101
1	0.929	0.0176	2	0.921	0.0145	3	0.923	0.0126	4	0.617	0.0097	5	1.474	0.0127
1	1.147	0.0195	2	1.368	0.0171	3	1.053	0.0131	4	0.724	0.0103	5	1.991	0.0155
1	2.001	0.0272	2	2.061	0.0208	3	1.516	0.0153	4	0.871	0.0109	5	2.786	0.0215
1	3.173	0.0342	2	2.536	0.0237	3	2.004	0.0182	4	1.030	0.0116	5	4.025	0.0256
1	3.952	0.0393	2	3.223	0.0316	3	2.983	0.0253	4	1.496	0.0140	5	5.941	0.0326
1	4.629	0.0430	2	4.087	0.0350	3	3.906	0.0311	4	2.056	0.0167	5	8.020	0.0376
1	5.941	0.0499	2	6.290	0.0422	3	5.785	0.0375	4	3.486	0.0254	5	10.054	0.0430
1	7.930	0.0597	2	7.976	0.0496	3	8.100	0.0440	4	5.018	0.0311	5	15.853	0.0586
1	10.241	0.0692	2	10.074	0.0571	3	10.117	0.0502	4	8.055	0.0422	5	18.437	0.0633
						3	17.232	0.0706	4	10.116	0.0476			
									4	18.135	0.0676			

Material:	CMC
Concentration/vol:	3.0%
Density kg/m³:	1018.2
T_y (Pa):	0.00
K (Pa.sⁿ):	0.175
n:	0.768
Flume width (mm):	150
Flume Shape	Semicircular

SLOPE	FLOW	DEPTH	SLOPE	FLOW	DEPTH	SLOPE	FLOW	DEPTH	SLOPE	FLOW	DEPTH	SLOPE	FLOW	DEPTH
FLUME	Q	h	FLUME	Q	h	FLUME	Q	h	FLUME	Q	h	FLUME	Q	h
(degrees)	(l.s ⁻¹)	(m)	(degrees)	(l.s ⁻¹)	(m)	(degrees)	(l.s ⁻¹)	(m)	(degrees)	(l.s ⁻¹)	(m)	(degrees)	(l.s ⁻¹)	(m)
1	0.128	0.0162	2	0.144	0.0133	3	0.145	0.0116	4	0.121	0.0096	5	0.328	0.0121
1	0.219	0.0184	2	0.247	0.0149	3	0.205	0.0121	4	0.193	0.0109	5	0.429	0.0127
1	0.288	0.0198	2	0.342	0.0164	3	0.298	0.0134	4	0.298	0.0124	5	0.522	0.0135
1	0.402	0.0217	2	0.402	0.0172	3	0.402	0.0149	4	0.401	0.0135	5	0.636	0.0143
1	0.558	0.0238	2	0.512	0.0183	3	0.506	0.0158	4	0.500	0.0144	5	0.719	0.0148
1	0.866	0.0270	2	0.643	0.0196	3	0.603	0.0167	4	0.592	0.0151	5	0.884	0.0154
1	0.993	0.0283	2	0.877	0.0215	3	0.803	0.0182	4	0.751	0.0161	5	1.026	0.0164
1	1.246	0.0304	2	1.004	0.0225	3	1.013	0.0194	4	0.997	0.0174	5	1.309	0.0179
1	1.539	0.0327	2	1.300	0.0245	3	1.295	0.0210	4	1.260	0.0191	5	1.613	0.0195
1	2.023	0.0358	2	1.695	0.0268	3	1.608	0.0229	4	1.519	0.0205	5	2.040	0.0209
1	2.846	0.0406	2	2.270	0.0299	3	2.100	0.0251	4	1.897	0.0222	5	2.994	0.0242
1	4.020	0.0474	2	2.640	0.0316	3	2.531	0.0271	4	2.257	0.0236	5	4.141	0.0281
1	4.948	0.0524	2	3.645	0.0364	3	3.609	0.0310	4	3.034	0.0263	5	5.008	0.0311
1	5.893	0.0568	2	4.267	0.0394	3	4.766	0.0360	4	4.125	0.0301	5	6.131	0.0342
1	6.769	0.0611	2	5.185	0.0430	3	6.446	0.0420	4	5.044	0.0337	5	7.070	0.0368
1	8.013	0.0672	2	6.285	0.0472	3	8.112	0.0471	4	6.066	0.0368	5	9.924	0.0446
1	10.019	0.0759	2	7.476	0.0523	3	10.162	0.0534	4	8.050	0.0433	5	15.833	0.0587
1	15.564	0.0967	2	9.483	0.0594	3	15.479	0.0686	4	10.120	0.0489	5	19.941	0.0688
1	19.738	0.1142	2	12.447	0.0692	3	19.412	0.0792	4	14.414	0.0603			
			2	14.934	0.0774				4	19.349	0.0718			

Material:	CMC
Concentration/vol:	4.0%
Density kg/m³:	1022.3
T_y (Pa):	0.00
K (Pa.sⁿ):	0.278
n:	0.749
Flume width (mm):	150
Flume Shape	Semicircular

SLOPE	FLOW	DEPTH	SLOPE	FLOW	DEPTH	SLOPE	FLOW	DEPTH	SLOPE	FLOW	DEPTH	SLOPE	FLOW	DEPTH
FLUME	Q	h	FLUME	Q	h	FLUME	Q	h	FLUME	Q	h	FLUME	Q	h
(degrees)	(l.s ⁻¹)	(m)	(degrees)	(l.s ⁻¹)	(m)	(degrees)	(l.s ⁻¹)	(m)	(degrees)	(l.s ⁻¹)	(m)	(degrees)	(l.s ⁻¹)	(m)
1	0.148	0.0200	2	0.141	0.0160	3	0.155	0.0140	4	0.101	0.0113	5	0.113	0.0108
1	0.195	0.0215	2	0.274	0.0184	3	0.282	0.0160	4	0.252	0.0143	5	0.201	0.0122
1	0.293	0.0241	2	0.382	0.0201	3	0.392	0.0176	4	0.406	0.0161	5	0.290	0.0135
1	0.393	0.0262	2	0.491	0.0217	3	0.500	0.0188	4	0.546	0.0174	5	0.395	0.0147
1	0.496	0.0279	2	0.592	0.0229	3	0.599	0.0197	4	0.613	0.0181	5	0.581	0.0161
1	0.684	0.0307	2	0.697	0.0239	3	0.802	0.0213	4	0.792	0.0193	5	0.587	0.0165
1	0.889	0.0332	2	0.888	0.0257	3	0.995	0.0229	4	0.988	0.0206	5	0.786	0.0174
1	1.179	0.0362	2	1.041	0.0269	3	1.489	0.0257	4	0.994	0.0211	5	0.984	0.0190
1	1.480	0.0389	2	1.455	0.0297	3	1.943	0.0282	4	1.489	0.0233	5	1.487	0.0214
1	1.788	0.0411	2	2.000	0.0330	3	2.492	0.0306	4	1.975	0.0256	5	1.990	0.0238
1	1.994	0.0426	2	2.911	0.0374	3	3.505	0.0349	4	2.554	0.0276	5	2.945	0.0272
1	2.902	0.0480	2	3.504	0.0401	3	4.161	0.0373	4	3.053	0.0299	5	4.136	0.0307
1	3.539	0.0518	2	4.075	0.0425	3	6.054	0.0440	4	3.972	0.0331	5	5.002	0.0339
1	4.057	0.0547	2	5.011	0.0465	3	7.122	0.0477	4	5.106	0.0366	5	5.984	0.0369
1	5.037	0.0596	2	6.105	0.0509	3	8.019	0.0507	4	6.118	0.0399	5	8.079	0.0425
1	6.102	0.0650	2	8.040	0.0582	3	10.275	0.0583	4	8.083	0.0461	5	10.046	0.0477
1	8.104	0.0747	2	10.080	0.0663				4	10.245	0.0524	5	16.390	0.0635
1	10.035	0.0838							4	17.063	0.0704			
									4	21.080	0.0803			

Material:	CMC
Concentration/vol:	5.3%
Density kg/m ³ :	1028.0
T _y (Pa):	0.00
K (Pa.s ⁿ):	0.920
n:	0.678
Flume width (mm):	150
Flume Shape	Semicircular

SLOPE	FLOW	DEPTH	SLOPE	FLOW	DEPTH	SLOPE	FLOW	DEPTH	SLOPE	FLOW	DEPTH	SLOPE	FLOW	DEPTH
FLUME	Q	h	FLUME	Q	h	FLUME	Q	h	FLUME	Q	h	FLUME	Q	h
(degrees)	(l.s ⁻¹)	(m)	(degrees)	(l.s ⁻¹)	(m)	(degrees)	(l.s ⁻¹)	(m)	(degrees)	(l.s ⁻¹)	(m)	(degrees)	(l.s ⁻¹)	(m)
1	0.227	0.0326				3	0.116	0.0185				5	0.121	0.0153
1	0.359	0.0376				3	0.211	0.0200				5	0.212	0.0174
1	0.454	0.0398				3	0.307	0.0245				5	0.330	0.0198
1	0.671	0.0454				3	0.404	0.0264				5	0.420	0.0214
1	0.737	0.0463				3	0.511	0.0283				5	0.506	0.0224
1	0.816	0.0475				3	0.605	0.0298				5	0.608	0.0238
1	0.976	0.0500				3	0.698	0.0310				5	0.693	0.0249
1	0.980	0.0501				3	0.801	0.0320				5	0.821	0.0256
1	1.092	0.0516				3	0.898	0.0330				5	0.883	0.0263
1	1.414	0.0566				3	0.996	0.0341				5	0.997	0.0272
1	1.542	0.0578				3	1.192	0.0358				5	1.196	0.0286
1	2.177	0.0652				3	1.391	0.0374				5	1.410	0.0301
1	2.247	0.0674				3	1.776	0.0404				5	1.693	0.0325
1	2.399	0.0678				3	1.980	0.0418				5	1.761	0.0314
1	2.485	0.0683				3	2.086	0.0421				5	2.078	0.0340
1	3.026	0.0730				3	2.237	0.0433				5	2.228	0.0343
1	3.159	0.0744				3	2.526	0.0450				5	2.651	0.0359
1	3.491	0.0796				3	2.999	0.0476				5	2.895	0.0372
1	4.355	0.0873				3	3.877	0.0519				5	3.159	0.0382
1	5.746	0.0982				3	4.325	0.0543				5	3.526	0.0398
1	7.437	0.1113				3	4.739	0.0560				5	4.421	0.0431
1	13.369	0.1459				3	5.745	0.0602				5	5.373	0.0460
1	15.390	0.1565				3	6.572	0.0633				5	6.247	0.0491
1	18.017	0.1722				3	7.502	0.0666				5	7.099	0.0515
						3	9.023	0.0704				5	7.954	0.0542
						3	12.020	0.0795				5	9.484	0.0585
						3	12.850	0.0823				5	10.378	0.0611
						3	15.990	0.0924				5	11.139	0.0633
												5	13.908	0.0684
												5	15.927	0.0731

Material:	Kaolin
Concentration/vol:	5.4%
Density kg/m³:	1089.0
T_y (Pa):	4.40
K (Pa.sⁿ):	0.084
n:	0.582
Flume width (mm):	150
Flume Shape	Semicircular

SLOPE	FLOW	DEPTH	SLOPE	FLOW	DEPTH	SLOPE	FLOW	DEPTH	SLOPE	FLOW	DEPTH	SLOPE	FLOW	DEPTH
FLUME	Q	h	FLUME	Q	h	FLUME	Q	h	FLUME	Q	h	FLUME	Q	h
(degrees)	(l.s ⁻¹)	(m)	(degrees)	(l.s ⁻¹)	(m)	(degrees)	(l.s ⁻¹)	(m)	(degrees)	(l.s ⁻¹)	(m)	(degrees)	(l.s ⁻¹)	(m)
1	0.094	0.0400	2	0.129	0.0205	3	0.377	0.0157	4	0.445	0.0130	5	1.099	0.0135
1	0.159	0.0415	2	0.154	0.0214	3	0.477	0.0163	4	0.579	0.0137	5	1.447	0.0156
1	0.214	0.0419	2	0.296	0.0221	3	0.596	0.0167	4	0.699	0.0143	5	1.519	0.0159
1	0.269	0.0425	2	0.401	0.0224	3	0.751	0.0173	4	0.899	0.0151	5	1.951	0.0180
1	0.324	0.0431	2	0.425	0.0225	3	0.922	0.0178	4	1.132	0.0159	5	2.176	0.0182
1	0.471	0.0442	2	0.470	0.0228	3	1.089	0.0185	4	1.294	0.0167	5	2.896	0.0206
1	0.579	0.0450	2	0.599	0.0234	3	1.338	0.0196	4	1.497	0.0176	5	3.088	0.0214
1	0.790	0.0471	2	0.697	0.0237	3	1.598	0.0210	4	1.797	0.0185	5	3.496	0.0229
1	1.039	0.0489	2	0.794	0.0243	3	1.863	0.0223	4	2.008	0.0197	5	5.306	0.0283
1	1.504	0.0525	2	1.031	0.0253	3	2.118	0.0234	4	2.477	0.0215	5	6.550	0.0316
1	2.018	0.0547	2	1.256	0.0259	3	2.633	0.0252	4	3.117	0.0235	5	8.071	0.0355
1	2.795	0.0562	2	1.538	0.0272	3	3.013	0.0266	4	3.507	0.0252	5	10.084	0.0410
1	3.103	0.0571	2	1.835	0.0282	3	4.069	0.0304	4	4.238	0.0271	5	14.727	0.0513
1	3.808	0.0573	2	2.029	0.0289	3	5.143	0.0342	4	5.074	0.0303			
1	4.027	0.0579	2	2.594	0.0313	3	6.985	0.0401	4	6.241	0.0336			
1	4.554	0.0594	2	2.845	0.0325	3	8.359	0.0442	4	7.076	0.0360			
1	4.955	0.0609	2	3.160	0.0327	3	10.198	0.0494	4	8.572	0.0403			
1	5.555	0.0623	2	3.458	0.0352	3	16.611	0.0662	4	10.295	0.0220			
1	6.642	0.0663	2	4.394	0.0380	3	21.997	0.0794	4	15.166	0.0565			
1	7.565	0.0697	2	5.075	0.0413				4	21.386	0.0704			
1	8.651	0.0740	2	7.927	0.0513									
1	10.074	0.0794	2	10.054	0.0576									
1	15.511	0.0982	2	15.193	0.0727									
1	20.435	0.1151	2	19.450	0.0848									
1	25.306	0.1317	2	23.667	0.0968									

Material:	Kaolin
Concentration/vol:	7.1%
Density kg/m³:	1118.0
T_y (Pa):	11.56
K (Pa.sⁿ):	0.148
n:	0.557
Flume width (mm):	150
Flume Shape	Semicircular

SLOPE	FLOW	DEPTH	SLOPE	FLOW	DEPTH	SLOPE	FLOW	DEPTH	SLOPE	FLOW	DEPTH	SLOPE	FLOW	DEPTH
FLUME	Q	h	FLUME	Q	h	FLUME	Q	h	FLUME	Q	h	FLUME	Q	h
(degrees)	(l.s ⁻¹)	(m)	(degrees)	(l.s ⁻¹)	(m)	(degrees)	(l.s ⁻¹)	(m)	(degrees)	(l.s ⁻¹)	(m)	(degrees)	(l.s ⁻¹)	(m)
1	0.999	0.0933	2	1.041	0.0547	3	1.017	0.0361	4	1.277	0.0277	5	1.953	0.0250
1	1.475	0.0985	2	1.935	0.0594	3	1.817	0.0381	4	1.790	0.0291	5	2.656	0.0269
1	1.883	0.1023	2	2.624	0.0608	3	2.064	0.0389	4	2.136	0.0299	5	2.921	0.0280
1	3.102	0.1111	2	3.144	0.0633	3	2.628	0.0407	4	2.805	0.0325	5	3.518	0.0299
1	3.595	0.1145	2	3.597	0.0641	3	3.297	0.0421	4	3.337	0.0338	5	4.050	0.0313
1	4.532	0.1207	2	4.421	0.0645	3	4.180	0.0438	4	3.828	0.0351	5	4.979	0.0340
1	5.498	0.1267	2	4.951	0.0653	3	4.664	0.0452	4	4.399	0.0365	5	5.895	0.0365
1	6.817	0.1330	2	5.621	0.0665	3	5.032	0.0464	4	4.938	0.0385	5	7.112	0.0396
1	7.863	0.1388	2	6.058	0.0675	3	5.826	0.0486	4	6.293	0.0420	5	8.300	0.0426
1	8.987	0.1439	2	6.594	0.0686	3	6.835	0.0516	4	7.107	0.0442	5	10.010	0.0469
1	10.072	0.1493	2	7.175	0.0702	3	7.844	0.0544	4	7.907	0.0465	5	12.322	0.0520
1	12.258	0.1580	2	7.869	0.0721	3	8.785	0.0570	4	9.448	0.0502	5	15.147	0.0583
1	14.994	0.1691	2	9.177	0.0756	3	10.010	0.0603	4	10.243	0.0522	5	18.008	0.0645
			2	10.126	0.0782	3	11.929	0.0650	4	11.928	0.0566	5	20.259	0.0691
			2	12.216	0.0840	3	14.075	0.0707	4	14.728	0.0633	5	22.990	0.0750
			2	12.627	0.0850	3	17.326	0.0788	4	17.217	0.0689			
			2	14.496	0.0905	3	19.659	0.0852	4	20.198	0.0759			
			2	15.746	0.0942	3	22.658	0.0922	4	23.035	0.0820			
			2	17.865	0.1000									
			2	20.264	0.1065									
			2	23.121	0.1144									

Material:	Kaolin
Concentration/vol:	9.0%
Density kg/m³:	1148.0
T_y (Pa):	19.00
K (Pa.sⁿ):	0.210
n:	0.616
Flume width (mm):	150
Flume Shape	Semicircular

SLOPE	FLOW	DEPTH	SLOPE	FLOW	DEPTH	SLOPE	FLOW	DEPTH	SLOPE	FLOW	DEPTH
FLUME	Q	h	FLUME	Q	h	FLUME	Q	h	FLUME	Q	h
(degrees)	(l.s ⁻¹)	(m)	(degrees)	(l.s ⁻¹)	(m)	(degrees)	(l.s ⁻¹)	(m)	(degrees)	(l.s ⁻¹)	(m)
2	2.138	0.1139	3	2.042	0.0805	4	2.145	0.0581	5	2.373	0.0460
2	2.707	0.1198	3	3.034	0.0848	4	2.953	0.0597	5	3.308	0.0474
2	3.917	0.1266	3	4.074	0.0895	4	3.749	0.0616	5	4.063	0.0489
2	5.415	0.1349	3	5.062	0.0915	4	4.906	0.0638	5	4.991	0.0506
2	6.664	0.1421	3	6.548	0.0937	4	6.164	0.0651	5	6.024	0.0522
2	7.633	0.1469	3	7.838	0.0967	4	7.306	0.0671	5	6.974	0.0539
2	8.816	0.1524	3	8.975	0.0978	4	9.345	0.0707	5	7.854	0.0556
2	10.045	0.1572	3	9.991	0.0986	4	10.084	0.0722	5	8.771	0.0576
2	12.186	0.1667	3	12.195	0.1016	4	11.547	0.0752	5	9.390	0.0589
2	15.371	0.1859	3	14.174	0.1051	4	13.184	0.0785	5	10.048	0.0604
			3	16.127	0.1095	4	15.162	0.0827	5	11.798	0.0637
			3	18.364	0.1146	4	18.015	0.0890	5	14.083	0.0688
			3	20.549	0.1195	4	20.298	0.0945	5	16.030	0.0728
			3	23.805	0.1274	4	24.310	0.1036	5	18.438	0.0780
									5	20.054	0.0814
									5	25.405	0.0926

Material:	Bentonite
Concentration/vol:	4.5%
Density kg/m³:	1027.0
T_y (Pa):	4.30
K (Pa.sⁿ):	0.0036
n:	1.000
Flume width (mm):	300
Flume Shape	Semicircular

SLOPE	FLOW	DEPTH	SLOPE	FLOW	DEPTH	SLOPE	FLOW	DEPTH	SLOPE	FLOW	DEPTH	SLOPE	FLOW	DEPTH
FLUME	Q	h	FLUME	Q	h	FLUME	Q	h	FLUME	Q	h	FLUME	Q	h
(degrees)	(l.s ⁻¹)	(m)	(degrees)	(l.s ⁻¹)	(m)	(degrees)	(l.s ⁻¹)	(m)	(degrees)	(l.s ⁻¹)	(m)	(degrees)	(l.s ⁻¹)	(m)
1	0.669	0.0420	2	0.824	0.0191	3	0.876	0.0152	4	0.539	0.0113	5	0.504	0.0108
1	0.752	0.0435	2	1.056	0.0206	3	1.006	0.0158	4	0.665	0.0119	5	0.543	0.0103
1	1.001	0.0452	2	1.263	0.0212	3	1.208	0.0169	4	0.763	0.0122	5	0.734	0.0116
1	1.241	0.0445	2	1.569	0.0222	3	1.312	0.0168	4	0.920	0.0131	5	0.810	0.0114
1	1.567	0.0451	2	1.866	0.0239	3	1.532	0.0181	4	1.054	0.0140	5	0.994	0.0123
1	1.861	0.0446	2	2.229	0.0249	3	1.943	0.0198	4	1.240	0.0148	5	1.216	0.0130
1	2.131	0.0440	2	2.635	0.0257	3	2.282	0.0206	4	1.400	0.0155	5	1.431	0.0133
1	2.445	0.0411	2	2.847	0.0261	3	2.675	0.0211	4	1.525	0.0157	5	1.630	0.0142
1	3.029	0.0427	2	3.857	0.0296	3	3.041	0.0224	4	1.687	0.0159	5	1.973	0.0152
1	3.612	0.0453	2	4.827	0.0322	3	3.535	0.0242	4	1.940	0.0170	5	2.538	0.0168
1	4.228	0.0469	2	6.057	0.0352	3	4.248	0.0258	4	2.234	0.0177	5	3.020	0.0179
1	4.701	0.0481	2	7.082	0.0379	3	4.646	0.0269	4	2.536	0.0188	5	3.478	0.0190
1	5.240	0.0496	2	8.194	0.0404	3	5.186	0.0286	4	3.032	0.0200	5	4.161	0.0202
1	6.066	0.0520	2	9.049	0.0423	3	6.091	0.0304	4	3.526	0.0213	5	5.086	0.0224
1	7.164	0.0554	2	10.157	0.0448	3	7.100	0.0331	4	4.139	0.0226	5	5.988	0.0246
1	7.612	0.0553	2	12.397	0.0493	3	8.140	0.0352	4	4.489	0.0236	5	7.078	0.0267
1	8.123	0.0570	2	18.854	0.0619	3	10.079	0.0396	4	5.182	0.0252	5	8.136	0.0288
1	9.282	0.0598	2	21.851	0.0674	3	11.995	0.0420	4	6.125	0.0272	5	11.805	0.0351
1	10.147	0.0617	2	26.257	0.0759	3	16.163	0.0495	4	7.081	0.0293	5	13.252	0.0374
1	11.734	0.0622				3	20.947	0.0576	4	8.028	0.0310	5	20.409	0.0475
1	15.678	0.0711				3	26.915	0.0656	4	10.084	0.0350			
1	18.159	0.0766				3	32.225	0.0740	4	14.225	0.0421			
1	22.846	0.0854							4	18.525	0.0487			
1	28.247	0.0967							4	23.162	0.0559			
1	33.630	0.1027												
1	38.434	0.1119												

Material:	Bentonite
Concentration/vol:	6.2%
Density kg/m³:	1038.0
T_y (Pa):	15.78
K (Pa.sⁿ):	0.0064
n:	1.000
Flume width (mm):	150
Flume Shape	Semicircular

SLOPE	FLOW	DEPTH	SLOPE	FLOW	DEPTH	SLOPE	FLOW	DEPTH	SLOPE	FLOW	DEPTH
FLUME	Q	h	FLUME	Q	h	FLUME	Q	h	FLUME	Q	h
(degrees)	(l.s⁻¹)	(m)	(degrees)	(l.s⁻¹)	(m)	(degrees)	(l.s⁻¹)	(m)	(degrees)	(l.s⁻¹)	(m)
2	0.794	0.0972	3	1.066	0.0622	4	3.270	0.0478	5	3.025	0.0235
2	1.424	0.1069	3	1.233	0.0658	4	4.172	0.0484	5	2.992	0.0366
2	1.817	0.1125	3	1.546	0.0697	4	4.581	0.0496	5	1.969	0.0355
2	2.481	0.1178	3	1.855	0.0692	4	4.935	0.0498	5	1.276	0.0342
2	3.053	0.1213	3	2.010	0.0682	4	5.357	0.0509	5	1.788	0.0351
2	5.378	0.1312	3	2.345	0.0685	4	5.845	0.0517	5	2.711	0.0367
2	5.773	0.1204	3	2.862	0.0685	4	6.449	0.0524	5	3.525	0.0388
2	6.288	0.1222	3	3.611	0.0693	4	7.402	0.0543	5	4.350	0.0399
2	7.134	0.1230	3	4.324	0.0696	4	8.102	0.0557	5	5.459	0.0424
2	8.096	0.1238	3	5.688	0.0702	4	8.313	0.0556	5	6.344	0.0443
2	8.731	0.1244	3	6.474	0.0689	4	10.470	0.0609	5	7.894	0.0478
2	9.248	0.1244	3	7.537	0.0704	4	11.575	0.0639	5	9.157	0.0518
2	13.805	0.1244	3	8.420	0.0719	4	13.733	0.0688	5	10.859	0.0540
2	11.102	0.1279	3	9.657	0.0745	4	15.119	0.0713	5	9.977	0.0522
2	12.007	0.1294	3	10.345	0.0756				5	12.604	0.059
2	14.225	0.1322	3	13.480	0.0826				5	14.486	0.063
2	15.359	0.1333	3	18.033	0.0940						
2	18.577	0.1369	3	21.167	0.1005						

Material:	Bentonite
Concentration/vol:	6.8%
Density kg/m³:	1042.0
T_y (Pa):	18.34
K (Pa.sⁿ):	0.0078
n:	1.000
Flume width (mm):	300
Flume Shape	Semicircular

SLOPE	FLOW	DEPTH	SLOPE	FLOW	DEPTH	SLOPE	FLOW	DEPTH	SLOPE	FLOW	DEPTH
FLUME	Q	h	FLUME	Q	h	FLUME	Q	h	FLUME	Q	h
(degrees)	(l.s⁻¹)	(m)	(degrees)	(l.s⁻¹)	(m)	(degrees)	(l.s⁻¹)	(m)	(degrees)	(l.s⁻¹)	(m)
2	1.631	0.1072	3	2.111	0.0580	4	1.363	0.0416	5	1.968	0.0316
2	1.996	0.0991	3	3.471	0.0595	4	2.292	0.0416	5	2.900	0.0340
2	2.635	0.1051	3	4.147	0.0611	4	3.022	0.0462	5	3.954	0.0353
2	3.062	0.1022	3	4.963	0.0610	4	4.013	0.0435	5	4.958	0.0374
2	4.027	0.1037	3	6.068	0.0627	4	5.020	0.0452	5	6.097	0.0391
2	4.988	0.1013	3	7.030	0.0621	4	6.099	0.0465	5	7.275	0.0405
2	6.059	0.1014	3	8.490	0.0620	4	7.067	0.0476	5	8.432	0.0417
2	6.897	0.1007	3	10.224	0.0645	4	8.460	0.0496	5	10.164	0.0444
2	8.443	0.0995	3	12.711	0.0666	4	10.221	0.0523	5	11.986	0.0459
2	12.468	0.1001	3	14.507	0.0682	4	12.728	0.0542	5	14.286	0.0507
2	14.463	0.1048	3	16.723	0.0719	4	14.493	0.0570	5	15.944	0.0526
2	17.642	0.1093	3	21.384	0.0778	4	16.625	0.0599	5	19.673	0.0579
2	22.975	0.1112	3	25.676	0.0841	4	21.213	0.0666	5	25.015	0.0647
2	30.217	0.1157	3	32.294	0.0944	4	25.701	0.0720	5	29.462	0.0708
2	34.629	0.1184	3	36.650	0.0989	4	31.684	0.0810			
2	40.516	0.1258	3	41.754	0.1047	4	36.569	0.0869			

Material:	CMC
Concentration/vol:	1.5%
Density kg/m³:	1008.4
T_y (Pa):	0.00
K (Pa.sⁿ):	0.015
n:	0.944
Flume width (mm):	300
Flume Shape	Semicircular

SLOPE	FLOW	DEPTH	SLOPE	FLOW	DEPTH	SLOPE	FLOW	DEPTH	SLOPE	FLOW	DEPTH	SLOPE	FLOW	DEPTH
FLUME	Q	h	FLUME	Q	h	FLUME	Q	h	FLUME	Q	h	FLUME	Q	h
(degrees)	(l.s ⁻¹)	(m)	(degrees)	(l.s ⁻¹)	(m)	(degrees)	(l.s ⁻¹)	(m)	(degrees)	(l.s ⁻¹)	(m)	(degrees)	(l.s ⁻¹)	(m)
1	0.156	0.0087	2	0.171	0.0072	3	0.306	0.0074	4	0.357	0.0072	5	0.458	0.0072
1	0.212	0.0095	2	0.270	0.0082	3	0.418	0.0082	4	0.505	0.0082	5	0.602	0.0081
1	0.325	0.0108	2	0.325	0.0086	3	0.513	0.0087	4	0.620	0.0085	5	0.794	0.0087
1	0.413	0.0115	2	0.416	0.0093	3	0.712	0.0098	4	0.753	0.0090	5	1.535	0.0116
1	0.514	0.0124	2	0.486	0.0097	3	1.039	0.0114	4	0.835	0.0096	5	2.109	0.0136
1	0.615	0.0131	2	0.618	0.0106	3	1.267	0.0124	4	1.043	0.0105	5	3.183	0.0161
1	0.837	0.0147	2	0.620	0.0106	3	1.540	0.0135	4	1.521	0.0129	5	4.143	0.0223
1	1.032	0.0160	2	0.715	0.0111	3	2.016	0.0156	4	2.062	0.0147	5	5.747	0.0255
1	1.442	0.0182	2	0.941	0.0124	3	3.805	0.0250	4	3.024	0.0188	5	8.007	0.0292
1	2.080	0.0215	2	1.240	0.0138	3	6.126	0.0297	4	4.147	0.0227	5	10.094	0.0335
1	3.346	0.0261	2	1.435	0.0147	3	8.075	0.0338	4	6.032	0.0270	5	20.031	0.0486
1	4.067	0.0307	2	2.156	0.0182	3	10.043	0.0382	4	8.045	0.0314	5	29.310	0.0618
1	4.525	0.0331	2	2.515	0.0196	3	19.790	0.0550	4	10.068	0.0363	5	39.827	0.0741
1	6.316	0.0392	2	3.494	0.0227	3	31.564	0.0728	4	17.356	0.0475			
1	8.024	0.0454	2	4.969	0.0288	3	39.954	0.0853	4	28.980	0.0646			
1	10.072	0.0514	2	6.149	0.0321				4	39.561	0.0805			
1	16.866	0.0688	2	8.086	0.0374									
1	41.781	0.1166	2	10.020	0.0419									
			2	20.032	0.0639									
			2	28.227	0.0767									
			2	40.368	0.0970									

Material:	CMC
Concentration/vol:	3.0%
Density kg/m³:	1016.9
T_y (Pa):	0.00
K (Pa.sⁿ):	0.126
n:	0.780
Flume width (mm):	300
Flume Shape	Semicircular

SLOPE	FLOW	DEPTH	SLOPE	FLOW	DEPTH	SLOPE	FLOW	DEPTH	SLOPE	FLOW	DEPTH	SLOPE	FLOW	DEPTH
FLUME	Q	h	FLUME	Q	h	FLUME	Q	h	FLUME	Q	h	FLUME	Q	h
(degrees)	(l.s ⁻¹)	(m)	(degrees)	(l.s ⁻¹)	(m)	(degrees)	(l.s ⁻¹)	(m)	(degrees)	(l.s ⁻¹)	(m)	(degrees)	(l.s ⁻¹)	(m)
1	0.088	0.0123	2	0.106	0.0101	3	0.164	0.0098	4	0.237	0.0096	5	0.658	0.0122
1	0.195	0.0149	2	0.178	0.0115	3	0.256	0.0108	4	0.376	0.0109	5	0.750	0.0124
1	0.418	0.0184	2	0.195	0.0118	3	0.314	0.0115	4	0.574	0.0121	5	0.839	0.0128
1	0.500	0.0192	2	0.286	0.0129	3	0.450	0.0126	4	0.677	0.0127	5	0.954	0.0134
1	0.602	0.0201	2	0.387	0.0140	3	0.607	0.0137	4	0.844	0.0135	5	1.088	0.0137
1	0.868	0.0223	2	0.528	0.0151	3	0.818	0.0151	4	0.953	0.0139	5	1.314	0.0142
1	1.023	0.0232	2	0.605	0.0157	3	1.039	0.0163	4	1.128	0.0147	5	1.486	0.0145
1	1.556	0.0265	2	0.827	0.0172	3	1.213	0.0168	4	1.350	0.0156	5	2.059	0.0165
1	1.841	0.0279	2	1.307	0.0197	3	1.326	0.0170	4	1.559	0.0162	5	2.813	0.0185
1	2.265	0.0291	2	2.068	0.0228	3	1.574	0.0176	4	1.989	0.0177	5	4.407	0.0234
1	2.717	0.0315	2	3.429	0.0277	3	1.876	0.0190	4	2.475	0.0196	5	5.502	0.0259
1	3.555	0.0356	2	5.164	0.0332	3	2.381	0.0206	4	2.868	0.0208	5	6.418	0.0278
1	4.029	0.0374	2	6.686	0.0383	3	3.062	0.0231	4	3.241	0.0219	5	8.158	0.0320
1	4.825	0.0404	2	8.464	0.0427	3	3.836	0.0254	4	4.280	0.0245	5	9.477	0.0351
1	5.720	0.0441	2	11.889	0.0507	3	5.680	0.0311	4	6.099	0.0292	5	15.818	0.0436
1	6.707	0.0470				3	7.526	0.0361	4	7.202	0.0317	5	24.236	0.0569
1	8.495	0.0527				3	9.471	0.0406	4	9.489	0.0367	5	33.925	0.0675
1	9.509	0.0553				3	16.963	0.0539	4	22.436	0.0560			
1	20.236	0.0803				3	25.462	0.0675	4	32.681	0.0698			
1	25.757	0.0913				3	35.361	0.0806	4	41.163	0.0822			
1	32.210	0.1045												
1	35.580	0.1108												
1	42.286	0.1213												
1	44.730	0.1253												

Material:	Kaolin
Concentration/vol:	3.5%
Density kg/m³:	1058.0
T_y (Pa):	0.50
K (Pa.sⁿ):	0.061
n:	0.560
Flume width (mm):	300
Flume Shape	Semicircular

SLOPE	FLOW	DEPTH	SLOPE	FLOW	DEPTH	SLOPE	FLOW	DEPTH	SLOPE	FLOW	DEPTH	SLOPE	FLOW	DEPTH
FLUME	Q	h	FLUME	Q	h	FLUME	Q	h	FLUME	Q	h	FLUME	Q	h
(degrees)	(l.s ⁻¹)	(m)	(degrees)	(l.s ⁻¹)	(m)	(degrees)	(l.s ⁻¹)	(m)	(degrees)	(l.s ⁻¹)	(m)	(degrees)	(l.s ⁻¹)	(m)
1	0.122	0.0104	2	0.066	0.0065	3	0.231	0.0065	4	0.319	0.0059	5	0.491	0.0074
1	0.158	0.0109	2	0.105	0.0068	3	0.320	0.0070	4	0.419	0.0065	5	0.670	0.0084
1	0.218	0.0114	2	0.159	0.0072	3	0.385	0.0073	4	0.528	0.0071	5	1.031	0.0104
1	0.264	0.0119	2	0.219	0.0077	3	0.465	0.0075	4	0.630	0.0075	5	1.452	0.0117
1	0.311	0.0122	2	0.262	0.0081	3	0.584	0.0093	4	0.773	0.0080	5	1.569	0.0121
1	0.374	0.0125	2	0.318	0.0085	3	0.668	0.0100	4	0.978	0.0088	5	2.039	0.0141
1	0.424	0.0130	2	0.383	0.0090	3	0.804	0.0105	4	1.495	0.0128	5	3.234	0.0179
1	0.478	0.0135	2	0.482	0.0096	3	1.047	0.0112	4	2.139	0.0148	5	4.113	0.0201
1	0.526	0.0138	2	0.576	0.0100	3	1.538	0.0138	4	3.576	0.0198	5	6.934	0.0263
1	0.586	0.0141	2	0.683	0.0106	3	2.116	0.0161	4	5.370	0.0237	5	10.105	0.0325
1	0.690	0.0148	2	0.765	0.0109	3	3.143	0.0196	4	7.061	0.0289	5	23.782	0.0560
1	0.801	0.0154	2	0.807	0.0112	3	4.235	0.0229	4	10.095	0.0349	5	34.722	0.0669
1	0.943	0.0160	2	0.916	0.0118	3	5.467	0.0260	4	19.114	0.0495	5	44.294	0.0791
1	1.013	0.0164	2	1.215	0.0131	3	8.093	0.0337	4	33.511	0.0695			
1	1.499	0.0193	2	2.185	0.0181	3	10.158	0.0380	4	45.471	0.0851			
1	2.071	0.0215	2	3.180	0.0219	3	17.676	0.0515						
1	3.119	0.0259	2	4.128	0.0254	3	28.609	0.0682						
1	4.072	0.0296	2	5.102	0.0286	3	46.740	0.0944						
1	5.081	0.0327	2	6.140	0.0317									
1	6.119	0.0359	2	7.098	0.0340									
1	7.208	0.0386	2	8.232	0.0368									
1	8.429	0.0436	2	10.099	0.0419									
1	9.562	0.0479	2	17.287	0.0569									
1	10.105	0.0493	2	30.715	0.0789									
1	15.782	0.0633	2	45.267	0.1019									
1	22.294	0.0796												
1	30.832	0.0946												
1	43.733	0.1160												

Material:	Kaolin
Concentration/vol:	5.4%
Density kg/m³:	1089.0
T_y (Pa):	4.40
K (Pa.sⁿ):	0.084
n:	0.582
Flume width (mm):	300
Flume Shape	Semicircular

SLOPE	FLOW	DEPTH	SLOPE	FLOW	DEPTH	SLOPE	FLOW	DEPTH	SLOPE	FLOW	DEPTH	SLOPE	FLOW	DEPTH
FLUME	Q	h	FLUME	Q	h	FLUME	Q	h	FLUME	Q	h	FLUME	Q	h
(degrees)	(l.s ⁻¹)	(m)	(degrees)	(l.s ⁻¹)	(m)	(degrees)	(l.s ⁻¹)	(m)	(degrees)	(l.s ⁻¹)	(m)	(degrees)	(l.s ⁻¹)	(m)
1	0.192	0.0358	2	0.257	0.0189	3	0.356	0.0141	4	1.212	0.0143	5	1.043	0.0119
1	0.276	0.0372	2	0.390	0.0197	3	0.406	0.0141	4	1.467	0.0151	5	1.312	0.0128
1	0.384	0.0382	2	0.510	0.0198	3	0.491	0.0145	4	1.704	0.0159	5	1.554	0.0139
1	0.548	0.0386	2	0.586	0.0204	3	0.576	0.0148	4	1.976	0.0169	5	1.892	0.0148
1	0.638	0.0391	2	0.697	0.0207	3	0.688	0.0152	4	2.449	0.0181	5	2.406	0.0161
1	0.842	0.0394	2	0.782	0.0209	3	0.804	0.0153	4	3.056	0.0196	5	3.008	0.0176
1	0.991	0.0406	2	0.942	0.0211	3	0.907	0.0158	4	3.974	0.0222	5	4.006	0.0199
1	1.341	0.0420	2	1.006	0.0216	3	1.018	0.0160	4	5.169	0.0245	5	5.304	0.0228
1	1.531	0.0423	2	1.312	0.0227	3	1.396	0.0176	4	6.168	0.0268	5	6.131	0.0245
1	2.129	0.0422	2	1.667	0.0237	3	1.649	0.0183	4	7.977	0.0306	5	8.221	0.0284
1	2.669	0.0423	2	2.069	0.0248	3	2.087	0.0197	4	10.192	0.0349	5	10.076	0.0322
1	2.925	0.0425	2	2.538	0.0262	3	2.559	0.0209	4	13.871	0.0412	5	14.855	0.0395
1	3.702	0.0460	2	2.956	0.0271	3	3.046	0.0224	4	22.477	0.0546	5	22.006	0.0499
1	4.604	0.0481	2	3.825	0.0303	3	4.032	0.0251	4	31.762	0.0658	5	31.437	0.0605
1	5.625	0.0502	2	4.584	0.0314	3	5.004	0.0275	4	42.132	0.0768			
1	6.754	0.0529	2	6.219	0.0364	3	6.109	0.0302	4	46.225	0.0822			
1	8.079	0.0562	2	7.092	0.0386	3	7.038	0.0323						
1	9.326	0.0585	2	10.096	0.0457	3	8.540	0.0357						
1	10.222	0.0610	2	14.297	0.0539	3	10.168	0.0389						
1	14.770	0.0712	2	22.181	0.0681	3	14.114	0.0459						
1	21.056	0.0838	2	33.603	0.0865	3	21.353	0.0582						
1	31.780	0.1036	2	42.322	0.0986	3	31.829	0.0731						
1	41.910	0.1203	2	46.015	0.1022	3	42.089	0.0864						
1	45.596	0.1259				3	46.358	0.0895						

Material:	Kaolin
Concentration/vol:	7.1%
Density kg/m³:	1118.0
T_y (Pa):	11.56
K (Pa.sⁿ):	0.148
n:	0.557
Flume width (mm):	300
Flume Shape	Semicircular

SLOPE	FLOW	DEPTH	SLOPE	FLOW	DEPTH	SLOPE	FLOW	DEPTH	SLOPE	FLOW	DEPTH	SLOPE	FLOW	DEPTH
FLUME	Q	h	FLUME	Q	h	FLUME	Q	h	FLUME	Q	h	FLUME	Q	h
(degrees)	(l.s ⁻¹)	(m)	(degrees)	(l.s ⁻¹)	(m)	(degrees)	(l.s ⁻¹)	(m)	(degrees)	(l.s ⁻¹)	(m)	(degrees)	(l.s ⁻¹)	(m)
1	0.273	0.0738	2	1.113	0.0479	3	1.005	0.0319	4	1.105	0.0246	5	1.288	0.0202
1	0.408	0.0747	2	1.557	0.0488	3	1.310	0.0323	4	1.271	0.0241	5	1.452	0.0211
1	0.615	0.0765	2	1.973	0.0505	3	1.610	0.0332	4	1.558	0.0253	5	1.789	0.0217
1	0.821	0.0781	2	2.637	0.0515	3	2.119	0.0335	4	1.973	0.0262	5	2.112	0.0223
1	1.020	0.0797	2	3.095	0.0522	3	2.583	0.0344	4	2.108	0.0264	5	2.566	0.0232
1	1.536	0.0826	2	3.522	0.0528	3	3.130	0.0356	4	2.558	0.0273	5	3.121	0.0241
1	2.034	0.0855	2	4.119	0.0530	3	3.449	0.0364	4	3.180	0.0285	5	3.631	0.0251
1	2.608	0.0877	2	4.515	0.0527	3	4.005	0.0373	4	3.560	0.0292	5	4.225	0.0263
1	3.471	0.0894	2	5.710	0.0537	3	4.525	0.0379	4	3.921	0.0302	5	4.774	0.0277
1	4.140	0.0926	2	6.653	0.0547	3	4.953	0.0385	4	4.423	0.0311	5	5.504	0.0292
1	4.998	0.0965	2	7.596	0.0562	3	5.600	0.0399	4	5.216	0.0321	5	6.549	0.0308
1	6.369	0.1009	2	8.573	0.0579	3	6.485	0.0416	4	6.035	0.0341	5	7.481	0.0327
1	7.195	0.1032	2	9.449	0.0596	3	7.553	0.0435	4	6.495	0.0350	5	8.573	0.0345
1	8.031	0.1052	2	10.158	0.0609	3	8.558	0.0452	4	7.551	0.0369	5	9.362	0.0359
1	9.161	0.1078	2	11.992	0.0637	3	9.608	0.0473	4	7.940	0.0374	5	10.193	0.0371
1	10.187	0.1101	2	12.464	0.0647	3	10.191	0.0481	4	8.641	0.0386	5	11.814	0.0397
1	12.716	0.1154	2	15.829	0.0707	3	12.467	0.0519	4	9.647	0.0406	5	15.107	0.0446
1	14.932	0.1195	2	17.791	0.0734	3	14.904	0.0558	4	10.194	0.0415	5	18.407	0.0493
1	17.446	0.1236	2	22.233	0.0802	3	18.114	0.0607	4	12.705	0.0455	5	22.671	0.0546
1	21.805	0.1284	2	25.512	0.0854	3	21.242	0.0657	4	15.901	0.0503	5	25.409	0.0588
1	26.207	0.1329	2	29.170	0.0907	3	24.731	0.0705	4	17.511	0.0531	5	28.952	0.0632
1	30.996	0.1387	2	35.167	0.0996	3	27.586	0.0750	4	24.585	0.0628	5	35.706	0.0711
1	35.020	0.1432	2	42.063	0.1100	3	31.253	0.0797	4	28.388	0.0682	5	42.503	0.0776
1	40.066	0.1490				3	37.297	0.0874	4	33.749	0.0748			
1	43.151	0.1531				3	42.058	0.0939	4	42.176	0.0847			

Material:	CMC
Concentration/vol:	1.5%
Density kg/m³:	1008.2
T_y (Pa):	0.00
K (Pa.sⁿ):	0.014
n:	0.944
Flume width (mm):	75
Flume Shape	Trapezoidal

SLOPE	FLOW	DEPTH	SLOPE	FLOW	DEPTH	SLOPE	FLOW	DEPTH	SLOPE	FLOW	DEPTH	SLOPE	FLOW	DEPTH
FLUME	Q	h	FLUME	Q	h	FLUME	Q	h	FLUME	Q	h	FLUME	Q	h
(degrees)	(l.s ⁻¹)	(m)	(degrees)	(l.s ⁻¹)	(m)	(degrees)	(l.s ⁻¹)	(m)	(degrees)	(l.s ⁻¹)	(m)	(degrees)	(l.s ⁻¹)	(m)
1	0.127	0.0069	2	0.135	0.0056	3	0.322	0.0063	4	0.599	0.0072	5	0.625	0.0067
1	0.241	0.0086	2	0.211	0.0063	3	0.534	0.0076	4	0.751	0.0078	5	0.811	0.0072
1	0.276	0.0092	2	0.263	0.0068	3	0.619	0.0081	4	0.910	0.0083	5	1.087	0.0084
1	0.341	0.0096	2	0.304	0.0073	3	0.727	0.0085	4	1.174	0.0095	5	1.514	0.0127
1	0.421	0.0103	2	0.432	0.0083	3	0.836	0.0091	4	1.508	0.0108	5	1.544	0.0096
1	0.510	0.0112	2	0.521	0.0089	3	0.922	0.0098	4	2.357	0.0179	5	2.143	0.0157
1	0.559	0.0116	2	0.610	0.0094	3	1.071	0.0104	4	2.851	0.0191	5	4.898	0.0256
1	0.605	0.0121	2	0.709	0.0101	3	1.553	0.0124	4	5.139	0.0290	5	7.841	0.0372
1	0.712	0.0129	2	0.817	0.0107	3	2.084	0.0150	4	7.622	0.0369	5	10.127	0.0411
1	0.828	0.0139	2	0.918	0.0112	3	3.007	0.0234	4	9.755	0.0440	5	15.847	0.0553
1	0.908	0.0147	2	1.316	0.0136	3	4.784	0.0316	4	9.759	0.0440	5	23.686	0.0754
1	1.026	0.0155	2	1.454	0.0146	3	5.780	0.0350	4	21.721	0.0728			
1	1.456	0.0186	2	2.193	0.0205	3	7.666	0.0441						
1	1.781	0.0212	2	2.778	0.0242	3	9.757	0.0494						
1	2.324	0.0268	2	4.170	0.0325	3	20.387	0.0787						
1	3.381	0.0354	2	5.808	0.0400	3	23.248	0.0861						
1	4.200	0.0413	2	7.822	0.0479									
1	5.591	0.0501	2	9.755	0.0556									
1	7.561	0.0583	2	17.428	0.0787									
1	9.754	0.0668	2	23.744	0.0974									
1	15.543	0.0892												
1	20.979	0.1092												

Material:	CMC
Concentration/vol:	3.0%
Density kg/m ³ :	1017.5
T _y (Pa):	0.00
K (Pa.s ⁿ):	0.145
n:	0.788
Flume width (mm):	75
Flume Shape	Trapezoidal

SLOPE	FLOW	DEPTH	SLOPE	FLOW	DEPTH	SLOPE	FLOW	DEPTH	SLOPE	FLOW	DEPTH	SLOPE	FLOW	DEPTH
FLUME	Q	h	FLUME	Q	h	FLUME	Q	h	FLUME	Q	h	FLUME	Q	h
(degrees)	(l.s ⁻¹)	(m)	(degrees)	(l.s ⁻¹)	(m)	(degrees)	(l.s ⁻¹)	(m)	(degrees)	(l.s ⁻¹)	(m)	(degrees)	(l.s ⁻¹)	(m)
1	0.109	0.0124	2	0.111	0.0097	3	0.158	0.0091	4	0.126	0.0078	5	0.283	0.0088
1	0.205	0.0152	2	0.204	0.0113	3	0.247	0.0106	4	0.211	0.0087	5	0.338	0.0093
1	0.308	0.0170	2	0.293	0.0126	3	0.348	0.0115	4	0.317	0.0099	5	0.447	0.0101
1	0.411	0.0187	2	0.403	0.0140	3	0.450	0.0126	4	0.414	0.0109	5	0.591	0.0111
1	0.503	0.0201	2	0.501	0.0151	3	0.641	0.0140	4	0.511	0.0116	5	0.751	0.0119
1	0.717	0.0229	2	0.634	0.0164	3	0.832	0.0154	4	0.608	0.0122	5	0.911	0.0129
1	0.937	0.0254	2	0.822	0.0179	3	1.041	0.0166	4	0.717	0.0130	5	1.015	0.0134
1	1.214	0.0279	2	0.975	0.0190	3	1.300	0.0180	4	0.851	0.0138	5	1.295	0.0145
1	1.566	0.0306	2	1.300	0.0212	3	1.602	0.0197	4	1.044	0.0148	5	1.431	0.0152
1	2.258	0.0353	2	1.654	0.0235	3	1.884	0.0208	4	1.259	0.0156	5	1.533	0.0156
1	3.068	0.0403	2	2.220	0.0264	3	2.112	0.0220	4	1.520	0.0172	5	1.729	0.0164
1	4.097	0.0467	2	3.087	0.0309	3	2.471	0.0238	4	1.813	0.0183	5	2.115	0.0179
1	5.246	0.0532	2	4.075	0.0365	3	3.056	0.0262	4	2.094	0.0195	5	2.531	0.0194
1	6.129	0.0580	2	5.056	0.0408	3	4.077	0.0309	4	2.524	0.0213	5	2.910	0.0207
1	8.072	0.0683	2	6.680	0.0480	3	5.143	0.0351	4	3.019	0.0231	5	3.358	0.0223
1	10.096	0.0774	2	7.979	0.0532	3	8.097	0.0470	4	4.046	0.0271	5	3.975	0.0246
1	13.120	0.0866	2	10.165	0.0615	3	10.186	0.0540	4	5.017	0.0310	5	4.840	0.0275
1	20.032	0.1176	2	14.756	0.0755	3	19.171	0.0787	4	6.142	0.0348	5	6.110	0.0316
			2	19.735	0.0907	3	25.179	0.0928	4	8.081	0.0419	5	7.626	0.0364
			2	21.653	0.0961				4	10.030	0.0479	5	10.097	0.0438
									4	12.089	0.0535	5	13.937	0.0537
									4	16.035	0.0642	5	21.045	0.0705
									4	19.635	0.0727	5	27.171	0.0834

Material:	CMC
Concentration/vol:	4.0%
Density kg/m³:	1022.8
T_y (Pa):	0.00
K (Pa.sⁿ):	0.330
n:	0.727
Flume width (mm):	75
Flume Shape	Trapezoidal

SLOPE	FLOW	DEPTH	SLOPE	FLOW	DEPTH	SLOPE	FLOW	DEPTH	SLOPE	FLOW	DEPTH	SLOPE	FLOW	DEPTH
FLUME	Q	h	FLUME	Q	h	FLUME	Q	h	FLUME	Q	h	FLUME	Q	h
(degrees)	(l.s ⁻¹)	(m)	(degrees)	(l.s ⁻¹)	(m)	(degrees)	(l.s ⁻¹)	(m)	(degrees)	(l.s ⁻¹)	(m)	(degrees)	(l.s ⁻¹)	(m)
1	0.173	0.0191	2	0.096	0.0119	3	0.143	0.0113	4	0.160	0.0104	5	0.170	0.0097
1	0.206	0.0199	2	0.194	0.0148	3	0.197	0.0126	4	0.202	0.0111	5	0.204	0.0103
1	0.344	0.0237	2	0.300	0.0167	3	0.294	0.0143	4	0.294	0.0125	5	0.390	0.0124
1	0.498	0.0267	2	0.397	0.0184	3	0.391	0.0154	4	0.391	0.0137	5	0.494	0.0134
1	0.605	0.0286	2	0.490	0.0197	3	0.498	0.0167	4	0.494	0.0146	5	0.591	0.0143
1	0.803	0.0311	2	0.595	0.0210	3	0.593	0.0176	4	0.595	0.0156	5	0.704	0.0151
1	0.981	0.0334	2	0.704	0.0222	3	0.703	0.0186	4	0.706	0.0164	5	0.807	0.0158
1	1.220	0.0360	2	0.810	0.0233	3	0.800	0.0195	4	0.835	0.0175	5	1.046	0.0170
1	1.403	0.0378	2	1.048	0.0253	3	1.005	0.0209	4	1.068	0.0188	5	1.492	0.0192
1	1.992	0.0430	2	1.436	0.0284	3	1.504	0.0240	4	1.432	0.0208	5	1.996	0.0213
1	2.525	0.0464	2	2.079	0.0324	3	2.001	0.0264	4	1.997	0.0233	5	2.555	0.0234
1	3.140	0.0506	2	2.524	0.0350	3	2.490	0.0291	4	3.050	0.0276	5	3.564	0.0270
1	3.911	0.0552	2	3.427	0.0392	3	3.515	0.0331	4	4.035	0.0315	5	4.517	0.0304
1	4.757	0.0592	2	5.063	0.0470	3	4.515	0.0376	4	4.999	0.0352	5	5.532	0.0336
1	5.392	0.0633	2	5.427	0.0485	3	5.509	0.0416	4	6.091	0.0389	5	7.047	0.0380
1	6.601	0.0690	2	6.500	0.0533	3	6.978	0.0475	4	7.556	0.0435	5	8.491	0.0424
1	8.089	0.0762	2	8.055	0.0597	3	8.032	0.0511	4	10.321	0.0517	5	10.303	0.0478
1	10.035	0.0855	2	10.023	0.0673	3	10.030	0.0578	4	13.885	0.0623	5	13.479	0.0571
1	16.306	0.1133	2	16.638	0.0893	3	14.579	0.0706	4	19.672	0.0766	5	16.377	0.0633
1	19.957	0.1292	2	19.732	0.0992	3	18.761	0.0822	4	21.529	0.0812	5	20.514	0.0732
1	22.546	0.1395	2	23.716	0.1123	3	21.380	0.0897	4	25.367	0.0898	5	26.459	0.0843
						3	24.686	0.0982						

Material:	Kaolin
Concentration/vol:	5.4%
Density kg/m³:	1089.0
T_y (Pa):	4.40
K (Pa.sⁿ):	0.084
n:	0.582
Flume width (mm):	75
Flume Shape	Trapezoidal

SLOPE	FLOW	DEPTH	SLOPE	FLOW	DEPTH	SLOPE	FLOW	DEPTH	SLOPE	FLOW	DEPTH	SLOPE	FLOW	DEPTH
FLUME	Q	h	FLUME	Q	h	FLUME	Q	h	FLUME	Q	h	FLUME	Q	h
(degrees)	(l.s ⁻¹)	(m)	(degrees)	(l.s ⁻¹)	(m)	(degrees)	(l.s ⁻¹)	(m)	(degrees)	(l.s ⁻¹)	(m)	(degrees)	(l.s ⁻¹)	(m)
1	0.093	0.0363	2	0.220	0.0171	3	0.161	0.0125	4	0.859	0.0120	5	0.792	0.0104
1	0.292	0.0373	2	0.265	0.0194	3	0.272	0.0130	4	0.957	0.0123	5	0.977	0.0105
1	0.312	0.0396	2	0.373	0.0199	3	0.377	0.0138	4	1.171	0.0131	5	1.087	0.0112
1	0.326	0.0392	2	0.486	0.0201	3	0.482	0.0142	4	1.305	0.0137	5	1.206	0.0111
1	0.472	0.0412	2	0.600	0.0208	3	0.583	0.0146	4	1.621	0.0148	5	1.518	0.0128
1	0.578	0.0419	2	0.784	0.0212	3	0.783	0.0148	4	2.060	0.0167	5	1.946	0.0140
1	0.611	0.0416	2	1.076	0.0221	3	1.027	0.0158	4	2.774	0.0189	5	2.311	0.0148
1	0.818	0.0436	2	1.587	0.0241	3	1.226	0.0165	4	3.082	0.0207	5	3.100	0.0185
1	1.001	0.0453	2	2.191	0.0263	3	1.530	0.0178	4	4.058	0.0247	5	4.182	0.0224
1	1.326	0.0472	2	2.977	0.0298	3	2.061	0.0198	4	5.417	0.0287	5	5.212	0.0257
1	1.624	0.0485	2	4.023	0.0352	3	2.950	0.0237	4	6.411	0.0327	5	6.269	0.0288
1	2.115	0.0502	2	5.485	0.0407	3	4.882	0.0318	4	8.198	0.0384	5	8.043	0.0338
1	3.104	0.0504	2	6.536	0.0450	3	5.413	0.0334	4	10.151	0.0440	5	10.095	0.0401
1	4.068	0.0543	2	8.084	0.0512	3	6.326	0.0369	4	13.318	0.0510			
1	5.097	0.0593	2	10.129	0.0580	3	8.121	0.0429	4	13.360	0.0522			
1	6.495	0.0645	2	14.209	0.0700	3	10.122	0.0495	4	18.233	0.0649			
1	8.245	0.0711				3	14.551	0.0618						
1	10.025	0.0780				3	20.192	0.0743						

Material:	Kaolin
Concentration/vol:	7.1%
Density kg/m³:	1118.0
T_y (Pa):	11.56
K (Pa.sⁿ):	0.148
n:	0.557
Flume width (mm):	75
Flume Shape	Trapezoidal

SLOPE	FLOW	DEPTH	SLOPE	FLOW	DEPTH	SLOPE	FLOW	DEPTH	SLOPE	FLOW	DEPTH	SLOPE	FLOW	DEPTH
FLUME	Q	h	FLUME	Q	h	FLUME	Q	h	FLUME	Q	h	FLUME	Q	h
(degrees)	(l.s ⁻¹)	(m)	(degrees)	(l.s ⁻¹)	(m)	(degrees)	(l.s ⁻¹)	(m)	(degrees)	(l.s ⁻¹)	(m)	(degrees)	(l.s ⁻¹)	(m)
1	1.314	0.0972	2	0.666	0.0528	3	0.941	0.0343	4	1.158	0.0256			
1	1.929	0.1029	2	1.717	0.0591	3	1.393	0.0349	4	1.357	0.0255	5	1.009	0.0201
1	2.226	0.1059	2	1.983	0.0595	3	1.702	0.0360	4	1.666	0.0263	5	1.129	0.0206
1	2.800	0.1117	2	2.500	0.0627	3	2.199	0.0367	4	2.064	0.0273	5	1.407	0.0210
1	4.324	0.1185	2	2.991	0.0638	3	2.678	0.0388	4	2.676	0.0290	5	1.622	0.0213
1	4.652	0.1227	2	3.453	0.0648	3	3.140	0.0399	4	3.107	0.0305	5	1.795	0.0218
1	5.654	0.1278	2	4.166	0.0661	3	3.667	0.0412	4	3.688	0.0325	5	2.109	0.0226
1	6.614	0.1326	2	4.412	0.0660	3	4.067	0.0425	4	4.189	0.0338	5	2.518	0.0239
1	8.044	0.1400	2	4.942	0.0669	3	4.719	0.0442	4	4.573	0.0350	5	2.775	0.0248
1	8.976	0.1439	2	5.891	0.0686	3	5.350	0.0465	4	5.262	0.0370	5	2.988	0.0253
1	10.121	0.1488	2	6.711	0.0697	3	6.024	0.0485	4	6.066	0.0396	5	3.202	0.0258
1	12.923	0.1612	2	7.384	0.0714	3	6.607	0.0504	4	7.009	0.0428	5	4.039	0.0284
1	14.554	0.1670	2	8.598	0.0745	3	7.264	0.0521	4	7.944	0.0457	5	4.339	0.0289
1	16.365	0.1743	2	9.612	0.0770	3	7.969	0.0545	4	10.120	0.0517	5	4.742	0.0296
1	18.143	0.1802	2	10.139	0.0783	3	9.215	0.0578	4	12.081	0.0571	5	5.028	0.0313
			2	12.053	0.0833	3	10.158	0.0606	4	14.903	0.0638	5	6.145	0.0344
			2	13.890	0.0884	3	11.939	0.0653	4	17.765	0.0703	5	7.024	0.0375
			2	15.104	0.0917	3	13.572	0.0696	4	22.061	0.0792	5	8.007	0.0404
			2	16.460	0.0951	3	16.520	0.0770	4	24.153	0.0834	5	8.860	0.0428
			2	17.529	0.0986	3	18.920	0.0827				5	10.195	0.0460
			2	19.205	0.1021	3	23.657	0.0944				5	12.308	0.0517
			2	20.693	0.1068							5	16.009	0.0599
			2	23.764	0.1149							5	20.518	0.0697

Material:	Bentonite
Concentration/vol:	4.5%
Density kg/m³:	1027.0
T_y (Pa):	4.30
K (Pa.sⁿ):	0.0036
n:	1.000
Flume width (mm):	150
Flume Shape	Trapezoidal

SLOPE	FLOW	DEPTH	SLOPE	FLOW	DEPTH	SLOPE	FLOW	DEPTH	SLOPE	FLOW	DEPTH	SLOPE	FLOW	DEPTH
FLUME	Q	h	FLUME	Q	h	FLUME	Q	h	FLUME	Q	h	FLUME	Q	h
(degrees)	(l.s ⁻¹)	(m)	(degrees)	(l.s ⁻¹)	(m)	(degrees)	(l.s ⁻¹)	(m)	(degrees)	(l.s ⁻¹)	(m)	(degrees)	(l.s ⁻¹)	(m)
1	0.645	0.0351	2	0.585	0.0156	3	0.617	0.0116	4	0.587	0.0090	5	0.654	0.0081
1	0.806	0.0351	2	0.793	0.0161	3	0.809	0.0117	4	0.784	0.0096	5	0.879	0.0085
1	1.049	0.0399	2	1.043	0.0168	3	1.027	0.0122	4	0.946	0.0106	5	1.182	0.0088
1	1.214	0.0404	2	1.403	0.0175	3	1.491	0.0131	4	1.029	0.0098	5	1.335	0.0097
1	1.357	0.0403	2	1.796	0.0192	3	1.762	0.0137	4	1.389	0.0107	5	1.526	0.0102
1	1.905	0.0412	2	2.290	0.0198	3	2.071	0.0148	4	1.390	0.0117	5	1.821	0.0107
1	2.631	0.0415	2	2.826	0.0199	3	2.324	0.0152	4	1.535	0.0113	5	2.129	0.0111
1	3.039	0.0375	2	3.501	0.0217	3	2.582	0.0150	4	1.806	0.0117	5	2.627	0.0120
1	3.814	0.0394	2	4.107	0.0236	3	2.994	0.0163	4	1.991	0.0120	5	3.086	0.0128
1	5.007	0.0412	2	4.563	0.0241	3	4.115	0.0188	4	2.473	0.0135	5	4.298	0.0145
1	6.181	0.0451	2	5.244	1.0000	3	5.034	0.0207	4	3.122	0.0147	5	5.009	0.0163
1	7.180	0.0472	2	6.240	0.0286	3	6.185	0.0229	4	3.942	0.0160	5	6.171	0.0178
1	8.033	0.0486	2	7.064	0.0309	3	7.203	0.0253	4	5.104	0.0180	5	8.242	0.0216
1	9.977	0.0532	2	8.044	0.0333	3	8.068	0.0271	4	6.131	0.0202	5	10.147	0.0252
1	12.575	0.0597	2	9.988	0.0376	3	9.825	0.0307	4	8.081	0.0240	5	12.711	0.0294
1	15.058	0.0650	2	12.213	0.0419	3	12.111	0.0353	4	10.060	0.0276	5	17.591	0.0374
1	20.047	0.0765	2	15.088	0.0486	3	15.572	0.0420	4	13.145	0.0330	5	22.845	0.0463
1	26.220	0.0900	2	19.935	0.0582	3	20.335	0.0508	4	16.644	0.0391	5	30.432	0.0560
1	32.134	0.1011	2	25.364	0.0679	3	30.680	0.0687	4	22.687	0.0490			
1	40.205	0.1141	2	30.287	0.0773	3	39.998	0.0826	4	30.318	0.0619			
			2	39.882	0.0934									

Material:	Bentonite
Concentration/vol:	6.2%
Density kg/m³:	1038.0
T_y (Pa):	15.78
K (Pa.sⁿ):	0.0064
n:	1.000
Flume width (mm):	75
Flume Shape	Trapezoidal

SLOPE	FLOW	DEPTH	SLOPE	FLOW	DEPTH	SLOPE	FLOW	DEPTH	SLOPE	FLOW	DEPTH
FLUME	Q	h	FLUME	Q	h	FLUME	Q	h	FLUME	Q	h
(degrees)	(l.s⁻¹)	(m)	(degrees)	(l.s⁻¹)	(m)	(degrees)	(l.s⁻¹)	(m)	(degrees)	(l.s⁻¹)	(m)
2	1.795	0.1182	3	0.985	0.0656	4	1.005	0.0446	5	0.915	0.0314
2	2.654	0.1210	3	1.642	0.0657	4	1.380	0.0446	5	1.493	0.0334
2	3.579	0.1235	3	2.523	0.0669	4	2.105	0.0466	5	2.098	0.0355
2	4.423	5.2337	3	2.880	0.0697	4	3.037	0.0492	5	3.060	0.0374
2	4.574	0.1034	3	3.993	0.0716	4	4.001	0.0503	5	4.047	0.0392
2	5.795	0.1267	3	5.120	0.0730	4	5.203	0.0515	5	5.000	0.0413
2	5.795	0.1267	3	6.165	0.0723	4	6.105	0.0532	5	6.141	0.0434
2	6.956	0.1310	3	7.121	0.0728	4	7.134	0.0551	5	7.100	0.0456
2	8.102	0.1313	3	8.023	0.0731	4	8.153	0.0573	5	8.098	0.0474
2	10.037	0.1305	3	9.084	0.0743	4	10.147	0.0609	5	9.008	0.0499
2	11.647	0.1349	3	10.073	0.0761	4	11.836	0.0649	5	10.157	0.0524
2	12.650	0.1437	3	12.083	0.0802	4	14.427	0.0707	5	12.783	0.0582
2	13.829	0.1434	3	14.336	0.0848	4	17.459	0.0775	5	15.908	0.0653
2	16.140	0.1428	3	16.951	0.0910	4	21.313	0.0861	5	23.752	0.0811
2	17.949	0.1468	3	19.300	0.0967	4	23.736	0.0909			
2	19.978	0.1492	3	21.587	0.1015						
2	22.564	0.1560	3	23.844	0.1072						

Material:	Bentonite
Concentration/vol:	6.8%
Density kg/m³:	1042.0
T_y (Pa):	18.34
K (Pa.sⁿ):	0.0078
n:	1.000
Flume width (mm):	150
Flume Shape	Trapezoidal

SLOPE	FLOW	DEPTH	SLOPE	FLOW	DEPTH	SLOPE	FLOW	DEPTH	SLOPE	FLOW	DEPTH
FLUME	Q	h	FLUME	Q	h	FLUME	Q	h	FLUME	Q	h
(degrees)	(l.s ⁻¹)	(m)	(degrees)	(l.s ⁻¹)	(m)	(degrees)	(l.s ⁻¹)	(m)	(degrees)	(l.s ⁻¹)	(m)
2	1.336	0.0845	3	1.454	0.0475	4	1.388	0.0356	5	1.391	0.0272
2	2.408	0.0835	3	2.336	0.0508	4	2.472	0.0422	5	2.338	0.0285
2	4.569	0.0865	3	3.353	0.0525	4	3.305	0.0351	5	3.280	0.0295
2	5.117	0.0917	3	4.198	0.0540	4	5.121	0.0389	5	4.068	0.0304
2	7.313	0.0931	3	6.094	0.0560	4	7.092	0.0416	5	5.559	0.0326
2	8.573	0.0917	3	7.470	0.0556	4	8.530	0.0424	5	7.025	0.0338
2	10.125	0.0909	3	9.754	0.0563	4	10.159	0.0446	5	8.543	0.0361
2	12.354	0.0931	3	10.182	0.0559	4	13.174	0.0482	5	10.093	0.0377
2	15.463	0.0932	3	13.213	0.0596	4	16.236	0.0527	5	12.605	0.0409
2	17.938	0.0936	3	16.244	0.0632	4	20.007	0.0582	5	17.034	0.0471
2	21.851	0.0967	3	20.680	0.0707	4	25.087	0.0650	5	20.387	0.0528
2	24.952	0.1016	3	25.858	0.0771	4	30.997	0.0753	5	25.967	0.0599
2	30.981	0.1096	3	30.599	0.0844	4	35.504	0.0798	5	31.746	0.0681
2	35.048	0.1130	3	35.321	0.0922						
2	39.824	0.1184	3	40.194	0.0988						
2	39.905	0.1162									

Material:	CMC
Concentration/vol:	1.5%
Density kg/m ³ :	1008.3
T _y (Pa):	0.00
K (Pa.s ⁿ):	0.014
n:	0.944
Flume width (mm):	150
Flume Shape	Trapezoidal

SLOPE	FLOW	DEPTH	SLOPE	FLOW	DEPTH	SLOPE	FLOW	DEPTH	SLOPE	FLOW	DEPTH	SLOPE	FLOW	DEPTH
FLUME	Q	h	FLUME	Q	h	FLUME	Q	h	FLUME	Q	h	FLUME	Q	h
(degrees)	(l.s ⁻¹)	(m)	(degrees)	(l.s ⁻¹)	(m)	(degrees)	(l.s ⁻¹)	(m)	(degrees)	(l.s ⁻¹)	(m)	(degrees)	(l.s ⁻¹)	(m)
1	0.163	0.0060	2	0.132	0.0043	3	0.276	0.0048	4	0.470	0.0049	5	0.419	0.0045
1	0.207	0.0065	2	0.223	0.0052	3	0.352	0.0053	4	0.535	0.0054	5	0.478	0.0048
1	0.270	0.0071	2	0.310	0.0058	3	0.429	0.0056	4	0.602	0.0056	5	0.563	0.0050
1	0.317	0.0075	2	0.423	0.0066	3	0.586	0.0062	4	0.814	0.0061	5	0.680	0.0053
1	0.364	0.0078	2	0.520	0.0070	3	0.751	0.0067	4	0.923	0.0064	5	0.867	0.0058
1	0.464	0.0085	2	0.743	0.0077	3	0.848	0.0072	4	1.052	0.0067	5	1.078	0.0063
1	0.554	0.0090	2	0.950	0.0085	3	1.106	0.0078	4	1.548	0.0076	5	1.325	0.0066
1	0.615	0.0094	2	1.565	0.0102	3	2.271	0.0110	4	2.004	0.0122	5	1.542	0.0072
1	0.714	0.0099	2	2.064	0.0120	3	3.138	0.0144	4	3.108	0.0146	5	2.061	0.0097
1	0.827	0.0103	2	2.994	0.0156	3	4.013	0.0186	4	4.821	0.0191	5	3.412	0.0128
1	0.936	0.0108	2	3.930	0.0191	3	5.765	0.0224	4	7.602	0.0244	5	4.846	0.0160
1	1.438	0.0128	2	6.024	0.0261	3	7.794	0.0281	4	10.141	0.0304	5	7.736	0.0221
1	1.838	0.0144	2	8.024	0.0315	3	10.252	0.0338	4	17.154	0.0436	5	10.126	0.0268
1	2.209	0.0160	2	10.114	0.0366	3	18.732	0.0505	4	30.785	0.0661	5	15.430	0.0380
1	2.948	0.0186	2	16.718	0.0532	3	25.098	0.0629	4	43.139	0.0837	5	29.954	0.0588
1	3.511	0.0231	2	25.562	0.0719	3	41.860	0.0894				5	43.547	0.0789
1	4.510	0.0277	2	39.995	0.0966									
1	5.997	0.0336												
1	7.907	0.0406												
1	10.105	0.0473												
1	17.084	0.0664												
1	22.740	0.0798												
1	44.691	0.1248												

Material:	CMC
Concentration/vol:	3.0%
Density kg/m³:	1017.5
T_y (Pa):	0.00
K (Pa.sⁿ):	0.126
n:	0.780
Flume width (mm):	150
Flume Shape	Trapezoidal

SLOPE	FLOW	DEPTH	SLOPE	FLOW	DEPTH	SLOPE	FLOW	DEPTH	SLOPE	FLOW	DEPTH	SLOPE	FLOW	DEPTH
FLUME	Q	h	FLUME	Q	h	FLUME	Q	h	FLUME	Q	h	FLUME	Q	h
(degrees)	(l.s ⁻¹)	(m)	(degrees)	(l.s ⁻¹)	(m)	(degrees)	(l.s ⁻¹)	(m)	(degrees)	(l.s ⁻¹)	(m)	(degrees)	(l.s ⁻¹)	(m)
1	0.107	0.0097	2	0.092	0.0068	3	0.098	0.0061	4	0.527	0.0089	5	0.781	0.0092
1	0.196	0.0112	2	0.145	0.0079	3	0.194	0.0074	4	0.652	0.0096	5	1.024	0.0103
1	0.309	0.0129	2	0.214	0.0089	3	0.335	0.0088	4	0.820	0.0103	5	1.491	0.0114
1	0.403	0.0141	2	0.308	0.0099	3	0.437	0.0095	4	1.003	0.0110	5	2.027	0.0126
1	0.608	0.0161	2	0.409	0.0108	3	0.608	0.0105	4	1.530	0.0126	5	3.080	0.0145
1	0.815	0.0176	2	0.493	0.0115	3	0.808	0.0116	4	2.048	0.0138	5	4.985	0.0182
1	1.047	0.0188	2	0.670	0.0127	3	1.106	0.0127	4	3.187	0.0161	5	7.039	0.0222
1	1.577	0.0215	2	0.842	0.0135	3	2.318	0.0161	4	5.073	0.0200	5	9.993	0.0273
1	2.090	0.0238	2	1.053	0.0146	3	3.159	0.0180	4	7.146	0.0246	5	20.185	0.0444
1	2.303	0.0247	2	1.310	0.0158	3	5.023	0.0222	4	8.044	0.0264	5	30.038	0.0593
1	2.917	0.0271	2	1.637	0.0168	3	7.269	0.0274	4	19.479	0.0476	5	40.161	0.0718
1	4.377	0.0326	2	2.340	0.0191	3	10.056	0.0336	4	31.327	0.0665			
1	5.717	0.0377	2	2.919	0.0204	3	17.512	0.0489						
1	7.452	0.0443	2	4.450	0.0247	3	27.723	0.0674						
1	9.446	0.0516	2	5.942	0.0287	3	37.272	0.0829						
1	21.012	0.0802	2	10.247	0.0398									
1	27.352	0.0956	2	21.025	0.0641									
1	42.648	0.1258	2	39.095	0.0975									
1	44.918	0.1285	2	41.556	0.1017									

Material:	CMC
Concentration/vol:	4.0%
Density kg/m ³ :	1022.6
T _y (Pa):	0.00
K (Pa.s ⁿ):	0.330
n:	0.727
Flume width (mm):	150
Flume Shape	Trapezoidal

SLOPE	FLOW	DEPTH	SLOPE	FLOW	DEPTH	SLOPE	FLOW	DEPTH	SLOPE	FLOW	DEPTH	SLOPE	FLOW	DEPTH
FLUME	Q	h	FLUME	Q	h	FLUME	Q	h	FLUME	Q	h	FLUME	Q	h
(degrees)	(l.s ⁻¹)	(m)	(degrees)	(l.s ⁻¹)	(m)	(degrees)	(l.s ⁻¹)	(m)	(degrees)	(l.s ⁻¹)	(m)	(degrees)	(l.s ⁻¹)	(m)
1	0.086	0.0124	2	0.088	0.0097	3	0.189	0.0101	4	0.206	0.0092	5	0.287	0.0093
1	0.203	0.0156	2	0.184	0.0117	3	0.291	0.0114	4	0.293	0.0103	5	0.394	0.0105
1	0.288	0.0174	2	0.284	0.0133	3	0.389	0.0124	4	0.389	0.0111	5	0.496	0.0113
1	0.406	0.0193	2	0.395	0.0147	3	0.518	0.0134	4	0.597	0.0125	5	0.614	0.0119
1	0.494	0.0206	2	0.485	0.0157	3	0.684	0.0146	4	0.844	0.0140	5	0.698	0.0125
1	0.672	0.0226	2	0.744	0.0178	3	0.892	0.0159	4	1.012	0.0148	5	0.898	0.0134
1	0.877	0.0247	2	0.874	0.0187	3	1.081	0.0169	4	1.437	0.0165	5	1.030	0.0140
1	1.039	0.0262	2	1.125	0.0203	3	1.460	0.0185	4	2.009	0.0182	5	1.438	0.0154
1	1.287	0.0279	2	1.457	0.0220	3	2.065	0.0206	4	3.008	0.0205	5	1.947	0.0167
1	1.619	0.0299	2	2.016	0.0244	3	3.010	0.0231	4	3.999	0.0228	5	3.037	0.0192
1	2.081	0.0326	2	2.483	0.0259	3	4.166	0.0258	4	4.886	0.0247	5	4.059	0.0213
1	2.656	0.0350	2	3.475	0.0289	3	6.008	0.0301	4	5.995	0.0268	5	5.174	0.0233
1	3.671	0.0391	2	4.498	0.0317	3	8.106	0.0346	4	8.044	0.0307	5	6.249	0.0251
1	4.473	0.0421	2	5.378	0.0341	3	10.271	0.0395	4	10.299	0.0353	5	8.052	0.0285
1	5.378	0.0451	2	6.817	0.0379	3	15.777	0.0515	4	15.628	0.0457	5	10.301	0.0328
1	7.010	0.0505	2	8.534	0.0423	3	21.056	0.0621	4	25.084	0.0625	5	16.160	0.0437
1	8.527	0.0553	2	10.147	0.0462	3	28.421	0.0755	4	31.025	0.0720	5	29.522	0.0638
1	10.064	0.0600	2	17.023	0.0621	3	38.474	0.0925	4	38.324	0.0833	5	35.641	0.0741
1	16.275	0.0780	2	31.159	0.0921							5	41.126	0.0820
1	20.961	0.0904	2	42.994	0.1125									
1	29.455	0.1107												
1	35.456	0.1225												
1	44.609	0.1392												
1	44.967	0.1390												

Material:	Kaolin
Concentration/vol:	5.4%
Density kg/m³:	1089.0
T_y (Pa):	4.40
K (Pa.sⁿ):	0.084
n:	0.582
Flume width (mm):	150
Flume Shape	Trapezoidal

SLOPE	FLOW	DEPTH	SLOPE	FLOW	DEPTH	SLOPE	FLOW	DEPTH	SLOPE	FLOW	DEPTH	SLOPE	FLOW	DEPTH
FLUME	Q	h	FLUME	Q	h	FLUME	Q	h	FLUME	Q	h	FLUME	Q	h
(degrees)	(l.s ⁻¹)	(m)	(degrees)	(l.s ⁻¹)	(m)	(degrees)	(l.s ⁻¹)	(m)	(degrees)	(l.s ⁻¹)	(m)	(degrees)	(l.s ⁻¹)	(m)
1	0.096	0.0304	2	0.152	0.0155	3	0.197	0.0114	4	1.009	0.0104	5	1.545	0.0098
1	0.108	0.0314	2	0.228	0.0163	3	0.387	0.0118	4	1.487	0.0110	5	2.072	0.0105
1	0.223	0.0327	2	0.311	0.0166	3	0.469	0.0122	4	2.001	0.0121	5	3.291	0.0124
1	0.296	0.0337	2	0.631	0.0174	3	0.675	0.0126	4	3.158	0.0141	5	4.072	0.0140
1	0.389	0.0345	2	0.695	0.0174	3	0.733	0.0129	4	4.096	0.0158	5	5.167	0.0160
1	0.519	0.0349	2	0.877	0.0177	3	0.873	0.0131	4	5.210	0.0181	5	6.395	0.0182
1	0.612	0.0354	2	1.181	0.0182	3	0.926	0.0133	4	6.151	0.0200	5	8.291	0.0216
1	0.788	0.0360	2	1.455	0.0186	3	1.472	0.0140	4	7.961	0.0237	5	10.122	0.0248
1	0.955	0.0361	2	2.048	0.0200	3	1.660	0.0145	4	10.109	0.0276	5	15.061	0.0328
1	1.188	0.0366	2	2.965	0.0216	3	2.091	0.0150	4	16.290	0.0388	5	15.109	0.0328
1	1.513	0.0378	2	3.724	0.0238	3	2.436	0.0208	4	25.956	0.0571	5	25.217	0.0495
1	2.164	0.0390	2	4.677	0.0260	3	2.594	0.0217	4	35.548	0.0693	5	35.462	0.0638
1	2.955	0.0399	2	6.002	0.0291	3	3.022	0.0167	4	43.339	0.0802	5	41.786	0.0722
1	4.034	0.0416	2	8.060	0.0340	3	3.953	0.0188						
1	4.859	0.0432	2	9.994	0.0386	3	5.119	0.0213						
1	5.999	0.0459	2	17.193	0.0542	3	5.666	0.0228						
1	6.884	0.0480	2	23.909	0.0673	3	7.750	0.0271						
1	8.126	0.0507	2	34.592	0.0848	3	10.180	0.0320						
1	9.803	0.0557	2	42.768	0.0986	3	15.266	0.0423						
1	16.843	0.0731				3	21.751	0.0567						
1	23.392	0.0873				3	32.035	0.0703						
1	34.372	0.1095				3	38.447	0.0791						
1	42.678	0.1240												
1	45.561	0.1264												

Material:	Kaolin
Concentration/vol:	7.1%
Density kg/m³:	1118.0
T_y (Pa):	11.56
K (Pa.sⁿ):	0.148
n:	0.557
Flume width (mm):	150
Flume Shape	Trapezoidal

SLOPE	FLOW	DEPTH	SLOPE	FLOW	DEPTH	SLOPE	FLOW	DEPTH	SLOPE	FLOW	DEPTH	SLOPE	FLOW	DEPTH
FLUME	Q	h	FLUME	Q	h	FLUME	Q	h	FLUME	Q	h	FLUME	Q	h
(degrees)	(l.s ⁻¹)	(m)	(degrees)	(l.s ⁻¹)	(m)	(degrees)	(l.s ⁻¹)	(m)	(degrees)	(l.s ⁻¹)	(m)	(degrees)	(l.s ⁻¹)	(m)
1	0.545	0.0688	2	0.500	0.0386	3	0.636	0.0261	4	1.014	0.0211	5	1.502	0.0176
1	0.826	0.0712	2	0.730	0.0397	3	0.860	0.0270	4	1.317	0.0218	5	1.800	0.0180
1	1.041	0.0726	2	0.918	0.0408	3	1.089	0.0276	4	1.710	0.0221	5	2.122	0.0187
1	2.051	0.0784	2	1.126	0.0416	3	1.522	0.0284	4	2.044	0.0227	5	2.428	0.0189
1	2.566	0.0811	2	1.595	0.0431	3	2.119	0.0291	4	2.501	0.0232	5	2.848	0.0195
1	3.267	0.0826	2	2.175	0.0444	3	2.566	0.0293	4	3.006	0.0238	5	3.521	0.0203
1	4.191	0.0868	2	2.596	0.0450	3	3.037	0.0294	4	4.045	0.0251	5	4.080	0.0213
1	5.077	0.0904	2	3.072	0.0453	3	4.110	0.0313	4	4.422	0.0252	5	4.439	0.0217
1	6.017	0.0939	2	4.181	0.0464	3	5.103	0.0328	4	5.055	0.0265	5	5.092	0.0226
1	8.041	0.0997	2	4.686	0.0474	3	6.160	0.0345	4	6.161	0.0280	5	6.263	0.0244
1	10.057	0.1044	2	5.251	0.0481	3	7.147	0.0362	4	7.066	0.0296	5	7.148	0.0257
1	15.411	0.1135	2	6.102	0.0489	3	7.998	0.0377	4	8.111	0.0315	5	8.046	0.0273
1	20.825	0.1209	2	6.960	0.0498	3	9.338	0.0402	4	9.146	0.0333	5	9.182	0.0291
1	24.689	0.1249	2	8.056	0.0515	3	10.199	0.0416	4	10.251	0.0349	5	10.170	0.0309
1	28.576	0.1293	2	9.106	0.0530	3	12.533	0.0459	4	12.653	0.0392	5	13.860	0.0363
1	33.534	0.1363	2	10.093	0.0548	3	14.379	0.0491	4	16.005	0.0450	5	22.048	0.0497
1	37.774	0.1424	2	13.102	0.0603	3	16.291	0.0529	4	22.258	0.0554	5	27.985	0.0581
1	40.948	0.1463	2	16.086	0.0660	3	20.038	0.0597	4	24.767	0.0596	5	35.189	0.0681
			2	22.680	0.0787	3	22.484	0.0639	4	30.657	0.0680			
			2	28.563	0.0892	3	28.507	0.0739	4	35.975	0.0754			
			2	33.090	0.0962	3	33.039	0.0812	4	39.918	0.0805			
			2	38.588	0.1044	3	40.076	0.0910	4	43.345	0.0846			
			2	44.308	0.1136				4	45.820	0.0874			

Material:	Bentonite
Concentration/vol:	3.5%
Density kg/m³:	1022.0
T_y (Pa):	3.00
K (Pa.sⁿ):	0.0036
n:	1.000
Flume width (mm):	300
Flume Shape	Triangular

SLOPE	FLOW	DEPTH	SLOPE	FLOW	DEPTH	SLOPE	FLOW	DEPTH	SLOPE	FLOW	DEPTH	SLOPE	FLOW	DEPTH
FLUME	Q	h	FLUME	Q	h	FLUME	Q	h	FLUME	Q	h	FLUME	Q	h
(degrees)	(l.s ⁻¹)	(m)	(degrees)	(l.s ⁻¹)	(m)	(degrees)	(l.s ⁻¹)	(m)	(degrees)	(l.s ⁻¹)	(m)	(degrees)	(l.s ⁻¹)	(m)
1	0.113	0.0505	2	0.079	0.0249	3	0.076	0.0177	4	0.145	0.0160	5	0.110	0.0128
1	0.154	0.0468	2	0.105	0.0256	3	0.108	0.0182	4	0.237	0.0177	5	0.164	0.0141
1	0.194	0.0470	2	0.128	0.0260	3	0.170	0.0190	4	0.325	0.0186	5	0.217	0.0153
1	0.232	0.0472	2	0.157	0.0260	3	0.235	0.0201	4	0.431	0.0199	5	0.294	0.0168
1	0.282	0.0484	2	0.195	0.0265	3	0.346	0.0216	4	0.598	0.0220	5	0.390	0.0179
1	0.397	0.0489	2	0.241	0.0269	3	0.408	0.0225	4	0.794	0.0241	5	0.606	0.0206
1	0.585	0.0496	2	0.285	0.0273	3	0.602	0.0247	4	1.005	0.0263	5	0.797	0.0226
1	0.794	0.0506	2	0.387	0.0285	3	0.816	0.0269	4	1.170	0.0277	5	1.015	0.0245
1	1.003	0.0517	2	0.598	0.0313	3	1.183	0.0307	4	1.401	0.0292	5	1.373	0.0271
1	1.472	0.0534	2	0.788	0.0332	3	1.395	0.0327	4	1.635	0.0310	5	1.695	0.0291
1	1.984	0.0567	2	1.167	0.0367	3	1.785	0.0352	4	2.147	0.0341	5	2.527	0.0341
1	2.585	0.0602	2	1.584	0.0400	3	2.409	0.0391	4	3.659	0.0418	5	3.494	0.0380
1	3.053	0.0610	2	2.076	0.0424	3	4.012	0.0472	4	4.416	0.0452	5	4.430	0.0420
1	4.053	0.0668	2	2.486	0.0447	3	6.306	0.0562	4	6.058	0.0521	5	6.647	0.0500
1	6.004	0.0761	2	3.093	0.0485	3	8.202	0.0634	4	8.180	0.0589	5	8.305	0.0557
1	8.029	0.0839	2	4.060	0.0538	3	10.053	0.0692	4	10.044	0.0640	5	10.042	0.0598
1	10.027	0.0913	2	6.049	0.0631	3	14.639	0.0798	4	15.430	0.0766	5	14.587	0.0724
1	14.866	0.1054	2	8.058	0.0705	3	22.065	0.0935	4	24.016	0.0957	5	25.179	0.0943
1	20.263	0.1197	2	10.059	0.0774				4	31.984	0.1104	5	30.418	0.1030
1	30.396	0.1398	2	14.182	0.0882									
			2	20.580	0.1031									
			2	30.021	0.1228									

Material:	Bentonite
Concentration/vol:	4.86%
Density kg/m³:	1029.5
T_y (Pa):	5.20
K (Pa.sⁿ):	0.0040
n:	1.000
Flume width (mm):	300
Flume Shape	Triangular

SLOPE	FLOW	DEPTH	SLOPE	FLOW	DEPTH	SLOPE	FLOW	DEPTH	SLOPE	FLOW	DEPTH	SLOPE	FLOW	DEPTH
FLUME	Q	h	FLUME	Q	h	FLUME	Q	h	FLUME	Q	h	FLUME	Q	h
(degrees)	(l.s ⁻¹)	(m)	(degrees)	(l.s ⁻¹)	(m)	(degrees)	(l.s ⁻¹)	(m)	(degrees)	(l.s ⁻¹)	(m)	(degrees)	(l.s ⁻¹)	(m)
1	0.173	0.0708	2	0.134	0.0384	3	0.124	0.0253	4	0.185	0.0213	5	0.345	0.0206
1	0.257	0.0732	2	0.217	0.0394	3	0.186	0.0264	4	0.334	0.0230	5	0.469	0.0222
1	0.341	0.0740	2	0.298	0.0396	3	0.292	0.0271	4	0.412	0.0233	5	0.605	0.0233
1	0.402	0.0744	2	0.386	0.0397	3	0.467	0.0282	4	0.593	0.0250	5	0.782	0.0253
1	0.605	0.0768	2	0.641	0.0414	3	0.608	0.0297	4	0.837	0.0274	5	0.983	0.0269
1	0.797	0.0765	2	0.831	0.0418	3	0.833	0.0318	4	1.030	0.0287	5	1.044	0.0265
1	1.032	0.0773	2	1.004	0.0429	3	1.013	0.0325	4	1.411	0.0317	5	1.427	0.0294
1	1.329	0.0772	2	1.367	0.0455	3	1.487	0.0358	4	2.074	0.0360	5	3.025	0.0388
1	2.074	0.0805	2	1.954	0.0476	3	2.036	0.0395	4	2.495	0.0381	5	4.090	0.0439
1	2.717	0.0799	2	2.817	0.0517	3	3.129	0.0463	4	3.247	0.0415	5	6.012	0.0512
1	3.595	0.0846	2	4.315	0.0598	3	4.062	0.0510	4	4.295	0.0462	5	8.146	0.0580
1	4.531	0.0862	2	6.019	0.0667	3	6.293	0.0594	4	6.066	0.0534	5	10.145	0.0629
1	6.336	0.0904	2	8.159	0.0740	3	8.319	0.0662	4	8.176	0.0604	5	15.781	0.0773
1	8.028	0.0959	2	10.060	0.0801	3	10.026	0.0714	4	10.149	0.0661	5	23.179	0.0909
1	9.991	0.1007	2	14.360	0.0919	3	14.935	0.0842	4	15.161	0.0782	5	31.913	0.1058
1	14.365	0.1113	2	25.517	0.1146	3	24.727	0.1037	4	25.499	0.0976			
1	24.451	0.1336	2	30.588	0.1246	3	34.112	0.1192	4	38.420	0.1183			
1	33.464	0.1495												

Material:	Bentonite
Concentration/vol:	5.4%
Density kg/m³:	1033.0
T_y (Pa):	7.25
K (Pa.sⁿ):	0.0038
n:	1.000
Flume width (mm):	300
Flume Shape	Triangular

SLOPE	FLOW	DEPTH	SLOPE	FLOW	DEPTH	SLOPE	FLOW	DEPTH	SLOPE	FLOW	DEPTH	SLOPE	FLOW	DEPTH
FLUME	Q	h	FLUME	Q	h	FLUME	Q	h	FLUME	Q	h	FLUME	Q	h
(degrees)	(l.s ⁻¹)	(m)	(degrees)	(l.s ⁻¹)	(m)	(degrees)	(l.s ⁻¹)	(m)	(degrees)	(l.s ⁻¹)	(m)	(degrees)	(l.s ⁻¹)	(m)
1	0.132	0.1045	2	0.233	0.0612	3	0.236	0.0389	4	0.363	0.0307	5	0.264	0.0255
1	0.342	0.1045	2	0.421	0.0628	3	0.436	0.0399	4	0.522	0.0316	5	0.491	0.0268
1	0.483	0.1047	2	0.630	0.0632	3	0.642	0.0400	4	0.721	0.0323	5	0.735	0.0283
1	0.686	0.1093	2	0.827	0.0652	3	0.831	0.0405	4	0.902	0.0336	5	0.988	0.0297
1	0.783	0.1081	2	1.132	0.0628	3	1.070	0.0415	4	1.353	0.0364	5	1.255	0.0316
1	0.957	0.1101	2	1.408	0.0627	3	1.519	0.0438	4	2.041	0.0400	5	1.611	0.0341
1	1.462	0.1151	2	1.853	0.0629	3	2.056	0.0468	4	3.014	0.0443	5	2.285	0.0375
1	2.064	0.1170	2	2.428	0.0631	3	2.986	0.0497	4	4.022	0.0496	5	2.976	0.0410
1	2.518	0.1164	2	3.450	0.0654	3	4.205	0.0562	4	6.171	0.0575	5	4.065	0.0455
1	3.069	0.1127	2	4.323	0.0668	3	6.084	0.0627	4	8.067	0.0634	5	6.333	0.0538
1	3.929	0.1177	2	6.384	0.0752	3	8.028	0.0690	4	10.187	0.0692	5	8.076	0.0591
1	6.113	0.1209	2	8.107	0.0804	3	10.208	0.0755	4	12.307	0.0743	5	10.199	0.0651
1	8.086	0.1235	2	10.209	0.0863	3	13.842	0.0844	4	15.371	0.0815	5	11.948	0.0691
1	10.221	0.1245	2	12.367	0.0918	3	18.480	0.0949	4	20.000	0.0913	5	14.863	0.0756
1	12.640	0.1289	2	14.980	0.0990	3	25.110	0.1076	4	26.504	0.1015	5	20.757	0.0870
1	14.753	0.1308	2	20.006	0.1105	3	35.284	0.1231	4	34.918	0.1156	5	31.904	0.1054
1	18.878	0.1418	2	26.208	0.1214									
1	23.839	0.1485	2	35.557	0.1360									
1	27.665	0.1551	2	43.315	0.1466									
1	41.022	0.1756												

Material:	CMC
Concentration/vol:	2.0%
Density kg/m ³ :	1012.9
T _y (Pa):	0.00
K (Pa.s ⁿ):	0.035
n:	0.776
Flume width (mm):	300
Flume Shape	Triangular

SLOPE	FLOW	DEPTH	SLOPE	FLOW	DEPTH	SLOPE	FLOW	DEPTH	SLOPE	FLOW	DEPTH	SLOPE	FLOW	DEPTH
FLUME	Q	h	FLUME	Q	h	FLUME	Q	h	FLUME	Q	h	FLUME	Q	h
(degrees)	(l.s ⁻¹)	(m)	(degrees)	(l.s ⁻¹)	(m)	(degrees)	(l.s ⁻¹)	(m)	(degrees)	(l.s ⁻¹)	(m)	(degrees)	(l.s ⁻¹)	(m)
1	0.062	0.0160	2	0.042	0.0123	3	0.103	0.0133	4	0.037	0.0095	5	0.028	0.0093
1	0.091	0.0176	2	0.062	0.0132	3	0.150	0.0142	4	0.061	0.0104	5	0.051	0.0102
1	0.128	0.0184	2	0.077	0.0136	3	0.198	0.0151	4	0.090	0.0115	5	0.072	0.0110
1	0.187	0.0203	2	0.104	0.0147	3	0.252	0.0160	4	0.122	0.0125	5	0.112	0.0121
1	0.290	0.0229	2	0.184	0.0167	3	0.282	0.0113	4	0.171	0.0135	5	0.153	0.0128
1	0.386	0.0251	2	0.285	0.0190	3	0.357	0.0173	4	0.269	0.0152	5	0.202	0.0142
1	0.583	0.0289	2	0.381	0.0208	3	0.430	0.0182	4	0.340	0.0188	5	0.281	0.0167
1	0.778	0.0339	2	0.491	0.0226	3	0.506	0.0196	4	0.446	0.0206	5	0.380	0.0193
1	1.064	0.0376	2	0.691	0.0249	3	1.105	0.0294	4	0.626	0.0237	5	0.494	0.0213
1	1.501	0.0428	2	0.972	0.0291	3	1.524	0.0341	4	0.834	0.0264	5	0.595	0.0227
1	2.016	0.0477	2	1.523	0.0338	3	1.978	0.0386	4	1.049	0.0284	5	0.755	0.0248
1	2.446	0.0507	2	3.035	0.0495	3	2.490	0.0425	4	1.503	0.0326	5	1.013	0.0272
1	3.036	0.0554	2	4.078	0.0564	3	3.066	0.0462	4	1.989	0.0367	5	1.511	0.0320
1	4.045	0.0624	2	5.993	0.0645	3	4.056	0.0524	4	2.468	0.0393	5	2.004	0.0357
1	5.834	0.0713	2	8.430	0.0732	3	5.983	0.0599	4	3.040	0.0427	5	4.035	0.0462
1	8.128	0.0817	2	10.096	0.0794	3	8.025	0.0667	4	4.099	0.0482	5	6.009	0.0536
1	10.154	0.0899	2	14.514	0.0915	3	8.161	0.0664	4	6.087	0.0561	5	7.867	0.0596
1	14.438	0.1042	2	19.932	0.1064	3	10.816	0.0752	4	8.086	0.0636	5	9.657	0.0652
1	19.884	0.1190	2	25.433	0.1173	3	15.238	0.0884	4	10.022	0.0685			
1	24.797	0.1318	2	32.169	0.1301	3	20.459	0.0997	4	14.547	0.0795			
1	33.643	0.1502	2	40.545	0.1417	3	27.075	0.1110	4	19.141	0.0903			
						3	35.468	0.1238	4	25.330	0.1001			
									4	28.979	0.1067			
									4	32.794	0.1128			

Material:	CMC
Concentration/vol:	3.1%
Density kg/m³:	1018.0
T_y (Pa):	0.00
K (Pa.sⁿ):	0.091
n:	0.823
Flume width (mm):	300
Flume Shape	Triangular

SLOPE	FLOW	DEPTH	SLOPE	FLOW	DEPTH	SLOPE	FLOW	DEPTH	SLOPE	FLOW	DEPTH	SLOPE	FLOW	DEPTH
FLUME	Q	h	FLUME	Q	h	FLUME	Q	h	FLUME	Q	h	FLUME	Q	h
(degrees)	(l.s ⁻¹)	(m)	(degrees)	(l.s ⁻¹)	(m)	(degrees)	(l.s ⁻¹)	(m)	(degrees)	(l.s ⁻¹)	(m)	(degrees)	(l.s ⁻¹)	(m)
1	0.051	0.0219	2	0.087	0.0193	3	0.084	0.0171	4	0.092	0.0164	5	0.071	0.0138
1	0.076	0.0237	2	0.133	0.0209	3	0.139	0.0188	4	0.132	0.0174	5	0.133	0.0160
1	0.091	0.0247	2	0.196	0.0228	3	0.193	0.0204	4	0.214	0.0191	5	0.188	0.0176
1	0.188	0.0288	2	0.285	0.0248	3	0.282	0.0223	4	0.309	0.0209	5	0.289	0.0194
1	0.291	0.0317	2	0.396	0.0269	3	0.380	0.0240	4	0.394	0.0223	5	0.379	0.0206
1	0.384	0.0335	2	0.530	0.0293	3	0.573	0.0267	4	0.638	0.0251	5	0.581	0.0230
1	0.610	0.0376	2	0.783	0.0322	3	0.772	0.0288	4	0.819	0.0272	5	0.781	0.0253
1	0.797	0.0400	2	1.054	0.0356	3	1.055	0.0321	4	1.008	0.0289	5	1.037	0.0280
1	1.095	0.0436	2	1.474	0.0393	3	1.479	0.0356	4	1.399	0.0323	5	1.359	0.0298
1	1.504	0.0479	2	1.937	0.0428	3	1.961	0.0390	4	2.042	0.0368	5	2.024	0.0349
1	2.073	0.0527	2	2.549	0.0474	3	2.789	0.0444	4	3.051	0.0421	5	2.634	0.0372
1	2.480	0.0560	2	3.082	0.0500	3	3.994	0.0506	4	4.028	0.0463	5	4.028	0.0443
1	3.218	0.0608	2	3.962	0.0551	3	5.329	0.0557	4	6.023	0.0556	5	6.018	0.0522
1	4.118	0.0667	2	6.025	0.0652	3	6.456	0.0601	4	8.005	0.0618	5	6.061	0.0525
1	6.141	0.0772	2	7.940	0.0724	3	10.131	0.0730	4	10.142	0.0680	5	10.103	0.0644
1	8.127	0.0857	2	9.900	0.0794	3	14.274	0.0825	4	14.802	0.0779	5	11.766	0.0685
1	10.107	0.0936	2	14.072	0.0908	3	20.305	0.0949	4	19.355	0.0869	5	13.266	0.0715
1	14.159	0.1063	2	19.023	0.1024	3	30.823	0.1141				5	18.268	0.0809
1	21.976	0.1264	2	24.939	0.1139							5	23.209	0.0889
1	32.003	0.1475	2	30.107	0.1229									
			2	30.150	0.1225									
			2	36.000	0.1327									

Material:	CMC
Concentration/vol:	4.0%
Density kg/m³:	1022.7
T_y (Pa):	0.00
K (Pa.sⁿ):	0.266
n:	0.748
Flume width (mm):	300
Flume Shape	Triangular

SLOPE	FLOW	DEPTH	SLOPE	FLOW	DEPTH	SLOPE	FLOW	DEPTH	SLOPE	FLOW	DEPTH	SLOPE	FLOW	DEPTH
FLUME	Q	h	FLUME	Q	h	FLUME	Q	h	FLUME	Q	h	FLUME	Q	h
(degrees)	(l.s ⁻¹)	(m)	(degrees)	(l.s ⁻¹)	(m)	(degrees)	(l.s ⁻¹)	(m)	(degrees)	(l.s ⁻¹)	(m)	(degrees)	(l.s ⁻¹)	(m)
1	0.101	0.0324	2	0.084	0.0251	3	0.121	0.0240	4	0.093	0.0201	5	0.169	0.0211
1	0.171	0.0357	2	0.135	0.0271	3	0.175	0.0259	4	0.142	0.0224	5	0.198	0.0219
1	0.285	0.0403	2	0.195	0.0295	3	0.275	0.0285	4	0.195	0.0240	5	0.294	0.0241
1	0.404	0.0437	2	0.297	0.0322	3	0.391	0.0307	4	0.291	0.0261	5	0.387	0.0258
1	0.602	0.0475	2	0.438	0.0350	3	0.579	0.0340	4	0.410	0.0283	5	0.597	0.0290
1	0.780	0.0511	2	0.623	0.0383	3	0.779	0.0366	4	0.588	0.0314	5	0.790	0.0311
1	1.109	0.0548	2	0.802	0.0414	3	1.125	0.0397	4	0.793	0.0335	5	1.053	0.0336
1	1.501	0.0590	2	1.048	0.0436	3	1.577	0.0436	4	1.048	0.0358	5	1.372	0.0360
1	2.116	0.0639	2	1.479	0.0481	3	2.067	0.0471	4	1.454	0.0390	5	1.996	0.0400
1	2.479	0.0668	2	2.015	0.0522	3	2.489	0.0495	4	2.106	0.0436	5	2.487	0.0427
1	3.214	0.0714	2	2.587	0.0559	3	3.101	0.0523	4	2.571	0.0460	5	3.015	0.0452
1	4.022	0.0762	2	3.110	0.0587	3	4.022	0.0573	4	3.024	0.0483	5	3.974	0.0490
1	6.046	0.0859	2	4.015	0.0635	3	5.045	0.0616	4	3.971	0.0529	5	5.912	0.0574
1	8.039	0.0954	2	5.016	0.0681	3	6.048	0.0650	4	5.118	0.0569	5	8.045	0.0642
1	10.185	0.1035	2	6.064	0.0726	3	8.110	0.0730	4	6.078	0.0608	5	10.220	0.0699
1	14.284	0.1172	2	8.160	0.0810	3	10.227	0.0804	4	8.034	0.0686	5	14.165	0.0791
1	20.239	0.1326	2	10.198	0.0877	3	14.314	0.0910	4	10.183	0.0746	5	19.291	0.0898
1	27.254	0.1487	2	15.179	0.1026	3	19.085	0.1009	4	14.257	0.0841	5	24.568	0.0992
			2	20.579	0.1148	3	24.221	0.1108	4	19.061	0.0940	5	30.569	0.1101
			2	26.110	0.1255	3	32.245	0.1248	4	23.962	0.1035	5	40.784	0.1229
			2	33.692	0.1379	3	41.333	0.1381	4	30.824	0.1140			
									4	41.821	0.1315			

Material:	CMC
Concentration/vol:	4.9%
Density kg/m³:	1027.6
T_y (Pa):	0.00
K (Pa.sⁿ):	0.599
n:	0.690
Flume width (mm):	300
Flume Shape	Triangular

SLOPE	FLOW	DEPTH	SLOPE	FLOW	DEPTH	SLOPE	FLOW	DEPTH	SLOPE	FLOW	DEPTH	SLOPE	FLOW	DEPTH
FLUME	Q	h	FLUME	Q	h	FLUME	Q	h	FLUME	Q	h	FLUME	Q	h
(degrees)	(l.s ⁻¹)	(m)	(degrees)	(l.s ⁻¹)	(m)	(degrees)	(l.s ⁻¹)	(m)	(degrees)	(l.s ⁻¹)	(m)	(degrees)	(l.s ⁻¹)	(m)
1	0.186	0.0451	2	0.182	0.0359	3	0.082	0.0273	4	0.089	0.0257	5	0.084	0.0234
1	0.288	0.0498	2	0.287	0.0398	3	0.188	0.0317	4	0.091	0.0253	5	0.186	0.0269
1	0.385	0.0537	2	0.436	0.0439	3	0.283	0.0351	4	0.185	0.0288	5	0.285	0.0303
1	0.534	0.0578	2	0.586	0.0466	3	0.433	0.0386	4	0.288	0.0320	5	0.426	0.0332
1	0.682	0.0613	2	0.829	0.0506	3	0.586	0.0411	4	0.395	0.0344	5	0.581	0.0355
1	0.882	0.0648	2	1.030	0.0534	3	0.782	0.0442	4	0.535	0.0372	5	0.737	0.0377
1	1.083	0.0681	2	1.535	0.0586	3	1.005	0.0466	4	0.726	0.0397	5	0.877	0.0390
1	1.479	0.0729	2	2.104	0.0629	3	1.341	0.0500	4	0.930	0.0420	5	1.127	0.0412
1	1.982	0.0779	2	2.765	0.0674	3	1.748	0.0532	4	1.186	0.0446	5	1.414	0.0435
1	2.485	0.0820	2	3.536	0.0712	3	2.196	0.0562	4	1.476	0.0468	5	1.676	0.0452
1	2.996	0.0856	2	4.526	0.0757	3	2.479	0.0581	4	2.043	0.0505	5	1.968	0.0471
1	4.025	0.0911	2	6.004	0.0821	3	3.537	0.0633	4	3.056	0.0558	5	2.478	0.0499
1	5.014	0.0959	2	7.597	0.0879	3	4.510	0.0675	4	4.023	0.0602	5	3.178	0.0533
1	6.993	0.1047	2	10.053	0.0958	3	6.054	0.0737	4	5.524	0.0661	5	4.015	0.0567
1	9.014	0.1121	2	14.454	0.1089	3	7.566	0.0787	4	7.012	0.0708	5	5.011	0.0603
1	13.269	0.1266	2	20.242	0.1234	3	10.116	0.0866	4	8.586	0.0762	5	6.480	0.0654
1	20.704	0.1469	2	25.533	0.1340	3	12.551	0.0943	4	10.179	0.0811	5	8.005	0.0707
			2	30.340	0.1420	3	15.057	0.1002	4	14.865	0.0923	5	10.022	0.0763
			2	35.456	0.1498	3	20.547	0.1116	4	20.027	0.1027	5	14.420	0.0860
						3	25.407	0.1203	4	25.171	0.1118	5	20.074	0.0974
						3	30.297	0.1281	4	30.150	0.1201	5	25.179	0.1067
						3	35.331	0.1365	4	35.459	0.1280	5	30.511	0.1150
						3	40.371	0.1436	4	40.000	0.1352	5	35.864	0.1234

Material:	Kaolin
Concentration/vol:	3.4%
Density kg/m³:	1056.0
T_y (Pa):	1.30
K (Pa.sⁿ):	0.051
n:	0.568
Flume width (mm):	300
Flume Shape	Triangular

SLOPE	FLOW	DEPTH	SLOPE	FLOW	DEPTH	SLOPE	FLOW	DEPTH	SLOPE	FLOW	DEPTH	SLOPE	FLOW	DEPTH
FLUME	Q	h	FLUME	Q	h	FLUME	Q	h	FLUME	Q	h	FLUME	Q	h
(degrees)	(l.s ⁻¹)	(m)	(degrees)	(l.s ⁻¹)	(m)	(degrees)	(l.s ⁻¹)	(m)	(degrees)	(l.s ⁻¹)	(m)	(degrees)	(l.s ⁻¹)	(m)
1	0.054	0.0261	2	0.084	0.0174	3	0.105	0.0139	4	0.074	0.0109	5	0.178	0.0128
1	0.086	0.0269	2	0.142	0.0179	3	0.131	0.0143	4	0.110	0.0120	5	0.273	0.0150
1	0.136	0.0285	2	0.185	0.0187	3	0.186	0.0150	4	0.150	0.0125	5	0.325	0.0158
1	0.185	0.0282	2	0.277	0.0205	3	0.289	0.0173	4	0.192	0.0133	5	0.433	0.0179
1	0.281	0.0301	2	0.382	0.0222	3	0.386	0.0187	4	0.237	0.0145	5	0.584	0.0201
1	0.387	0.0317	2	0.588	0.0252	3	0.503	0.0203	4	0.322	0.0162	5	0.785	0.0222
1	0.584	0.0336	2	0.793	0.0277	3	0.795	0.0246	4	0.468	0.0184	5	0.994	0.0245
1	0.788	0.0357	2	1.020	0.0302	3	1.005	0.0268	4	0.730	0.0223	5	1.476	0.0287
1	1.028	0.0381	2	1.527	0.0346	3	1.494	0.0315	4	1.005	0.0256	5	1.991	0.0326
1	1.493	0.0427	2	2.039	0.0385	3	1.989	0.0351	4	1.367	0.0284	5	3.005	0.0387
1	2.051	0.0474	2	3.023	0.0442	3	4.058	0.0465	4	1.958	0.0325	5	4.045	0.0428
1	2.943	0.0538	2	4.085	0.0504	3	7.932	0.0620	4	2.462	0.0357	5	6.069	0.0514
1	4.016	0.0604	2	6.076	0.0595	3	9.734	0.0671	4	4.128	0.0440	5	8.043	0.0574
1	6.008	0.0705	2	9.774	0.0734	3	14.918	0.0806	4	5.616	0.0507	5	9.822	0.0620
1	8.078	0.0794	2	14.197	0.0869	3	22.135	0.0962	4	7.986	0.0593	5	14.435	0.0736
1	9.736	0.0854	2	22.204	0.1050	3	32.670	0.1155	4	9.691	0.0648	5	20.128	0.0844
1	14.504	0.1002	2	32.046	0.1235				4	14.237	0.0750			
1	22.121	0.1197							4	21.933	0.0905			
1	32.224	0.1398												

Material:	Kaolin
Concentration/vol:	5.0%
Density kg/m³:	1082.0
T_y (Pa):	3.58
K (Pa.sⁿ):	0.060
n:	0.630
Flume width (mm):	300
Flume Shape	Triangular

SLOPE	FLOW	DEPTH	SLOPE	FLOW	DEPTH	SLOPE	FLOW	DEPTH	SLOPE	FLOW	DEPTH	SLOPE	FLOW	DEPTH
FLUME	Q	h	FLUME	Q	h	FLUME	Q	h	FLUME	Q	h	FLUME	Q	h
(degrees)	(l.s ⁻¹)	(m)	(degrees)	(l.s ⁻¹)	(m)	(degrees)	(l.s ⁻¹)	(m)	(degrees)	(l.s ⁻¹)	(m)	(degrees)	(l.s ⁻¹)	(m)
1	0.082	0.0479	2	0.089	0.0285	3	0.098	0.0216	4	0.101	0.0185	5	0.072	0.0167
1	0.194	0.0505	2	0.218	0.0305	3	0.188	0.0225	4	0.142	0.0189	5	0.113	0.0165
1	0.314	0.0534	2	0.309	0.0311	3	0.315	0.0244	4	0.223	0.0201	5	0.197	0.0178
1	0.407	0.0548	2	0.399	0.0319	3	0.429	0.0257	4	0.288	0.0205	5	0.304	0.0188
1	0.615	0.0573	2	0.625	0.0335	3	0.632	0.0276	4	0.424	0.0220	5	0.404	0.0200
1	0.845	0.0591	2	0.811	0.0355	3	0.927	0.0296	4	0.593	0.0237	5	0.594	0.0219
1	1.306	0.0616	2	1.235	0.0389	3	1.184	0.0325	4	0.814	0.0258	5	0.844	0.0237
1	1.554	0.0622	2	1.407	0.0404	3	1.417	0.0340	4	1.196	0.0291	5	1.197	0.0274
1	1.968	0.0632	2	1.649	0.0421	3	1.751	0.0365	4	1.385	0.0305	5	1.382	0.0288
1	3.348	0.0678	2	2.080	0.0452	3	2.571	0.0413	4	1.863	0.0333	5	1.832	0.0316
1	4.276	0.0728	2	3.546	0.0533	3	4.012	0.0486	4	3.435	0.0417	5	3.046	0.0374
1	6.140	0.0819	2	4.479	0.0579	3	4.862	0.0520	4	4.218	0.0456	5	4.059	0.0420
1	8.474	0.0902	2	6.031	0.0645	3	6.159	0.0578	4	6.240	0.0531	5	6.322	0.0507
1	10.066	0.0965	2	8.320	0.0730	3	8.261	0.0645	4	8.038	0.0593	5	8.235	0.0565
1	16.476	0.1132	2	10.004	0.0788	3	10.032	0.0706	4	10.192	0.0656	5	10.075	0.0617
1	28.121	0.1407	2	16.679	0.0961	3	15.134	0.0836	4	14.873	0.0771	5	14.626	0.0720
1	36.695	0.1551	2	26.074	0.1169	3	25.049	0.1069	4	22.261	0.0923	5	20.447	0.0837
			2	35.666	0.1313	3	36.435	0.1258	4	32.844	0.1096	5	25.342	0.0925
									4	40.157	0.1187	5	34.950	0.1014

Material:	Kaolin
Concentration/vol:	7.0%
Density kg/m³:	1115.0
T_y (Pa):	8.18
K (Pa.sⁿ):	0.142
n:	0.570
Flume width (mm):	300
Flume Shape	Triangular

SLOPE	FLOW	DEPTH	SLOPE	FLOW	DEPTH	SLOPE	FLOW	DEPTH	SLOPE	FLOW	DEPTH	SLOPE	FLOW	DEPTH
FLUME	Q	h	FLUME	Q	h	FLUME	Q	h	FLUME	Q	h	FLUME	Q	h
(degrees)	(l.s ⁻¹)	(m)	(degrees)	(l.s ⁻¹)	(m)	(degrees)	(l.s ⁻¹)	(m)	(degrees)	(l.s ⁻¹)	(m)	(degrees)	(l.s ⁻¹)	(m)
1	1.128	0.1015	2	0.172	0.0557	3	0.112	0.0395	4	0.179	0.0329	5	0.104	0.0255
1	1.285	0.1028	2	0.280	0.0584	3	0.247	0.0426	4	0.204	0.0334	5	0.168	0.0269
1	1.494	0.1043	2	0.350	0.0594	3	0.342	0.0428	4	0.279	0.0344	5	0.311	0.0288
1	1.714	0.1060	2	0.543	0.0621	3	0.536	0.0453	4	0.399	0.0351	5	0.409	0.0295
1	2.081	0.1084	2	0.789	0.0641	3	0.710	0.0464	4	0.556	0.0360	5	0.571	0.0307
1	3.145	0.1131	2	1.033	0.0654	3	0.936	0.0471	4	0.761	0.0368	5	0.792	0.0316
1	4.484	0.1200	2	1.424	0.0667	3	1.372	0.0483	4	1.012	0.0380	5	0.992	0.0326
1	6.227	0.1271	2	1.665	0.0678	3	1.845	0.0501	4	1.219	0.0392	5	1.198	0.0337
1	8.375	0.1327	2	1.986	0.0689	3	2.725	0.0534	4	1.457	0.0404	5	1.429	0.0345
1	9.968	0.1364	2	2.621	0.0696	3	4.531	0.0607	4	1.457	0.0404	5	1.748	0.0369
1	13.439	0.1388	2	4.169	0.0741	3	5.995	0.0658	4	1.749	0.0417	5	2.255	0.0395
1	16.674	0.1451	2	6.112	0.0793	3	7.690	0.0716	4	2.291	0.0441	5	3.208	0.0433
1	26.975	0.1626	2	7.966	0.0861	3	9.763	0.0774	4	3.387	0.0480	5	4.268	0.0481
1	36.115	0.1750	2	9.883	0.0919	3	15.766	0.0926	4	4.334	0.0528	5	6.135	0.0542
			2	16.034	0.1064	3	24.477	0.1100	4	6.160	0.0596	5	8.277	0.0615
			2	26.214	0.1277	3	34.185	0.1259	4	8.132	0.0660	5	10.023	0.0662
			2	36.201	0.1435				4	9.993	0.0714	5	15.310	0.0783
									4	15.404	0.0841	5	25.184	0.0970
									4	27.124	0.1063	5	34.149	0.1109
									4	36.256	0.1199			

Material:	Kaolin
Concentration/vol:	9.2%
Density kg/m³:	1152.0
T_y (Pa):	18.90
K (Pa.sⁿ):	0.194
n:	0.550
Flume width (mm):	300
Flume Shape	Triangular

SLOPE	FLOW	DEPTH	SLOPE	FLOW	DEPTH	SLOPE	FLOW	DEPTH	SLOPE	FLOW	DEPTH	SLOPE	FLOW	DEPTH
FLUME	Q	h	FLUME	Q	h	FLUME	Q	h	FLUME	Q	h	FLUME	Q	h
(degrees)	(l.s ⁻¹)	(m)	(degrees)	(l.s ⁻¹)	(m)	(degrees)	(l.s ⁻¹)	(m)	(degrees)	(l.s ⁻¹)	(m)	(degrees)	(l.s ⁻¹)	(m)
1	0.987	0.1421	2	0.445	0.1004	3	0.262	0.0711	4	0.154	0.0551	5	0.108	0.0467
1	1.110	0.1449	2	0.638	0.1027	3	0.360	0.0733	4	0.275	0.0575	5	0.130	0.0468
1	1.201	0.1463	2	0.855	0.1053	3	0.447	0.0748	4	0.385	0.0593	5	0.188	0.0485
1	1.477	0.1489	2	1.055	0.1063	3	0.603	0.0763	4	0.435	0.0586	5	0.232	0.0488
1	1.838	0.1517	2	1.312	0.1091	3	0.780	0.0771	4	0.550	0.0607	5	0.326	0.0505
1	2.214	0.1546	2	1.537	0.1101	3	0.993	0.0785	4	0.671	0.0615	5	0.407	0.0503
1	2.649	0.1578	2	1.802	0.1115	3	1.186	0.0799	4	0.819	0.0625	5	0.629	0.0521
1	3.769	0.1639	2	2.301	0.1141	3	1.356	0.0806	4	0.955	0.0631	5	0.729	0.0527
1	4.235	0.1649	2	3.127	0.1159	3	1.590	0.0811	4	1.135	0.0637	5	0.878	0.0529
1	5.102	0.1705	2	4.313	0.1208	3	1.785	0.0821	4	1.295	0.0645	5	1.030	0.0533
1	7.360	0.1799	2	6.385	0.1268	3	2.094	0.0831	4	1.467	0.0654	5	1.148	0.0537
1	9.844	0.1884	2	8.161	0.1306	3	2.383	0.0842	4	1.688	0.0661	5	1.337	0.0542
1	15.194	0.2007	2	11.207	0.1327	3	2.858	0.0852	4	1.885	0.0668	5	1.571	0.0545
1	25.940	0.2219	2	14.279	0.1361	3	3.631	0.0878	4	2.034	0.0660	5	1.771	0.0548
1	35.965	0.2372	2	20.236	0.1417	3	5.254	0.0904	4	2.452	0.0665	5	2.002	0.0551
			2	27.586	0.1535	3	7.236	0.0928	4	2.923	0.0684	5	2.320	0.0559
			2	35.806	0.1650	3	9.057	0.0960	4	4.086	0.0707	5	3.051	0.0583
						3	15.863	0.1092	4	5.027	0.0729	5	3.795	0.0592
						3	25.418	0.1259	4	5.986	0.0754	5	4.950	0.0632
						3	34.840	0.1400	4	7.127	0.0779	5	6.473	0.0672
									4	8.449	0.0809	5	8.068	0.0717
									4	15.026	0.0952	5	9.905	0.0763
									4	22.726	0.1091	5	15.789	0.0881
									4	28.415	0.1187	5	22.134	0.1002
									4	34.483	0.1270	5	28.730	0.1105
												5	35.966	0.1203

Material:	Bentonite
Concentration/vol:	6.8%
Density kg/m³:	1042.0
T_y (Pa):	18.34
K (Pa.sⁿ):	0.0078
n:	1.000
Flume width (mm):	300
Flume Shape	Rectangular

SLOPE	FLOW	DEPTH	SLOPE	FLOW	DEPTH	SLOPE	FLOW	DEPTH	SLOPE	FLOW	DEPTH
FLUME	Q	h	FLUME	Q	h	FLUME	Q	h	FLUME	Q	h
(degrees)	(l.s ⁻¹)	(m)	(degrees)	(l.s ⁻¹)	(m)	(degrees)	(l.s ⁻¹)	(m)	(degrees)	(l.s ⁻¹)	(m)
2	1.781	0.0820	3	1.474	0.0461	4	1.420	0.0320	5	1.794	0.0264
2	2.986	0.0878	3	2.845	0.0487	4	2.524	0.0360	5	2.977	0.0268
2	4.033	0.0900	3	4.022	0.0483	4	3.046	0.0338	5	4.010	0.0272
2	5.030	0.0905	3	5.065	0.0493	4	4.092	0.0354	5	5.079	0.0281
2	6.021	0.0916	3	6.217	0.0495	4	5.055	0.0352	5	6.196	0.0291
2	7.290	0.0923	3	7.180	0.0487	4	6.054	0.0347	5	7.236	0.0291
2	8.831	0.0881	3	8.492	0.0493	4	7.126	0.0351	5	8.437	0.0302
2	10.097	0.0891	3	10.156	0.0515	4	8.430	0.0360	5	10.187	0.0308
2	13.522	0.0837	3	12.950	0.0501	4	10.176	0.0370	5	15.147	0.0337
2	14.867	0.0806	3	16.633	0.0523	4	11.892	0.0373	5	11.778	0.0309
2	20.958	0.0862	3	18.360	0.0534	4	14.107	0.0384	5	16.065	0.0345
2	24.700	0.0847	3	22.629	0.0582	4	16.375	0.0405	5	20.259	0.0386
2	1.000	0.0847	3	26.062	0.0616	4	17.958	0.0421	5	24.974	0.0431
2	31.669	0.0936	3	31.254	0.0665	4	21.258	0.0452	5	31.425	0.0483
2	35.791	0.0930	3	35.490	0.0701	4	21.211	0.0450	5	35.830	0.0509
2	41.375	0.1001	3	40.808	0.0759	4	25.225	0.0499			
						4	31.882	0.0556			
						4	39.870	0.0632			

Material:	Bentonite
Concentration/vol:	4.8%
Density kg/m³:	1029.0
T_y (Pa):	5.66
K (Pa.sⁿ):	0.0036
n:	1.000
Flume width (mm):	150
Flume Shape	Rectangular

SLOPE	FLOW	DEPTH	SLOPE	FLOW	DEPTH	SLOPE	FLOW	DEPTH	SLOPE	FLOW	DEPTH	SLOPE	FLOW	DEPTH
FLUME	Q	h	FLUME	Q	h	FLUME	Q	h	FLUME	Q	h	FLUME	Q	h
(degrees)	(l.s ⁻¹)	(m)	(degrees)	(l.s ⁻¹)	(m)	(degrees)	(l.s ⁻¹)	(m)	(degrees)	(l.s ⁻¹)	(m)	(degrees)	(l.s ⁻¹)	(m)
1	0.501	0.0457	2	0.554	0.0201	3	0.616	0.0137	4	0.523	0.0109	5	1.899	0.0115
1	0.736	0.0480	2	0.781	0.0201	3	0.910	0.0145	4	0.799	0.0114	5	1.054	0.0102
1	1.001	0.0487	2	1.103	0.0214	3	1.270	0.0156	4	1.137	0.0120	5	1.343	0.0108
1	1.369	0.0506	2	1.413	0.0233	3	1.652	0.0159	4	1.560	0.0125	5	2.158	0.0123
1	1.846	0.0503	2	2.049	0.0234	3	2.151	0.0174	4	2.044	0.0128	5	2.560	0.0130
1	2.459	0.0441	2	2.571	0.0235	3	2.571	0.0177	4	2.575	0.0133	5	3.165	0.0139
1	2.976	0.0500	2	3.052	0.0252	3	3.075	0.0185	4	3.155	0.0155	5	3.571	0.0147
1	3.483	0.0509	2	3.524	0.0264	3	3.554	0.0198	4	3.602	0.0161	5	4.148	0.0157
1	4.188	0.0518	2	3.975	0.0281	3	4.059	0.0211	4	4.135	0.0177	5	4.653	0.0166
1	4.953	0.0528	2	4.597	0.0293	3	4.542	0.0219	4	4.607	0.0183	5	5.274	0.0175
1	6.030	0.0556	2	5.110	0.0306	3	5.182	0.0232	4	2.777	0.0145	5	7.226	0.0217
1	7.737	0.0568	2	5.593	0.0317	3	6.043	0.0255	4	5.645	0.0209	5	8.028	0.0230
1	8.929	0.0606	2	6.589	0.0344	3	7.241	0.0282	4	7.919	0.0255	5	9.465	0.0258
1	11.676	0.0708	2	7.507	0.0367	3	8.524	0.0313	4	10.028	0.0304	5	10.166	0.0272
1	10.085	0.0658	2	10.152	0.0441	3	10.193	0.0351	4	13.926	0.0387	5	12.032	0.0306
1	12.796	0.0738	2	8.833	0.0422	3	13.374	0.0430	4	21.552	0.0540	5	17.250	0.041
1	14.350	0.0802	2	15.434	0.0580	3	20.142	0.0586				5	24.219	0.055
1	17.433	0.0897	2	12.302	0.0493	3	17.631	0.0529						
1	20.262	0.0997	2	20.007	0.0699	3	25.809	0.0695						

Material:	Bentonite
Concentration/vol:	4.5%
Density kg/m³:	1027.0
T_y (Pa):	4.30
K (Pa.sⁿ):	0.0036
n:	1.000
Flume width (mm):	300
Flume Shape	Rectangular

SLOPE	FLOW	DEPTH	SLOPE	FLOW	DEPTH	SLOPE	FLOW	DEPTH	SLOPE	FLOW	DEPTH	SLOPE	FLOW	DEPTH
FLUME	Q	h	FLUME	Q	h	FLUME	Q	h	FLUME	Q	h	FLUME	Q	h
(degrees)	(l.s ⁻¹)	(m)	(degrees)	(l.s ⁻¹)	(m)	(degrees)	(l.s ⁻¹)	(m)	(degrees)	(l.s ⁻¹)	(m)	(degrees)	(l.s ⁻¹)	(m)
1	0.823	0.0086	2	0.659	0.0156	3	0.602	0.0106	4	0.827	0.0086	5	1.138	0.0076
1	0.487	0.0353	2	0.808	0.0160	3	0.902	0.0113	4	1.183	0.0096	5	1.502	0.0082
1	0.720	0.0363	2	1.120	0.0162	3	1.346	0.0120	4	1.567	0.0100	5	2.022	0.0087
1	1.028	0.0367	2	1.507	0.0166	3	2.058	0.0129	4	2.120	0.0105	5	2.494	0.0095
1	1.552	0.0376	2	2.071	0.0174	3	2.521	0.0133	4	2.579	0.0102	5	3.047	0.0099
1	2.057	0.0372	2	2.577	0.0184	3	3.089	0.0128	4	3.046	0.0109	5	3.514	0.0101
1	2.684	0.0393	2	3.643	0.0187	3	4.090	0.0145	4	3.516	0.0120	5	4.118	0.0107
1	3.298	0.0346	2	3.039	0.0187	3	3.838	0.0141	4	3.974	0.0123	5	4.536	0.0110
1	4.032	0.0360	2	0.602	0.0106	3	4.512	0.0150	4	4.830	0.0131	5	4.953	0.0113
1	5.134	0.0351	2	4.590	0.0206	3	5.097	0.0156	4	1.000	0.0131	5	6.001	0.0124
1	6.219	0.0368	2	5.103	0.0210	3	6.105	0.0166	4	6.110	0.0140	5	8.009	0.0141
1	7.012	0.0382	2	6.059	0.0221	3	8.025	0.0183	4	8.030	0.0156	5	10.038	0.0159
1	8.003	0.0371	2	7.081	0.0231	3	10.147	0.0208	4	10.102	0.0179	5	13.250	0.0190
1	10.142	0.0401	2	8.065	0.0242	3	12.596	0.0238	4	12.392	0.0203	5	18.231	0.0239
1	11.496	0.0416	2	9.905	0.0262	3	15.677	0.0274	4	16.572	0.0247	5	23.008	0.0284
1	13.283	0.0448	2	12.543	0.0294	3	20.616	0.0336	4	22.388	0.0308	5	30.208	0.036
1	14.908	0.0475	2	15.119	0.0331	3	29.364	0.0424	4	30.855	0.0408			
1	19.065	0.0531	2	21.822	0.0417	3	39.897	0.0541						
1	24.418	0.0626	2	29.883	0.0519									
1	30.201	0.0699	2	39.856	0.0640									
1	36.034	0.0778												
1	40.075	0.0841												

Material:	Kaolin
Concentration/vol:	5.4%
Density kg/m³:	1089.0
T_y (Pa):	4.40
K (Pa.sⁿ):	0.0840
n:	0.582
Flume width (mm):	300
Flume Shape	Rectangular

SLOPE	FLOW	DEPTH	SLOPE	FLOW	DEPTH	SLOPE	FLOW	DEPTH	SLOPE	FLOW	DEPTH	SLOPE	FLOW	DEPTH
FLUME	Q	h	FLUME	Q	h	FLUME	Q	h	FLUME	Q	h	FLUME	Q	h
(degrees)	(l.s ⁻¹)	(m)	(degrees)	(l.s ⁻¹)	(m)	(degrees)	(l.s ⁻¹)	(m)	(degrees)	(l.s ⁻¹)	(m)	(degrees)	(l.s ⁻¹)	(m)
1	0.243	0.0297	2	0.241	0.0150	3	0.698	0.0111	4	1.270	0.0094	5	1.306	0.0079
1	0.357	0.0299	2	0.366	0.0155	3	0.915	0.0114	4	1.469	0.0097	5	2.057	0.0086
1	0.443	0.0300	2	0.564	0.0159	3	1.187	0.0116	4	2.106	0.0103	5	1.793	0.0085
1	0.522	0.0302	2	0.795	0.0164	3	1.488	0.0121	4	2.523	0.0106	5	2.434	0.0091
1	0.699	0.0300	2	0.986	0.0164	3	1.845	0.0124	4	3.536	0.0114	5	3.419	0.0098
1	0.980	0.0302	2	1.363	0.0171	3	2.394	0.0128	4	4.588	0.0123	5	4.723	0.0108
1	1.221	0.0298	2	1.647	0.0175	3	2.565	0.0128	4	5.475	0.0131	5	5.605	0.0116
1	1.422	0.0307	2	2.061	0.0178	3	3.597	0.0142	4	7.015	0.0147	5	7.095	0.0128
1	1.964	0.0318	2	2.993	0.0182	3	4.839	0.0152	4	8.377	0.0157	5	8.460	0.0141
1	3.155	0.0342	2	3.644	0.0191	3	5.729	0.0159	4	10.026	0.0177	5	10.082	0.0156
1	3.715	0.0349	2	4.854	0.0203	3	6.970	0.0172	4	17.417	0.0256	5	16.007	0.0215
1	4.637	0.0356	2	5.549	0.0211	3	8.500	0.0191	4	25.286	0.0339	5	24.692	0.0299
1	5.021	0.0357	2	7.208	0.0228	3	10.153	0.0208	4	35.672	0.0435	5	35.437	0.0395
1	6.454	0.0366	2	8.632	0.0246	3	18.124	0.0303	4	45.158	0.0527	5	44.935	0.0486
1	7.662	0.0379	2	10.040	0.0267	3	23.588	0.0368						
1	8.817	0.0392	2	16.127	0.0348	3	34.384	0.0487						
1	10.099	0.0408	2	22.458	0.0433	3	45.172	0.0599						
1	14.875	0.0482	2	33.385	0.0573									
1	19.618	0.0557	2	44.725	0.0712									
1	23.881	0.0624												
1	30.455	0.0726												
1	36.908	0.0824												
1	44.008	0.0933												

Material:	Kaolin
Concentration/vol:	7.1%
Density kg/m³:	1118.0
T_y (Pa):	11.56
K (Pa.sⁿ):	0.1480
n:	0.557
Flume width (mm):	300
Flume Shape	Rectangular

SLOPE	FLOW	DEPTH	SLOPE	FLOW	DEPTH	SLOPE	FLOW	DEPTH	SLOPE	FLOW	DEPTH	SLOPE	FLOW	DEPTH
FLUME	Q	h	FLUME	Q	h	FLUME	Q	h	FLUME	Q	h	FLUME	Q	h
(degrees)	(l.s ⁻¹)	(m)	(degrees)	(l.s ⁻¹)	(m)	(degrees)	(l.s ⁻¹)	(m)	(degrees)	(l.s ⁻¹)	(m)	(degrees)	(l.s ⁻¹)	(m)
1	1.206	0.0633	2	1.044	0.0353	3	0.965	0.0249	4	0.917	0.0184	5	1.507	0.0160
1	2.054	0.0675	2	2.172	0.0378	3	2.016	0.0260	4	1.635	0.0194	5	2.040	0.0166
1	2.584	0.0691	2	3.093	0.0391	3	2.990	0.0268	4	2.099	0.0198	5	2.565	0.0173
1	3.038	0.0703	2	4.131	0.0404	3	4.149	0.0278	4	2.561	0.0207	5	3.105	0.0178
1	4.135	0.0732	2	5.399	0.0417	3	5.089	0.0286	4	3.377	0.0210	5	3.492	0.0177
1	5.140	0.0756	2	6.042	0.0416	3	6.119	0.0292	4	4.076	0.0217	5	3.929	0.0183
1	6.063	0.0774	2	7.170	0.0423	3	7.138	0.0296	4	4.557	0.0219	5	4.888	0.0185
1	7.007	0.0796	2	8.103	0.0428	3	8.110	0.0303	4	5.020	0.0224	5	5.603	0.0191
1	8.065	0.0813	2	9.052	0.0432	3	9.042	0.0311	4	6.165	0.0232	5	6.726	0.0197
1	9.082	0.0830	2	10.153	0.0444	3	10.247	0.0318	4	6.963	0.0235	5	7.555	0.0203
1	10.158	0.0849	2	12.713	0.0457	3	13.100	0.0345	4	7.618	0.0241	5	8.505	0.0210
1	13.634	0.0897	2	15.924	0.0490	3	17.043	0.0386	4	8.577	0.0247	5	9.421	0.0218
1	19.849	0.1023	2	17.800	0.0509	3	18.962	0.0405	4	9.437	0.0254	5	10.123	0.0224
1	22.889	0.0978	2	20.168	0.0542	3	23.351	0.0454	4	10.159	0.0260	5	13.860	0.0252
1	28.571	0.1044	2	24.059	0.0591	3	27.316	0.0499	4	12.422	0.0278	5	12.500	0.0241
1	33.360	0.1102	2	27.408	0.0625	3	30.588	0.0535	4	16.255	0.0314	5	18.345	0.029
1	38.570	0.1170	2	30.089	0.0662	3	35.379	0.0589	4	15.299	0.0305	5	25.222	0.036
1	44.609	0.1254	2	34.154	0.0715	3	39.500	0.0633	4	19.676	0.0349	5	35.567	0.046
			2	38.813	0.0772	3	42.162	0.0665	4	22.668	0.0378	5	39.398	0.050
			2	44.036	0.0837				4	25.454	0.0407			
									4	29.940	0.0454			
									4	35.637	0.0512			
									4	39.557	0.0559			
									4	42.539	0.0576			

Material:	cmc
Concentration/vol:	1.5%
Density kg/m ³ :	1008.2
T _y (Pa):	0.00
K (Pa.s ⁿ):	0.0140
n:	0.944
Flume width (mm):	150
Flume Shape	Rectangular

SLOPE	FLOW	DEPTH	SLOPE	FLOW	DEPTH	SLOPE	FLOW	DEPTH	SLOPE	FLOW	DEPTH	SLOPE	FLOW	DEPTH
FLUME	Q	h	FLUME	Q	h	FLUME	Q	h	FLUME	Q	h	FLUME	Q	h
(degrees)	(l.s ⁻¹)	(m)	(degrees)	(l.s ⁻¹)	(m)	(degrees)	(l.s ⁻¹)	(m)	(degrees)	(l.s ⁻¹)	(m)	(degrees)	(l.s ⁻¹)	(m)
1	0.114	0.0053	2	0.107	0.0041	3	0.449	0.0057	4	0.548	0.0053	5	1.061	0.0058
1	0.207	0.0065	2	0.175	0.0045	3	0.884	0.0071	4	0.983	0.0065	5	1.240	0.0064
1	0.273	0.0071	2	0.385	0.0062	3	1.426	0.0085	4	1.218	0.0070	5	1.240	0.0079
1	0.314	0.0074	2	0.517	0.0069	3	2.099	0.0113	4	1.535	0.0081	5	1.914	0.0095
1	0.401	0.0080	2	0.755	0.0078	3	2.758	0.0141	4	1.550	0.0095	5	3.422	0.0139
1	0.541	0.0089	2	1.000	0.0086	3	4.520	0.0190	4	2.259	0.0112	5	6.373	0.0217
1	0.659	0.0094	2	1.387	0.0098	3	7.142	0.0273	4	5.885	0.0211	5	9.813	0.0279
1	0.770	0.0101	2	1.743	0.0109	3	9.589	0.0341	4	8.802	0.0277	5	19.992	0.0493
1	0.938	0.0109	2	2.605	0.0156	3	16.147	0.0502	4	14.340	0.0404			
1	1.032	0.0113	2	3.103	0.0179				4	21.448	0.0555			
1	1.383	0.0127	2	4.778	0.0246									
1	1.702	0.0142	2	6.373	0.0300									
1	2.138	0.0177	2	9.675	0.0406									
1	1.911	0.0155	2	14.592	0.0538									
1	2.479	0.0196	2	18.172	0.0641									
1	3.294	0.0246												
1	4.187	0.0289												
1	7.391	0.0434												
1	9.756	0.0537												
1	9.775	0.0537												
1	15.386	0.0734												

Material:	cmc
Concentration/vol:	1.5%
Density kg/m ³ :	1008.2
T _y (Pa):	0.00
K (Pa.s ⁿ):	0.0140
n:	0.944
Flume width (mm):	300
Flume Shape	Rectangular

SLOPE	FLOW	DEPTH	SLOPE	FLOW	DEPTH	SLOPE	FLOW	DEPTH	SLOPE	FLOW	DEPTH	SLOPE	FLOW	DEPTH
FLUME	Q	h	FLUME	Q	h	FLUME	Q	h	FLUME	Q	h	FLUME	Q	h
(degrees)	(l.s ⁻¹)	(m)	(degrees)	(l.s ⁻¹)	(m)	(degrees)	(l.s ⁻¹)	(m)	(degrees)	(l.s ⁻¹)	(m)	(degrees)	(l.s ⁻¹)	(m)
1	0.131	0.0046	1	8.603	0.0293	2	26.728	0.0478	4	1.225	0.0057	5	1.150	0.0050
1	0.206	0.0054	1	9.801	0.0318	2	33.561	0.0584	4	1.729	0.0064	5	1.757	0.0058
1	0.305	0.0060	1	13.305	0.0379	3	0.574	0.0049	4	2.001	0.0067	5	2.381	0.0067
1	0.409	0.0066	1	18.763	0.0476	3	0.942	0.0057	4	2.580	0.0075	5	2.908	0.0079
1	0.513	0.0070	1	27.153	0.0617	3	1.483	0.0066	4	3.309	0.0082	5	3.832	0.0093
1	0.623	0.0075	1	34.498	0.0735	3	2.050	0.0075	4	3.882	0.0108	5	4.967	0.0111
1	0.716	0.0078	2	0.147	0.0036	3	2.484	0.0080	4	5.663	0.0134	5	5.768	0.0121
1	0.797	0.0081	2	0.242	0.0042	3	2.874	0.0086	4	7.680	0.0159	5	7.500	0.0144
1	1.029	0.0088	2	0.407	0.0051	3	3.727	0.0097	4	9.796	0.0189	5	9.820	0.0168
1	1.130	0.0091	2	0.607	0.0058	3	4.625	0.0140	4	19.242	0.0282	5	17.367	0.0245
1	1.325	0.0096	2	0.819	0.0064	3	5.741	0.0150	4	25.654	0.0350	5	29.564	0.0375
1	1.512	0.0101	2	1.000	0.0068	3	7.671	0.0177	4	36.020	0.0457			
1	1.766	0.0107	2	1.376	0.0077	3	9.792	0.0202						
1	1.873	0.0108	2	1.953	0.0086	3	16.542	0.0288						
1	2.971	0.0134	2	2.716	0.0099	3	24.542	0.0380						
1	3.422	0.0144	2	3.302	0.0107	3	29.810	0.0448						
1	3.850	0.0152	2	3.946	0.0117									
1	4.449	0.0165	2	4.776	0.0156									
1	4.483	0.0191	2	5.869	0.0174									
1	5.446	0.0204	2	7.822	0.0208									
1	6.461	0.0236	2	9.820	0.0243									
1	7.274	0.0260	2	17.470	0.0351									

Material:	cmc
Concentration/vol:	3.0%
Density kg/m³:	1017.5
T_y (Pa):	0.00
K (Pa.sⁿ):	0.1450
n:	0.788
Flume width (mm):	300
Flume Shape	Rectangular

SLOPE	FLOW	DEPTH	SLOPE	FLOW	DEPTH	SLOPE	FLOW	DEPTH	SLOPE	FLOW	DEPTH	SLOPE	FLOW	DEPTH
FLUME	Q	h	FLUME	Q	h	FLUME	Q	h	FLUME	Q	h	FLUME	Q	h
(degrees)	(l.s ⁻¹)	(m)	(degrees)	(l.s ⁻¹)	(m)	(degrees)	(l.s ⁻¹)	(m)	(degrees)	(l.s ⁻¹)	(m)	(degrees)	(l.s ⁻¹)	(m)
1	0.095	0.0075	2	0.141	0.0065	3	0.185	0.0062	4	0.288	0.0064	5	0.283	0.0058
1	0.200	0.0092	2	0.210	0.0074	3	0.316	0.0072	4	0.398	0.0070	5	0.432	0.0067
1	0.316	0.0109	2	0.305	0.0082	3	0.534	0.0085	4	0.605	0.0079	5	0.552	0.0072
1	0.407	0.0117	2	0.503	0.0096	3	0.719	0.0093	4	0.834	0.0087	5	0.720	0.0077
1	0.503	0.0126	2	0.700	0.0107	3	0.913	0.0101	4	1.016	0.0093	5	0.913	0.0083
1	0.713	0.0141	2	0.884	0.0115	3	1.236	0.0112	4	1.314	0.0102	5	1.263	0.0092
1	0.915	0.0152	2	1.246	0.0128	3	1.537	0.0119	4	1.638	0.0109	5	1.630	0.0100
1	1.081	0.0160	2	1.620	0.0140	3	2.180	0.0132	4	2.045	0.0116	5	2.112	0.0108
1	2.036	0.0195	2	2.029	0.0150	3	3.025	0.0147	4	3.077	0.0131	5	3.006	0.0121
1	3.100	0.0223	2	3.011	0.0170	3	4.066	0.0154	4	4.089	0.0144	5	4.016	0.0132
1	4.205	0.0244	2	4.007	0.0187	3	5.266	0.0176	4	4.998	0.0154	5	5.145	0.0143
1	5.127	0.0266	2	5.203	0.0203	3	6.638	0.0192	4	6.631	0.0171	5	6.511	0.0156
1	6.182	0.0285	2	6.432	0.0223	3	8.016	0.0209	4	8.138	0.0187	5	7.957	0.0170
1	7.107	0.0304	2	8.060	0.0246	3	10.100	0.0236	4	10.270	0.0210	5	10.199	0.0191
1	8.158	0.0324	2	10.004	0.0275	3	15.580	0.0303	4	17.113	0.0285	5	14.651	0.0235
1	9.075	0.0343	2	14.647	0.0343	3	20.192	0.0362	4	23.547	0.0357	5	20.570	0.029
1	10.223	0.0367	2	20.659	0.0434	3	29.316	0.0478	4	30.279	0.0434	5	27.792	0.037
1	13.503	0.0433	2	24.664	0.0493	3	42.140	0.0625	4	42.043	0.0560	5	38.118	0.046
1	16.934	0.0499	2	32.718	0.0608							5	43.633	0.050
1	21.560	0.0591	2	43.511	0.0755									
1	26.813	0.0680												
1	34.976	0.0821												
1	43.385	0.0964												

Material:	cmc
Concentration/vol:	3.0%
Density kg/m³:	1017.5
T_y (Pa):	0.00
K (Pa.sⁿ):	0.1450
n:	0.788
Flume width (mm):	75
Flume Shape	Rectangular

SLOPE	FLOW	DEPTH	SLOPE	FLOW	DEPTH	SLOPE	FLOW	DEPTH	SLOPE	FLOW	DEPTH
FLUME	Q	h	FLUME	Q	h	FLUME	Q	h	FLUME	Q	h
(degrees)	(l.s⁻¹)	(m)	(degrees)	(l.s⁻¹)	(m)	(degrees)	(l.s⁻¹)	(m)	(degrees)	(l.s⁻¹)	(m)
1	0.025	0.0078	2	0.130	0.0099	3	0.131	0.0082	4	0.140	0.0081
1	0.042	0.0089	2	0.202	0.0114	3	0.223	0.0098	4	0.233	0.0095
1	0.071	0.0107	2	0.240	0.0120	3	0.285	0.0106	4	0.298	0.0102
1	0.092	0.0116	2	0.293	0.0128	3	0.345	0.0112	4	0.402	0.0112
1	0.123	0.0129	2	0.348	0.0136	3	0.402	0.0119	4	0.507	0.0122
1	0.173	0.0145	2	0.386	0.0141	3	0.495	0.0128	4	0.606	0.0129
1	0.202	0.0153	2	0.495	0.0154	3	0.603	0.0138	4	0.718	0.0137
1	0.355	0.0184	2	0.591	0.0164	3	0.698	0.0146	4	0.911	0.0152
1	0.572	0.0220	2	0.720	0.0177	3	0.796	0.0154	4	1.216	0.0174
1	1.008	0.0283	2	0.803	0.0186	3	1.030	0.0173	4	1.561	0.0204
1	1.516	0.0363	2	0.899	0.0196	3	1.185	0.0186	4	2.081	0.0245
1	1.938	0.0421	2	1.041	0.0210	3	1.242	0.0193	4	2.546	0.0275
1	2.395	0.0486	2	1.135	0.0219	3	1.745	0.0233	4	3.188	0.0321
1	2.995	0.0564	2	1.321	0.0242	3	2.284	0.0281	4	3.671	0.0356
1	4.004	0.0692	2	1.733	0.0283	3	3.487	0.0376	4	4.694	0.0426
1	4.969	0.0822	2	1.897	0.0302	3	4.476	0.0449	4	5.777	0.0501
			2	2.294	0.0344						
			2	3.714	0.0477						
			2	4.063	0.0511						
			2	5.135	0.0603						
			2	7.443	0.0814						

Material:	cmc
Concentration/vol:	3.1%
Density kg/m³:	1018.2
T_y (Pa):	0.00
K (Pa.sⁿ):	0.1750
n:	0.768
Flume width (mm):	150
Flume Shape	Rectangular

SLOPE	FLOW	DEPTH	SLOPE	FLOW	DEPTH	SLOPE	FLOW	DEPTH	SLOPE	FLOW	DEPTH	SLOPE	FLOW	DEPTH
FLUME	Q	h	FLUME	Q	h	FLUME	Q	h	FLUME	Q	h	FLUME	Q	h
(degrees)	(l.s ⁻¹)	(m)	(degrees)	(l.s ⁻¹)	(m)	(degrees)	(l.s ⁻¹)	(m)	(degrees)	(l.s ⁻¹)	(m)	(degrees)	(l.s ⁻¹)	(m)
1	0.107	0.0095	2	0.128	0.0082	3	0.107	0.0067	4	0.107	0.0059	5	0.638	0.0092
1	0.199	0.0122	2	0.205	0.0093	3	0.207	0.0080	4	0.192	0.0070	5	0.698	0.0097
1	0.300	0.0139	2	0.312	0.0105	3	0.306	0.0091	4	0.311	0.0081	5	0.988	0.0106
1	0.393	0.0150	2	0.417	0.0116	3	0.400	0.0099	4	0.407	0.0088	5	1.447	0.0121
1	0.512	0.0163	2	0.510	0.0124	3	0.575	0.0110	4	0.514	0.0094	5	1.979	0.0132
1	0.582	0.0170	2	0.608	0.0132	3	0.805	0.0123	4	0.696	0.0103	5	2.497	0.0146
1	0.705	0.0181	2	0.787	0.0143	3	1.013	0.0133	4	0.913	0.0114	5	3.077	0.0157
1	0.934	0.0197	2	1.647	0.0181	3	1.420	0.0149	4	1.259	0.0127	5	3.566	0.0166
1	1.271	0.0219	2	1.106	0.0159	3	1.947	0.0163	4	1.797	0.0141	5	4.503	0.0187
1	1.595	0.0240	2	2.025	0.0193	3	2.949	0.0190	4	2.167	0.0153	5	6.128	0.0222
1	1.955	0.0256	2	2.544	0.0213	3	3.452	0.0202	4	2.983	0.0170	5	7.965	0.0266
1	2.245	0.0270	2	2.950	0.0225	3	4.032	0.0219	4	4.111	0.0191	5	10.001	0.0311
1	2.840	0.0292	2	4.097	0.0261	3	5.297	0.0253	4	5.098	0.0219	5	14.364	0.0404
1	4.170	0.0350	2	4.573	0.0278	3	6.615	0.0287	4	6.112	0.0241	5	19.617	0.0522
1	5.072	0.0391	2	3.552	0.0244	3	8.045	0.0330	4	8.065	0.0288	5	25.557	0.0653
1	5.970	0.0432	2	5.990	0.0323	3	9.881	0.0383	4	9.938	0.0336			
1	7.548	0.0507	2	8.072	0.0398	3	15.161	0.0520	4	16.267	0.0485			
1	8.931	0.0571	2	10.178	0.0466	3	20.231	0.0656	4	23.055	0.0648			
1	10.230	0.0624	2	14.502	0.0630	3	25.229	0.0776						
1	14.760	0.0805												
1	19.738	0.1035												
1	23.112	0.1133												

Material:	cmc
Concentration/vol:	4.0%
Density kg/m³:	1022.8
T_y (Pa):	0.00
K (Pa.sⁿ):	0.3300
n:	0.727
Flume width (mm):	150
Flume Shape	Rectangular

SLOPE	FLOW	DEPTH	SLOPE	FLOW	DEPTH	SLOPE	FLOW	DEPTH	SLOPE	FLOW	DEPTH	SLOPE	FLOW	DEPTH
FLUME	Q	h	FLUME	Q	h	FLUME	Q	h	FLUME	Q	h	FLUME	Q	h
(degrees)	(l.s ⁻¹)	(m)	(degrees)	(l.s ⁻¹)	(m)	(degrees)	(l.s ⁻¹)	(m)	(degrees)	(l.s ⁻¹)	(m)	(degrees)	(l.s ⁻¹)	(m)
1	0.100	0.0132	2	0.156	0.0117	3	0.105	0.0086	4	0.188	0.0088	5	0.109	0.0071
1	0.296	0.0177	2	0.193	0.0119	3	0.194	0.0101	4	0.291	0.0101	5	0.200	0.0082
1	0.294	0.0177	2	0.298	0.0135	3	0.298	0.0114	4	0.404	0.0110	5	0.309	0.0093
1	0.390	0.0195	2	0.396	0.0151	3	0.395	0.0127	4	0.548	0.0122	5	0.463	0.0106
1	0.497	0.0209	2	0.505	0.0161	3	0.489	0.0136	4	0.706	0.0134	5	0.639	0.0116
1	0.589	0.0222	2	0.599	0.0171	3	0.602	0.0145	4	0.837	0.0141	5	0.873	0.0128
1	0.791	0.0245	2	0.805	0.0187	3	0.762	0.0156	4	1.100	0.0153	5	1.041	0.0137
1	1.052	0.0270	2	1.070	0.0205	3	0.953	0.0166	4	1.399	0.0165	5	1.286	0.0145
1	1.218	0.0284	2	1.207	0.0213	3	1.165	0.0179	4	1.407	0.0165	5	1.980	0.0168
1	1.530	0.0315	2	1.539	0.0231	3	1.480	0.0192	4	1.988	0.0185	5	2.827	0.0188
1	2.035	0.0344	2	2.036	0.0255	3	2.074	0.0216	4	1.996	0.0186	5	3.656	0.0206
1	2.541	0.0373	2	2.744	0.0284	3	2.524	0.0230	4	3.072	0.0213	5	4.972	0.0233
1	3.024	0.0397	2	3.495	0.0307	3	3.140	0.0247	4	3.894	0.0225	5	6.489	0.0264
1	4.053	0.0446	2	4.360	0.0338	3	4.538	0.0285	4	4.259	0.0244	5	8.146	0.0299
1	5.024	0.0494	2	6.213	0.0398	3	5.521	0.0312	4	5.066	0.0260	5	10.194	0.0346
1	6.118	0.0541	2	8.078	0.0464	3	6.561	0.0339	4	6.077	0.0284	5	17.139	0.050
1	7.035	0.0587	2	9.983	0.0533	3	8.072	0.0382	4	6.991	0.0308	5	22.371	0.062
1	10.110	0.0730	2	15.148	0.0698	3	10.073	0.0437	4	10.275	0.0388	5	27.026	0.073
1	17.540	0.1065	2	19.152	0.0823	3	16.938	0.0631	4	16.972	0.0557			
1	21.974	0.1242	2	24.356	0.0990				4	23.742	0.0722			

Material:	cmc
Concentration/vol:	5.3%
Density kg/m ³ :	1028.0
T _y (Pa):	0.00
K (Pa.s ⁿ):	0.9200
n:	0.678
Flume width (mm):	150
Flume Shape	Rectangular

SLOPE	FLOW	DEPTH	SLOPE	FLOW	DEPTH	SLOPE	FLOW	DEPTH	SLOPE	FLOW	DEPTH	SLOPE	FLOW	DEPTH
FLUME	Q	h	FLUME	Q	h	FLUME	Q	h	FLUME	Q	h	FLUME	Q	h
(degrees)	(l.s ⁻¹)	(m)	(degrees)	(l.s ⁻¹)	(m)	(degrees)	(l.s ⁻¹)	(m)	(degrees)	(l.s ⁻¹)	(m)	(degrees)	(l.s ⁻¹)	(m)
1	0.120	0.0199	2	0.108	0.0141	3	0.108	0.0114	4	0.114	0.0104	5	0.131	0.0098
1	0.214	0.0241	2	0.222	0.0174	3	0.224	0.0148	4	0.212	0.0127	5	0.213	0.0116
1	0.317	0.0278	2	0.316	0.0199	3	0.333	0.0164	4	0.312	0.0144	5	0.312	0.0131
1	0.420	0.0308	2	0.415	0.0215	3	0.411	0.0179	4	0.431	0.0158	5	0.412	0.0143
1	0.506	0.0331	2	0.615	0.0247	3	0.521	0.0194	4	0.531	0.0169	5	0.523	0.0154
1	0.592	0.0348	2	0.703	0.0257	3	0.615	0.0205	4	0.617	0.0181	5	0.610	0.0163
1	0.716	0.0370	2	0.875	0.0280	3	0.711	0.0216	4	0.709	0.0188	5	0.713	0.0172
1	0.851	0.0389	2	1.085	0.0299	3	0.887	0.0232	4	0.902	0.0204	5	0.818	0.0179
1	0.932	0.0400	2	1.951	0.0366	3	1.023	0.0244	4	1.047	0.0213	5	0.893	0.0185
1	0.988	0.0407	2	3.040	0.0435	3	1.993	0.0301	4	1.478	0.0236	5	1.043	0.0194
1	1.440	0.0470	2	3.422	0.0457	3	1.601	0.0280	4	2.049	0.0263	5	1.548	0.0218
1	2.058	0.0534	2	4.282	0.0499	3	2.630	0.0331	4	3.027	0.0302	5	2.003	0.0238
1	2.961	0.0624	2	5.303	0.0544	3	3.031	0.0352	4	3.846	0.0334	5	3.093	0.0278
1	3.827	0.0709	2	6.119	0.0582	3	3.869	0.0385	4	4.756	0.0362	5	3.884	0.0301
1	4.880	0.0800	2	7.954	0.0660	3	4.842	0.0422	4	5.705	0.0388	5	4.767	0.0326
1	5.726	0.0863	2	8.813	0.0696	3	5.830	0.0455	4	6.563	0.0415	5	5.641	0.035
1	6.525	0.0917	2	11.635	0.0786	3	6.600	0.0483	4	7.491	0.0441	5	6.609	0.037
1	7.522	0.0992	2	13.535	0.0858	3	8.385	0.0545	4	8.474	0.0471	5	7.515	0.040
1	9.180	0.1061	2	15.243	0.0923	3	10.372	0.0612	4	11.187	0.0528	5	8.980	0.042
1	10.445	0.1133	2	17.332	0.1004	3	12.051	0.0667	4	11.590	0.0547	5	10.136	0.045
1	12.319	0.1246	2	17.887	0.1039	3	14.883	0.0726	4	14.212	0.0610	5	12.124	0.049
1	14.527	0.1372	2	20.229	0.1109	3	17.089	0.0804	4	16.523	0.0673	5	14.166	0.054
1	16.584	0.1485	2	23.128	0.1164	3	18.884	0.085	4	19.669	0.0745	5	16.857	0.0602
1	17.648	0.1543	2	25.561	0.1271	3	20.957	0.0919	4	21.488	0.0804	5	17.946	0.0628
1	19.578	0.1637				3	23.006	0.0981	4	23.463	0.0853	5	19.275	0.0662
1	21.167	0.1732				3	25.218	0.1040				5	20.508	0.0693
												5	22.102	0.0728

Appendix B. Error propagation analysis

The following appendix contains the error propagation analysis calculator equations (Dr. N.J. Alderman)

Friction factor

$$f = \frac{2g R_h \sin\theta}{V^2} \quad (2.11)$$

Simplify to

$$f = \frac{2g R_h \theta}{V^2} \text{ assuming } \sin\theta \approx \theta \text{ when } \theta \text{ is in radians}$$

Hence

$$(f \pm \delta f) = \frac{2g (R_h \pm \delta R_h) (\theta \pm \delta\theta)}{(V \pm \delta V)^2}$$

Error in f

$$\delta f = |f| \sqrt{\left(\frac{\delta R_h}{R_h}\right)^2 + \left(\frac{\delta\theta}{\theta}\right)^2 + \left(\frac{2\delta V}{V}\right)^2}$$

Velocity

$$V = \frac{Q}{A} \quad (B.1)$$

Hence

$$(V \pm \delta V) = \frac{(Q \pm \delta Q)}{(A \pm \delta A)}$$

Error in V

$$\delta V = |V| \sqrt{\left(\frac{\delta Q}{Q}\right)^2 + \left(\frac{\delta A}{A}\right)^2}$$

Hydraulic Radius

$$R_h = \frac{A}{P} \quad (2.8)$$

Hence

$$(R_h \pm \delta R_h) = \frac{(A \pm \delta A)}{(P \pm \delta P)}$$

Error in R_h

$$\delta R_h = |R_h| \sqrt{\left(\frac{\delta A}{A}\right)^2 + \left(\frac{\delta P}{P}\right)^2}$$

Channel shape	Area	Perimeter
Assume b, x and D are exact		
Rectangular	$A = bh$ $(A \pm \delta A) = (b(h \pm \delta h))$ Error in A $\delta A = b\delta h$	$P = b + 2h$ $(P \pm \delta P) = b + 2(h \pm \delta h)$ Error in P $\delta P = 2\delta h$
Triangular	$A = h^2$ $(A \pm \delta A) = (h \pm \delta h)^2$ Error in A $\delta A = 2h\delta h$	$P = 2h\sqrt{2}$ $(P \pm \delta P) = 2(h \pm \delta h)\sqrt{2}$ Error in P $\delta P = 2\sqrt{2}\delta h$
Trapezoidal	$A = h(b + xh)$ with $x = 1/\tan\theta$ $(A \pm \delta A) = b(h \pm \delta h) + x(h \pm \delta h)^2$ Error in A $\delta A = (b + 2xh)\delta h$	$P = b + 2h\sqrt{1 + x^2}$ with $x = 1/\tan\theta$ $(P \pm \delta P) = b + 2\sqrt{1 + x^2}(h \pm \delta h)$ Error in P $\delta P = 2\sqrt{1 + x^2}\delta h$
Semi-circular	$A = \frac{D^2}{8}(\theta - \sin\theta)$ with $\theta = 2\cos^{-1}(1 - \frac{2h}{D})$ $(A \pm dA) = \frac{D^2}{8}((\theta \pm d\theta) - \sin(\theta \pm d\theta))$ Error in A $\delta A = \frac{D^2}{8} \frac{1 - \cos\theta}{\sqrt{h(D-h)}} \delta h = \sqrt{h(D-h)}\delta h$	$P = D\left(\frac{\theta}{2}\right)$ with $\theta = 2\cos^{-1}(1 - \frac{2h}{D})$ $P = D\left(\frac{(\theta \pm d\theta)}{2}\right)$ Error in P $\delta P = \frac{D}{\sqrt{h(D-h)}}\delta h$

Flow curve using tube viscometry

Wall shear stress

$$\tau_w = \frac{P_f D}{4L} \tag{B.2}$$

Hence

$$(\tau_w + \delta\tau_w) = \frac{(P_f \pm \delta P_f)(D \pm \delta D)}{4(L \pm \delta L)}$$

Error in τ_w

$$\delta\tau_w = |\tau_w| \sqrt{\left(\frac{\delta P_f}{P_f}\right)^2 + \left(\frac{\delta D}{D}\right)^2 + \left(\frac{\delta L}{L}\right)^2}$$

Wall shear rate

$$\dot{\gamma} = \frac{32Q}{\pi D^3} \quad (\text{B.3})$$

hence

$$(\dot{\gamma} + \delta\dot{\gamma}) = \frac{32(Q \pm \delta Q)}{\pi(D \pm \delta D)^3}$$

Error in $\dot{\gamma}$

$$\delta\dot{\gamma} = |\dot{\gamma}| \sqrt{\left(\frac{\delta Q}{Q}\right)^2 + \left(\frac{3\delta D}{D}\right)^2}$$

Flow curves

Plot $\tau_w + \delta\tau_w$ versus $\dot{\gamma} + \delta\dot{\gamma}$

Plot τ_w versus $\dot{\gamma}$

Plot $\tau_w - \delta\tau_w$ versus $\dot{\gamma} - \delta\dot{\gamma}$

Fit Herschel- Bulkley model to (i) and obtain τ_y , k and n

Fit Herschel- Bulkley model to (ii) and obtain τ_y , k and n

Fit Herschel- Bulkley model to (iii) and obtain τ_y , k and n

Obtain $(\tau_y \pm \delta\tau_y)$, $(k \pm \delta k)$ and $(n \pm \delta n)$

Reynolds Number

$$\text{Re} = \frac{8\rho V^2}{\tau_y + k\left(\frac{2V}{R_h}\right)^n} \quad (2.59)$$

Hence

$$(\text{Re} \pm \delta\text{Re}) = \frac{8(\rho \pm \delta\rho)(V \pm \delta V)^2}{(\tau_y \pm \delta\tau_y) + (k \pm \delta k)\left(\frac{2(V \pm \delta V)}{(R_h \pm \delta R_h)}\right)^{(n \pm \delta n)}}$$

Error in Re

$$\frac{\partial \text{Re}}{\partial V} = \frac{(8\rho\delta\rho^2 \left(\tau_y + k \left(\frac{2V}{R_h} \right)^n \right) - (8\rho\delta^2) \left(\frac{2kn}{R_h} \right)}{\left(\tau_y + k \left(\frac{2V}{R_h} \right)^n \right)^2}$$

$$\frac{\partial \text{Re}}{\partial \rho} = \frac{8V^2}{\tau_y + k \left(\frac{2V}{R_h} \right)^n}$$

$$\frac{\partial \text{Re}}{\partial \tau_y} = - (8\rho\delta^2) \left(\tau_y + k \left(\frac{2V}{R_h} \right)^n \right)^{-2}$$

$$\frac{\partial \text{Re}}{\partial K} = - (8\rho\delta^2) \left(\tau_y + k \left(\frac{2V}{R_h} \right)^n \right)^{-2} \left[\left(\frac{2V}{R_h} \right)^n n k^{n-1} \right]$$

$$\frac{\partial \text{Re}}{\partial n} = - (8\rho\delta^2) \left(\tau_y + k \left(\frac{2V}{R_h} \right)^n \right)^{-2} \left[k \left(\frac{2V}{R_h} \right)^n \ln \left(k \left(\frac{2V}{R_h} \right) \right) \right]$$

$$\delta \text{Re} = \sqrt{\left(\frac{\partial \text{Re}}{\partial V} \delta V \right)^2 + \left(\frac{\partial \text{Re}}{\partial \rho} \delta \rho \right)^2 + \left(\frac{\partial \text{Re}}{\partial \tau_y} \delta \tau_y \right)^2 + \left(\frac{\partial \text{Re}}{\partial k} \delta k \right)^2 + \left(\frac{\partial \text{Re}}{\partial n} \delta n \right)^2}$$

K value

$$K = f \text{Re} \tag{3.1}$$

Hence

$$(K \pm dK) = (f \pm df)(\text{Re} \pm \delta \text{Re})$$

Error in K

$$\delta K = |K| \sqrt{\left(\frac{\delta f}{f} \right)^2 + \left(\frac{\delta \text{Re}}{\text{Re}} \right)^2}$$

Appendix C. Fundamental derivations for non-Newtonian open channel flow

The following appendix contains the derivations for non-Newtonian open channel flow by (Chhabra & Richardson, 2008).

C.1 For the flow of any fluid down an inclined plane where the flow is steady, incompressible, fully developed (no end effects) and there are no side walls.

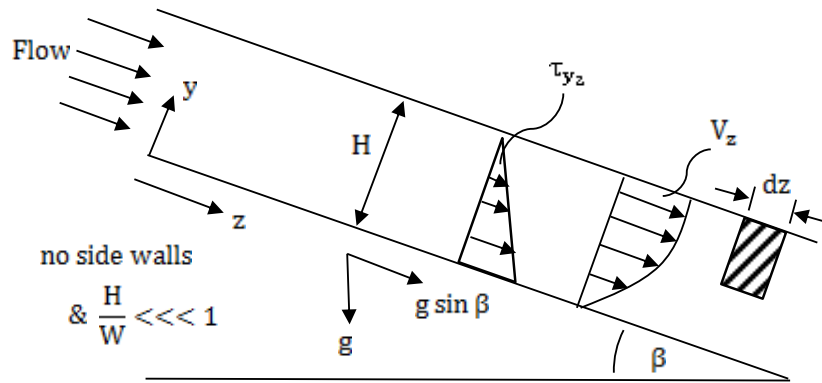


Figure 2.5

Writing a force balance on a differential element of the fluid:

$$W(H - y)dz\rho g \sin \beta = \tau_{yz}Wdz \quad (2.14)$$

let $dz \rightarrow 0$

$$\therefore \tau_{yz} = \frac{W(H - y)\rho g \sin \beta}{W} = (H - y)\rho g \sin \beta \quad (2.15)$$

where

$$\tau_{yz\min} = 0 \text{ at } y = H$$

and

$$\tau_{yz\max} = H\rho g \sin \beta$$

For the flow of a power law fluid down an inclined plane- no side walls

$$\tau_{yz} = k \left(\frac{dV_z}{dy} \right)^n \quad (2.16)$$

and from Eq. (2.15)

$$\tau_{yz} = (H - y)\rho g \sin \beta$$

gives

$$\frac{dV_z}{dy} = \left(\frac{\rho g \sin \beta}{k}\right)^{\frac{1}{n}} (H - y)^{\frac{1}{n}} \quad (2.17)$$

integrating Eq.(2.17) with respect to y

$$V_z = \left(\frac{\rho g \sin \beta}{k}\right)^{\frac{1}{n}} \int (H - y)^{\frac{1}{n}} dy + c$$

$$V_z = \left(\frac{\rho g \sin \beta}{k}\right)^{\frac{1}{n}} (-1)(H - y)^{\frac{n+1}{n}} \left(\frac{n}{n+1}\right) + c \quad (C.1)$$

$V_z = 0$ at $y=0$ to get c

giving

$$c = \left(\frac{\rho g \sin \beta}{k}\right)^{\frac{1}{n}} \left(\frac{n}{n+1}\right) (H)^{\frac{n+1}{n}}$$

Substitute c into Eq. (C.1)

$$V_z = \left(\frac{\rho g \sin \beta}{k}\right)^{\frac{1}{n}} (-1)(H - y)^{\frac{n+1}{n}} \left(\frac{n}{n+1}\right) + \left(\frac{\rho g \sin \beta}{k}\right)^{\frac{1}{n}} \left(\frac{n}{n+1}\right) (H)^{\frac{n+1}{n}}$$

Factorising

$$V_z = \left(\frac{\rho g \sin \beta}{k}\right)^{\frac{1}{n}} \left(\frac{n}{n+1}\right) H^{\frac{n+1}{n}} \left[1 - \left(\frac{1}{H^{\frac{n+1}{n}}}\right) (H - y)^{\frac{n+1}{n}} \right]$$

Simplifying

$$V_z = \left(\frac{\rho g \sin \beta}{k}\right)^{\frac{1}{n}} \left(\frac{n}{n+1}\right) H^{\frac{n+1}{n}} \left[1 - \left(1 - \frac{y}{H}\right)^{\frac{n+1}{n}} \right] \quad (2.18)$$

For the volumetric flow

$$Q = \int_0^H V_z W dy \quad (2.19)$$

Substitute for V_z from Eq.(2.18) into Eq.(2.19) and integrating

$$Q = W \left(\frac{\rho g \sin \beta}{k} \right)^{\frac{1}{n}} \left(\frac{n}{n+1} \right) H^{\frac{n+1}{n}} + 1 \int_0^H \left[1 - \left(1 - \frac{y}{H} \right)^{\frac{n+1}{n}} \right] dy$$

gives

$$Q = W \left(\frac{\rho g \sin \beta}{k} \right)^{\frac{1}{n}} \frac{n}{(2n+1)} H^{\frac{2n+1}{n}} \quad (2.20)$$

C.2 For the flow of a Hershel – Bulkley fluid down an inclined plane where the flow is steady, incompressible, fully developed (no end effects), and laminar.

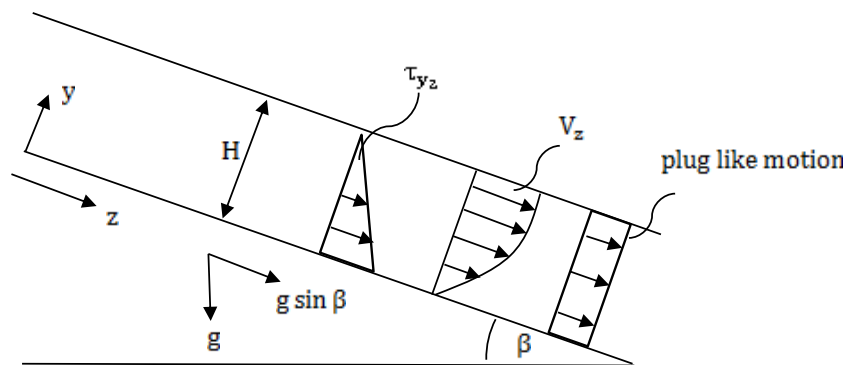


Figure C.1

$$\tau_{yz} = (H - y)\rho g \sin \beta$$

For the Hershel-Bulkley fluid model find the relationship for: H - β - τ_0^H - k - n

case I:

where

$$\tau_{yz_{max}} = \tau_{yz_{y=0}} = \rho g H \sin \beta < \tau_0^H$$

there is plug like motion

case II:

where $\tau_{yz_{max}} > \tau_0^H$

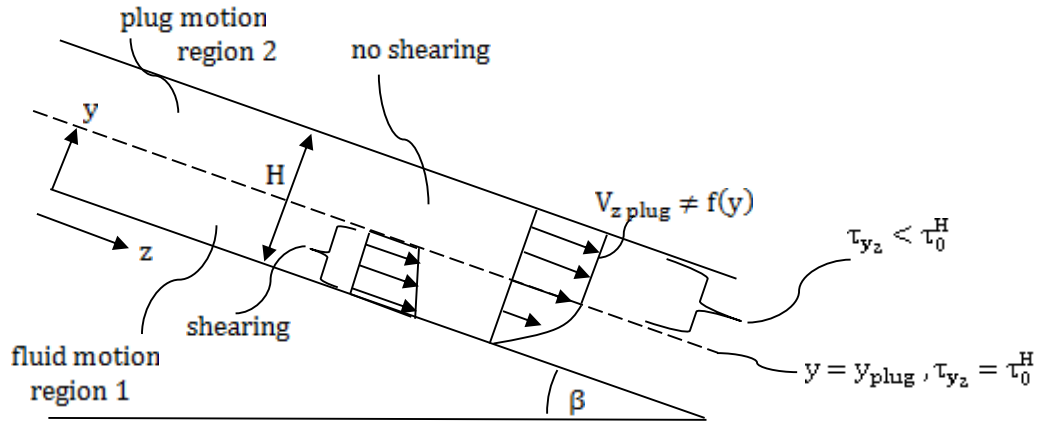


Figure 2.6

Region 1:

$$0 \leq y \leq y_{\text{plug}}$$

$$\tau_{yz} = (H - y) \rho g \sin \beta = \tau_0^H + k \left(\frac{dV_z}{dy} \right)^n$$

Rearranging this equation

$$\frac{dV_z}{dy} = \left[\frac{(H - y) \rho g \sin \beta - \tau_0^H}{k} \right]^{\frac{1}{n}}$$

Integrating

$$V_z = \int \left(\frac{(H - y) \rho g \sin \beta - \tau_0^H}{k} \right)^{\frac{1}{n}} dy + c$$

$$V_z = \frac{-k}{\rho g \sin \beta} \left(\frac{n}{n+1} \right) \left[\frac{(H - y) \rho g \sin \beta - \tau_0^H}{k} \right]^{\frac{n+1}{n}} + c$$

At $y = 0, V_z = 0$, find c

and substitute c

results in:

$$V_z = \frac{k}{\rho g \sin \beta} \left(\frac{n}{n+1} \right) \left[\left(\frac{H \rho g \sin \beta - \tau_0^H}{k} \right)^{\frac{n+1}{n}} - \left(\frac{(H - y) \rho g \sin \beta - \tau_0^H}{k} \right)^{\frac{n+1}{n}} \right] \quad (2.22)$$

Region 2:

$y_{\text{plug}} \leq y \leq H$: plug velocity = constant $\neq f(y)$

$$V_{zp} = V_{zy=y_{plug}} = \frac{k}{\rho g \sin \beta} \left(\frac{n}{n+1} \right) \left[\left(\frac{H \rho g \sin \beta - \tau_0^H}{k} \right)^{\frac{n+1}{n}} - \left(\frac{(H - y_{plug}) \rho g \sin \beta - \tau_0^H}{k} \right)^{\frac{n+1}{n}} \right]$$

noting at $y = y_{plug}$

$$\tau_{yzy=y_{plug}} = (H - y_p) \rho g \sin \beta = \tau_0^H$$

and

$$\tau_w = H \rho g \sin \beta$$

Substitute and simplifying gives

$$V_{zp} = V_{zy=y_{plug}} = \frac{k}{\rho g \sin \beta} \left(\frac{n}{n+1} \right) \tau_w^{\frac{n+1}{n}} \left[\frac{1 - \frac{\tau_0^H}{\tau_w}}{k} \right]^{\frac{n+1}{n}} \quad (2.23)$$

The total flow is the sum of the flow in region 1 plus the flow in region2. Hence,

$$Q = \int_0^H W dy \cdot V_z = \int_0^{y_{plug}} W dy \cdot V_z + \int_{y_{plug}}^H W dy \cdot V_{z_{plug}} \quad (2.21)$$

C.3 For the flow in noncircular cross sections, the flow is assumed to be steady, incompressible, fully developed, with no-slip, laminar and no end effects.

Flow in circular pipe:

$$\dot{\gamma}_w = \frac{1}{4} \tau_w \frac{d \left(\frac{8V}{D} \right)}{d\tau_w} + \frac{3}{4} \left(\frac{8V}{D} \right) \quad (2.24)$$

Slit flow:

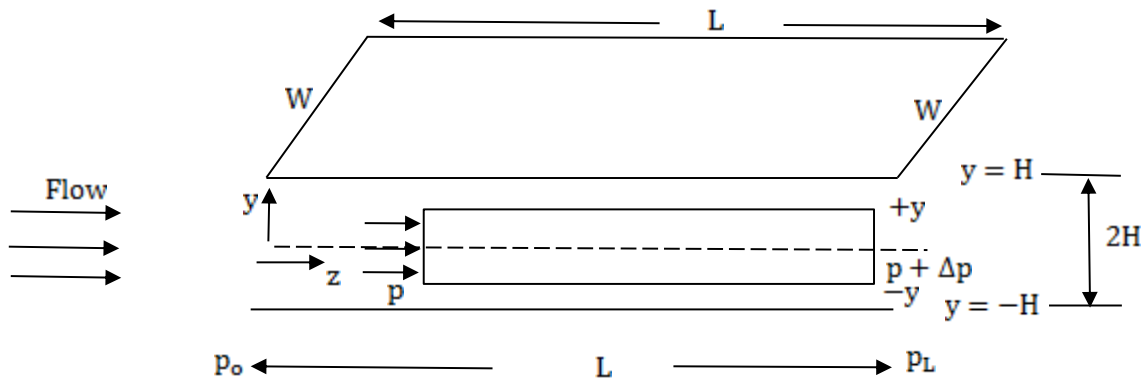


Figure 2.7

Momentum balance in Z direction

$$p \cdot 2Wy - (p + \Delta p)2Wy = \tau_{yz} 2WL$$

gives

$$\tau_{yz} = \left(\frac{-\Delta p}{L}\right)y$$

the volumetric flow rate

$$Q = W \cdot dy \cdot V_z$$

integrating between limits

$$= \int_{-H}^H W \cdot dy \cdot V_z = 2W \int_0^H V_z \cdot 1 dy$$

integrating gives

$$Q = 2W \left[yV_z \Big|_0^H - \int_0^H y \frac{dz}{dy} \cdot dy \right]$$

noting the first term inside the bracket becomes zero for no slip condition

giving

$$Q = 2W \int_0^H y \left(\frac{-dV_z}{dy}\right) dy$$

noting that : $\frac{y}{H} = \frac{\tau_{yz}}{\tau_w}$ & $dy = \frac{H}{\tau_w} \cdot d\tau_{yz}$ & $\frac{-dV_z}{dy} = \gamma = f(\tau_{yz})$

and substituting

gives

$$Q = 2W \int_0^{\tau_w} \frac{H}{\tau_w} \tau_{yz} f(\tau_{yz}) \frac{H}{\tau_w} d\tau_{yz}$$

$$Q = \frac{2WH^2}{\tau_w^2} \int_0^{\tau_w} \tau_{yz} f(\tau_{yz}) d\tau_{yz}$$

$$\frac{Q}{(2WH)(H)} \tau_w^2 = \int_0^{\tau_w} \tau_{yz} f(\tau_{yz}) d\tau_{yz}$$

$$\left(\frac{V}{H}\right) \tau_w^2 = \int_0^{\tau_w} \tau_{yz} f(\tau_{yz}) d\tau_{yz}$$

Differentiating both sides wrt τ_w

$$2\tau_w \left(\frac{V}{H}\right) + (\tau_w^2) \frac{d\left(\frac{V}{H}\right)}{d\tau_w} = \tau_w f(\tau_w)$$

$$f(\tau_w) = \dot{\gamma}_w = \left(\frac{2V}{H}\right) + \tau_w \frac{d\left(\frac{V}{H}\right)}{d\tau_w}$$

Noting:

$$D_h = 4R_h = \frac{4 \times \text{flow area}}{\text{wetted perimeter}}$$

for a circular tube $D_h = D$

noting that for a slit $D_h = 4H$

gives

$$\dot{\gamma}_w = \frac{1}{2} \tau_w \frac{d}{d\tau_w} \left(\frac{8V}{D_h}\right) + \left(\frac{8V}{D_h}\right) \quad (2.25)$$

for any arbitrary shape

$$\dot{\gamma}_w = a\tau_w \frac{d}{d\tau_w} \left(\frac{8V}{D_h}\right) + b \left(\frac{8V}{D_h}\right) \quad (2.26)$$

Appendix D. Experimental set-up

The experimental set-up consists of a 10 meter long tilting flume with the test fluid supplied from a 2000 litre mixing tank by a progressive cavity positive displacement pump (fitted with a pulsation damping unit) via a heat exchanger to three tube in-line tube viscometers into a 600 litre inlet tank which discharges into the flume inlet. For higher flow rates a centrifugal pump was used via a heat exchanger to the flume.

An isometric view of the experimental set -up is shown in Figure D.1

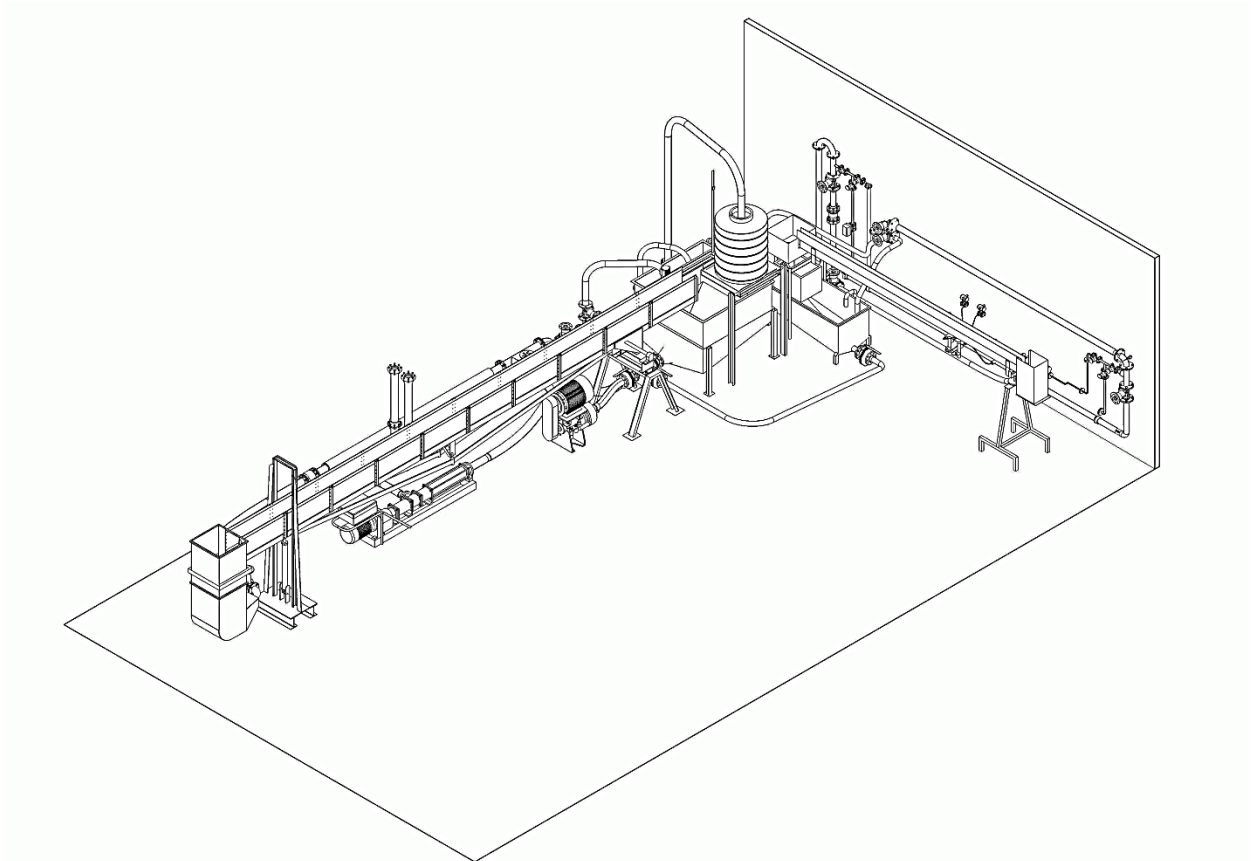


Figure D.1 Isometric view of flume and pipe viscometer

D.1.1 Flume

The flume shown in Figure D.1a is 10m long with a width of 300 mm and a depth of 300 mm. A partitioning section can be fitted in the flume to form a 150 mm wide flume. By inserting different cross-sectional inserts, the rectangular flume can be changed into a trapezoidal, semi-circular or triangular shaped flume. The slope of the flume can be altered from 0 to 5 degrees with the horizontal by using the hydraulic ram and locking device. Figure D.1b shows the flume fitted with the partition to change the flume width from 300 mm to 150 mm. The material of the flume sides and inserts were smooth acrylic with a maximum roughness of a few microns.

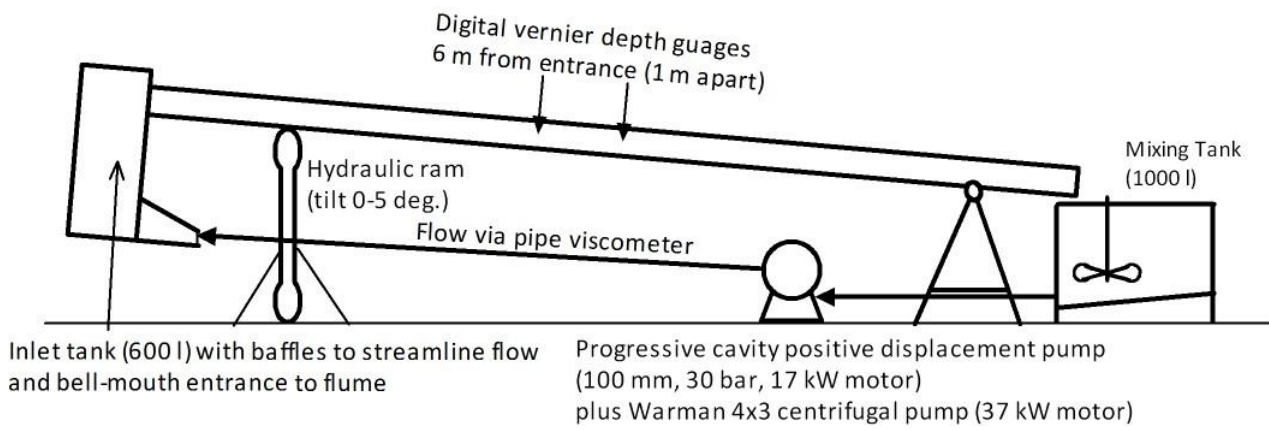


Figure D.1a Schematic of the 10 m tilting flume.



Figure D.1b Flume with partition fitted to form a 150 mm wide rectangular flume.

Figure D.1c shows the flume hydraulic ram and locking device. The 600 L flume inlet tank can also be seen. The inlet tank is fitted with a stainless steel baffle made up of 64 sections of 70 mm wide x 70 mm wide x 400 mm long sections in a square grid.

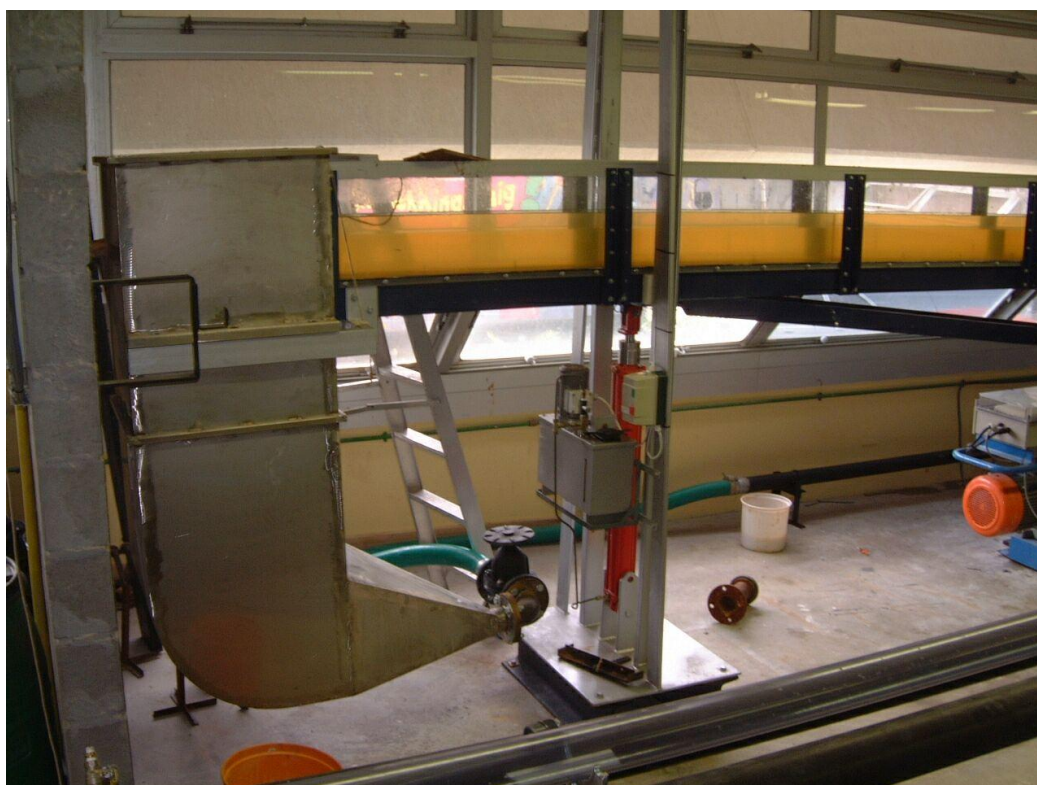


Figure D.1c The flume hydraulic lifting ram with a locking device and the flume inlet tank.

The flume was leveled using a contractor's automatic dumpy level. By setting up in the middle of the flume, the level can be checked to within 1 mm over 10 m (i.e. 0.01% accuracy). The vertical heights for the slopes of 1, 2, 3, 4 and 5 degrees were then calculated and used to set the slopes required. A ruler was mounted vertically on the frame next to the flume and a marker was connected to the flume. This was done at the position next to the hydraulic ram. The various slopes can then easily be set to within 1 mm and locked in that position for the duration of the test.

D.1.2 Flow depth measurement

To measure the flow depth, two digital vernier type depth gauges were fitted as shown in Figure D.1a. Figure D.2a shows the two Mitutoyo digital depth gauges (having a 0.01 mm accuracy from 0 to 100 mm and 0.02 mm accuracy from 100 mm to 250 mm) located at 5 and 6 m positions from the flume entrance. The depth gauges are linked electronically to the PC with an RS232 interface. Haldenwang, (2003) determined that the location of the two depth gauges at position 5 m and 6 m from the flume entrance coincided with where the flow was found to be steady and uniform as shown in Figure D.2b.

Haldenwang, (2003) estimated that the accuracy of flow depth measurement is better than 0.5 mm when the flow is laminar and better than 1 mm when the flow is turbulent. For a flow depth of 20 mm in laminar flow, the accuracy would be 2.5%. If the flow depth is then 50 mm in turbulent flow the accuracy would be 2%. It is very difficult to precisely predict the accuracy of flow depth measurements.



Figure D.2a Two Mitutoyo digital depth gauges mounted on the flume at 5 m and 6 m from the entrance

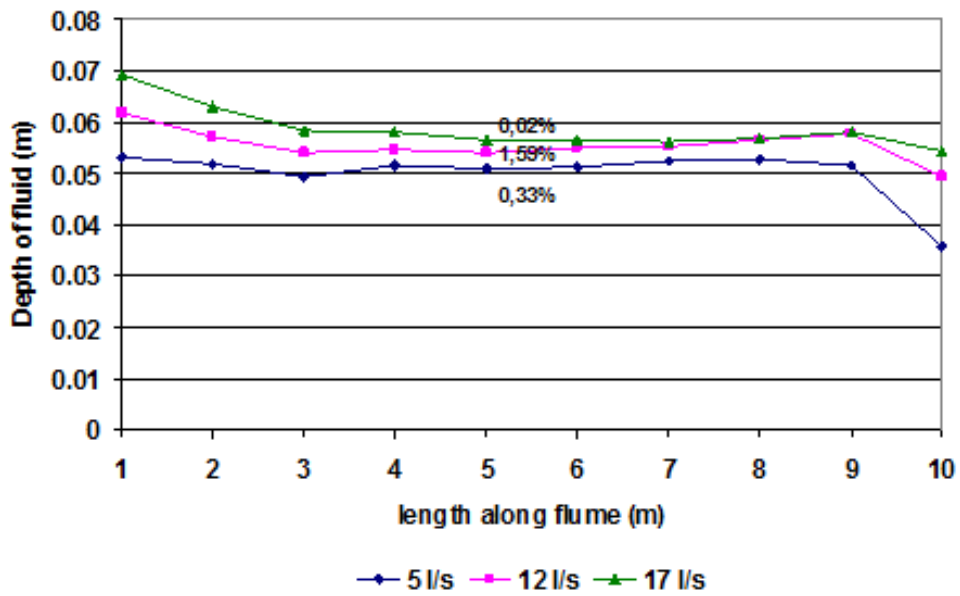


Figure D.2b Fluid flow depth measured at 1 m intervals from inlet to outlet for 10% kaolin flowing in a 300 mm wide flume at 3 degree slope to the horizontal. (Haldenwang, 2003)

It can be seen from Figure D.2b that between 5 m and 6 m the difference between the depth gauge measurements is very small and therefore the flow was considered to be steady and uniform.

D.1.3 The flume rig operating procedure

The procedure implemented by Haldenwang, (2003) was followed to establish a range of values of volumetric flow rate, (Q) and fluid depth, (h). The procedure which is the same for all four flume shapes and sizes tested, is as follows.

- The flume slope is adjusted to the correct slope with the hydraulic ram and locked in place.
- The slurry is diverted to the flume and is now circulating through the tube viscometer rig and the flume rig. This is to enable one to check whether the rheology of the slurry has changed during the flume test at regular intervals.
- The data logger is switched on and the visual basic programme on the PC is activated. The data is exported to an Excel spreadsheet.
- The two depth gauges are fitted to the flume and connected to the data logger.
- The depth gauges are zeroed on the bottom of the flume.
- When the correct flow rate is set, the depth gauges are manually lowered to the fluid surface.
- The data-logger is triggered and the program samples flow rates over the set time interval.
- The average flow rate and the fluid height recorded by the two depth gauges are exported to the spreadsheet.
- The procedure is repeated for a range of flow rates, as well as for different slopes.
- The spreadsheet contains a Moody diagram and the Reynolds numbers and Fanning friction factors are plotted directly on the diagram.
- This ensures that the range of data points covered is covered sufficiently.

D.2.1 The tube viscometer rig

The in-line tube viscometer consists of three parallel tubes of 13, 28 and 80 mm diameter PVC tubes, three magnetic flow meters, one mass flow meter a heat exchanger, two differential pressure transducers and flow regulating valves. A front elevation of the tube viscometer layout is shown in Figure D.2a. The surface roughness of the pipes was determined by Haldenwang, (2003) to be 1 μm for the 13 and 28 mm pipes and 3 μm for the 80 mm pipe.

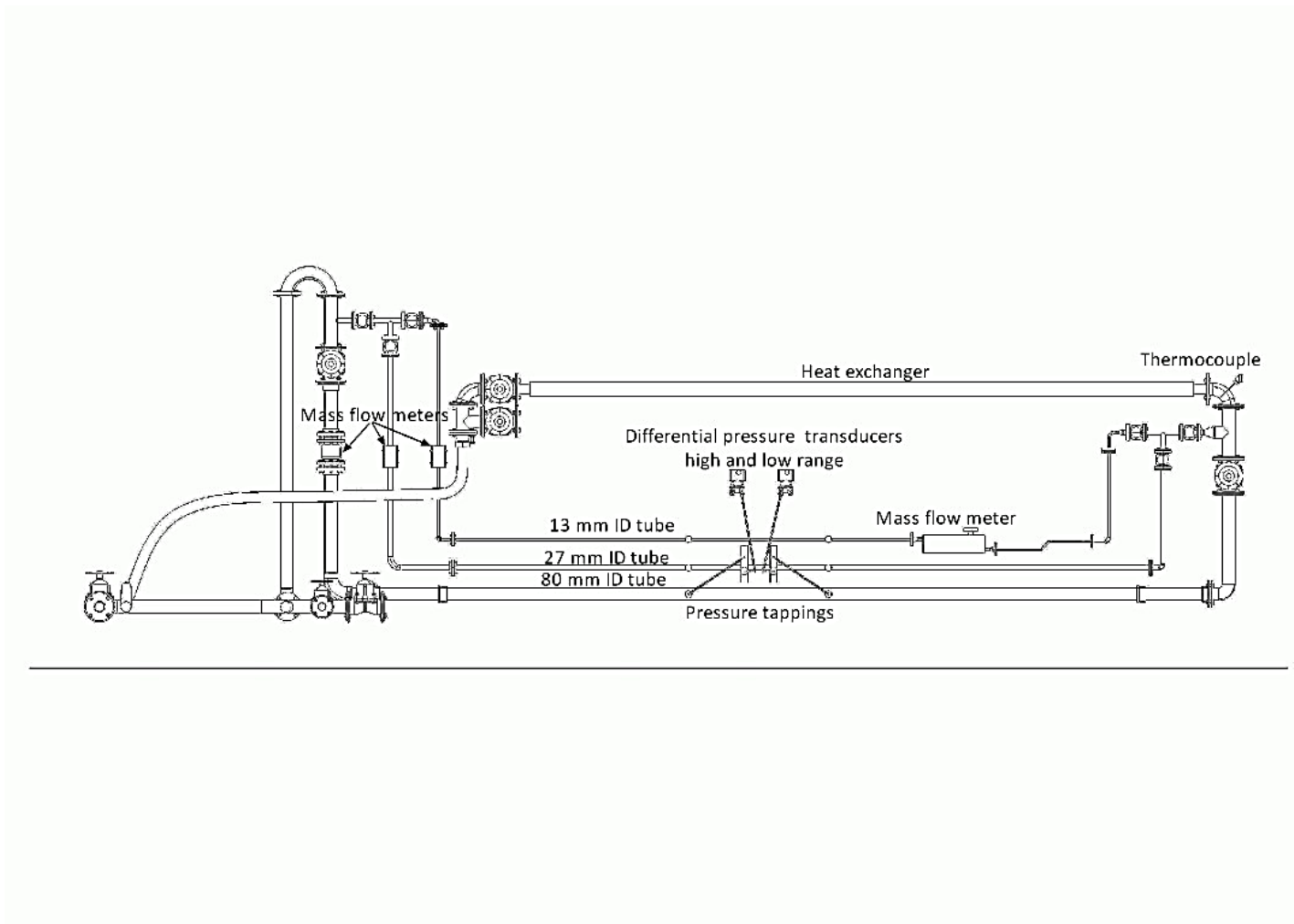


Figure D.2a Front view of tube viscometer.

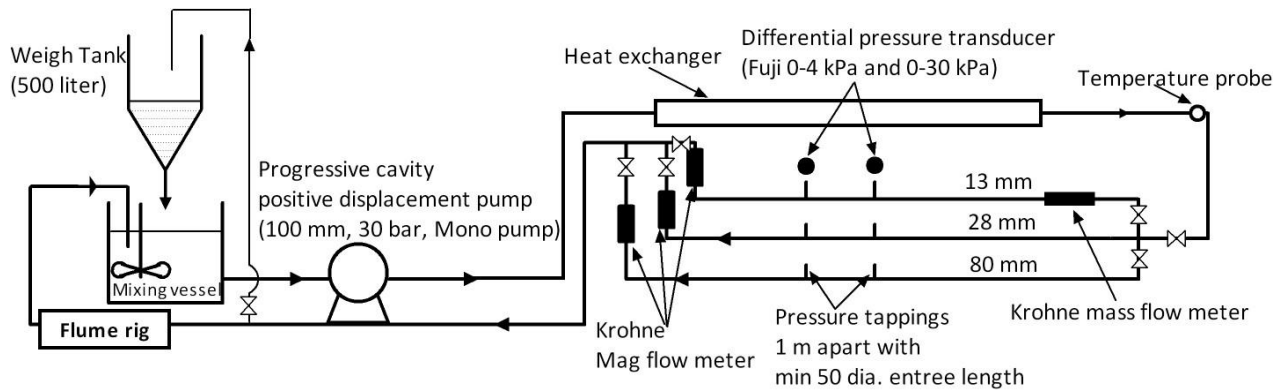


Figure D.2b Schematic of flume rig linked to the 3 tube in- line viscometer.

D.2.2 Flow meters

To measure the flow in the tube viscometer and the flow going to the 10m flume rig, three Krohne magnetic flow meters are used as shown in Figure D.2b. Figure D.2c shows the three Krohne in-line magnetic flow meters.

The three PVC tubes in Figure D.2b are in parallel and have 13 mm, 28 mm and 80 mm diameters respectively. Each tube has an in-line magnetic flow meter as shown in Figure D.2c. All three flow meters are fitted in the vertical position. The maximum error of the flow meters in the range measured is 4%. The 80 mm diameter tube was not used for volumetric flow rates below 2 l/s and the 28 mm diameter tube was not used for volumetric flow rates below 0.4 l/s. The 13 mm diameter tube was not used for flow rates below 0.07 l/s

The Krohne flow meter manufacturer specifies a straight pipe minimum length before the flow meter to be 5 pipe diameters and a straight pipe minimum length after the flow meter to be 2 pipe diameters. The minimum lengths used in the rig set-up are ≥ 10 pipe diameters before and ≥ 5 pipe diameters after the flow meters. The 13 mm pipe also has an in-line mass flow meter that allows measurement of temperature and density of the slurry.



Figure D.2c Krohne in- line magnetic flow meters used in the 80 mm, 28 mm and 13 mm diameter PVC tubes.

D.2.3 Differential pressure transducers

Each of the 80 mm, 28 mm and 13 mm PVC tube has two pressure tapings 1 m apart, so that the differential pressure can be measured during tube viscometry, Figure D.2d. Flushing pods are connected to the pressure tapping, and then the fluid or slurry is fed into the isolation pods to make sure no solids enter the differential pressure (DP) cells. A water line is then fed into the pods to flush the system i.e. remove any entrapped air.

According to the manufacturer, the accuracy of the differential pressure transducers (DPTs), Figure D.2e are within 0.1% of full scale. This means that for the high range DPT, the differential pressure error is ± 25 Pa and for the low range DPT the differential pressure error is ± 4 Pa.

A straight unobstructed pipe section of at least 50 pipe diameters was kept before the pressure tapings (Govier & Aziz, 1972; Hanks, 1981). This is to ensure that flow is fully developed and does not influence the pressure readings.



Figure D.2d Pressure tapings and flushing pods.



Figure D.2e Differential pressure transducers

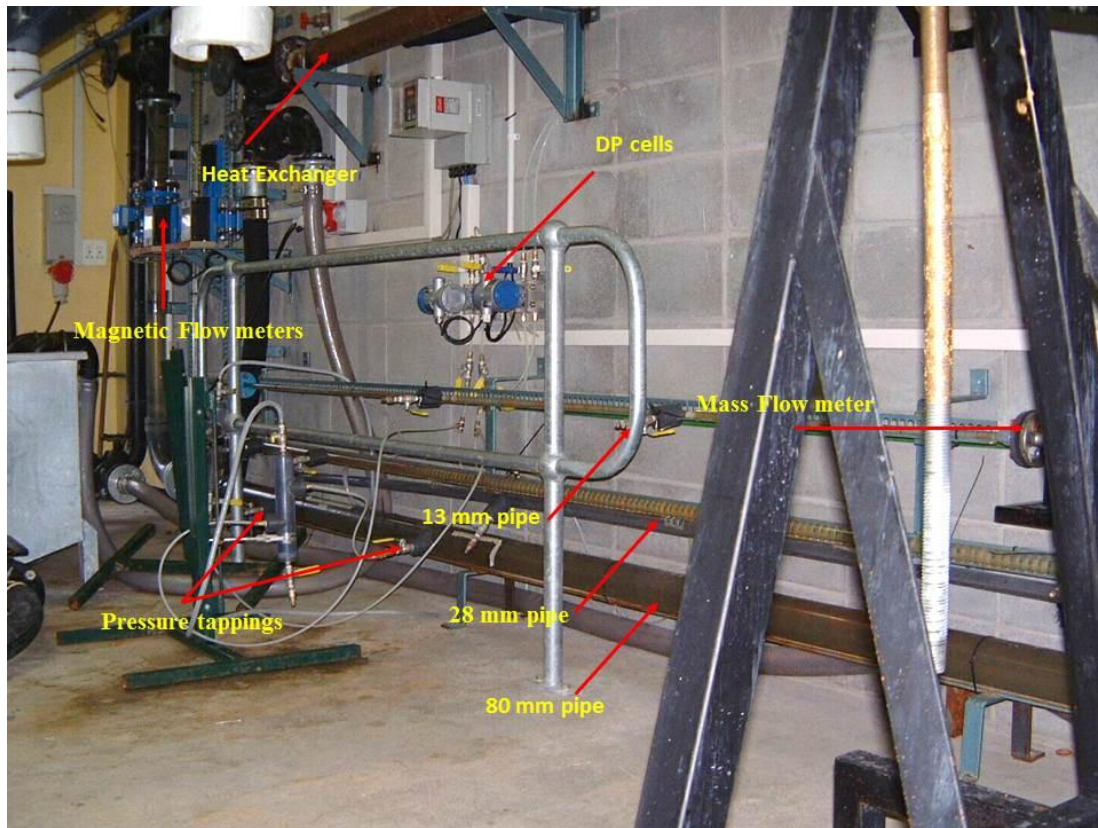


Figure D.2f Tube viscometer and heat exchanger.

D.2.4 Tube viscometer rig procedure

The procedure implemented by Haldenwang, (2003) for the tube viscometer shown in Figure D.2f was followed to establish a range of values of Δp and V . The procedure, is the same for all three the tube diameters, and is as follows:

- Before any slurry is tested, the flow meters and the differential pressure transducers are calibrated.
- Water tests are then conducted in all three tubes and the values compared with the Colebrook-White equation.
- About 2 000 litres of slurry are mixed in the main mixing tank until the slurry is well mixed.
- A representative sample is taken and the relative density is calculated. If the required concentration is not achieved, more solids are added and mixed.
- During the mixing process the slurry is circulated through all three tubes so that any water in the system is mixed in the slurry and will not afterwards influence the final concentration.
- The pods that prevent solids from entering the differential pressure transducers (Figure D.2d) are connected to the pressure tappings. The lines linking the tappings and DPTs are flushed with water. This sometimes has to be repeated during tests when solids start entering the system. The amount of fluid in the system is more than 2000 litres and the volume for flushing is extremely small and therefore did not affect the rheology.
- The flow rate is regulated by means of a series of valves, and as the pump cannot achieve the low flow rates, the excess flow is diverted through a by-pass line back into the mixing tank. This helps to ensure that the slurry is well mixed.

- The data logger is switched on and the visual basic programme on the PC is activated. The data is exported to an Excel spreadsheet.
- When the correct flow rate is set, the data-logger is triggered and the programme samples flow rates and differential pressures over a preset time interval.
- The average flow rate and differential pressure are exported to the spreadsheet and are visually displayed on a wall shear stress versus $8V/D$ plot.
- This is repeated with a range of flow rates until sufficient data points are available for the pseudo shear diagram.
- The process is repeated for the 13 mm, 28 mm and 80 mm tubes.
- All three sets of data are plotted on one graph, which enables one to see whether there are any obvious errors in the data sets. If the laminar flow data of all three tubes form collapse onto a single line, confirming that there is now wall slip occurring in the tube
- During the flume tests, the in-line tube viscometer was used to see whether the rheology has changed. This was very important as the flume testwork often took a day to complete.

D.3 Heat exchanger

The temperature was monitored to stay within a range during the tests to insure similar test conditions for the fluids tested. Slurry temperatures varied from 19° to 25° Celsius. The cooling system kept the temperature of the slurries tested from rising above 25° Celsius.

D.4 Pumps

A 100 mm, 30 bar progressive cavity positive displacement pump Figure D.4a, driven by a 17 kW motor fitted with a variable speed drive, feeds the closed system linking the flume and the pipe viscometer. This pump is able to deliver approximately 25 l/s of water through the pipe rig.

To minimise pump pulsations, a damper was fitted at the supply end of the pump. This is shown in Figure D.4a. The effectiveness of the damper unit could be observed by observing the pulsations of the fluids in the clear section of the unit. The vertical pipes are 100 mm clear acrylic with steel end caps on and steel nipples to let air into the system when required. The flow in the flumes was more regular after fitting the damping unit (Haldenwang 2003).

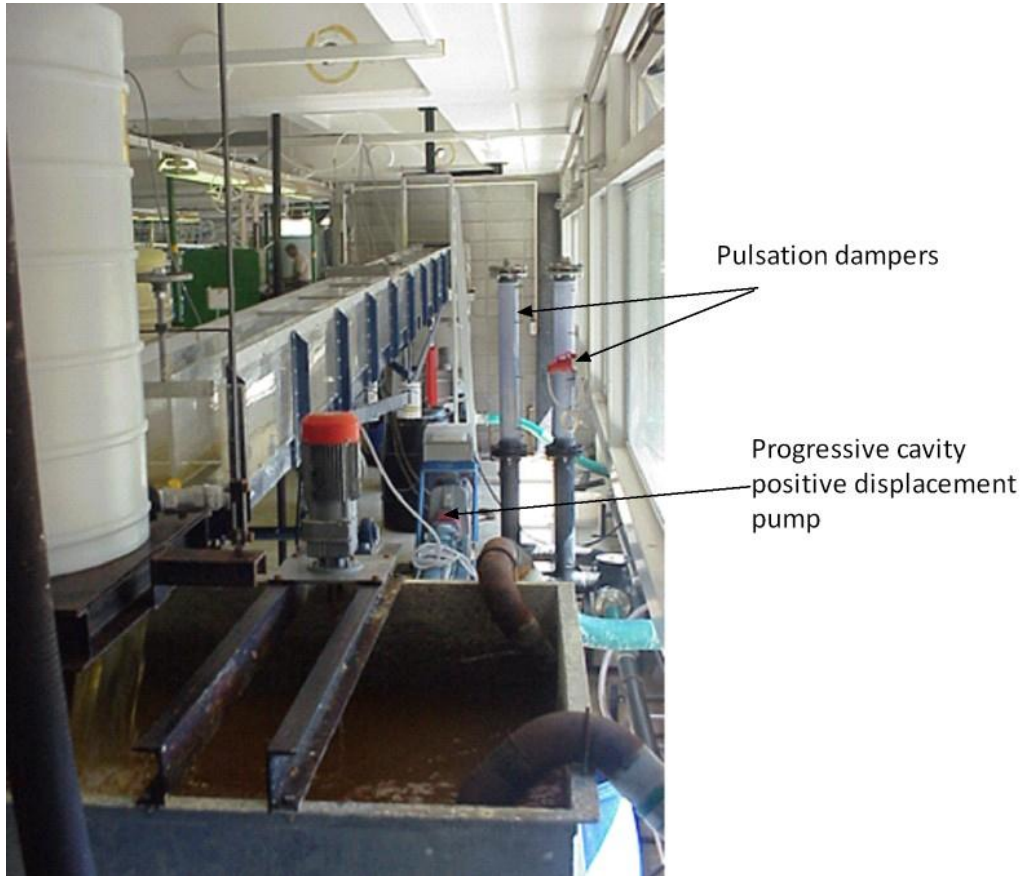


Figure D.4a Flume, mixing tank, progressive cavity positive displacement pump and pulsation dampening unit.

For higher flow rates a Warman 4x3 centrifugal pump, Figure D.4b was installed, driven by a 37 kW motor and regulated by a variable speed drive. To minimise losses, the pump was not linked to the in-line pipe viscometer, but linked via a heat exchanger and 100 mm electromagnetic flow meter directly to the inlet of the flume.



Figure D.4b Warman 4x3 centrifugal pump

D.5 Slurry density

The process to obtain the slurry density (ρ) and relative density (S_m) are calculated according to standard procedures as follows.

- The equipment required is a one litre volumetric flask and a scale that can measure to a milligram.
- Dry the flask thoroughly and weigh (M_1).
- Take a well-mixed slurry sample from the mixing tank. This can be done by taking a few samples from different places in the tank and mixing them.
- Fill the flask partially with slurry and weigh (M_2).
- Fill up the remainder of the flask to the graduated mark with water and weigh (M_3).
- Empty the flask, clean and fill with water to the same graduated mark, and weigh (M_4).
- The procedure is repeated at least three times to check the accuracy of testing.
- The relative density (S_m) is defined as:

$$S_m = \frac{\rho}{\rho_w} \quad (D1)$$

This can be written as:

$$S_m = \frac{\text{Mass of slurry sample}}{\text{Mass of equal volume of water}} \quad (D2)$$
$$\therefore S_m = \frac{M_2 - M_1}{(M_3 - M_2) - (M_4 - M_1)}$$

From Equation (D1)

$$\rho_m = S_m \rho_w \quad (D3)$$

D.6 Error analysis

Error propagation analysis for all measured variables were performed as outlined in Appendix B.